Synthesis and Blend Behaviour of Multi-End Capped Polyethylene

HARDMAN, SARAH,JEAN

Synthesis and Blend Behaviour of Multi-End Capped Polyethylene

Sarah Jean Hardman

Trevelyan College
Department of Chemistry
University of Durham

May 2011

Thesis submitted to the University of Durham in partial fulfillment of the regulations for the Degree of Doctor of Philosophy.

Declaration

The work reported in this thesis was carried out in the laboratories of the Department of Chemistry, University of Durham and at the Rutherford Appleton Laboratory in Oxfordshire between October 2007 and September 2010. This work has not been submitted for any other degree in Durham or elsewhere and, unless otherwise stated, is the original work of the author.

Statement of Copyright

Financial Support

I gratefully thank the Engineering and Physical Sciences Research Council's Doctoral Training Account for their generous funding of this research. I must also thank Macro Group UK and the Royal Society of Chemistry for funding my attendance at conferences and meetings to present this research.

Abstract

There is an ever-growing need for polymers with specific surface properties for the production of modified materials. Recently, extremely efficient polymer surface modification has been achieved by incorporating dendritically end functionalised polymers into blends, which combine sufficient mobility, with optimal functionality, to cause dramatic changes in surface properties. This method has significant advantages over traditional coating technologies in that no additional processing step is required.

It has already been established that blends of dendritically functionalised polymers have great potential in amorphous systems, but for commercial uptake similar results in semi-crystalline materials must be achieved. Polyethylene (PE) is the world's most widely produced polymer, coming in many grades of molecular weight, branch content, and crystallinity. Semi-crystalline materials, such as PE possess excellent bulk properties, but their surfaces are notoriously difficult to functionalise except by harsh chemical treatments, or corona discharge methods. By bridging the gap between polymer science that is well understood, and polymer modification, will add value to commercially important materials. However to do this the effect that crystalline domains have on spontaneous surface segregation must be understood. Do crystalline regions exclude lower energy additives and drive them to the surface or are the additives trapped in the bulk?

In this study new synthetic methodologies were developed for the preparation of fluoro-end-capped polymers with well defined multiple hydrophobic groups, via anionic polymerisation, resulting in analogues of end-functionalised LLDPE. Physical properties have been characterised using a variety of techniques, namely ion beam analysis (IBA), contact angle measurements and several neutron scattering measurements, including neutron reflectivity (NR), small angle neutron scattering (SANS) and quasi-elastic neutron scattering (QENS) and studies proved surface enrichment with fluoro-chain ends.

This work has shown that blends of fluoro-polymer preferentially segregate to the air surface interface and the subsequent surface free energies of these blends were near that of polytetrafluoroethylene (measured surface energy was 8.95 mNm^{-2}) with minimal amounts of fluorine. For example blends with 12 wt% (with respect to matrix polymer) fluorocarbon end-functionalised PE, which is equivalent to ~1% fluorocarbon, result in a measured surface energy of 8.44 mNm^{-2}.

Acknowledgments

I am deeply indebted to a number of people for their support and patience throughout my Ph.D. but especially to my supervisor, Richard Thompson, even after I suggested that we purchase kryptonite from Aldrich to make “green plasma”! His guidance and support over the past three years has been endless, and his enthusiasm at exploring the pubs in Cambridge, during an Ion Beam Conference, admiral.

Similarly, my thanks also go to my co-supervisors Lian Hutchings, whose advice throughout my synthesis proving invaluable, and Nigel Clarke, whose enthusiastic outlook on neutron scattering was encouraging.

The neutron scattering experiments would not have been possible if it was not for the help and expertise of the instrument scientists at Oxford. Special thanks must go to Victoria Garcia-Sakai who without her continued support the QENS interpretation, and experiment, would not have been salvaged! Secondly, John Webster’s help during the neutron reflection experiment and Sarah Rogers during the SANS.

I must also thank Doug Carswell for the many DSC samples he ran for me and Alan Kenwright for his help during the interpretation of NMR spectra. In addition thanks must go to Catherine Heffernan and Ian McKeag for their help recording NMR spectra, especially the high temperature samples. Gratitude must also go to Emily Smith who ran XPS samples for me at the open access Nottingham XPS facility funded by EPSRC and to William Berguis who supplied one of the alkyl bromides used during end-capping.

To everyone in MC105 and the Musgrave room, past and present, thank you for making it such a diverse and enjoyable place to work and have coffee. Also a mention must go the person with a “special” sense of humour who signed me up to the Durham Swingers Society, you kept my inbox full!

Finally, I would like to thank Scott for keeping me smiling, even on the most difficult of days and to Mildred – you kept me sane!

Contents

Units and Symbols

Abbreviations

"a"	End group 3,5-(Di-3-(perfluorooctyl)propyloxy) benzyl bromide
ATRP	Atom Transfer Radical polymerisation
ACCA	Actual contact angle
APCA	Apparent contact angle
AFM	Atomic force microscopy
"b"	End group 3,4,5-(Tri-3-(perfluorooctyl)propyloxy) benzyl bromide
"c"	End group $(C_8F_{17}(CH_2)_3O)_4$-[G-1]-Br
CA	Contact Angle
CF	Fluorocarbon groups (C_8F_{17})
PEyx	Deuterated ethylene molecular weight x kg/mol, with end group y
DSC	Differential scanning calorimetry
hPEx	Hydrogenated polyethylene molecular weight x kg/mol
IBA	Ion Beam Analysis
kg/mol	Kilograms per mole
LDPE	Low density polyethylene
LLDPE	Linear low density polyethylene
NMR	Nuclear Magnetic Resonance
NR	Neutron Reflection
NRA	Nuclear Reaction Analysis
OZ	Ornstein-Zernike
PB	Polybutadiene

PBx	Polybutadiene molecular weight x kg/mol
PByx	Polybutadiene molecular weight x kg/mol, with end group y
PE	Polyethylene
PS	Polystyrene
PTFE	Polytetrafluoroethylene
QENS	Quasielastic Neutron Scattering
RAFT	Reversible Addition Fragmentation Transfer polymerisation
RBS	Rutherford Backscattering Spectroscopy
ROMP	Ring Opening Metathesis Polymerisation
RPA	Random Phase Approximation
SANS	Small Angle Neutron Scattering
SCMFT	Self-consistent mean field theory
SEC	Size Exclusion Chromatography
TGA	Thermogravimetric Analysis
TCA	True contact angle
UHDPE	Ultra high density polyethylene
XPS	X-ray Photoelectron Spectrometry

Roman Symbols

A	Surface area per lattice site
a	Kuhn length
b	Scattering length
B	Phase shift of neutron beam
d	Layer thickness

ΔHm^*	Theoretical heat of fusion 1g of 100% crystalline polymer
ΔHm	Heat associated with fusion
D_m	Diffusion coefficient
E_a	Activation energy
E_K	Kinetic energy of the photoemitted electron
$I(\lambda,Q)$	Measure SANS intensity
$I_0(\lambda)$	Incident flux
$I_{inc}(Q,E)$ *or* $I(Q,t)$	Elastic incoherent structure factor (EISF)
$I_{inc}(Q,t)$	Intermediate incoherent scattering function
k_i	Rate of Initiation
k_p	Rate of Propagation
L	Brush layer height
M	Molar mass
M_n	Number average molar mass
M_w	Weight average molar mass
n	Monomer molecular weight
N	Number of scattering bodies
N_a	Atomic number density
n_i	Refractive index
PDI	Polydispersity index
Q	Momentum Transfer
r	Normalised polymer chain length
$R(Q)$	Q dependent reflectivity

R_f	Fresnel reflectivity
R_g	Radius of gyration
r_i	Fresnel coefficient
	Position Vector
$S_{inc}(Q,t)$ or $S(Q,\omega)$	Incoherent dynamic structure factor
t	Time
T	Temperature
T_g	Glass transition temperature
T_m	Measured melting temperature
	The melting point for a perfectly crystalline polymer of high molar mass
v_r	Repeat unit volume
v_{ref}	Lattice volume
w	Work function of the spectrometer
X	Number of monomer units / Degree of polymerisation
Z	Number of functional groups per polymer chain
z	Depth
z^*	Surface excess concentration

Greek Symbols

β	Sticking energy
χ	Flory-Huggins interaction parameter
γ	Surface energy
χ_s	Surface interaction parameter

χ_b	Bulk interaction parameter
δ	Solubility parameter
μ	Chemical potential
σ	Grafting density
φ	Volume fraction
ζ	Size of the lattice layer
λ	Wavelength
θ	Scattering Angle
$\phi(z)$	Depth composition profile
θ_c	Critical angle
ψ	Kohlrausch-Williams-Watts (KWW) shape parameter
τ_{KWW}	KWW relaxation time
τ_c	Effective relaxation times
η	Frequency of photon
	Function of the molecular properties of two phases
γ_{LV}	Liquid-vapour surafce tension
γ_{SL}	Solid-liquid surface tension
γ_{SV}	Solid-vapour surface tension
$\Delta\Omega$	Detector solid angle
$\eta(\lambda)$	Detector efficiency

List of Figures

List of Tables

1 Introduction

1.1 History of Polymers

A polymer is 'a molecule of relatively high molecular mass, the structure of which essentially comprises of the multiple repetition of units derived from molecules of low relative molecular mass'[1] which is composed of macromolecules, or polymer molecules. The repeat units come from monomers which are simply 'molecules which can undergo polymerisation'.

People have been utilising polymers for thousands of years without realising it. For example silk is simply a protein, wood, is lignin, both of which are polymers. The importance of polymers was not realised until Goodyear[2], in 1839, who crosslinked natural rubber with sulphur (Vulcanisation) making it more useful, and in 1910 Hendrik Baekeland[3] invented the first commercially available synthetic polymer, Bakelite.

By the early 20th century the chemical and physical nature of polymers was being explored and in 1920, Hermann Staudinger[4] coined the name macromolecules. He argued polymers were in fact giant chainlike molecules, rather than aggregates of smaller molecules. However, it was not until Herman Francis Mark proved their existence that the concept of macromolecules was accepted[5, 6].

Paul Flory, a student of Wallace Carothers[7-10] (who synthesised nylon in 1935 and is widely credited for introducing the world to macromolecules), went on to determine the fundamental behaviour of macromolecules. His book, Principles of Polymer Chemistry[11], is still a principle reference for any polymer chemist. He received the Nobel Prize in chemistry in 1974, which he dedicated to his mentor Carothers.

1.2 Polymer Classification

Polymers are formed by chemical reactions in which a large number of monomers are joined sequentially forming a chain. These polymers may be classified according to their structure, their physical properties and by the characteristics of the reactions by which they are formed.

1.2.1 Polymer Classification According to Skeletal Structure

In many polymers only one monomer is used, termed *homopolymers* (AA). In others, two or more different monomers may be combined to form *copolymers* (AB), where A and B are types of monomers. Copolymers can have a statistical, alternating, di-block, tri-block or multiblock sequence type. These are all examples of *linear* polymers, figure 1:1.

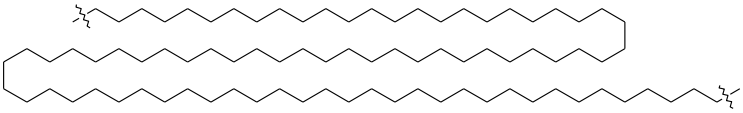

Figure 1:1 The skeletal structure of linear polyethylene

Other types of polymer structures are branched polymers, figure 1:2. If the polymer has branches of different sizes irregularly spaced along the chain it is classified as a non-linear (branched) polymer e.g. linear low density polyethylene. If the polymer has identical pendant groups, e.g. CH_3 groups, along the backbone in a regular array it is classified as a linear polymer, e.g. polypropylene.

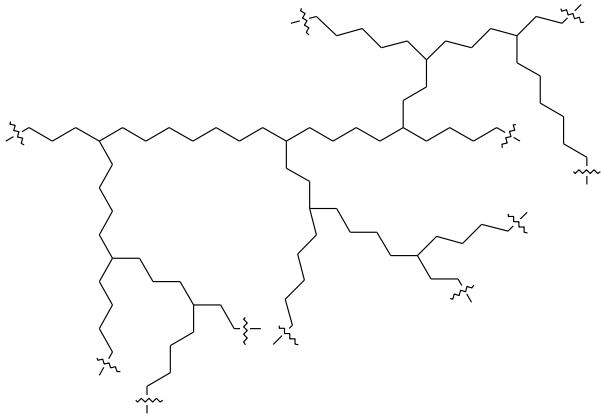

Figure 1:2 The general skeletal structure of a branched polymer

Branches prevent the molecules from packing closely, reducing crystallinity thus density. The final type of polymer skeletal structure, is known as a network polymer, figure 1:3. These polymers have cross-links between their chains creating three-dimensional networks. In some networks the high density of cross-links restricts motion leading to a rigid material. A result of this is that these networks cannot be dissolved and instead swell in a good solvent.

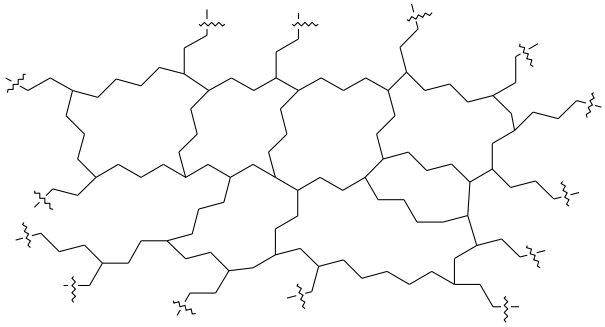

Figure 1:3 The general skeletal structure of a network polymer

1.2.2 Polymer Classification According to Physical Properties

Today there exist several types of polymeric materials from elastomers to natural polymers, figure 1:4. These can be broadly divided into three types of polymer; thermoplastic and thermosetting (behaviour to heat), and the third type by their elastic modulus – elastomers. Thermoplastics are further subdivided into three types - crystalline, amorphous and semi-crystalline.

1.2.2.1 Response to Heat

Thermoplastic polymers contain linear or branched chains, are solid at room temperature and become rubbery when heated above their T_g (glass transition temperature[*]) or T_m (melt temperature[†]). As a result thermoplastic polymers can be processed as viscous liquids that solidify on cooling. Reheating can be performed many times without affecting the polymers properties; this phenomenon is due to their relatively weak intermolecular forces. The majority of thermoplastics are produced by chain polymerisation.

Thermosetting polymers are network polymers with a high degree of cross-linking that develops as the polymer is heated ("cured"). After heating, a thermosetting plastic solidifies on cooling and cannot be remoulded. This is because the high degree of irreversible cross-linking within the polymer network which restricts the motion of the chains. Thermosetting polymers are more durable than thermoplastics and have uses in the car and construction industries.

Elastomers are soft rubbery polymers with some crosslinks that can be stretched but then recover when stress is removed. This is due to their low degree of cross-linking. These polymer chains have some freedom to move, but are prevented from permanently moving relative to each other. However, due to the cross-links they cannot be processed. Thermoplastic elastomers have elements of thermoplastics and thermosets where at room temperature behave as normal elastomers but at elevated temperatures they are thermoplastics and can be heated and processed cooled and then reheated. This is because the cross-links are not permanent covalent bonds but reversible physical cross-links.

[*] The glass transition temperature (T_g) of a non-crystalline material is the temperature at which the material changes its behaviour from being 'glassy' to being 'rubbery'

[†] The melting point of a polymer is the temperature at which a transition from a crystalline or semi-crystalline phase to a solid amorphous phase occurs.

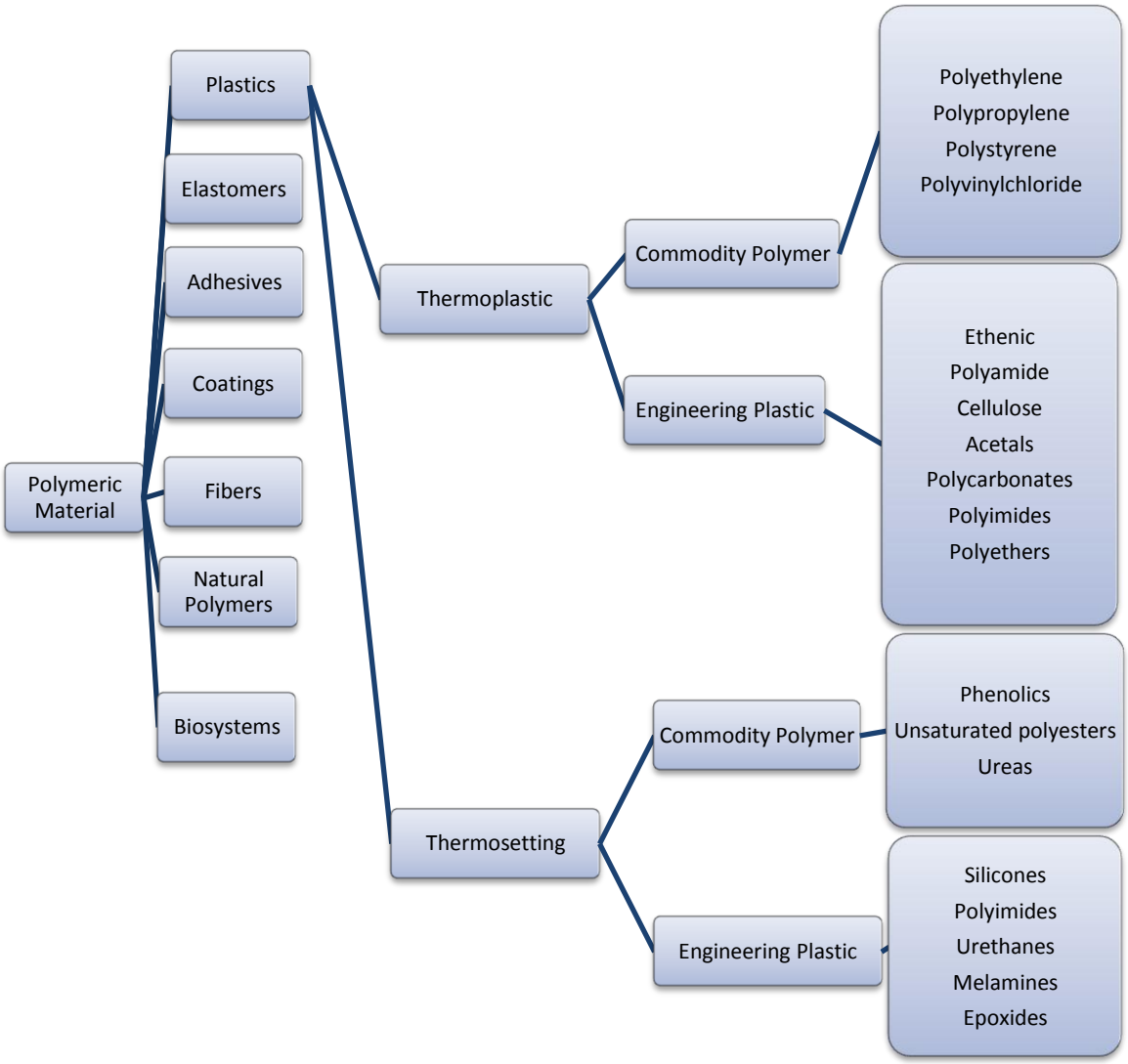

Figure 1:4 Classification of polymeric materials according to their response to heat after Koutsos[12]

1.2.2.2 Polymer Morphology

Polymer morphology has a significant impact upon the thermal properties of a polymer such as the glass transition and the melting point. At sufficiently low temperatures all polymers are hard rigid solids. As temperature is raised each polymer chain eventually obtains sufficient thermal energy for its chains to move freely enough for it to behave as a viscous liquid. Upon lowering the temperature some polymers are able to crystallise and lamella are formed. The different morphologies of a polymer are a direct result of the type of "packing" that a polymer undergoes due to its skeletal structure and molecular weight which influences the overall crystallinity of the polymer. Polymers therefore can be amorphous or semi-crystalline.

1.2.2.2.1 Amorphous Polymers

Amorphous chains are disordered in the solid state. Below T_g, the polymer is a glass. T_g can phenomenologically be defined as a temperature where a polymer experiences a significant change in properties, typically, a change in Young's Modulus of several orders of magnitude. With increasing temperature the molecular motion in an amorphous polymer increases, the polymer passes from a glass, through a rubber like state, until finally it becomes a viscous liquid. The T_g is governed by the molecular and structural nature of the polymer chains:

- *Free Volume* (spaces in between chains, V_f) where V is the specific volume and V_i is the volume of the atoms/bonds. The greater the free volume the more likely the material is rubbery.
- *Chain Flexibility* – is a measure of the ability of a chain to rotate about the constituent chain bonds, hence a flexible polymer, comprising of flexible chains, has a low T_g, whereas a rigid polymer chain has a higher T_g. Flexible polymers have no bulky groups in the main chain, e.g. phenyl rings, and are attached by easily rotatable bond sequences such as $\{CH_2\text{-}CH_2\}$, $\{CH_2\text{-}O\text{-}CH_2\}$, or $\{Si(CH_3)\text{ -}O\}$.
- *Molecular structure (steric effects)* –
    1. Bulky side groups - groups restrict rotation about the backbone and increase T_g.
    2. Flexible side groups - by increasing the size of the side group the effect is accentuated as the free volume of the repeat unit increases therefore lowering the T_g (N.B if the side groups are short the T_g increases because stiffness increases).
    3. Polar side groups - polar side groups increase the T_g, compared to a non-polar group of similar size and the more polar the less flexible it becomes.
- *Molar Mass* –chain ends have significantly higher free volume then the main polymer chain. The lower a polymer's molar mass the more chain ends a polymer has, thus the greater the contribution to free volume, therefore the T_g is lowered. However, this is only measurable for lower molar mass polymers.
- *Crosslinking* - when crosslinking is introduced the density of the sample increases, the molecular motion decreases, free volume decreases and the T_g increases.

1.2.2.2.2 Crystalline and Semi-crystalline Polymers

In a perfectly crystalline polymer all the chains would have 3D order and no T_g, because of the absence of disordered chains. Above T_m^0 a crystalline polymer would become a viscous liquid[‡]. Semi-crystalline polymers contain varying degrees of order and disorder. Because of the different size of crystals present T_m is broad and lower than T_m^0. No fundamental property affects the physical properties of a polymer so profoundly as the degree of crystallinity[13, 14]. It can affect the storage modulus, permeability, density, brittleness, toughness and melting temperature.

[‡] T_m^0 is the melting point for a perfectly crystalline polymer of high molar mass.

Crystalline polymers show order at a variety of dimensional levels, from interatomic spacing to macroscopic measures[15]. The extent to which a polymer crystallises depends on the type of polymer and its skeletal structure and thermal/process history[16]. When crystallising from the melt, chain entanglements are extremely important and the crystals that are formed are more irregular than those obtained from dilute solution.

Imperfect polycrystalline aggregates are formed in association with a substantial amorphous content. This is a consequence of chain entanglement and high viscosity hindering the diffusion of the chains into ordered arrays. The basic characteristic feature is still lamella crystallite with amorphous regions. There are several types of lamellar crystallites that can be produced during melt crystallisation obtained from the different ways of packing lamellae.

- Crystallites – matrix of small crystalline regions with disordered interfacial areas. The size of the crystallites are small compared to the fully extended polymer chain, independent of the molar mass, and rarely exceed 1-100nm.
- Hedrites – crystalline polyhedral structures composed of lamellae joined together along a common plane, produced for polymers that have been allowed to crystallise from concentrated solutions.
- Spherulites - literally little spheres[16], are birefringent with circular symmetry. Each spherulite grows radially from a nucleus formed either from an impurity or from density fluctuations, which result in the initial chain ordering process. The structures are not single crystals and their sizes range from slightly larger than a crystallite to a few millimetres. They are the most common structure obtained from melt crystallised polymers. Spherulites are also believed to be associated, and due to the segregation of different molecular species in a sample. E.g. shorter molecules are likely to occupy inter-spherulitic boundaries leading to regions of differing mechanical properties resulting in fracture points[15].

In figure 1:5a the structure of a typical spherulite is sketched. From this picture it is seen that a single polymer chain can be partly crystalline and partly amorphous. The polymer chains can even originate in from one lamellar domain unit and end in another; these are called *tie molecules*-amorphous regions holding the crystals together.

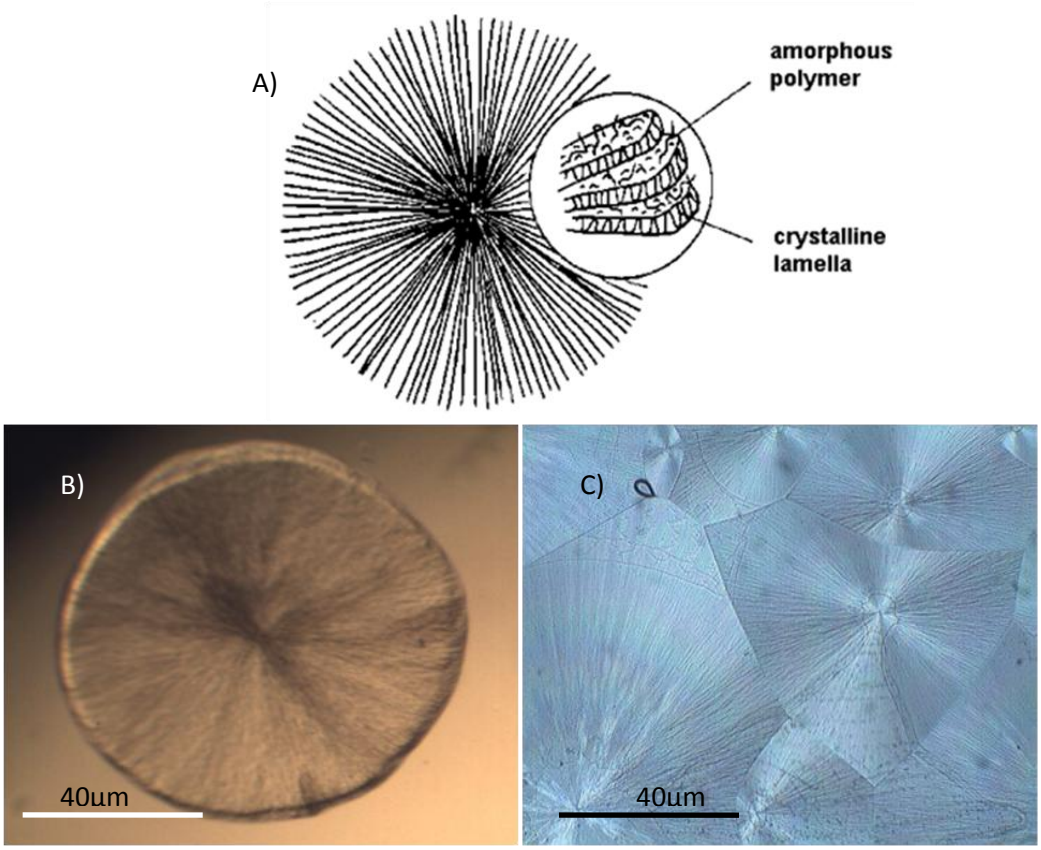

Figure 1:5 Illustration showing a) spherulite schematic after the University of Cambridge Department of Materials Science and Metallurgy[§], b) optical microscope image of single spherulite, c) spherulites impeding on each other[**]

1.2.2.2.3 Theory of Crystallisation

In the melt, polymers consist of randomly coiled and entangled chains, which have high entropy with respect to the crystalline state. Upon cooling to a temperature below T_m the polymer crystallises leading to a reduction in entropy.

Heterogeneous crystallisation occurs by nucleation and growth from impurities. A nucleus is created during slow cooling from the melt, stimulated by intermolecular forces, brought about by the ordering of chains in a parallel array. Secondary valence forces stabilise the long range order which aids the packing of molecules into 3D ordered structure[17-19]. This entropy penalty, from forming a regular structure, is offset by the large reduction in enthalpy that occurs during crystallisation. Once the crystals have reached a critical size, or the melt has been quenched rapidly, the crystals can spontaneously grow – homogenous crystallisation[15, 20, 21]. Two models have been proposed to describe the fine structure of the lamellae and their surface characteristics

[§] http://www.doitpoms.ac.uk/tlplib/polymers/spherulites.php
[**] Reproduced with permission of Neil Sim (image B) and Ben Knappet (image C), Durham University

in semi-crystalline polymers and the models differ mainly in the way the chains are thought to enter and leave the ordered lamellae regions.

- *Regular fold array*, figure 1:6, with adjacent re-entry of the chains. When there is a sharp phase boundary between the crystal and amorphous phase, the mode of re-entry is the adjacent neighbour. In this case a smooth surface is obtained, figure 1:6a. Where there is no sharp phase boundary between the crystal and amorphous phase, the mode of re-entry is still the adjacent neighbour but the variation in fold length is large. In this case a rough surface is obtained, figure 1:6b.

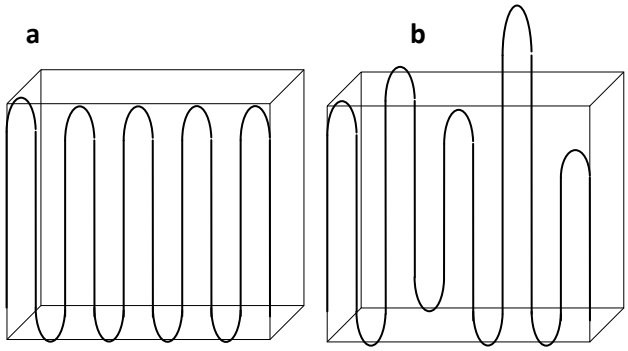

Figure 1:6 Sketch of the polymer chains alignment in the Regular Fold Array Model for a a) smooth surface and b) rough surface

- The *Switchboard model,* , figure 1.7 where there is some folding of the chains but re-entry is now random, is more likely to explain the formation of crystal from the melt.

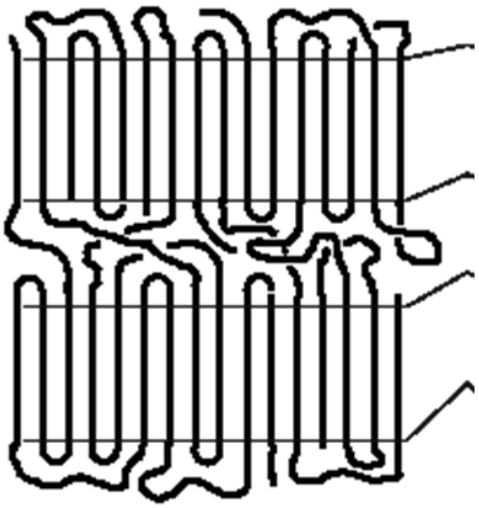

Figure 1:7 Sketch of the polymer chains linking semi-crystalline regions in the Switchboard Model

Thermodynamically, crystallisation will be favoured if the entropy penalty is outweighed by the enthalpy change. Crystallisation is an exothermic process whereas melting is endothermic as energy is required to disassociate molecules. T_m is usually higher than T_c due to the high viscosity of molten polymers. Crystallisation is therefore determined by kinetics as well as thermodynamics.

A polymer's structure largely affects its crystallinity. The more regular and ordered its structure, e.g. without branching and with defined tacticity, the easier it will pack into crystals. Intermolecular forces increase the amount of crystallinity in a sample[24]. The attractive forces between polymer chains play a large part in determining a polymer's crystallinity. Since polymer chains are so long, the interchain forces are amplified when compared to conventional molecules. Furthermore, long chains are subject to conformational and translational entropic effects which also have an impact on the polymer properties.

Some polymers, such as atactic polystyrene and poly(methylmethacrylate), are amorphous glasses in the solid state and never crystallise whereas syndiotactic polystyrene is semicrystalline. Even polymers, such as polyethylene, that do crystallise, are at most *semi-crystalline*, that is, some fraction of the polymer is inevitably amorphous chains and will not crystallise. The extent of crystallisation will depend upon the crystallisation cooling rate, solvent, thermal history, degree of branching and molar mass, and, in turn, will affect the melting temperature. As such there are several factors that affect crystallinity and increase T_m.

Variable	Increase T_m	Why?
Symmetry	Increase symmetry/linearity	Pack more efficiently thus increasing the number of crystallites conversely the many small crystals results in a low T_m.
Intermolecular Bonding	Increase number of polar groups/packing	Strong dipole-diople interactions and more van der Waals forces
Tacticity / Symmetry	Increase number of large rigid pendant groups	increase the rigidity, restricts rotation
Branching	Increase branching in the side groups	stiffen the chain
	Decrease branching of the main polymer chain	Increases packing efficiency, hence increases crystallinity
Molar mass	Decreases number of chain ends (increase M_w)	Chain ends are relatively free to move and the less of them the less energy required to stimulate chain motion and melting Chain ends can be thought of as impurities and they introduce defects into the polymer crystals and so lower the T_m
Stiffness	Excluding groups that allow rotation about the chemical bonds	Reduces flexibility

However, most of these variables are interconnected. For example, if the number of large rigid pendant groups is increased then the ability to pack closely is decreased; this counter effect can be overcome if the groups are arranged in a regular fashion along the chain.

1.2.2.3 Molar Mass Distribution

During polymerisation it is not possible to make polymer chains all the same length. Hence, there will always be a distribution of chain lengths. Two common ways of calculating the average molar mass are the number average molar mass, M_n, and the weight average molar mass, M_w.

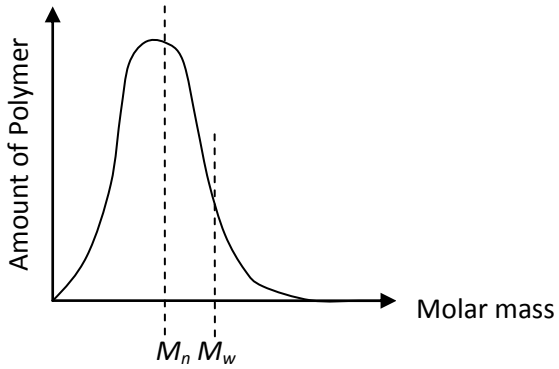

Figure 1:8 Bell curve showing the molar mass distribution in polymers

The number average molar mass of the polymer is only sensitive to the number of molecules present whereas, the weight average molar mass of the polymer is sensitive to both the number of molecules present and the size or weight of each polymer molecule. Equations 1:1 and 1:2 are used to calculate the number average molar mass and the weight average molar mass of the polymer,

Equation 1:1

Equation 1:2

where N_i is the number of polymer chains of i units and M_i is the molar mass of chains of i units and w_i is the weight fraction of i units of polymer. The width of the molecular weight distribution, sketched in figure 1:8, is often characterised by the polydispersity index (*PDI*). This is the "range" of molar mass in the polymer sample. The *PDI* can be calculated using equation 1:3 by dividing the weight average molar mass by the number average molar mass.

Equation 1:3

The weight average molar mass distribution is always greater than the number average molar mass because each chain contributes to the weight average molar mass in proportion to M^2, therefore larger heavier chains make a greater contribution, *PDI* is always greater than 1.

Finally, the degree of polymerisation (X) can be either weight averaged (X_w) or number averaged (X_n) and defined as the molar mass of the polymer divided by the molar mass of the repeat unit.

When calculating the weight averaged degree of polymerisation, equation 1:4, the weight average molar mass is divided by the molar mass of the repeat unit.

—— Equation 1:4

1.2.2.4 Polymer Tacticity

There are three configurations, isotactic, syndiotactic and atactic, figure 1:9. Polymer tacticity is important because stereochemistry can have an important effect on chain packing, and thus the degree of crystallinity and density. An isotactic polymer is a macromolecule comprising of essentially only one species of configurational base unit. A syndiotactic polymer is a macromolecule comprising of alternating configurational base units. Finally, an atactic polymer is a regular macromolecule but the configurations are random.

Isotactic	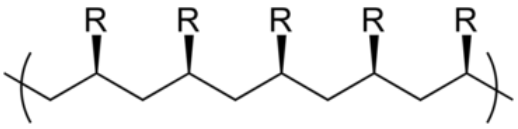
Syndiotatctic	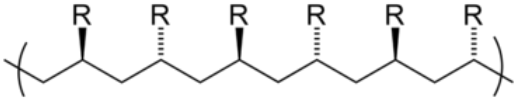
Atactic	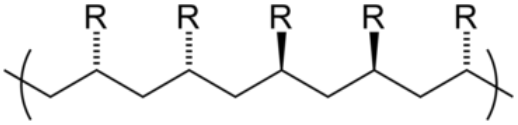

Figure 1:9 The three different types of polymer tacticity

1.2.3 Polymer Classification According to Synthetic Methodology

There are two families of synthetic mechanisms used to form polymers; step growth and chain growth polymeriations.

Polyfunctional monomers, monomers that have two different functional groups (for example – NH_2 or COOH groups), polymerise by step wise addition, resulting in for example, ester or amide links. No initiator is required but the reaction is often catalysed and the polymer chains grow by reaction between any two molecular species. The average molar mass increases as the reaction goes to higher conversion. The general characteristics are that:

- any two molecular species can react,
- the monomers are consumed very early in the reaction,

- the molar mass distribution of molecular species can be calculated at any time during the reaction

Step growth polymerisations are further sub-divided into polycondensation reactions and polyaddition reactions. If some of the atoms of the monomers are released as small molecules, such as water, then it is a polycondensation reaction and classified as a *condensation polymer* e.g. polyamides (Nylon) and polyesters. If the monomers react together without the elimination of other molecules e.g. *polyurethanes* it is classified as a polyaddition reaction.

The second type of polymerisation is a *chain growth polymerisation*. It involves the initiation and rapid growth of a polymer chains by adding monomers form an "active centre" at the end of the chain. During this type of polymerisation there is no by-product elimination. The stages of the polymerisation reaction are:

- initiation,
- propagation,
- termination

Most chain polymers are made from monomers containing a double bond between carbon atoms. Such monomers are called olefins and most commercial polymers are polyolefins.

Today there exist several specialised mechanisms to synthesise polymers, figure 1:10. Anionic polymerisation will be discussed in detail (section 1.3) as a method of synthesising model end functionalised polyethylene additives – the focus of this thesis.

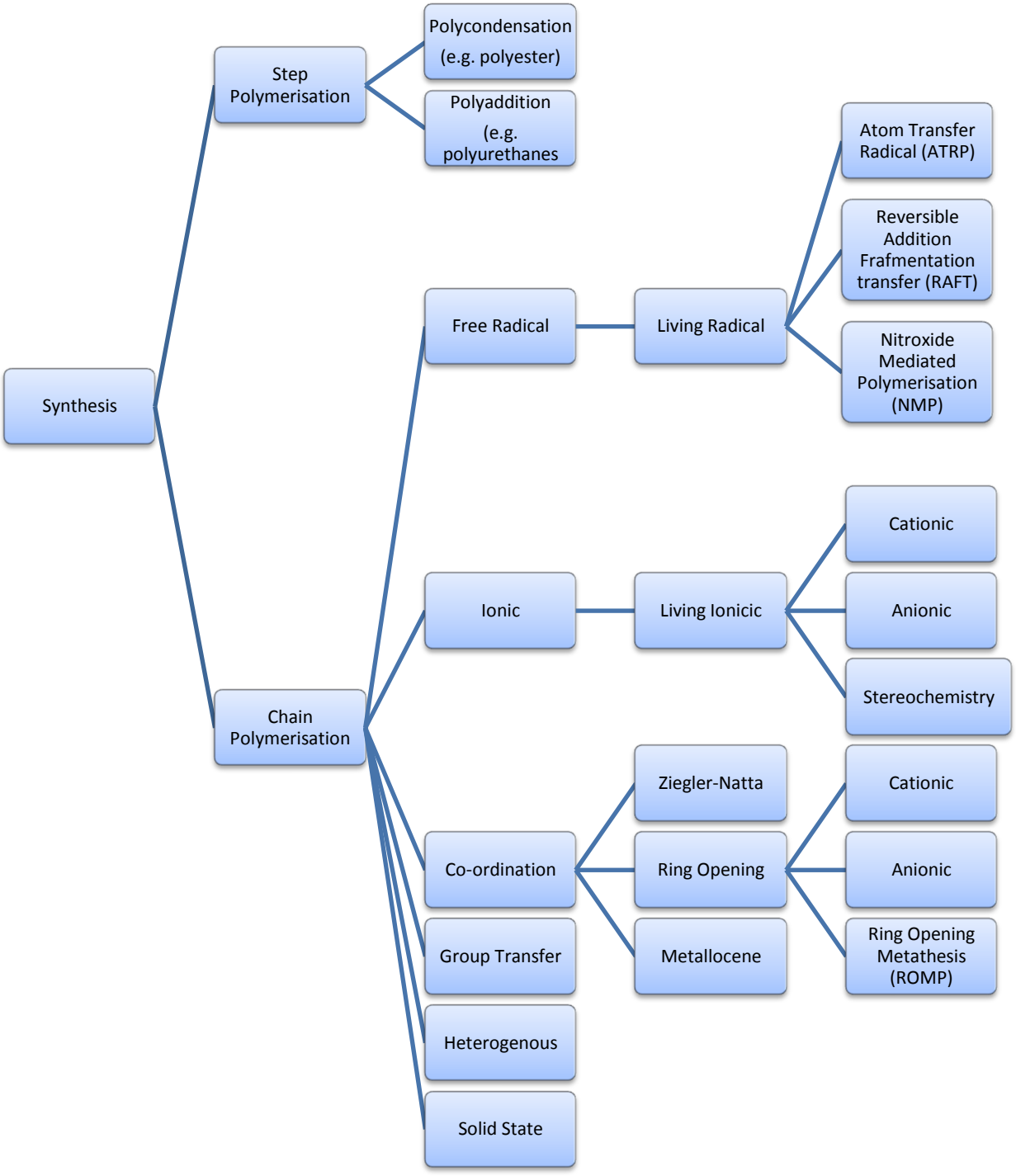

Figure 1:10 Classification of polymer synthesis mechanisms according to the monomers mode of addition

1.2.4 Polyolefin Synthesis

In the following section the synthesis of three polyolefins of relevance to the current work will be discussed. These are polybutadiene, polyethylene and polytetrafluoroethylene (PTFE).

1.2.4.1 Polybutadiene

In 1932 SV Lebedev in the USSR first polymerized 1,3-butadiene to give a rubbery material – polybutadiene (PB). Polybutadiene's very low glass transition temperature (typically < -90 ^{0}C)[25] makes it ideal for use in cold environments, e.g. as a component in car tyres, hoses etc, and as impact modifiers, in other polymers. Polybutadiene can be easily hydrogenated yielding saturated PB which crystallises in a similar manner to LLDPE making hydrogenated PB a useful model for polyethylene[26]. The synthesis of PB by anionic polymerisation is discussed in greater detail in chapter 3.

1.2.4.2 Polyethylene

Polyethylene is the world's highest tonnage plastic with an annual consumption[27] in excess of 70 billion kg. Polyethylene is a very versatile material with many applications, e.g. food-packaging, cable jackets, artificial hip joints and even bullet proof vests (UHDPE). Molecularly, it is the simplest of all commercial polymers, composing entirely of long chains of CH_2 groups. PE is a low melting and flexible polymer, composed of non polar segments. However, it is susceptible to branching during manufacture[13].

The first known sample of polyethylene was accidently prepared by a German chemist Hans von Pechmann in 1898 whilst heating diazomethane. Its production was not reported again until 1933 when two ICI chemists Eric Fawcett and Reginald Gibson synthesised it by applying extremely high pressure (several hundred atmospheres) to a mixture of ethylene and benzaldehyde. However, even though they realised the importance of their discovery they were unable to replicate the experiment. Unknown to them the reaction was only made possible by a trace of oxygen contamination in their apparatus which initiated the reaction. Two years later another ICI chemist, Michael Perrin, developed a reproducible high-pressure free radical synthesis for polyethylene that became the basis for industrial low density polyethylene (LDPE) and production began in 1939.

In 1953 a new process for synthesizing polymers was discovered that made the synthesis of now common plastics possible, including high-density polyethylene. By using this new process, scientists could make the double bonds in monomers join up in a more disciplined manner using a catalyst. When applied to ethylene monomers, polyethylene with the rigid linear chains known as high density polyethylene was synthesised. Karl Ziegler (1898–1973) and Giulio Natta (1903–1979) shared the Nobel Prize for Chemistry in 1963 for developing this process. The second method developed was a chromium trioxide based catalyst discovered in 1951 by Robert Banks and J. Paul Hogan at Phillips Petroleum and is known today as Phillips catalyst.

Today in industry, polyethylene, branched or otherwise, table 1:1, is generally made by free radical polymerisation or catalytic polymerisation. The catalyst could be a Ziegler-Natta, metallocene or Phillips type. Phillips catalyst is cheaper and easier to handle, but does require some pressure, 0.2-15 MPa.

Type	Industrial Name	Description	Mechanism	Structure
Low Density PE	LDPE	Highly branched polyethylene	Ziegler/Phillips or by free radical polymerisation	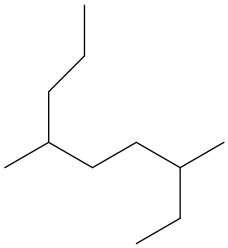
High Density PE	HDPE	No/very little branching present	chromium/silica catalysts, Ziegler-Natta catalysts or metallocene	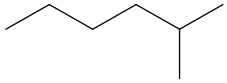
Ultra High Density PE	UHDPE	No branching	Ziegler catalysts polymerisation	
Ultra high molecular mass PE	UHMWPE	No branching, high M_w (very very strong fibres which have replaced Kevlar)	Ziegler catalysts polymerisation	
Linear Low Density PE	LLDPE	short branches	Copolymerisation	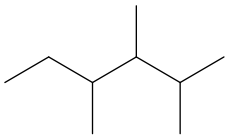

Table 1:1 Five types of polyethylene

The intramolecular chain transfer, through hydrogen abstraction, results in long alkyl side chains during free radical polymerisations.

Linear Low Density Polyethylene (LLDPE) is slowly taking over the polyethylene market. It does not require the same level of engineering as HDPE but owing to its reduced branching (or shorter branches) it has a higher density than LDPE. It is mainly used for film extrusion and packaging applications. It is also used for injection moulding and wire and cable extrusion. However, the difficulty of adhesion to its surface, owing to its low surface energy and therefore low wettability, is a major problem. A pre-treatment is required in order to create a surface with a satisfactory level of adhesion, for purposes such as printing, bonding, painting and coating. These two factors limit the use of PE in many applications. Over recent years surface fluorination has proved an

effective pre-treatment technique for increasing the barrier properties of PE[28]. The increase in adhesion, despite being a low surface energy surface could be due to the increased polarity of the surface.

1.2.4.3 Polytetrafluoroethylene

Roy Plunkett in 1938, working for DuPont, whilst experimenting on new chlorofluorocarbon refrigerants, observed that a chemical sample of tetrafluoroethylene gas had changed its properties into a white, waxy solid. This substance was polytetrafluoroethylene (PTFE) and was patented and is commonly known as Teflon™ today[29].

Teflon is an inert thermoplastic polymer and has a low coefficient of friction which is important for applications where low adhesion features are important. For example, it has revolutionized the cookware industry, and is widely used in other areas including aerospace, communications, electronics and in industrial processes where it acts as a lubricant. Interestingly PTFE's weak van der Waals forces means that it is the only known surface to which a gecko cannot stick[30].

1.3 Synthesis of End-Functionalised Polymers

It is the objective of this work to study the effect of the addition of end functionalised polymer additives on the surface properties of semi crystalline polymers and we have chosen to study polyethylene as a commercially important semi crystalline polymer.

When synthesising an end-functionalised polymers, a low *PDI*, a controlled molar mass and a high degree of end-capping are important aspirations. There are generally three techniques employed to synthesise end-capped polymers with controlled structures; namely anionic polymerisation, atom transfer radical polymerisation (ATRP) and reversible addition fragmentation transfer polymerisation (RAFT); the latter two are controlled radical polymerisation mechanisms.

Each technique has its advantages and disadvantages. Anionic polymerisation can achieve the lowest *PDI* ~ 1-1.1, where as ATRP and RAFT give slightly higher *PDI*s - typically~1.1-1.5. The molar mass can be controlled for all three techniques, however, for ATRP and RAFT, control is lost at higher molar masses because of the nature of the radical mechanism. Finally a high degree of end-capping is achievable with each technique.

Anionic polymerisation is very sensitive to different functionalities because of the reactive nature of the active anion. Therefore the solvent and the initiator used and the monomer need to be carefully considered. In this situation ATRP and RAFT are more versatile owing to the wider range of functionalities that the active chain can be exposed to. (But living radical polymerisations are

sensitive to species which destroy radicals, e.g. oxygen). Finally, anionic polymerisation is a very challenging laborious technique to use and specialist equipment needs to be commissioned.

One of the major disadvantages of the controlled polymerisations is that none of them can directly polymerise ethylene. Although the uncontrolled polymerisations (radical, metallocene and Ziegler Natta) can synthesise polyethylene they do not allow the preparation of polymer additives which are well defined in terms of molecular weight and polydispersity and (more importantly) allow close to quantitative end functionalisation with the desired functional groups.

1.3.1 Living Radical Polymerisation

Living/controlled radical polymerisation is not living in the true sense, in contrast to anionic polymerisation, as termination does occur. The rate of termination, which occurs by either recombination or disproportionation, is suppressed by the establishment of an equilibrium that exists between dormant and active radical species. Considering the kinetics of living radical polymerisation the rate of propagation, k_p, is proportional to the concentration of monomers and the concentration of active chain ends, P_n*, whereas, the rate of termination if proportional to the concentration of active chain ends squared.

Equation 1:5

Equation 1:6

Due to the difference in rate order, the decreasing concentration of active chain ends, , has a bigger impact on k_t than k_p. The equilibrium stage reduces the concentration of active chain ends, so k_t reduces and $k_p > k_t$, therefore at any one time the majority of chains are dormant, so cannot terminate. However, as k_t is only suppressed (rather than eliminated) synthesising higher molar mass polymers is increasingly challenging because during the reaction , and [monomer] decreases as the reaction continues, whereas , and is constant, so gradually k_p decreases towards the value of k_t ( ).

1.3.1.1 Introduction to Atom Transfer Radical Polymerisation (ATRP)

During ATRP polymerisations there are two methods that can be used to produce end-functionalised polymers. These are the use of functionalised initiators (RBr), or by the nucleophillic substitution of the terminal halogen atom. The main advantage of using functional initiators is that no post-polymerization modification is required as direct functionalisation is achieved from the start, figure 1:11, leading to 100% end functionalised polymers, as a functionalised initiator is used. This is the huge advantage of ATRP.

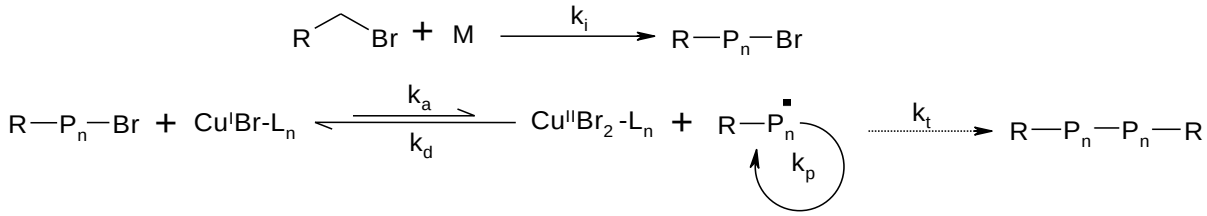

Figure 1:11 General mechanism of ATRP polymerisation

Figure 1:11 illustrates the general mechanism for ATRP. M is the monomer, P_n is the polymer chain, k_i, k_a, k_d, k_p and k_t are the rates of initiation, activation, deactivation, propagation and termination, and L_n is a ligand which aids in dissolving the copper catalyst. The catalyst used is generally, but not limited to, copper halides. Other examples include ruthenium and iron. ATRP utilises a redox equilibrium reaction where the equilibrium reduces the concentration of the reactive radicals, therefore, reducing the rate of termination and allowing the molar mass to be controlled. The functionalities, R groups, that can be easily introduced are OH, N_3, C≡C, C=C, trichlorosilyl and thiol groups, to name a few.

One specific problem associated with ATRP is that it is catalysed by Cu(I). Therefore polymers need to be stripped of any residual copper before it can be commercialised as copper is extremely toxic. This adds extra time and waste chemicals, however recent advances by K. Matyjaszewski et al. from Carnegie Mellon University have, in some cases, reduced the level of copper down to less than 1 part per million after purification[31].

1.3.1.2 Introduction to Reversible Addition Fragmentation Transfer Polymerisation (RAFT)

The advantages of RAFT polymerisation are that it is a very versatile technique, can use a wide range of solvents, temperatures and monomers. During RAFT polymerisation a RAFT agent[32, 33] is required, figure 1:12.

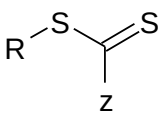

Figure 1:12 General illustration of a RAFT agent

Although the RAFT agent needs to be tailored for each monomer, it is versatile in that it allows end-functionalities to be introduced in three different ways after initiation of the polymerisation, figure 1:13. Firstly, a α-functionality can be introduced on the polymer from the R groups of the

chain transfer agent. The R group is the only group guaranteed to be on the end of every polymer chain. Therefore, the S-R bond should be labile, and R a good leaving group and good re-initiator (see figure 1: 14 and 1:15). However, the R group should also be able to make strong bonds with the monomer, when initiating, to ensure that it remains on every chain. Secondly a ω-functionality can be introduced via the Z group. The role of Z is very important also; as it controls the fragmentation addition step, see figure 1:14, by stabilising the radical, which it does by either resonance or by electron withdrawal. Finally, an ω-functionality can also be introduced via the modification of the thiocarbonylthio group post-polymerisation. In an ideal RAFT polymerisation there is a thiocarbonylthio group that is at the end of the polymer but during the reaction some chains may lose the thiocarbonylthio end group, thus also the Z functionality. Disadvantages include the colour, usually pink or yellow and the smell during the reaction.

RAFT polymerisation is characterised by four steps: initiation; addition fragmentation; re-initiation and equilibration. The polymerisation is started by radical initiators, e.g. AIBN, where upon reaction with a monomer, a radical species is generated which starts the polymer chain.

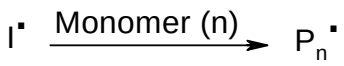

Figure 1:13 First step during RAFT polymerisation – Initiation to produce radical species

The active chains, $P^{\bullet}_{n}$, that are not functionalised, react with the RAFT agent resulting in the R group leaving. The radical R group is then used to initiate further chains, figure 1:14, during addition fragmentation.

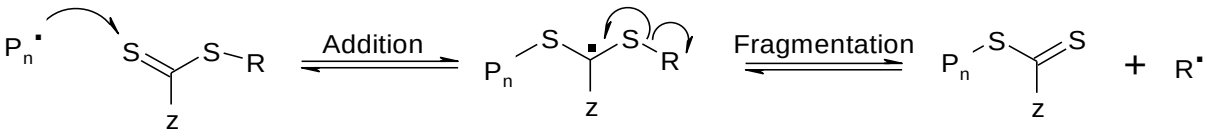

Figure 1:14 Second step during RAFT polymerisation - Addition Fragmentation Step producing a radical R species and a thiol terminated polymer

The next step is re-initiation. During this step the leaving groups' radicals react with another monomer species, initiating the growth of another active chain. All P_m chains are functionalised.

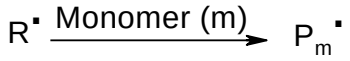

Figure 1:15 Third step during RAFT polymerisation - Re-initiation step producing functionalised radical active polymer chains

This then undergoes another addition fragmentation.

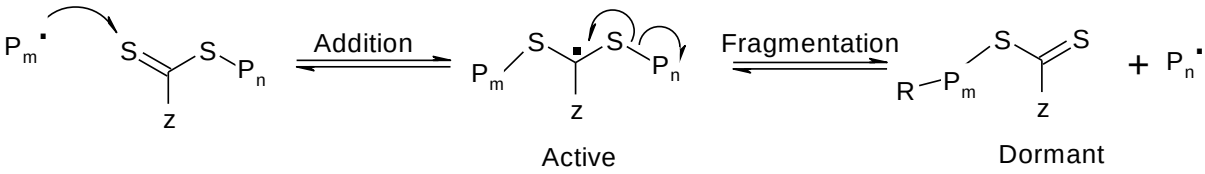

Figure 1:16 Subsequent addition fragmentation during RAFT polymerisation

The final step is equilibration, figure 1:17. During this stage equilibrium exists between the active and dormant polymer chains, limiting termination steps such as radical combination and disproportionation increasing the polymer length.

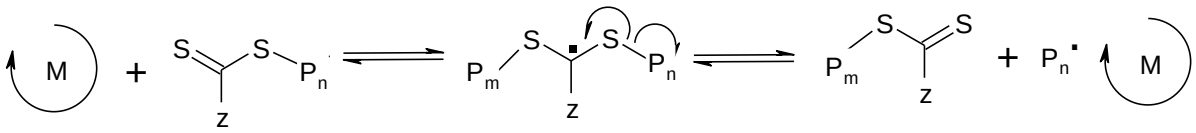

Figure 1:17 Fourth and final step during RAFT polymerisation - Equilibration producing longer polymer chains

Via the R and Z groups carboxyl and hydroxyl end-functionalised polymers can be produced. For example RAFT can also be used in conjunction with other polymerisation techniques e.g. ATRP and ROMP, opening up the possibility to synthesis complex molecular architectures[34].

1.3.2 Living Anionic Polymerisation

Through the use of living anionic polymerisation, a variety of end-functionalized polymers can be quantitatively synthesised whilst maintaining a narrow polydispersity index and a predictable degree of polymerization. The term living anionic polymerization was first coined in 1956 by Swzarc and was defined as when “growing polymers retain indefinitely their propensity of growth and their propagation proceeds with exclusion of termination and chain transfer” [11,13,16]. However,

all living polymers will lose their activity eventually through decomposition or reaction with external contaminants. Criteria used to define a living polymerisation are[93];

- propagation continues until all monomer is consumed and the addition of more monomer results in further chain growth,
- the number average molecular weight, M_n, is a linear function of conversion,
- the number of polymer molecules (and active centres) is constant, and independent of conversion,
- the molecular weight can be controlled by the stoichiometry of the reaction,
- the resulting polymers have a narrow polydispersity index[94],
- block copolymers can be prepared by sequential addition of monomer,
- chain-end functionalized polymers can be prepared in quantitative yield,
- have a linear kinetic plot of k_p versus time: $\ln([M_o]/[M]) = k_{obs}t$ where $[M_0]$ is the initial monomer concentration and $[M]$ is the monomer concentration at some time during the polymerisation.

Like all chain growth polymerisation mechanisms, anionic polymerisation comprises of three stages, initiation, propagation and termination. However in a living anionic polymerisation, termination should not occur on a timescale comparable to propagation.

1.3.2.1 Initiation

Anionic polymerizations are chain growth polymerizations that are initiated by anions form materials such as sodium naphthalene, metal amides or in most cases alkyl lithium reagents. This is due to their solubility in non-polar hydrocarbons. When using an organometallic initiator it is assumed that the metal is strongly electropositive relative to the carbon atom at the tip of the growing chain, hence, the metal becomes a cation. The first reported use of lithium in polymerisation reactions with dienes was by Ziegler and co-workers in 1934[35-37]. Later, Swzarc et al[38] showed that sodium naphthalene initiated anionic polymerizations by electron transfer processes. However, when other organometallic initiators were used, initiation results from direct anionic attack leading to a monofunctional propagating chain, rather than a difunctional as with electron transfer. Szwarc observed that during the polymerization of butadiene the viscosity of the polymer solution increased linearly with the theoretical calculated molecular weight, which confirmed the termination-free nature of the propagation[39].

The initiator and the propagating anion can exist in different forms. For example as contact ion-pairs, solvent separated ion-pairs and free ions (in a polar solvent). All these forms have differing

inter ionic distances, extent of solvation and intermolecular association[40]. The extent of the association is dependent upon the size of the alkyllithium and the polarity if the solvent.

1.3.2.2 Propagation

Ideally the propagation rate should be proportional to the number of growing chains and for free ions it is independent of the counter-ion and solvent used[41]. If initiation is faster than the rate of propagation, R_p, is dependent on the monomer concentration, [*M*], and the concentration of active chain ends, $[P_n^*]$, proportional to the rate constant of propagation, k_p. In polar solvents R_p is calculated using equation 1:7.

Equation 1:7

Introducing the monomer conversion, x_p, into the integrated form of equation 1:7, the rate of propagation becomes where t is the polymerisation time:

Equation 1:8

Equation 1:9

In non-polar solvents, equation 1:10, only the free chains are involved in propagation,

Equation 1:10

so R_p is reduced as the concentration of active chain end is dependent of the degree of aggregation, *x*, which is different for different monomers e.g. for polystyrene in benzene *x*=2, whereas, for polybutadiene in benzene *x*=6.

The absence of termination is one of the requirements for living polymerisations. If termination is absent then $[P_n^*]$ is constant and $k_p[P_n^*]=k_{apps}$ (apps = apparent) which can be regarded as a first order rate constant. This was proved by Szwarc *et al*[42]. The plot of the first order time relation, figure 1:18, indicates by the linearity that $[P_n^*]$ remains constant throughout the polymerisation and when termination occurs $[P_n^*]$ depletes and the slope decreases.

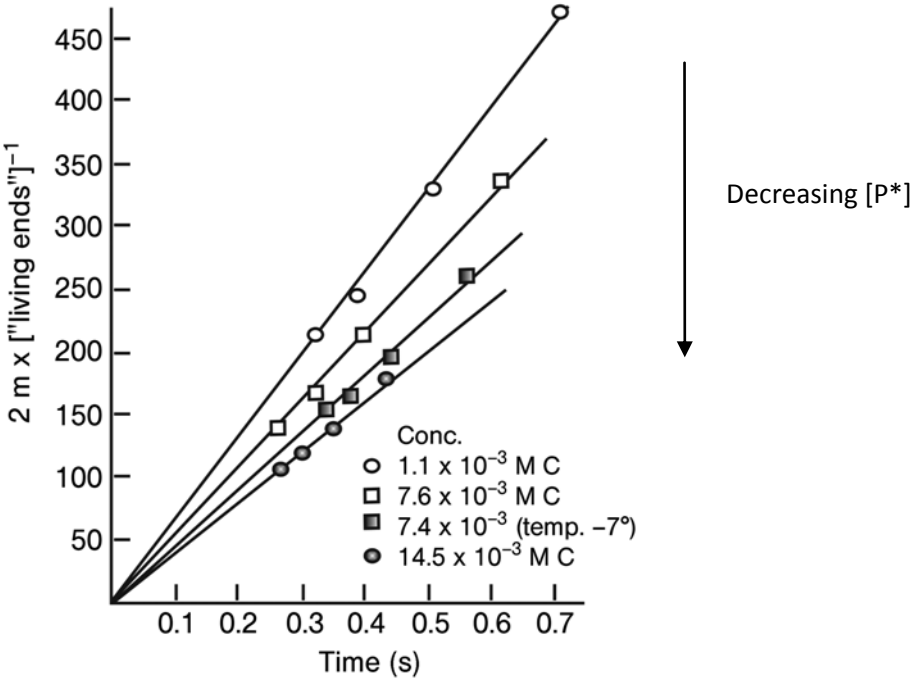

Figure 1:18 Rate of polymerisation of polystyrene in THF at 25°C after Geacintov *et al*[42]

Another requirement for living anionic polymerisations is the absence of transfer. The evidence for this was provided by *Schulz et* al[43] by plotting the number average degree of polymerisation *versus* conversion. The number average degree of polymerisation is given by a slight modification of equation 1:4, owing to the living nature of the polymerisation,

Equation 1:11

where the [*P*] is the total concentration of chains, active or inactive, that are generated in the transfer process.

In an ideal polymerisation [*P*]= [P_n*]=*f*[*I*]$_0$ where [*I*]$_0$ is the initial concentration of initiator and f is the initiator efficiency. This should lead to a linear dependence of *X* on conversion[39].

The absence of termination and transfer leads to a linear growth of polymer chains with respect to the monomer consumption. The result of this is a narrow distribution of chain lengths, which theoretically can be expressed as, but is rarely satisfied:

Equation 1:12

Although it is now known that that the rate determining step in an anionic polymerization is initiation, the rate of propagation is still important. This is due to the fact that narrow PDI is only obtained if the rate of initiation is much faster than that of propagation. Ideally the propagation rate should be proportional to the number of growing chains and for free ions it is independent of the counter-ion and solvent used[41]. Since chain ends in anionic polymerizations can exist in various states, e.g., covalent species, aggregates, various types of ion pairs or free anions, propagation can occur at different rates. If the rate of exchange between these species is slow compared to the rate of propagation, it can lead to a significant broadening of the *PDI*. This can occur when the counter-ions and the carbanionic active centres are in close proximity, where the propagation rate is suppressed compared to if the carbanionic active centres were free. By increasing the reactivity of the ion pair, the rate constant for ion pair propagation increases. Thus the rate of propagation can be influenced by the type of solvent, increasing or decreasing the degree of solvation, the size of the initiator used, the carbanion structure, and the temperature of the reaction.

1.3.2.2.1 Effect of Solvents on the Rate of Propagation

Aggregation, solvation and ion-pair dissociation of anionic chain ends primarily dictates the rate of anionic polymerization in polar and non polar solvents. In anionic polymerisation the propagating species is a carbanionic active centre and associated with it is a counter-ion. The anion present in solution may be either tightly associated with the counter-ion or loosely associated with a solvated counter-ion.

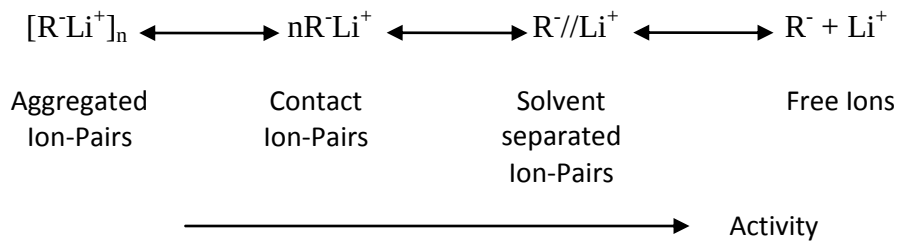

Figure 1:19 Fuoss-Winstein[44] spectrum of anion-pairs as solvent polarity increases

The stabilisation of electronic charges through intermolecular association leads to the formation of aggregates in non-polar solvents and different forms of ion pairs in polar solvents. The coexistence of different forms of ion pairs depends on the experimental conditions e.g. type of monomer/chain end, solvent polarity, chain end concentration and temperature. Therefore, the rate of addition of the monomer to the initiator and the propagating anion is strongly dependent on the reaction conditions.

1.3.2.2.2 Effect of Counter-ion on the Rate of Propagation

Initiators for anionic polymerisations of vinyl monomers can be broadly divided into three categories (i) radical anions, (ii) carbanions, and (iii) oxyanions. In the present work only carbanions, specifically alkyl metals will be considered.

The effect that the counter-ion has on the rate of propagation is twofold. Firstly, the interaction between the counter-ion and the carbanion decreases with increasing size of the cations. When solvation is absent or weak, e.g. benzene, the rate constant for propagation increases as the size of the counter-ion increases due to the separation of the ions, i.e. $K^+ > Na^+ > Li^+$. However, in polar solvents the opposite trend is observed because the smaller counter-ions are more strongly solvated. The second factor is the solvation of the cation where the interaction of the solvent with the cation decreases with increasing size of the cation.

1.3.2.2.3 Effect of Temperature on the Rate of Propagation

Various factors influence the rate of propagation with temperature, and the overall temperature dependence is determined by the balance of these factors. For polymerisation to proceed the Gibbs free energy of polymerisation, ΔG should be negative, so increasing temperature above a certain ceiling temperature makes ΔG positive and unfavourable. In certain situations if the temperature is high enough that ΔG is positive the reverse reaction occurs and the monomer can be produced in 100% conversion. More precisely, in non-polar solvents, free ions and solvent-separated ion-pairs are not present and instead the contact ion-pairs are aggregated. In this situation the R_p increases as the temperature increases. In polar solvents reducing the temperature increases R_p, because the formation of free ions and solvent-separated ion-pairs is exothermic, and solvents have higher dielectric constants at lower temperatures.

1.3.2.3 Termination

Anionic polymerisation is a truly living mechanism and in many cases there are no intrinsic termination reactions. Usually the active chain ends are terminated by proton donors, usually alcohols, added at the end of the polymerisation, where the metal salt is the by-product. Controlled deactivation can also be achieved and terminal functional groups introduced, for example, by utilising reactions analogous to Grignard reactions, carboxylic acid and hydroxyl end groups can be introduced.

However, in some cases unwanted termination reactions can occur and special care needs to be taken. For example, when using lithium initiators, reaction can occur between either the initiator and/or propagating species and ether solvents such as THF. The rate of the first order termination of chain ends by ethers decreases for organometallic compounds in the order of Li > Na > K and the rate of decomposition of organometallic compounds in ethers depends on the structure of

the organometallic compound, the structure of the ether and the temperature. THF is the most reactive of all commonly used ethers towards organolithium compounds and figure 1:20, illustrates the decomposition of *sec*-BuLi in THF. This type of decomposition is a cyclo-elimination degradation cleavage reaction which occurs when T>10 °C.

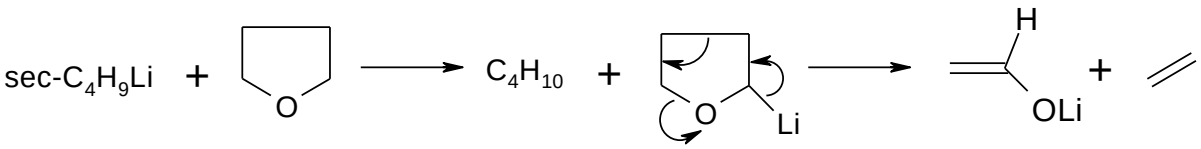

Figure 1:20 Mechanism of decomposition of *sec*-BuLi in THF

1.3.2.3.1 Termination by Impurities

Termination by impurities is the principal challenge when attempting to carry out living anionic polymerisation and as such every effort must be made to exclude impurities from the polymerisation. The living carbanions are very reactive towards a wide variety of functionalities and environmental impurities. Such impurities may be present in the monomer or solvent and both must be purified rigorously prior to their use. Environmental impurities such as water, oxygen and carbon dioxide must also be excluded. The impact of impurities upon the resulting polymer can vary dramatically depending upon the rate of reaction with the carbanion and the reaction mechanism.

If the impurities are fast reacting, e.g. H_2O, then the initiator or propagating species is deactivated very quickly. If there are insufficient impurities to deactivate all the polymer chains, the residual active chains will have an increased molecular weight but there will be little effect on the PDI. If the impurities are slow reacting, the initiation, $k_i >> k_p$, will have already finished and therefore the impurities will continue to react with the growing chains. From a SEC trace this will be obvious as the molecular weight will be shifted to higher molecular weights and there will be a long tail in the lower molecular weight region, increasing the *PDI*.

Chain coupling reactions can also occur as a result of the presence impurities. When oxygen and carbon dioxide are introduced coupling can occur. Figure 1:21 illustrates the complex mixture of products that are produced when oxygen diffuses into an unstirred solution of lithium initiated polymer at room temperature[45].

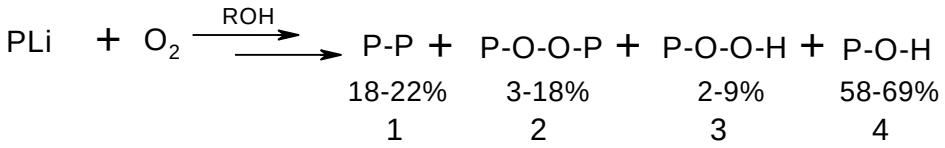

Figure 1:21 Products obtained due to polymer termination by oxygen

The presence of carbon dioxide can also lead to chain coupling. Carbon dioxide is often added to a polyalkyllithium species to functionalise the chain end by carbonation, resulting in the formation of a carboxylic acid end group. This reaction is not always quantitative and two side products may be obtained. If CO_2 is present at low concentrations, as an impurity, three products may be obtained; the carboxylated polymer, a ketone and an alcohol see figure 1:22. The formation of products 2 and 3 are favoured relative to 1 because of the aggregation of the chain ends in hydrocarbon solution.

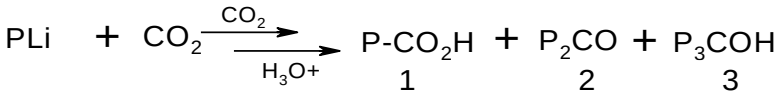

Figure 1:22 Products obtained on addition of CO_2 to a living polymer

To minimise the presence of impurities, anionic polymerisation is usually carried out under high vacuum conditions or under an inert atmosphere.

Coupling reactions that can also occur during diene polymerisations are lithium halogen exchange, intermolecular elimination of LiH and Wurtz coupling, and are discussed in more detail in section 1.4.

1.3.2.4 Anionic polymerisation of dienes

Butadiene is a conjugated 1,3-diene and acts as an electrophile during anionic polymerisations, where one of the C=C bonds reacts with nucleophillic carbanions. There are three basic modes for addition in a growing polymer chain of butadiene (1,2-addition, *cis*-1,4-addition and *trans*-1,4-addition) and if one of the hydrogens is replaced with an alkyl group, e.g. isoprene, then there is a fourth (3,4-addition), figure 1:23.

a)

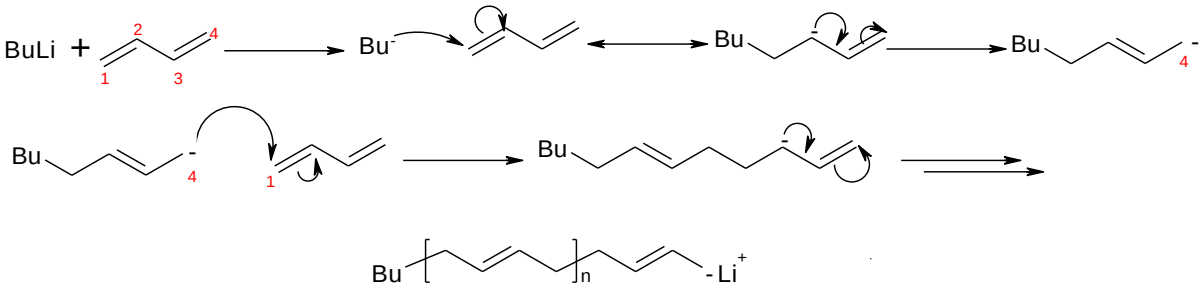

b)

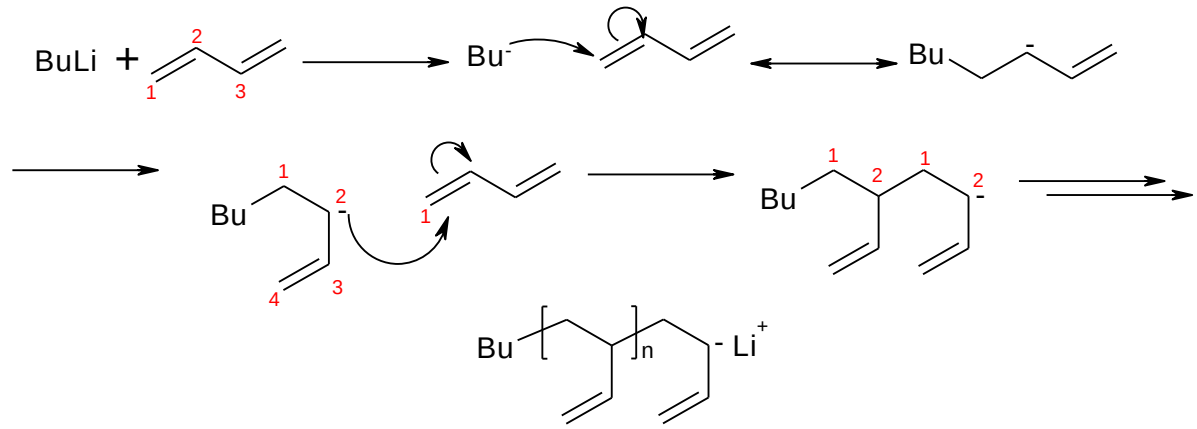

c)

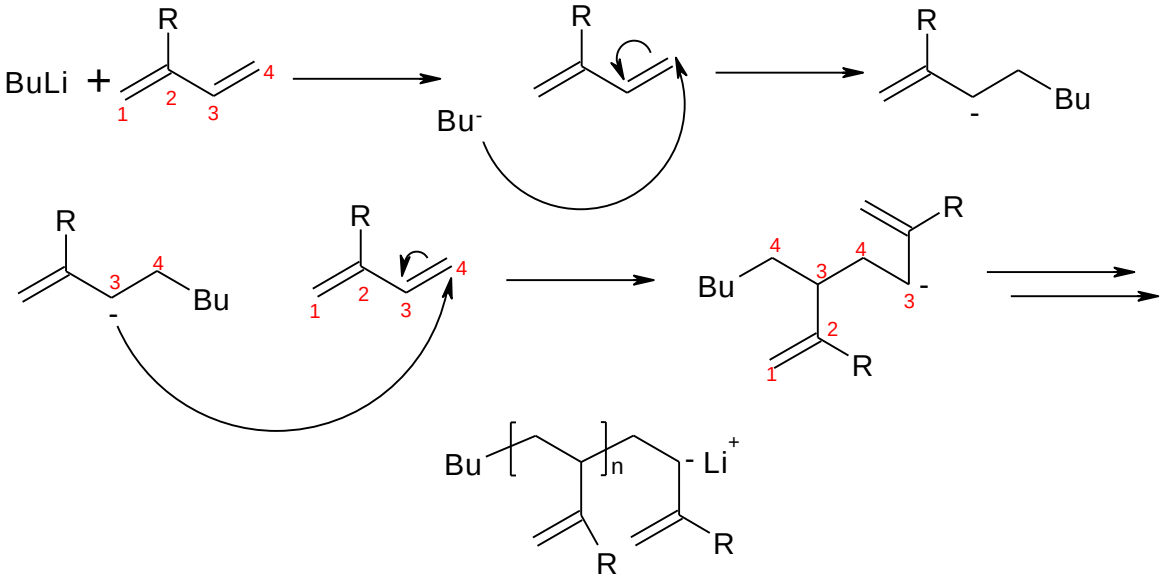

Figure 1:23 Mechanisms representing the microstructure formation of a) 1,4 addition, b) 1,2 addition and c) 3,4 addition for a diene monomer

The stereochemistry (microstructure) of anionic diene polymerisation depends on the counterion, the solvent, the chain end concentration, the temperature and the presence of Lewis bases additives.

The proportion of 1,4 addition decreases for increasing electropositive character of the alkali metal[46] and increasing polarity of the solvent where 1,2 addition dominates[46, 47, 48, 49]. This is because secondary carbanions are more stable than primary[46, 50], table 1:2.

Polymerisation conditions		**Microstructure (mole fractions)**		
Solvent	Counter Ion	*Cis*-1,4	*Trans*-1,4	1,2
Hexane	Li^+	0.68	0.28	0.04
Diethyl ether	Li^+	0.08	0.17	0.75

Table 1:2 The effect on microstructure when using a lithium counter-ion in different solvents during an Anionic Polymerisation of Butadiene

Decreasing the temperature generally leads to an increase in 1,4 addition because the σ-bonded chain end is preferentially stabilised. Finally, the concentration of initiator can affect the microstructure. Increasing the concentration of chain ends results in a higher proportion of 1,2 addition. A very clear example of this is highlighted in table 3:1 in section 3.1.

1.3.2.5 Synthesis of End-Functionalised Polymers

To achieve a high degree of end functionalisation a highly sophisticated approach, specific to each monomer, is required[51, 52]. The most widely used approach is anionic polymerisation[53, 54] as it proceeds without chain termination or chain transfer reactions[55]. End-functionalised polymers produced by anionic polymerisation are generally made in one of two ways[55-57]. The first approach utilizes functionalised initiators, which can initiate the polymerisation of specific monomers[32, 33]. The use of functional initiators ensures complete functionalisation, and should have low Lewis base character and be soluble in hydrocarbon solvents in order to maintain a low vinyl content in the specific case of diene polymerisations. However, this approach often encounters solubility problems, is limited by the type of monomers that can be polymerised in a living manner and control over the functionalisation reaction is sometimes lost. The biggest limitation is incorporating functionality onto the initiator without affecting the polymerisation. The second approach requires the addition of specific electrophilies to functionally terminate living polymerisations[52]. The more reactive the electrophile, the more efficient, and quantitative the terminating reaction. For example, chlorosilanes are more reactive than alkyl halides, due to their highly polarised silicon-chloride bond hence are more efficient terminating agents. Care should be taken in the choice of the suitable terminating agent, since this reaction can be subject to several side reactions, leading to incomplete functionalisation. For example, end-capping halides with a lower alkyl halide bond polarity results in the increased likelihood of unwanted side reactions, e.g. Wurtz-coupling. For alkyl halides the likelihood of unwanted reactions follows the order RI > RBr > RCl[51,58,59]. Examples of end functionalisation by anionic polymerisation include end-

functionalisation of polystyrl and polybutadienyllithium by chloroalkyl derivates to yield oxygen bearing end-groups[59] and amino end-groups[58, 60].

1.4 Surface Modification

A wide spectrum of surface modification techniques are available, which can be classified into four groups: (i) physical deposition/adsorption, e.g. blending, (ii) chemical modification e.g. radiation (UV, X-ray and gamma), laser, electron and ion beam treatment, (iii) plasma and flame techniques and (iv) grafting. A consequence of surface modification is that often functionalised surfaces have a finite lifetime and may revert to a more thermodynamically stable state given sufficient time[61-63].

1.4.1 Surface Properties

Through modifying a surface chemical functionality a surface will have different surface energy. Blended polymers will spontaneously minimise their surface energy by favouring an excess of the lower surface energy component. A hydrophobic surface has a low surface free energy. A completely fluorinated surface has the lowest overall surface energy where the surface energy decreases in the order $-CH_2>-CH_3>-CF_2>-CF_2H>-CF_3$[64].

1.4.2 Phase and Surface Separation

Incompatible polymer blends will usually phase separate. Where one of the blended components has a much lower energy, surface segregation will be enhanced by the incompatibility since this process reduces the contact between dissimilar polymers.

1.4.2.1 Theory of Phase Separation

There are two mechanisms for phase separation. The first is by nucleation and growth. This occurs for a system that is metastable, a stable intermediate stage of a system the energy of which may be lost in discrete amounts, where a droplet's growth proceeds by diffusion and reaches equilibrium. Further growth results by coalescence or by Ostwald Ripening. Mixtures of this type must overcome a free energy barrier in order to form stable phase separated nuclei[65]. The second is a mixture where spontaneous de-mixing occurs by spinodal decomposition[65]. A great variety of microphases may be obtained during phase separation of either diblock copolymers or a mixture of two distinct polymers which can be varied by the molecular architecture, the composition and the molar mass[66, 67].

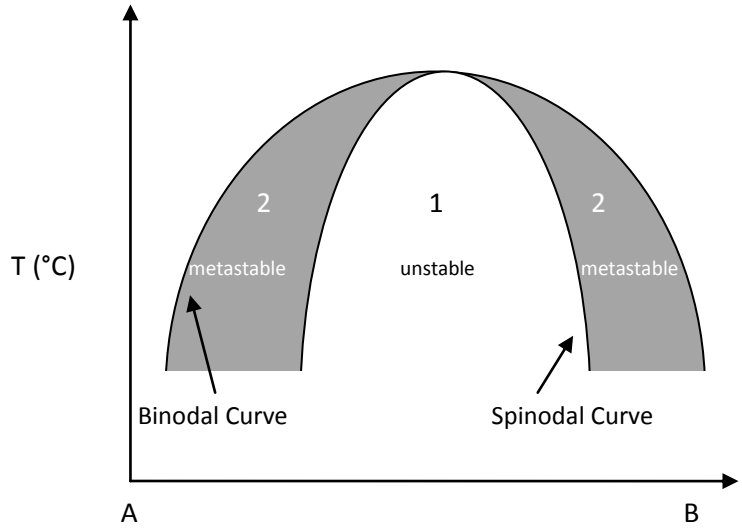

Figure 1:24 Phase Diagram for Binodal/Spinodal Decomposition where area 1 is unstable and area 2 is metastable

1.4.2.2 Theory of Surface Segregation

To reduce the surface free energy the lower surface component of the blend must first diffuse from the bulk to the surface, adsorb and reorientate themselves at the interface[68]. The quantity of adsorbed polymer is calculated using the surface excess concentration, *z**. The surface excess concentration is defined as the difference between the surface volume fraction, *φ(x)*, and the bulk volume fraction, φ_b and can be expressed mathematically by:

Equation 1:13

where *x* is the depth normal to the surafce[69, 70].

The driving force of phase separation is the incompatibility existing between the different polymer blocks and phase separation decreases the enthalpy of the system[71]. The major contributing factors for surface segregation are based on surface energies, entropy of the polymer chains, and various specific segmental interactions. This behaviour is generally dominated by adsorption of the lower surface energy component. The entropic loss of placing polymers at a surface increases with molar mass. Therefore segregation of smaller polymers is favoured if the surface energy difference is small. In single phase blends, segregation is ultimately limited by the ability of end-functional polymers to be added to a dense brush layer where chain stretching is required but is entropically unfavourable.

The Gibbs-Duhem adsorption isotherm[62] classically represents the differences between the chemical potential of the polymers in a polymer blend:

Equation 1:14

where is the surface tension, z^* the surface excess and μ is the chemical potential of components 1 and 2.

The required change in chemical potential associated with functional group segregations is related to the bulk interaction parameter χ between the functional groups and the chain backbone. Bulk interactions increase the degree of surface segregation but do not alter the qualitative nature of segregation. The surface interaction parameter, χ_s, relates the differences in adsorption energies of the functional group and repeat unit segment,

Equation 1:15

where is the change in energy associated with moving a segment of type *i* from the bulk to the surface. The surface area per lattice site, *A*, is given by , where v_{ref} is a reference volume.

When , that is the end group has a lower surface energy that that of the repeat unit on the polymer backbone then $\chi_s<0$ and the additive adsorbs preferentially at the surface[72]. The magnitude of enrichment increases as χ_s becomes more negative. Surface segregation is favourable for functional groups that have low forces of interaction, that is, only London dispersive interactions[73]. These types of surfaces are often termed "release surfaces" due to their low adhesion properties.

When , that is the functional group has a higher surface energy that that of the polymer backbone then $\chi_s>0$ and the additive is depleted from the surface[72]. The magnitude of depletion increases as χ_s becomes more positive. Functional groups must have high interaction potentials (or are reactive in nature). Often these surfaces are unstable and susceptible to reorganisation[73]. These types of surfaces are often termed "adhesive surfaces".

1.4.2.3 Polymer Brushes

A polymer brush is a polymer chain that is tethered to the surface or an interface with such high grafting density that the chains are forced to stretch away from the tethered site[74, 75]. The tethered chains can be formed by polymer either "grafting to" or "grafting from" a surface. The chains can be grafted by either physisorption or chemisorption. Physisorption can occur when a diblock copolymer is used to strongly adsorb to the surface, whereas chemisorption is by

covalently grafting to the surface. Physisorption has inherent thermal and solvolytic instabilities whereas covalent attachment has none of these inherent instabilities[76].

"Grafting to" the surface is where polymer chains have a suitable end-functionalised groups that are tethered to the surface[74, 76, 77]. "Grafting from" is where a polymer brush layer is generated *in* situ from a surface immobilised initiator, for example, using ATRP or RAFT polymerisation[78]. Using this method, thicker brush layers of higher density are generated because the thickness is controlled by the monomer diffusion to the propagating chain end rather than macromolecular diffusion to the surface. The main advantage of "grafting from" is control over the brush thickness via control of molar mass and polydispersity, and the ability to create specific architectures[77, 78]. Polymer brushes can exist in either solvent or melt where the reason for stretching is affinity for the solvent or to avoid overlap respectively.

The first brush theory to be published was by Alexander[79] in 1977 and he concluded that when a flexible polymer with Kuhn length a, permanently attached at a grafting density of σ chains per unit area, to a surface, has a layer height is given by;

Equation 1:16

where the number of chains per unit area[43] is σa^{-2}.

If $\sigma^{1/2} << R_g$ then the distance between the grafting sites is extremely small and the polymer will not be able to maximise its configurational entropy, which is done by forming short dense brushes, random walk configuration or by stretching if it has a favourable external environment. The free energy cost for these contradictory tendencies is firstly unfavourable overlapping and secondly stretching which decreases configurational entropy. Therefore the equilibrium height will be determined by the balance between these terms[79].

Brushes can be classified as being dry (matrix excluded) or wet (matrix included in the brush or solvated). When the molar mass of the matrix is much smaller than the molar mass of the brush then the matrix is mixed into the additive because of the high entropic penalty to exclude it, e.g. a wet brush. However, as the molar mass of the matrix increases the volume fraction mixed in the additive decreases until a limit where further increase in matrix molar mass does not affect the properties of the brush, e.g. dry brush[80].

There are several types of systems that can be considered as brushes. Block copolymers, mixtures and polyelectrolyte polymers can all be described in terms of polymer brushes where they can be either mixed into a polymer blend and segregate to the surface, be grafted to/from the surface by

surface functionalisation then reaction, or by surface initiated polymerisation. There exist several reviews in the literature which discuss the physics and chemistry of polymer brushes in detail [81-84].

1.4.2.4 Theoretical Descriptions of End-Attached Polymers

There are two theoretical descriptions of end-attached polymers which are scaling theories and self-consistent mean field calculations.

1.4.2.4.1 Scaling theories

Scaling theories produce equations relating the brush height to the areal density of the adsorbed chains but contain no information about the concentration profile of the polymer normal to the surface. Following from the work of Alexander, De Gennes[85] and Schmidt[83] extended scaling theories for polymer brushes.

Their theory can be briefly summarised as follows: as additional chains are added to the brush increases and therefore the free energy increases as a result of the entropic cost of chain stretching. Different scaling exponents relate brush height to grafting density depending on brush and matrix molecular weights. When the chains are collapsed the free energy is independent of z^*.

1.4.2.4.2 SCMFT

Adsorption isotherms at the air polymer interface may be quantitatively described by a self-consistent mean field theory[86, 87] (SCMFT). This approach was originally developed by Scheutjens and Fleer[88] to study adsorption in polymer solutions. SCMFT are used to predict the concentration profile of an adsorbed layer as a function of the attraction of the functional group to the film surface[70], where the mean field is the free energy required to place a segment of volumes v_0 into its surroundings[89], and the chemical potential of the adsorbing end is the relevant parameter[90]. Theodorou[91, 92] furthered this and developed a model for the surface structure of end-functionalised polymers. This model requires the knowledge of three parameters; the normalised chain length, r; Flory-interaction parameter, χ; and the surface interaction parameter, χ_S. The calculated end group surface volume fractions, $v_{f,1}$, are a function of r and the surface interaction parameter where the output of the calculation is the functional group concentration for each layer. An advantage of SCMFT over scaling theories is that the former gives information on the density profile of the brush and can therefore be related to experimental data from NR.

SCMFT can only be applied to amorphous blends as it does not account for density fluctuations. Therefore SCMFT cannot be used for polyethylene as it is semi-crystalline and below its T_m. However, when PE films are heated above T_m, the polymers are amorphous and SCMFT can be used to analyse adsorption isotherms obtained by NR.

1.4.2.4.2.1 Sticking Energies

Using the self-consistent mean field theory of Shull[80, 87], it is possible to relate the normalised surface excess to the thermodynamic "sticking energy", , of the end-functionalised polymer to the surface. is an experimentally accessible quantity which can be compared with the results from numerical SCMFT calculations.

The sticking energy can be calculated by assuming that each segment in the adsorbing molecule has equal sticking energy to the surface[93]. Equation 1:17 mathematically describes the sticking energy,

— — Equation 1:17

where and are the interaction parameters of the end functional groups with the surface and the bulk, respectfively, and is the free energy of transfer of the functional group from the bulk of the film to the surface, i.e. enthalpic term for confining the adsorbing chain end to the first lattice layer[69]. The logarithmic term accounts for the entropic penalty associated with confining the end-functional group in the surface layer, where ζ is the size of the lattice layer[69, 70].

A value of can be estimated using solubility parameters[93] where the values of the solubility parameters, δ, are obtained from the literature and the lattice volume, $V_{ref} = \zeta^3$, is calculated using $R_g = a(N/6)^{1/2}$,

— Equation 1:18

— Equation 1:19

where n_L is the number of lattice cells per square metre, and is the difference in surface energies of the two components. However, solubility parameters are inaccurate for crystalline polymers below T_m therefore these parameters cannot always be reliably estimated.

1.4.2.4.2.2 Group Contribution Methods

The interaction parameter for diblock systems can be estimated from the solubility parameter, δ, of the individual components. In the absence of surface segregation, the surface tension of a homogenous two constituent blend follows a simple group additivity relationship. It states that

the dilution of the end-group concentration, as molar mass increases, causes a change in the surface tension[94]. Any deviation would indicate surface segregation and the larger the difference in δ the higher the χ for the system and lower the chance of rearrangement[95-97]. Following from equation 1:13, if the end-groups are randomly distributed through the materials, the surface tension can then be calculated from the surface energies of the end group, , and the repeat units, , using group contributions methods.

Equation 1:20

1.4.2.5 Effect of Molar Mass on Segregation

Characteristics of a surface are determined by the molar mass of the adsorbing species, the molar mass of the matrix, and the areal density of the adsorbed polymer chains at the interface. There is a configurational entropy cost associated with confining a polymer to a surface. Therefore when considering purely entropic effects, the shorter chains partition preferentially to the surface, in order to enable the system to reach maximum entropy thus decreasing the free energy of the system[61, 67, 98]. Where the adsorption energy of the end-groups has to be large enough to compensate for the large entropy loss caused by stretching, thus a low energy end-group e.g. fluoro-groups, has to be used[99, 100]. It follows that the degree of end-group surface enrichment decreases with increasing molar mass when a low energy end-group is used.

When the molar mass of the additive is kept constant and the molar mass of the matrix is increased there is an increase in additive surface segregation expected, which is associated with reduction in the mixing entropy[101, 102]. Experimental results have shown that when an additive molar mass is constant yet the matrix molar mass increases the tendency of the additive to adsorb to the surface increases[99, 100, 103-105]. Le Grand and Gaines[106] reported that relationships exist between the molar mass of the matrix and the surface tension. They concluded that as the molar mass of the matrix increases the surface tension would increase, presuming there were no other additives[62]. They represent the surface tension as proportional to:

Equation 1:21

The entropy of mixing is generally very small therefore only a small enthaply of adsoprtion is required to induce adsorption [98]. For example the molar mass dependence of additives on the surface free energy for various end-capped poly(dimethylsiloxane) polymers (X-PDMS) is related to the difference in the surface energy between the chain backbone and the end-group[94]. Three

amorphous different end-capped polymers were synthesised, one with a lower surface tension than the polymer backbone (CH_3-PDMS), one with approximately the same (OH-PDMS) and one with higher surface tension (NH_2-PDMS). The surface tension increases with increasing molar mass for CH_3-PDMS, decreases for NH_2-PDMS and almost independent for OH-PDMS.

1.4.2.6 Types of Modifying Additives

Blending a small amount of functional additive with a matrix has advantages. Firstly, polymer blends have very low entropies of mixing compared to polymer solutions, so one expects large surface effects from relatively small perturbations. Secondly, blending polymers provides the possibility of continued supply from the bulk if the surface is damaged[86]. Some of the many types of additive are given in table 1:3.

Type	Function
Mechanical Property Modifiers	
Fillers	Increase strength at a reduced cost
Impact Modifier	Improve impact strength
Nucleating Agent	Promote crystallinity or reduce crystal size
Plasticisers	Increase flexibility and reduce melt viscosity
Reinforcing Fibres	Increase strength and stiffness
Compatibilsers	Join two distinct phases
Chemical and Aesthetic Property Modifiers	
Antioxidants	Prevent oxidative degradation
Flame Retardants	Reduce flammability
UV Stabilizers	Prevent degradation by UV
Colouring Agents	Add colour
Odorants	Add/mask smell
Nucleating Agents	Improve light transmission
Surface and Processing Modifiers	
Antiblocking Agents	Prevent sheets/films sticking together
Antifogging Agents	Prevents moisture from obscuring clarity
Antistatic Agent	Prevents build up of static charge
Coupling Agents	Improve bonding
Release Agents	Prevent sticking
Adhesive Agents	Improve sticking
Cross linking Agents	Promote curing
Emulsifiers	Stabilise emulsions

Table 1:3 Types of polymer modifying additives and their uses[††]

There are many types of polymer additive that exist from those that aid the mechanical properties of the system[107], chemical and aesthetic properties[108] , modify the surface and processing properties[109], and those which have a compatibilising effect of block copolymers[110].

[††] http://www.bpf.co.uk/plastipedia/additives/default.aspx last accessed on 1st December 2010

The problem of micellisation and aggregation is specific to block copolymers and end functional polymers are a promising alternative because they usually have a lower volume fraction of incompatible block than the block copolymer. By employing end-modified polymers as surface modifying agents the formation of aggregates may be avoided which can adversely affect physical properties of the bulk, such as optical transparency[69].

1.4.2.7 Effect of Additive Architecture on Segregation

Surface segregation of end groups requires reorientation of the chain backbone and commensurate loss in configurationally entropy. Thus where the functional groups are, relative to the polymer backbone, is very important in determining their surface preference. Koberstein *et al*[72, 73, 101] reported on surface segregation of different chain architectures and determined that two adjacent end-functional groups is the most effective to induce segregation.

The optimum architecture for a low energy release surfaces is adjacent placement of low energy functional groups located at one end where both enthalpic, associated with surface energy reduction, and entropic factors, configurational entropy loss, serve to drive the chain-ends to the surface. Usually the incorporation of low energy fluorocarbon or silicone components are used to lower the surface tension. Selective adsorption of polymers with an attractive end group is accompanied by depletion in deeper layers, resulting from chain connectivity[91, 92].

The optimum architecture for high energy adhesive surfaces is adjacent high energy functional groups at the centre of the chain where they locate preferentially in the second lattice layer. From here they can migrate readily to the surface when it is in contact with any other high surface energy medium. The result of this is that the sign of χ_S changes instantly and the functional polymer interface reorganises, in an attempt to reach a new equilibrium with the substrate. However, this only applies to pure additive - once the additive is mixed with a homopolymer there is little prospect of getting the polar groups to the second layer in large quantities.

1.4.2.8 Effect of Deuterium on Segregation

It has been observed that deuterated components of isotopic blends segregate to surfaces preferentially indicating that deuterated polymers have a lower surface energy than their protonated counterparts[111]. This is because the C-D bond length is shorter than the C-H length, therefore there is a slight reduction in electron distribution resulting in C-D bond having a slightly lower polarisability relative to a C-H bond and a very slightly lower cohesive energy density[112, 113]. Furthermore C-D has a shorter segmental volume so from surface free energy predictions a D/H mixture will have a small positive χ because of the excess free energy of mixing[113-115]. Thus in a mixture of a deuterated and a hydrogenated polymer the surface is expected to be enriched by

the deuterated component[115]. Isotopic effects are normally only significant when close to a phase boundary as is the case for very high molar mass perdeuterated polymers.

1.4.3 Current Surface Modified Polymers

In recent years there has been an increase in the number of applications that use polymer blends with functional surfaces. Their applications are very varied and range from adhesion, drug delivery[116, 117] , polymer coated stendts[118] to release surfaces. They can broadly be divided into two main categories that are low energy (release surfaces) and high energy (adhesive surfaces).

1.4.3.1 Low energy surfaces

Fluorinated materials have advanced significantly since 1930s and now many commercially available low energy polymers exist[119] but there is increasing demand for chemical robustness, reduced bulk cost and low adhesion. So alternatives that produce the same effect have been investigated over recent years and many examples have been described in the literature[61, 69, 83, 84, 120-123]. Adding low energy polymeric additives to polymers can induce thermodynamically controlled surface segregation where the new surface is inherently robust and has "self-healing" properties[61, 123]. Examples of surface enriching additives include polymers end-capped with fluoro-groups[124-126], butyl chain ends[61, 124], deuterated additives[61, 127]. Materials with a surface free energy as low as 8 mN/m have be claimed[128, 129] and because of the good oxygen compatibility[130] that fluorinated polymers have they can be used to manipulate specific blood and cellular protein interactions with polymer surfaces, e.g. during drug degradation[131]. Unusually, fluorocarbon surface groups also show not only hydrophobicity but lipophobicity.

Low energy surfaces are also biologically inert and resistant to attack from biological systems thus they are often employed as non toxic marine coating, however, it turns out that they are not very good for preventing bio-adhesion[132-134].

1.5 Aims & Structure of Thesis

The aim of the research presented in this thesis was to synthesise a range of end-functionalised polyethylenes. Currently, no polymerisation technique allows the preparations of well-defined end-functionalised polyethylene. Through the use of living anionic polymerisation an analogue to end-functionalised polyethylene was made by saturating end-functionalised polybutadiene. Developing a one step synthesis allows surface properties to be tailored with no detriment to the bulk which can be achieved by adding a comparatively small amount of additive. Doing this would be very advantageous in terms of durability of the modified surface.

This thesis describes the first ever preparation of semi-crystalline multi-end functionalised polymers and their surface properties. The surface properties of blended polymers were studied and related to the bulk and the crystalline regions of the polymer. The effect the molar mass of the multi-end functionalised additive along with the effect the matrix molar mass has on surface enrichment was explored. The influence that different degrees of end-functionalisation had on the surface properties was discovered and a quantitative study was performed to determine the effects the degree of crystallinity has on surface enrichment.

The following chapter discusses the experimental techniques that were used to characterise novel materials and how the samples were prepared and handled for each of these techniques. Chapter 3 provides detailed account of the synthesis required to make several different multi-end functionalised polymers and the path taken to obtain a standard working protocol for synthesising end-capped polybutadiene. Subsequent chapters explore the surface properties, surface organisation and bulk organisation in detail and at the end of each of these chapters an evaluation of the results will be made. The final chapter, chapter 7, collates results and discusses an overall conclusion to this project and identifies areas of further work that would be appropriate.

1.6 References

1. Jenkins, A. D.; Kratochvil, P.; Stepto, R. F. T.; Suter, U. W., *Pure and Applied Chemistry* **1996,** *68* (12), 2287-2311.
2. Goodyear, C. Improvement in the Process of Divesting Caoutchouc, Gum-Elastic, or India-Rubber of its Adhesive Properties, and also of Bleaching the Same, and Thereby Adapting it to Various Useful Purposes. 1844. U.S. Patent No. 240
3. Baekeland, L. H., *Journal of the Franklin Institute* **1910,** *169*, 55-60.
4. Staudinger, H., *Berichte der deutschen chemischen Gesellschaft (A and B Series)* **1920,** *Staudinger, H. (1920), Über Polymerisation. Berichte der deutschen chemischen Gesellschaft (A and B Series), 53: 1073–1085. doi: 10.1002/cber.19200530627*
5. Leuck, G. J.; Mark, H., *Journal of the American Chemical Society* **1934,** *56* (7), 1959-1962.
6. Fankuchen, I.; Mark, H., *Journal of Applied Physics* **1944,** *15* (4), 364-370.
7. Smith, J. K.; Hounshell, D. A., *Science* **1985,** *229* (4712), 436-442.
8. Carothers, W. H. Diamine dicarboxylic acid salt (suitable for forming spun fibers, etc.). 1938. U.S. Patent No. 2,130,947
9. Carothers, W. H. Linear polyamides suitable for spinning into strong pliable fibers. 1938. U.S. Patent No. 2,130,523
10. Carothers, W. H. Synthetic fibers, which describes the polymerisation of hexamethylenediamine adipate acid to form poly(hexamethyleneadipamide). 1938. U.S. Patent No. 2,130,948
11. Flory, P. J., *Principles of Polymer Chemistry*. 11th ed.; Cornell University Press, NY: 1981.
12. Koutsos, V., Polymeric materials: an Introduction, Edinburgh University, Edinburgh.
13. Fred W. Billmeyer, J., *Textbook of Polymer Science*. 2nd ed.; Wiley-Interscience, John Wiley & Sons, Inc, NY: 1971.
14. Cowie, J. M. G., *Polymers: Chemsitry & Physics of Modern Materials*. 2nd Eddition ed.; Blackie and Son Ltd, Glasgow: 1991.
15. Bassett, D. C., *Principles of Polymer Morphology*. Cambridge University Press, London: 1981.
16. Young, R. J.; Lovell, P. A., *Introduction to Polymers*. 2nd ed.; CRC Press: 1991.
17. Hoffman, J. D.; Miller, R. L., *Polymer* **1997,** *38* (13), 3151-3212.
18. Long, Y.; Shanks, R. A.; Stachurski, Z. H., *Progress in Polymer Science* **1995,** *20* (4), 651-701.
19. Armistead, K.; Goldbeckwood, G.; Keller, A., *Advances in Polymer Science* **1992,** *100*, 221-312.
20. Frank, F. C.; Tosi, M., *Proceedings of the Royal Society of London Series a-Mathematical and Physical Sciences* **1961,** *263* (131), 323-&.
21. Phillips, P. J., *Materials Science and Technology* **2003,** *19*, 1153-1160.
22. Dettenmaier, M.; Fischer, E. W.; Stamm, M., *Colloid and Polymer Science* **1980,** *258* (3), 343-349.
23. Boettinger, W. J.; Coriell, S. R.; Greer, A. L.; Karma, A.; Kurz, W.; Rappaz, M.; Trivedi, R., *Acta Materialia* **2000,** *48* (1), 43-70.
24. Boyer, R. F., *Journal of Polymer Science Part C-Polymer Symposium* **1975,** (50), 189-242.
25. Janowska, G.; Slusarski, L., *Journal of Thermal Analysis and Calorimetry* **2001,** *65* (1), 205-212.
26. Raju, V. R.; Smith, G. G.; Marin, G.; Knox, J. R.; Graessley, W. W., *Journal of Polymer Science Part B-Polymer Physics* **1979,** *17* (7), 1183-1195.

27. Hustad, P. D., *Science* **2009,** *325* (5941), 704-707.
28. Kharitonov, A. P.; Kharitonova, L. N., *Pure and Applied Chemistry* **2009,** *81* (3), 451-471.
29. Plunkett, R. J. Teflon. 1941.
30. Autumn, K.; Peattie, A. M., *Integrative and Comparative Biology* **2002,** *42* (6), 1081-1090.
31. Mueller, L.; Matyjaszewski, K., *Macromolecular Reaction Engineering* **2010,** *4* (3-4), 180-185.
32. Schulz, D. N.; Halasa, A. F., *Journal of Polymer Science Part a-Polymer Chemistry* **1977,** *15* (10), 2401-2410.
33. Broze, G.; Jerome, R.; Teyssie, P., *Makromolekulare Chemie-Macromolecular Chemistry and Physics* **1978,** *179* (5), 1383-1386.
34. Barner-Kowollik, C., *Handbook of RAFT Polymerisation*. Wiley-VCH: 2008.
35. Ziegler, K.; Dersch, F.; Wollthan, H., *Justus Liebigs Annalen Der Chemie* **1934,** *511*, 13-44.
36. Ziegler, K.; Jakob, L., *Justus Liebigs Annalen Der Chemie* **1934,** *511*, 45-63.
37. Ziegler, K.; Jakob, L.; Wollthan, H.; Wenz, A., *Justus Liebigs Annalen Der Chemie* **1934,** *511*, 64-88.
38. Szwarc, M.; Levy, M.; Milkovich, R., *Journal of the American Chemical Society* **1956,** *78* (11), 2656-2657.
39. Brody, H.; Ladacki, M.; Milkovitch, R.; Szwarc, M., *Journal of Polymer Science* **1957,** *25* (109), 221-224.
40. Baskaran, D.; Muller, A. H. E., *Progress in Polymer Science* **2007,** *32* (2), 173-219.
41. Schmitt, B. J.; Schulz, G. V., *European Polymer Journal* **1975,** *11* (2), 119-130.
42. Geacintov, C.; Smid, J.; Szwarc, M., *Journal of the American Chemical Society* **1962,** *84* (13), 2508.
43. Aubouy, M.; Fredrickson, G. H.; Pincus, P.; Raphael, E., *Macromolecules* **1995,** *28*, 2979-2981.
44. Fuoss, R. M.; Kraus, C. A., *Journal of the American Chemical Society* **1933,** *55*, 2387-2399.
45. Hsieh, H. L., Quirk, R.P, *Anionic Polymerization: Principles and Practical Applications*. Marcel Dekker Inc: 1996.
46. Morton, M. a. L. J. F., *Rubber Chemistry and Technology 48*, 359-409.
47. Koenig, J. L., *Chemical Microstructure of Polymer Chains*. Wiley-Interscience, John Wiley & Sons, Inc, NY: 1980.
48. Glaze, W. H.; Chaudhur.J; Hanicak, J. E.; Moore, M., *Journal of Organometallic Chemistry* **1972,** *44* (1), 39-&.
49. Stellman, J. M.; Woodward, A. E., *Journal of Polymer Science Part a-2-Polymer Physics* **1971,** *9* (1), 59-&.
50. Stavely, F. W.; Dunbrook, R. F.; Forman, L. E.; Foster, F. C.; Stearns, R. S.; Talcott, T. B.; Wakefield, L. B.; Alliger, G.; Russell, J. R.; Smith, S.; Smith, W. A.; Willis, J. M.; Binder, J. L.; Forster, M. J.; Hanson, E. E.; Liska, J. W.; Ransaw, H. C.; Barzan, M.; Gates, R. D.; Johnson, B. L.; Downing, J. P.; Hammond, C. H.; Hanson, E. S.; Mayes, C. G.; Para, A.; Smith, F. M.; Brock, M. J.; Eberly, K. C., *Industrial and Engineering Chemistry* **1956,** *48* (4), 778-783.
51. Peters, M. A.; Belu, A. M.; Linton, R. W.; Dupray, L.; Meyer, T. J.; Desimone, J. M., *Journal of the American Chemical Society* **1995,** *117* (12), 3380-3388.
52. P.R.Quirk, *Anionic Synthesis of Polymers with Functional Groups*. Pergamon Press: Oxford, 1992; Vol. First Supplement, p p83.
53. Hadjichristidis, N.; Iatrou, H.; Pitsikalis, M.; Mays, J., *Progress in Polymer Science* **2006,** *31* (12), 1068-1132.

54. Hadjichristidis, N.; Pitsikalis, M.; Pispas, S.; Iatrou, H., *Chemical Reviews* **2001,** *101* (12), 3747-3792.
55. Young, R. N.; Quirk, R. P.; Fetters, L. J., *Advances in Polymer Science* **1984,** *56*, 1-90.
56. Quirk, R. P.; Yin, J.; Guo, S. H.; Hu, X. W.; Summers, G.; Kim, J. G.; Zhu, L. F.; Schock, L. E., *Makromolekulare Chemie-Macromolecular Symposia* **1990,** *32*, 47-59.
57. Schulz, D. N.; Datta, S.; Waymouth, R. M., *Abstracts of Papers of the American Chemical Society* **1997,** *213*, 2-PMSE.
58. Ueda, K.; Hirao, A.; Nakahama, S., *Macromolecules* **1990,** *23* (4), 939-945.
59. Labeau, M. P.; Cramail, H.; Deffieux, A., *Polymer International* **1996,** *41* (4), 453-462.
60. Quirk, R. P.; Lee, Y., *Journal of Polymer Science Part a-Polymer Chemistry* **2000,** *38* (1), 145-151.
61. Schaub, T. F.; Kellogg, G. J.; Mayes, A. M.; Kulasekere, R.; Ankner, J. F.; Kaiser, H., *Macromolecules* **1996,** *29* (11), 3982-3990.
62. Wu, S., *Polymer Interface and Adhesion*. Marcel Dekker: New York, NY, 1982.
63. Garbassi, F.; Morra, M.; Occhiello, E., *Polymer Surfaces: From Physics to Technology*. John Wiley and Sons: New York, NY, 1994.
64. Nishino, T.; Meguro, M.; Nakamae, K.; Matsushita, M.; Ueda, Y., *Langmuir* **1999,** *15* (13), 4321-4323.
65. Bates, F. S., *Science* **1991,** *251* (4996), 898-905.
66. Paiksung, C. S.; Schneider, N. S., *Journal of Materials Science* **1978,** *13* (8), 1689-1699.
67. Rosen, S. L., *Fundamental Principles of Polymeric Materials*. 2nd ed.; John Wiley: 1993.
68. Eastoe, J.; Rankin, A.; Wat, R.; Bain, C. D., *International Reviews in Physical Chemistry* **2001,** *20* (3), 357-386.
69. Hutchings, L. R.; Narrainen, A. P.; Eggleston, S. M.; Clarke, N.; Thompson, R. L., *Polymer* **2006,** *47* (24), 8116-8122.
70. Ansari, I. A.; Clarke, N.; Hutchings, L. R.; Pillay-Narrainen, A.; Terry, A. E.; Thompson, R. L.; Webster, J. R. P., *Langmuir* **2007,** *23* (8), 4405-4413.
71. Bauer, B. J.; Fetters, L. J., *Macromolecules* **1980,** *13* (5), 1027-1031.
72. O'Rourke-Muisener, P. A. V.; Koberstein, J. T.; Kumar, S., *Macromolecules* **2003,** *36* (3), 771-781.
73. Koberstein, J. T., *Journal of Polymer Science Part B-Polymer Physics* **2004,** *42* (16), 2942-2956.
74. Mansky, P.; Liu, Y.; Huang, E.; Russell, T. P.; Hawker, C. J., *Science* **1997,** *275* (5305), 1458-1460.
75. Milner, S. T., *Science* **1991,** *251* (4996), 905-914.
76. Zhao, B.; Brittain, W. J., *Progress in Polymer Science* **2000,** *25* (5), 677-710.
77. Boyes, S. G.; Granville, A. M.; Baum, M.; Akgun, B.; Mirous, B. K.; Brittain, W. J., *Surface Science* **2004,** *570* (1-2), 1-12.
78. Granville, A. M.; Boyes, S. G.; Akgun, B.; Foster, M. D.; Brittain, W. J., *Macromolecules* **2004,** *37* (8), 2790-2796.
79. Alexander, S., *Journal De Physique* **1977,** *38* (8), 983-987.
80. Shull, K. R., *Journal of Chemical Physics* **1991,** *94* (8), 5723-5738.
81. Barbey, R.; Lavanant, L.; Paripovic, D.; Schuwer, N.; Sugnaux, C.; Tugulu, S.; Klok, H. A., *Chemical Reviews* **2009,** *109* (11), 5437-5527.
82. Zhang, J. L.; Han, Y. C., *Chemical Society Reviews* **2010,** *39* (2), 676-693.

83. Schmidt, D. L.; Coburn, C. E.; Dekoven, B. M.; Potter, G. E.; Meyers, G. F.; Fischer, D. A., *Nature* **1994,** *368* (6466), 39-41.
84. Genzer, J.; Efimenko, K., *Science* **2000,** *290* (5499), 2130-2133.
85. Degennes, P. G., *Macromolecules* **1980,** *13* (5), 1069-1075.
86. Iyengar, D. R.; Perutz, S. M.; Dai, C. A.; Ober, C. K.; Kramer, E. J., *Macromolecules* **1996,** *29* (4), 1229-1234.
87. Shull, K. R.; Kramer, E. J., *Macromolecules* **1990,** *23* (22), 4769-4779.
88. Scheutjens, J.; Fleer, G. J., *Journal of Physical Chemistry* **1979,** *83* (12), 1619-1635.
89. Shull, K. R., *Macromolecules* **1996,** *29* (7), 2659-2666.
90. Shull, K. R.; Kramer, E. J.; Hadziioannou, G.; Tang, W., *Macromolecules* **1990,** *23* (22), 4780-4787.
91. Theodorou, D. N., *Macromolecules* **1988,** *21* (5), 1411-1421.
92. Theodorou, D. N., *Macromolecules* **1988,** *21* (5), 1422-1436.
93. Hopkinson, I.; Kiff, F. T.; Richards, R. W.; Bucknall, D. G.; Clough, A. S., *Polymer* **1997,** *38* (1), 87-98.
94. Jalbert, C.; Koberstein, J. T.; Yilgor, I.; Gallagher, P.; Krukonis, V., *Macromolecules* **1993,** *26* (12), 3069-3074.
95. Zhao, B.; Brittain, W. J.; Zhou, W. S.; Cheng, S. Z. D., *Macromolecules* **2000,** *33* (23), 8821-8827.
96. Zhulina, E. B.; Singh, C.; Balazs, A. C., *Macromolecules* **1996,** *29* (19), 6338-6348.
97. Zhulina, E. B.; Singh, C.; Balazs, A. C., *Macromolecules* **1996,** *29* (25), 8254-8259.
98. Hariharan, A.; Kumar, S. K.; Russell, T. P., *Macromolecules* **1990,** *23* (15), 3584-3592.
99. Hadziioannou, G.; Patel, S.; Granick, S.; Tirrell, M., *Journal of the American Chemical Society* **1986,** *108* (11), 2869-2876.
100. Belder, G. F.; tenBrinke, G.; Hadziioannou, G., *Langmuir* **1997,** *13* (15), 4102-4105.
101. Muisener, P.; Jalbert, C. A.; Yuan, C. G.; Baetzold, J.; Mason, R.; Wong, D.; Kim, Y. J.; Koberstein, J. T., *Macromolecules* **2003,** *36* (8), 2956-2966.
102. Dai, K. H.; Kramer, E. J.; Shull, K. R., *Macromolecules* **1992,** *25* (1), 220-225.
103. Clarke, C. J.; Jones, R. A. L.; Edwards, J. L.; Shull, K. R.; Penfold, J., *Macromolecules* **1995,** *28* (6), 2042-2049.
104. Shull, K. R.; Winey, K. I.; Thomas, E. L.; Kramer, E. J., *Macromolecules* **1991,** *24* (10), 2748-2751.
105. Jones, R. A. L.; Norton, L. J.; Shull, K. R.; Kramer, E. J.; Felcher, G. P.; Karim, A.; Fetters, L. J., *Macromolecules* **1992,** *25* (9), 2359-2368.
106. Legrand, D. G.; Gaines, G. L., *Journal of Colloid and Interface Science* **1969,** *31* (2), 162-&.
107. Stevens, M. P., *Journal of Chemical Education* **1993,** *70* (6), 444-448.
108. Stevens, M. P., *Journal of Chemical Education* **1993,** *70* (7), 535-538.
109. Stevens, M. P., *Journal of Chemical Education* **1993,** *70* (9), 713-718.
110. Anastasiadis, S. H.; Gancarz, I.; Koberstein, J. T., *Macromolecules* **1989,** *22* (3), 1449-1453.
111. Harton, S. E.; Stevie, F. A.; Griffis, D. P.; Ade, H., *Applied Surface Science* **2006,** *252* (19), 7224-7227.
112. Bates, F. S.; Fetters, L. J.; Wignall, G. D., *Macromolecules* **1988,** *21* (4), 1086-1094.
113. Jones, R. A. L.; Kramer, E. J.; Rafailovich, M. H.; Sokolov, J.; Schwarz, S. A., *Physical Review Letters* **1989,** *62* (3), 280-283.
114. Bhatia, Q. S.; Pan, D. H.; Koberstein, J. T., *Macromolecules* **1988,** *21* (7), 2166-2175.

115. Jones, R. A. L.; Norton, L. J.; Kramer, E. J.; Composto, R. J.; Stein, R. S.; Russell, T. P.; Mansour, A.; Karim, A.; Felcher, G. P.; Rafailovich, M. H.; Sokolov, J.; Zhao, X.; Schwarz, S. A., *Europhysics Letters* **1990,** *12* (1), 41-46.
116. Langer, R., *Nature* **1998,** *392* (6679), 5-10.
117. Zhang, Z. B.; Ying, S. K.; Zhang, Q. L.; Xu, X. D., *Journal of Polymer Science Part a-Polymer Chemistry* **2001,** *39* (15), 2670-2676.
118. Morice, M.; Serruys, P. W.; Sousa, J. E.; Fajadet, J.; Hayashi, E. B.; Perin, M.; Colombo, A.; Schuler, G.; Barragan, P.; Guagliumi, G.; Molnar, F.; Falotico, R.; Grp, R. S., *New England Journal of Medicine* **2002,** *346* (23), 1773-1780.
119. Grainger, D. W.; Stewart, C. W., *Fluorinated Coatings and Films: Motivation and Significance*. American Chemical Society: Washington, DC, 2001.
120. Narrainen, A. L.; Hutchings, L. R.; Ansari, I. A.; Clarke, N.; Thompson, R. L., *Soft Matter* **2006,** *2* (2), 126-128.
121. McLain, S. J.; Sauer, B. B.; Firment, L. E., *Macromolecules* **1996,** *29* (25), 8211-8219.
122. Hirao, A.; Sakai, S.; Sugiyama, K., *Polymers for Advanced Technologies* **2004,** *15* (1-2), 15-25.
123. Thompson, R. L.; Narrainen, A. P.; Eggleston, S. M.; Ansari, I. A.; Hutchings, L. R.; Clarke, N., *Journal of Applied Polymer Science* **2007,** *105* (2), 623-628.
124. Elman, J. F.; Johs, B. D.; Long, T. E.; Koberstein, J. T., *Macromolecules* **1994,** *27* (19), 5341-5349.
125. Hwang, S. S.; Ober, C. K.; Perutz, S.; Iyengar, D. R.; Schneggenburger, L. A.; Kramer, E. J., *Polymer* **1995,** *36* (6), 1321-1325.
126. McCloskey, C. B.; Yip, C. M.; Santerre, J. P., *Macromolecules* **2002,** *35* (3), 924-933.
127. Frantz, P.; Leonhardt, D. C.; Granick, S., *Macromolecules* **1991,** *24* (8), 1868-1875.
128. Pike, J. K.; Ho, T.; Wynne, K. J., *Chemistry of Materials* **1996,** *8* (4), 856-860.
129. Wang, J. G.; Mao, G. P.; Ober, C. K.; Kramer, E. J., *Macromolecules* **1997,** *30* (7), 1906-1914.
130. Chapman, T. M., *Journal of Polymer Science Part a-Polymer Chemistry* **1989,** *27* (6), 1993-2005.
131. McCarthy, S. J.; Meijs, G. F.; Mitchell, N.; Gunatillake, P. A.; Heath, G.; Brandwood, A.; Schindhelm, K., *Biomaterials* **1997,** *18* (21), 1387-1409.
132. Bartels, J. W.; Cheng, C.; Powell, K. T.; Xu, J. Q.; Wooley, K. L., *Macromolecular Chemistry and Physics* **2007,** *208* (15), 1676-1687.
133. Gudipati, C. S.; Finlay, J. A.; Callow, J. A.; Callow, M. E.; Wooley, K. L., *Langmuir* **2005,** *21* (7), 3044-3053.
134. Xu, J. Q.; Bohnsack, D. A.; Mackay, M. E.; Wooley, K. L., *Journal of the American Chemical Society* **2007,** *129*, 506-507.

2 Experimental

This chapter is concerned with the experimental methods that were used to synthesise and characterise the polymers used as part of this study and ultimately the properties of end functionalised polyethylenes and their blends. The protocol under which these experiments were carried out, and for key techniques the theoretical basis is briefly outlined. All the methods reported here were carried out 'hands-on' with the exception of XPS, which was provided by the University of Nottingham, and transmission electron microscopy which was provided by Dr Budikha Mendis, Durham University. To analyse the molecular structure NMR, IR and size exclusion chromatography (SEC) were used. To analyse the surface properties a range of techniques were used. These include contact angles analysis, x-ray photo-electron spectrometry and electron microscopy. To determine the surface organisation several complementary techniques were utilised including neutron reflectometry and ion beam analysis. Finally, the bulk properties were characterised using small angle neutron scattering, quasi elastic neutron scattering and differential scanning calorimetry.

2.1 Molecular Structure

2.1.1 Nuclear Magnetic Resonance (NMR)

^{1}H NMR analyses were recorded on both on a Bruker Avance-400 spectrometer, for rapid analysis to follow reactions and a Varian Inova-700MHz spectrometer for final product analysis, using CD_2Cl_2 as the NMR solvent for the dendrimer synthesis, and 1% concentration. The ^{1}H NMR allowed the final product to be differentiated from the starting materials through the peak shifts and intensity ratios. All polymers were also analysed by ^{1}H NMR (Varian Inova-700MHz) to establish the microstructure of the polybutadiene and to the extent of end-capping. The end-capped polymers were further analysed by ^{13}C (Varian 500) and ^{19}F (Varian 200) in DCM-d_2 to qualitatively analyse the fluorine content. The fraction of saturated double bonds when converting polybutadiene to polyethylene was examined using ^{1}H NMR using TCE-d_2 at 100^{0}C and the disappearance of the C=C peaks observed.

2.1.2 Infra-red (IR) Spectroscopy

A Perkin-Elmer Paragon FT-IR spectrometer was used to quatinfy the disappearance of the C=C vibration after hydrogenation/deuteration. Firstly, a background spectrum of the sample environment was run, then samples, ~0.1g, were loaded onto the diamond analyser so it was

completely covered, and the spectrum was recorded. The absence of absorbances at 1650cm^{-1} and CH stretch band near 3000cm^{-1} were used to verify the extent of the saturation reaction.

2.1.3 Size exclusion chromatography

Size exclusion chromatography (SEC), developed in the mid 1960s, is one of the most versatile analytical techniques available for understanding and predicting polymer performance[1]. It is also the only proven technique for characterizing the complete molecular weight distribution of a polymer. Molecular weight analysis of the butadiene polymers was carried out using a Viscotek TDA 302 with refractive index, viscosity, and light scattering detectors and 2 x 300mm PLgel 5µm mixed C columns, THF was used as the eluent with a flow rate of 1.0 ml/min and at a constant temperature of 35^{o}C. Molecular weights were obtained using triple detection where the detectors were calibrated with a single narrow molecular weight distribution polystyrene standard using a refractive index increment of 0.185 and a value of 0.124 was used for polybutadiene.

Dilute polymer solution (1 mg/ml) was injected into a solvent stream which then flowed through a column packed with solvent swollen crosslinked polystyrene beads (polymer gel). The beads selected had pore sizes in the range of 10^2–10^5 Å, figure 2:1.

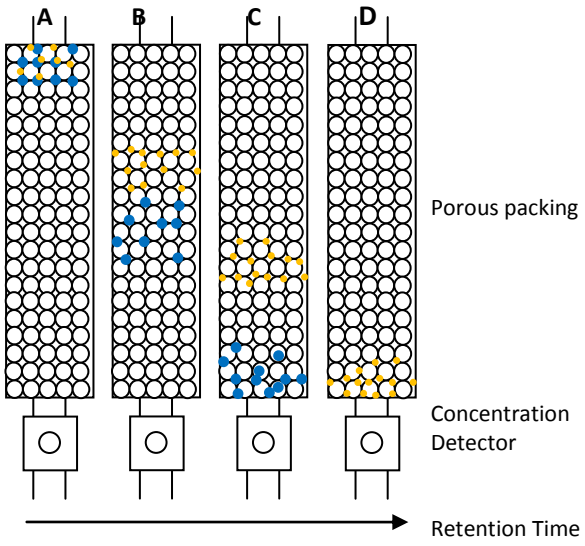

Figure 2:1 Illustration of polymer molecules (blue and yellow) travelling through the porous media and the mechanism of size separation by SEC (a) sample injected, (b) size separation, (c) large solutes eluted, and (d) small solutes eluted.

The retention time (i.e. the length of time it takes to emerge from the column) is shortest for large molecules and longest for shorter ones. This is because SEC separates molecules in solution by their “effective size in solution”. The column retains lower molecular weight materials longer than higher ones because the larger polymer molecules are excluded from all but the largest

pores due to their greater molecular size. (The conformational entropy loss prevents the larger chain from entering the gel consequently they have a much shorter flow path). Conversely, the small solvent molecules pass through and around the beads, carrying the polymer molecules with them where possible. The competition between the two types of entropy, ΔS_{mix} (favourable entropy of mixing of polymer and solvent inside pores), and ΔS_{conf} (unfavourable loss of conformation entropy of large polymers, high M_w, when entering smaller pores in the gel), results in the smaller polymer molecules having a longer flow path because the mixing entropy gain drives the smaller chains to enter and diffuse throughout the entire gel.

SEC can determine the molecular weight distribution from which several important parameters are derived. These include number average molecular weight (M_n)**,** weight average molecular weight (M_w), *Z* weight average molecular weight (M_z), and the molecular weight at the top of the peak (M_p), this is the highest obtained molecular weight. These values are important since they affect many of the characteristic physical properties of a polymer. M_n is sensitive to small molecules and thermodynamic properties, e.g. T_g, whereas M_w is sensitive to larger molecules and determines the bulk properties. Finally, M_z is sensitive to very large molecules and the viscosity is dependent on it.

To obtain these important parameters the molar mass distribution of the polymer being eluted was measured. This was achieved using refractive index and a right angle laser light scattering detector (RAL), which gives a mass distribution as a function of the retention volume.

Refractive index detectors measure the concentration of molecules in a weight to volume ratio, where the intensity is directly proportional the concentration (Raleigh's law). (GPC cannot measure the number of molecules in a sample, instead it measures the concentration). The RAL detector also measures the concentration of molecules where the absorbance is directly proportional to concentration (Beer Lambert law).

2.1.4 Fractionation

If a polymer has a broader polydispersity (PDI) than desired it can be fractioned. For polybutadiene a thermodynamically stable polymer solution is made by dissolving it in toluene in a 1% solution. Methanol, a poor solvent, is added drop wise and the temperature increased slowly until the polymer re-dissolves. The temperature is then reduced and the fractionated polymer removed.

2.2 Polymer Synthesis

The preparation of polymers used in this study can be divided into two sections; polymer synthesis and polymer saturation. Firstly, a series of polybutadiene (PB) polymers were prepared

with a range of molecular weights (from 5 to 200 $kgmol^{-1}$), three of which were hydrogenated and used as matrix polymer in subsequent studies and one sample was deuterated and used to study the effects of deuterium on surface segregation. Secondly, a series of end-capped PB polymers were prepared with molecular weights in the range of 5 to 50 $kgmol^{-1}$. The polymers were end capped with one of three types of fluoroalkylbromides, two of which have been synthesised in this work and a third supplied by another group member[2]; with type "a" end capping agent carrying 2 CF groups, type "b" carrying 3 CF groups, and type "c" carrying 4CF groups were prepared. Every CF group represents C_8F_{17}. The eight end functionalised polybutadiene polymers were deuterated to form a series of deuterium labelled end functionalised polyethylenes.

The nomenclature used throughout this work is as follows: The end-capped polybutadiene polymers (PB) are labelled as PBx00, where the x represents the type of CF group attached to the end and 00 is the approximate molar mass in $kgmol^{-1}$. After saturation PE is used as shorthand for polyethylene, instead of PB. Depending on whether hydrogenated or deuterated, h or d is used as a prefix.

2.2.1 Materials

Hexane (Reagentplus >99.9%, Aldrich) was dried and degassed over CaH_2 (95%, Aldrich). 1,3-Butadiene (Aldrich), sec-BuLi (1.4M in cyclohexane, Aldrich), 3-(perfluorooctyl)propanol (Fluorochem), 3,5-dihydroxybenzyl alcohol (99%, Aldrich), CBr_4 (Aldrich), PPh_3 (Aldrich), K_2CO_3 (Aldrich), 18-crown-6 (Aldrich) and benzyl bromide (Aldrich), benzene (Aldrich), cyclohexane (Aldrich), diphenylethylene (Aldrich), 2,6-Di-tert-butyl-4-methylphenol (Aldrich) and tetramethylethylenediamine(Aldrich) were all used as received. Hydrogen and deuterium (100L, 19.4bar, BOC) and $Pd/CaCO_3$ (5% reduced, Alfa Aesar) were all used as received.

2.2.2 Polymer Synthesis

2.2.2.1 Synthesis of Polybutadiene

2.2.2.1.1 Synthesis of polybutadiene with a predetermined molecular weight of 50$kgmol^{-1}$

Living anionic polymerization was carried out under high vacuum using standard Schlenk techniques[3-5] with *sec*-butyllithium as an initiator and hexane as a solvent. Butadiene polymerization was typically carried out as follows to obtain a molecular weight of 50 $kgmol^{-1}$: Approximately 300mL of hexane (Aldrich) was dried with calcium hydride, degassed by a series of freeze – pump – thaw cycles and vacuum distilled into the "Christmas tree" reaction apparatus immediately prior to use, figure 2:1. The required amount of butadiene, 6.23 g, (1.24 mmol of polybutadiene), was passed through a drying column prior to use and collected in a pre-weighed

flask before being transferred to the "Christmas tree" apparatus. The polymerisation was initiated with *sec*-buLi (0.9 ml, 1.3 mmol) for a target molecular weight of 50 $kgmol^{-1}$ and the polymerisation allowed to proceed at 50 °C for 36 hours. After this time the living anions were terminated by the addition of an excess of methanol (purged with N_2 ~2 mL). Antioxidant solution, BHT, was added to the polymer solution before adding the solution to a large excess of methanol, where the polybutadiene "precipitates" out of solution as a sticky solid and rests on the bottom of the beaker where it can then be separated, dried in vacuo to constant mass and stored in the freezer. 89% Yield M_n 59500, M_w 60500, M_w/M_n 1.02.

A series of polybutadiene samples with different molecular weights were prepared by the same method except;

Sample Code: PB5

For a target molecular weight of 5 $kgmol^{-1}$, 2.93 g of butadiene and 0.4 2mL of *sec*-BuLi was used 73% Yield; M_n 4900, M_w 5000, M_w/M_n 1.02,

Sample Code: PB10

For a target molecular weight of 10 $kgmol^{-1}$, 5.53 g of butadiene and 0.395 mL of *sec*-BuLi was used to make PB10, 85% Yield M_n 10700, M_w 11000, M_w/M_n 1.03,

Sample Code: PB20

For a target molecular weight of 20 $kgmol^{-1}$, 7.13 g of butadiene and 0.25 mL of *sec*-BuLi was used to make PB20, 95% Yield M_n 23700, M_w 25400, M_w/M_n 1.07,

Sample Code: PB50

For a target molecular weight of 50 $kgmol^{-1}$, 36.21 g of butadiene and 0.52 mL of *sec*-BuLi was used to make PB50, 97% Yield M_n 56600, M_w 58900, M_w/M_n 1.04,

Sample Code: PB100

For a target molecular weight of 100 $kgmol^{-1}$, 37.57 g of butadiene and 0.27 mL of *sec*-BuLi was used to make PB100, 83% Yield M_n 113000, M_w 117000, M_w/M_n 1.04,

Sample Code: PB200

For a target molecular weight of 150 $kgmol^{-1}$,34.37 g of butadiene and 0.16 mL of *sec*-BuLi was used to make PB200, 67% Yield M_n 135000, M_w 200000, M_w/M_n 1.48.

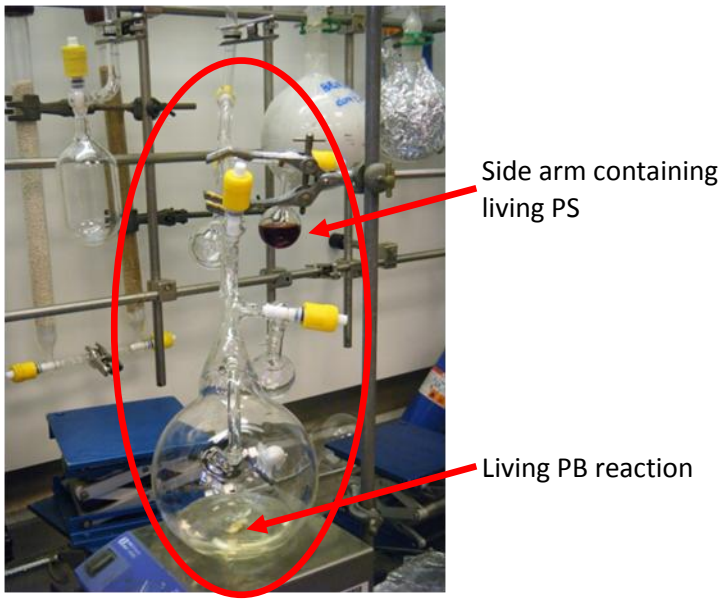

Figure 2:2 Reaction vessel colloquially named a "Christmas tree"

2.2.2.1.2 Standard High Vacuum Techniques - Schlenk techniques

The Schlenk technique is a method of transferring solvents, or materials, under very high vacuum or in inert conditions. Using a turbo pump all apparatus used for the polymerisation was evacuated to 10^{-6} Torr and sealed with Young's taps to ensure no leaks.

2.2.2.2 Synthesis of Fluoroalkylbromides

2.2.2.2.1 Synthesis of 3-(perfluorooctyl)propyl bromide (1)

Following the procedure previously reported in the literature[6] 3-(perfluorooctyl)propyl bromide was synthesised by adding triphenylphosphine (92.6 g, 355 mmol) in THF/CH_2Cl_2 (47 mL/87 mL) to a mixture of 3-perfluorooctyl-1-propanol (100 g, 237 mmol) and carbon tetrabromide (118.2 g, 356 mmol) in THF/CH_2Cl_2 (20 mL/40 mL) at 0 ^{0}C. The reaction mixture was stirred for 20 hours at room temperature and quenched with a small amount of water. The excess solvent was removed on a rotary vacuum until only slurry remained. The slurry was then partitioned between dichloromethane and water, the organic layer being washed twice more with water then dried over $MgSO_4$. The organic layer was filtered to remove $MgSO_4$ and the solvent removed. Fractional distillation gave 3-perfluorooctylpropyl bromide (63.1 g, 116.6 mmol) as a colourless liquid in 63% yield. (bp: 64-65 ^{0}C/3 mmHg). ^{1}H NMR (400MHz, $CDCl_3$, δ, ppm): 2.19 (m, 2H, $CH_2CH_2CH_2$), 2.29 (m, 2H, CF_2CH_2), 3.48 (t, 2H, CH_2Br).

2.2.2.2.2 Synthesis of 3,5-(di-3-(perfluorooctyl)propyloxy) benzyl alcohol (2)

Following the procedure previously reported by *Narrainen et al*[7] 3,5-(Di-3-(perfluorooctyl)propyloxy) benzyl alcohol was synthesised by adding a mixture of **1** (63.1 g, 116.6

mmol), 3,5-dihydroxybenzyl alcohol (8.17 g, 58 mmol), K_2CO_3 (20.15 g, 145.8 mmol) and 18-crown-6 (1.92 g, 7.3 mmol) in dry acetone (250 mL). This mixture was stirred vigorously and refluxed under a N_2 atmosphere for 24 hrs. The excess solvent was removed on a rotary vacuum until only slurry remained. The slurry was then partitioned between EtOAc and H_2O, the organic layer being washed twice more with water then dried over $MgSO_4$. After filtration and removal of solvent, the crude product was recrystallized from a small amount of Et_2O to afford the product **2** a white powder (40.48 g, 38.17 mmol, 65.5%). ^{1}H NMR (700MHz, $CDCl_3$, δ, ppm): 1.55 (s, 1H, OH), 2.09 (m, 4H, $CH_2CH_2CH_2$), 2.29 (m, 4H, CF_2CH_2), 4.02 (t, 4H, CH_2O), 4.63 (s, 2H, CH_2OH), 6.36 (t, 1H, ArH), 6.53 (d, 2H, ArH).

2.2.2.2.3 Synthesis of 3,5-(di-3-(perfluorooctyl)propyloxy) benzyl bromide (3)

Following the procedure previously reported by *Narrainen et al*[7] 3,5-(di-3-(perfluorooctyl)propyloxy) benzyl bromide was synthesised by adding CBr_4 (25.02 g, 75.4 mmol) and **2** (32.08 g, 30.25 mmol) in dry THF (250 mL) under N_2. The reaction mixture was stirred and PPh_3 (8.5 g, 32.4 mmol) is added in 3 aliquots over 6hrs and left stirring for a further 20 hrs at room temperature and quenched with a small amount of water. The excess solvent was removed on a rotary vacuum until only slurry remained. The slurry was then partitioned between dichloromethane and water, the organic layer being washed twice more with water then dried over $MgSO_4$. The organic layer was filtered and the solvent removed. The crude product was recrystallized by first stirring vigorously with MeOH, to dissolve the Ph_3PO then EtOAc was added to afford the product **3** a white powder (20.13 g, 76.01%) . ^{1}H NMR (700MHz, $CDCl_3$, δ, ppm): 2.09 (m, 4H, $CH_2CH_2CH_2$), 2.29 (m, 4H, CF_2CH_2), 4.02 (t, 4H, CH_2O), 4.39 (s, 2H, CH_2Br), 4.63 (s, 2H, CH_2OH), 6.37 (t, 1H, ArH), 6.54 (d, 2H, ArH).

2.2.2.2.4 Synthesis of $(C_8F_{17}(CH_2)_3O)_4$-[G-1]-OH (4)

Following the procedure previously reported in the literature [7] $(C_8F_{17}(CH_2)_3O)_4$-[G-1]-OH was synthesised by adding a mixture of **3** (10.5 g, 9.34 mmol), 3,5-dihydroxybenzyl alcohol (0.65 g, 4.67 mmol), K_2CO_3 (1.94 g, 14.02 mmol) and 18-crown-6 (0.12 g, 0.46 mmol) in dry acetone (20 mL). This mixture was stirred vigorously and refluxed under a N_2 atmosphere for 24 hrs. The reaction was followed by NMR and when gone to completion the solvent was removed and partitioned between EtOAc and H_2O, the organic layer being washed twice more with water then dried over $MgSO_4$. After filtration and removal of solvent, the crude product was purified by column chromatography eluting with pure CH_2Cl_2, gradually changing to pure EtOAc to give **4** a white powder (8.39 g, 80.68%). ^{1}H NMR (700MHz, $CDCl_3$, δ, ppm): 1.55 (s, 1H, OH), 2.08 (m, 8H, $CH_2CH_2CH_2$), 2.29 (m, 8H, CH_2CF_2), 4.01 (t, 8H, CH_2CH_2O), 4.63 (s, 2H, CH_2OH), 4.95 (s, 4H, CCH_2O), 6.38 (t, 2H, Ar_2H), 6.51 (t, 1H, Ar_1H), 6.56 (d, 4H, Ar_2H), 6.61 (d, 2H, Ar_1H).

2.2.2.2.5 Synthesis of $(C_8F_{17}(CH_2)_3O)_4$-[G-1]-Br (5)

$(C_8F_{17}(CH_2)_3O)_4$-[G-1]-Br was synthesised[7] by adding **4** (8.39 g, 3.77 mmol), CBr_4 (1.22 g, 3.68 mmol), and PPh_3 (2.09 g, 7.98 mmol) in dry THF (100 mL) under N_2. The reaction mixture was stirred and PPh_3 (8.5 g, 32.4 mmol) was added in 3 aliquots over 6hrs and left stirring for a further 15 hrs at room temperature, the reaction was followed by NMR (^1H) and when complete, was quenched with a small amount of water (~2 mL). The solvent was removed and partitioned between EtOAc and H_2O, the organic layer being washed twice more with water then dried over $MgSO_4$. The organic layer was filtered and the solvent removed. The crude product was stirred for several hours in MeOH (to dissolve any residual $Ph_3P=O$) then recrystallized from CH_2Cl_2 to afford the product **5** a white powder (6.82 g, 79.05%). 1H NMR (700 MHz, CDCl3, δ, ppm): 2.09 (m, 8H, $CH_2CH_2CH_2$), 2.30 (m, 8H, CH_2CF_2), 4.03 (t, 8H, CH_2CH_2O), 4.41 (s, 2H, CH_2Br), 4.96 (s, 4H, CCH_2O), 6.40 (t, 2H, Ar_2H), 6.51 (t, 1H, Ar_1H), 6.57 (d, 4H, Ar_2H), 6.64 (d, 2H, Ar_1H).

2.2.2.3 Synthesis of Polybutadiene end-capped with Fluoroalkylbromides

2.2.2.3.1 Synthesis of polybutadiene end capped with type A end capping agent with 2 fluoroalkyl groups with a target molecular weight of 5 $kgmol^{-1}$ (PBa5)

Living anionic polymerization was carried out under high vacuum using standard Schlenk techniques using *sec*-butyllithium (1.4 M solution in cyclohexane), as an initiator and hexane as a solvent. Butadiene polymerization was typically carried out as follows to obtain a molecular weight of 5 $kgmol^{-1}$: Approximately 100 mL of hexane was dried with calcium hydride, degassed by a series of freeze – pump – thaw cycles and vacuum distilled into vessel 1 of the "Christmas tree A" reaction apparatus and some decanted into the side arm 2, immediately prior to use, figure 2:3. The required amount of butadiene, 6.68 g (1.34 mmol of PB of the target molecular weight), was passed through a drying column prior to use and collected in pre weighed flask before being transferred to the "Christmas tree" apparatus. The polymerisation was initiated with *sec*-BuLi (0.95 mL, 1.33 mmol) for a target molecular weight of 5 $kgmol^{-1}$ and the polymerisation proceed at 50 °C for 36 hrs. When the polymerization had finished the hexane was distilled out of the reaction flask and replenished with fresh, dry hexane. This process was repeated a further two times. Diphenylethylene, DPE, (0.35 mL, 2.00 mmol), sec-BuLi, (0.19 mL, 0.27 mmol) used to activate the DPE, and tetramethylethylenediamine, TMEDA, (0.60 mL, 4.00 mmol) was injected into the side arm (2), and the contents of the side arm were decanted into the main reaction vessel (1) and left stirring for 48 hrs at 50 ^0C, the resulting solution was red which deepened over time. A sample was taken and quenched with MeOH. In side arm (3) 3,5-(Di-3-(perfluorooctyl)propyloxy) benzyl bromide, (1.80 g, 1.60 mmol) was azeotropically dried with benzene three times and 10 mL THF added. THF, 20 mL, was then distilled into the living polymer

solution and cooled to -78 ^{0}C using a dry ice bath whilst stirring. The contents of (3) was also cooled and then decanted into the living polymer solution at -78 ^{0}C, left stirring for 3hrs then allowed to warm to room temperature over 2 hrs. After this time any unreacted polymer was terminated by the addition of an excess of MeOH (purged with N_2 ~2 mL) before the polymer is precipitated out, antioxidant, BHT, was added before the solution was added to a ×7 excess of MeOH. The end-capped polybutadiene "precipitates" out of solution and rests on the bottom of the beaker where it can then be separated, dried in vacuo to constant mass and stored in the freezer. 96% Yield, 84% end-capping M_n 7100, M_w 7500, M_w/M_n 1.07. ^{1}H NMR (700MHz, DCM-d_2, δ, ppm): 5.6 (**C** CH_2CH), 5.4 (**A** *CHCH*), 5.0 (**B** CH_2CH), 2.1 (d, CH_2, polymer backbone), 2.09 (m, 4H, $CH_2CH_2CH_2$), 2.29 (m, 4H, CF_2CH_2), 3.7 (m, 4H, CH_2O), 3.3 (m, 2H, CH_2DPE), 6.2 (t, 1H, ArH), 5.7 (d, 2H, ArH). See Chapter 3 for NMR discussion and references to **A,B** and **C**.

Elemental analysis, SEC, F^{19} NMR, H^1 NMR and C^{13} NMR was performed on all the end-capped polymers to fully characterise them. As some of the peaks in the ^{1}H NMR moved to the region where THF appears so a C^{13} NMR was run to make sure the polymer was completely dry. A series of end-capped polybutadiene samples were prepared by the same method except that:

Sample Code: PBa10

5.03 g of butadiene (equivalent to 0.50 mmol of PB of the target molecular weight), 0.36 mL of *sec*-BuLi (0.50 mmol), 0.13 mL of DPE (0.76 mmol) with 0.07 mL (0.10 mmol) *sec*-BuLi, 0.23 mL (1.51 mmol) TMEDA and 0.67 g (0.60 mmol) 3,5-(Di-3-(perfluorooctyl)propyloxy) benzyl bromide was used to make 10 kgmol^{-1} end-capped PB, 67% Yield, 86% end-capping M_n 15400, M_w 16100, M_w/M_n 1.05.

Sample Code: PBa20

12.8 g of butadiene (equivalent to 0.64 mmol of PB of the target molecular weight), 0.46 mL of *sec*-BuLi (0.64 mmol), 0.17 mL of DPE (0.96 mmol) with 0.09 mL (0.13 mmol) *sec*-BuLi, 0.29 mL (1.92 mmol) TMEDA and 0.86 g (0.77 mmol) 3,5-(Di-3-(perfluorooctyl)propyloxy) benzyl bromide was used to make 20 kgmol^{-1} end-capped PB, 99% Yield, 81% end-capping, M_n 26800, M_w 27500, M_w/M_n 1.03.

Sample Code: PBb5

8.56 g of butadiene (equivalent to 1.71 mmol of PB of the target molecular weight), 1.22 mL of *sec*-BuLi (1.71 mmol), 0.45 mL of DPE (2.57 mmol) with 0.24 mL (0.34 mmol) *sec*-BuLi, 0.77 mL (5.13 mmol) TMEDA and 2.31 g (2.05 mmol) 3,4,5-(Tri-3-(perfluorooctyl)propyloxy) benzyl bromide was used to make 5 kgmol^{-1} end-capped PB, 99% Yield, 75% end-capping M_n 6900, M_w

7200, M_w/M_n 1.04. ^{1}H NMR (700MHz, DCM-d_2, δ, ppm): .6 (**C** CH_2CH), 5.4 (**A** *CHCH*), 5.0 (**B** CH_2CH), 2.1 (d, CH_2, polymer backbone), 2.02 (m, 2H, $CH_2CH_2CH_2$), 2.12 (m, 4H, $CH_2CH_2CH_2$), 2.32 (m, 6H, CH_2CF_2), 3.99 (t, 2H, CH_2O), 4.07 (t, 4H, CH_2O), 6.60 (s, 2H, ArH).

Sample Code: PBc5

5.86 g of butadiene (equivalent to 1.17 mmol of PB of the target molecular weight), 0.84 mL of *sec*-BuLi (1.17 mmol), 0.31 mL of DPE (1.76 mmol) with 0.17 mL (0.23 mmol) *sec*-BuLi, 0.53 mL (3.51 mmol) TMEDA and 3.22 g (1.41 mmol) $(C_8F_{17}(CH_2)_3O)_4$-[G-1]-Br was used to make 5 kgmol^{-1} end-capped PB, 97% Yield, 86% end-capping M_n 4200, M_w 5500, M_w/M_n 1.31.

Sample Code: PBc10

4.5 g of butadiene (equivalent to 0.45 mmol of PB of the target molecular weight), 0.32 mL of *sec*-BuLi (0.45 mmol), 0.12 mL of DPE (0.68 mmol) with 0.06 mL (0.09 mmol) *sec*-BuLi, 0.20 mL (1.35 mmol) TMEDA and 1.24 g (0.54 mmol) $(C_8F_{17}(CH_2)_3O)_4$-[G-1]-Br was used to make 10 kgmol^{-1} end-capped PB, 87% Yield, 99% end-capping M_n 13500, M_w 14000, M_w/M_n 1.04.

Sample Code: PBc20

4.96 g of butadiene (equivalent to 0.25mmol of PB of the target molecular weight), 0.18 mL of *sec*-BuLi (0.25 mmol), 0.07 mL of DPE (0.37 mmol) with 0.04 mL (0.05 mmol) *sec*-BuLi, 0.11 mL (0.74 mmol) TMEDA and 0.68 g (0.30 mmol) $(C_8F_{17}(CH_2)_3O)_4$-[G-1]-Br was used to make 20 kgmol^{-1} end-capped PB, 91% Yield, 79% end-capping M_n 24200, M_w 24900, M_w/M_n 1.03.

Sample Code: PBc50

7.5 g of butadiene (equivalent to 0.15 mmol of PB of the target molecular weight), 0.11 mL of *sec*-BuLi (0.15 mmol), 0.04 mL of DPE (0.23 mmol) with 0.21 mL (0.03 mmol) *sec*-BuLi, 0.07 mL (0.45 mmol) TMEDA and 0.41 g (0.18 mmol) $(C_8F_{17}(CH_2)_3O)_4$-[G-1]-Br was used to make 50 kgmol^{-1} end-capped PB, 86% Yield, 65% end-capping M_n 758000, M_w 78300, M_w/M_n 1.03.

1H NMR (700 MHz, DCM-d_2, δ, ppm): 5.6 (**C** CH_2CH), 5.4 (**A** *CHCH*), 5.0 (**B** CH_2CH), 2.1 (d, CH_2, polymer backbone), 2.09 (m, 8H, $CH_2CH_2CH_2$), 2.30 (m, 8H, CH_2CF_2), 4.1 (t, 8H, CH_2CH_2O), 3.3 (s, 2H, CH_2DPE), 4.96 (s, 4H, CCH_2O), 6.6 (t, 2H, Ar_2H), 6.51 (t, 1H, Ar_1H), 6.4 (d, 4H, Ar_2H), 5.7 (d, 2H, Ar_1H).

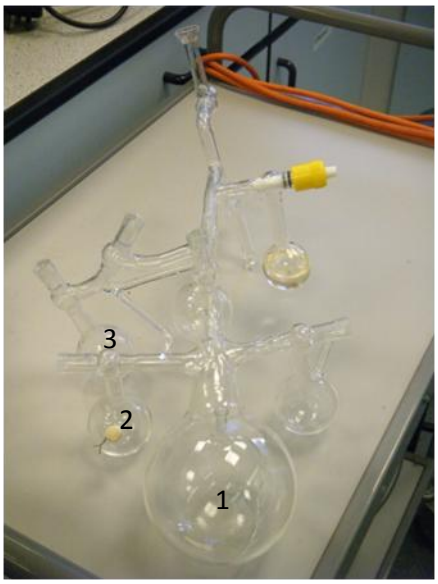

Figure 2:3 Modified "Christmas Tree" reaction vessel used for end-capping polymerisations

2.2.3 Polymer Saturation

2.2.3.1 Saturation of polybutadiene

In a round bottom flask, nitrogen was bubbled through a stirring solution of 3 g PB in 300 mL cyclohexane (1 g in 100 mL) overnight. The catalyst, 5 g, 5% Pd supported on $CaCO_3$, was then activated in a 2 L Parr reactor vessel by heating to 100°C under 100 psi H_2 for 2.5 hrs and cooled to room temperature. The amount of catalyst used was 1.5 times the weight of the polymer (or approximately 0.01 moles metal/mole of double bonds). Once cooled the PB solution was transferred by canulation, to the autoclave under nitrogen. The autoclave was then returned to the high pressure lab where it was filled with H_2 to 500 psi, heated to 100 °C and stirred for 16 hrs. This procedure has been reported previously[8-11]. Upon completion the reactor was cooled to room temperature and transported to the lab where any unreacted hydrogen was vented with care. The polymer suspension was removed, heated to around 70 ^{0}C and filtered hot to remove the catalyst. The solution was then concentrated and finally the polymer was precipitated out with methanol and dried to produce a white powder. ^{1}H NMR at 100^{0}C in TCE-d_1 is performed to establish the extent of saturation, FT-IR to show the characteristic band disappearance and DSC so the melting temperature of hydrogenated polyethylene can be directly compared with that of LLDPE.

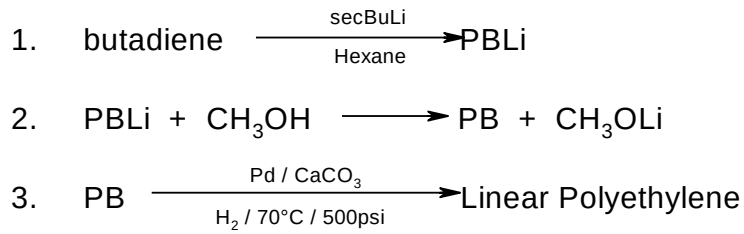

Figure 2:4 Reaction Scheme for production of LLDPE from butadiene monomer

The same procedure was followed for the 50, 100 and 200 kgmol-1PB. For the 5 $kgmol^{-1}$ PB the same procedure was also followed except that deuterium was used instead of hydrogen and the reaction was left to run for 48 hours yielding deuterium labelled polyethylene (dPE).

Sample Code: hPE50 Batch 1

Made from PB50, 3.11 g, 58% Yield M_n 56600, M_w 58900, M_w/M_n 1.04, 99.7% saturation.

Sample Code: hPE50 Batch 2

hPE50 batch 2, 3.42 g, 54% Yield, 100% saturation.

Sample Code: hPE100 Batch 1

Made from PB100, 3.14 g, 53% Yield, M_n 113000, M_w 117000, M_w/M_n 1.04, 98.62% saturation.

Sample Code: hPE100 Batch 2

hPE100 batch 2, 3.12 g, 57% Yield, 100% saturation.

Sample Code: hPE200 Batch 1

Made from PB200 Batch 1, 4.74 g, 81% Yield M_n 188000, M_w 203000, M_w/M_n 1.08, 99.4 % saturation.

Sample Code: hPE200 Batch 2

hPE120 batch 2, 3.56 g, 63% Yield, 100% saturation.

Beyond this point only 100% saturated polymers were used.

2.2.3.2 Saturation of End-capped Polybutadiene

The same procedure was followed for the eight fluoro-end-capped polymers but again deuterium was used instead of hydrogen and the reaction was left to run for 48 hrs yielding deuterium labelled end-capped polyethylene. The results are displayed in table

Made From	Mass /g	% Yield	% Deuteration	Sample Code
PBa5	0.96	31%	99%	**PEa5**
PBa10	0.96	96%	99%	**PEa10**
PBa20	2.56	69%	99%	**PEa10**
PBb5	3.71	64%	99%	**PEb5**
PBc5	1.66	72%	73%	**PEc5**
PBc10	1.03	82%	99.8%	**PEc10**
PBc20	0.87	73%	98%	**PEc20**
PBc50	1.98	44%	81%	**PEc50**

Table 2:1 Results from deuteration of end-capped polymers

2.3 Surface Properties

2.3.1 Spin Casting

Thin films were prepared for use in neutron reflectometry, ion beam experiments and contact angle measurements. 1% solutions in 1 mL of xylene were prepared with different concentrations of additive in different matrix polymers, see table 2:2. The matrix polymers used were 50 $kgmol^{-1}$, 100 $kgmol^{-1}$, 200 $kgmol^{-1}$ and the additives were PEa5, PEa10, PEa10, PEb5, PEc5, PEc10, PEc20 and PEc50, so 24 solution sets were prepared.

% Additive	% Matrix
0	100
1	99
2	98
4	96
8	92
12	88
16	84
20	80

Table 2:2 Ratio of additive to matrix mixtures

Thin films were prepared according to the following protocol:

1. The depth of SiO_2 layer on a silicon wafer substrate was measured using ellipsometry
2. The substrate was placed on the vacuum chuck and heated with a hot air gun
3. The polymers were dissolved in hot xylene solvent and deposited onto the substrate

4. The substrate was then rotated at ~1500 rpm resulting in the solution spreading evenly over the surface
5. Most of the solvent evaporates, leaving a thin polymer blend film.

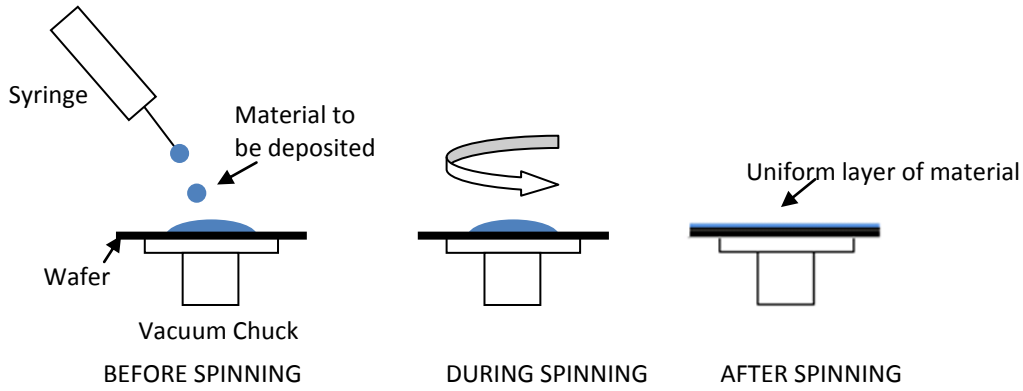

Figure 2:5 Procedure for thin film preparation by spin casting

6. The films were then annealed for 1 hr at 110 ^{0}C
7. Thickness of the thin film was measured again by elipometry.

2.3.2 Ellipsometry

A Sentech SE500 combined ellipsometer/reflectometer, equipped with a 632.8 nm He-Ne laser and a white light source (500 – 900 nm for reflectometry) was used. Only the elliposmeter was used and a refractive index of 1.46 and 1.51 was programmed in when measuring the SiO_2 layer and the polymer film depth respectively.

2.3.3 Contact Angles (CA)

The apparatus used for contact angle measurements was a Rame-Hart goniometer model 100-00-230, where a droplet (5 µm) of purified water, glycerol or dodecane was put on the material by the means of a micropipette. The results of the two contact angle fluids were used to determine the surface free energy of the film. Owens and Wendt[12] developed a method which divides the surface tension into two components, dispersive and polar, and uses a Geometric Mean Approach to combine their contributions. When combined with Young's equation it yields:

Equation 2:1

where the square root of the surface tension, γ, for the polar (P) and dispersive (D) components of the liquid (l) and solid (s) parameters are multiplied. Six CA measurements were taken and averaged, to ensure reliability of the results and estimate the error. The results of surface free energy versus % additive were then plotted and directly compared. Samples used for CA analysis

were prepared using spin casting, described in section 2.3.1, as a result seven different compositions were made (1-20% additive) for each of the 8 additives in 3 different matrices.

2.3.3.1 Data Analysis

Samples were analysed using two contact fluids water and either dodecane or glycerol. Using the Owens-Wendt equation their surface free energy was calculated.

2.3.4 X-ray Photoelectron Spectometry (XPS)

X-ray photoelectron spectroscopy (XPS) is a surface sensitive technique that provides quantitative compositional information 1-10 nm from the surface. It measures the distribution in photoelectron kinetic energy and converts this information into atomic surface compositions and can detect all elements except hydrogen and helium[13, 14]. To generate quantitative elemental composition each raw XPS signal must be corrected by dividing its signal intensity by a "relative sensitivity factor" and normalised over all the elements detected. The kinetic energy of the electrons can act as a unique fingerprint to indentify the atom and orbital from which it originated. To do this XPS must be performed under ultra-high vacuum. Samples used for XPS analysis were prepared as follows, table 2:3, and spun cast on Si substrates:

Additive = PEa5 Matrix = hPE100	
% Additive	**% Matrix**
4	96
12	98
20	80

Additive = PEc5 Matrix = hPE100	
% Additive	**% Matrix**
4	96
12	98
20	80

Additive = PEc5 Matrix = hPE200	
% Additive	**% Matrix**
4	96
12	98
20	80

Additive = PEb5 Matrix = hPE50	
% Additive	**% Matrix**
1	99
4	96
12	98
20	80

Additive = PEb5 Matrix = hPE100	
% Additive	**% Matrix**
1	99
2	98
4	96
8	92
12	88
16	84
20	80

Additive = PEb5 Matrix = hPE200	
% Additive	**% Matrix**
1	99
4	96
8	92
12	98
16	84
20	80

Table 2:3 Samples prepared for XPS measurements of various blends of additives and matrices

2.3.4.1 Data Analysis

XPS analysis was carried out by Emily Smith at the open access Nottingham XPS facility funded by EPSRC. The software used to view the data was CASAXPS. The percentage concentrations of

fluorine and carbon were then used to calculate the percentage composition of fluorocarbons at the surface.

2.4 Surface Organisation

2.4.1 Ion Beam Analysis (IBA)

The NEC 5SDH Pelletron accelerator at Durham University produces a monoenergetic beam of helium ions. At the source a 100 kHz radio frequency pulse converts He into a plasma. The source is held under a constant potential of 6kV and is insulated. Rubidium vapour, which is produced under reflux conditions, then converts the He^+ to neutral or negative charge. The negative He ions in the plasma are then extracted towards the Pelletron using a gap lens. An einzel lens focuses the negative ions which are accelerated to the positive terminal of the tandem accelerator. Once inside the accelerator the negative He ions collide with the N_2 gas, which strips their electrons changing their charge to positive or neutral. The positive ions are accelerated away due to their charge repulsion from the centre of the accelerator towards the quadropole magnets. After the positive He ions have exited the accelerator quadropole magnets focus the beam and then bending magnets separate the ions according to their mass to charge ratio. The magnetic field can be tuned so the correct species is directed down the beam line. The ion beam is then deflected by steering magnets and further re-focused using additional quadropoles. Finally the beam reaches the end station (sample chamber). It is important that a high vacuum is used and no air leaks into the system so that the detected atoms can be properly analysed, as energy is lost on particle collision e.g. air leaks.

Deuterium can be profiled using helium where the energy of the detected fast proton depends on the depth of the deuterium in the sample[15] according to the equation, where the short hand is $^2D(^3He,p)\alpha$ + 18.35 MeV:

$$^3He + D \rightarrow \alpha + p + 18.353MeV$$

Films previously characterised by CA analysis were placed in the end-station and analysed using nuclear reaction analysis (NRA). The samples were aligned in the end-station by using the ion beam as a marker, the polymer glows when the ion beam is grazing off the surface, at an angle of -85° and -83°. The details of Ion Beam Analysis and nuclear reaction analysis are discussed in more detail in Appendix 1.

2.4.1.1 Data Analysis

The data obtained is of the form Counts (of recoil particles detected) *vs* Channel (energy of recoil particles) from which the energy of the detected proton is known and a depth profile can be

calculated. A simulation of the intensity at a given channel can be calculated for any polymer using proprietary software such as SIMNRA[15] or DataFurnace[16]. Then the experimental counts can be converted into a "corrected volume fraction" and plotted against the calculated deuterium depth at the appropriate channel. The experimental data can be modelled using a Fortran program with the following variables:

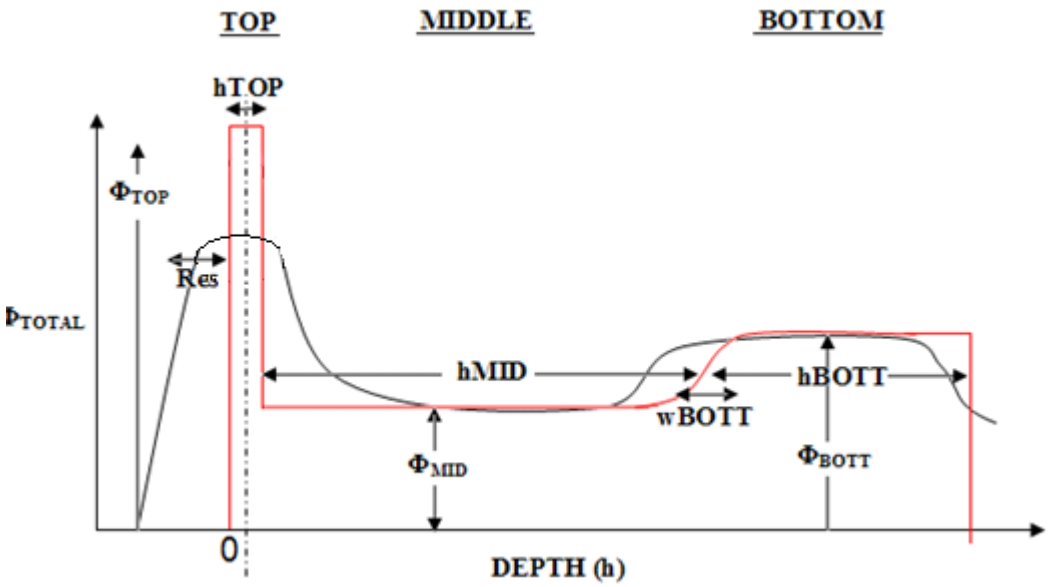

Figure 2:6 Illustration describing the physical representation of the fitting parameters for NRA

The model composition profile (red) is convolved with the instrument resolution to yield the black curve which is fitted to experimental data be adjusting the parameters which were smeared by the resolution of the measurement.

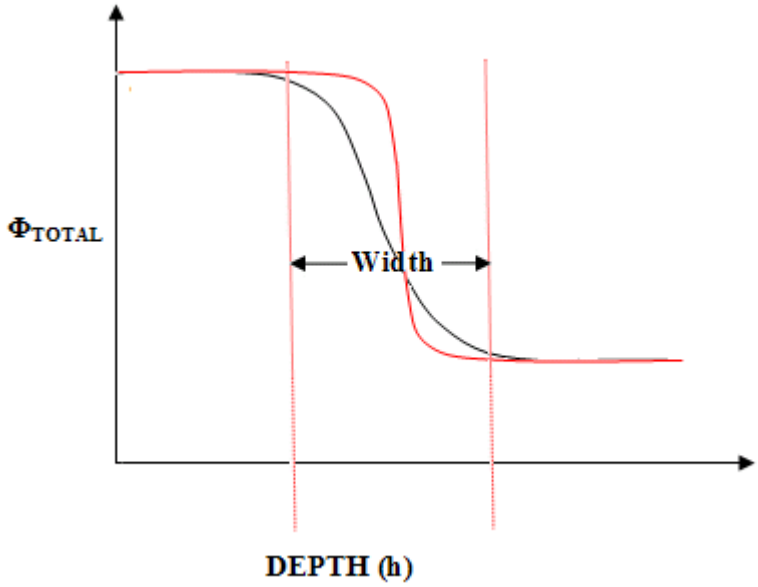

Figure 2:7 Illustration of the "width" variable used in NRA modelling

The depth scale is defined in terms of how much matter was transversed by the incident and detected particles. Thus, the depth scale is reported in units of atoms/cm^2. To convert the depth scale into more familiar units, e.g. nm or microns, then the density of the sample needs to be supplied. The surface excess, z^*, is then calculated by the following equation:

Equation 2:2

2.4.2 Neutron Reflectometry (NR)

Neutron reflectometry measures the specular reflection of neutrons off smooth surfaces as a function of scattering vector and is sensitive to deuterium. The scattering vector, Q, is defined as the change in momentum measured between the initial and final direction of a neutron beam ($Q = (4\pi/\lambda) \sin\theta$ (where λ is the wavelength of the neutron)). In chapter 5 the specular reflection is discussed in terms of the reflectivity *R(Q)* as a function of Q, where *R(Q)* is the ratio of the reflected intensity to the incident intensity.

The Inter reflectometer at ISIS is equipped with three fully shielded ^{3}He gas detectors for routine measurement of both transmitted and reflected beams and a two-dimensional multi-detector. A Q range from 0.008 to 0.5 Å^{-1} was used in this study, which necessitated the use of two different incident angles of 0.6 and 2.3°.

Samples prepared for NR analysis were prepared as follows, table 2:4, and spun cast onto thick Si blocks.

Additive = PEa5 Matrix = hPE35	
% Additive	**% Matrix**
1	99
2	98
4	96
8	92
12	88
16	84
20	80

Additive = PEa5 Matrix = hPE50	
% Additive	**% Matrix**
1	99
2	98
4	96
8	92
12	88
16	84
20	80

Additive = PEa5 Matrix = hPE100	
% Additive	**% Matrix**
1	99
2	98
4	96
8	92
12	88
16	84
20	80

Table 2:4 Samples prepared for NR analysis of various blends of additives and matrices

The beam was collimated to ensure that the footprint of the beam was the same as the sample surface area, then the sample was aligned to maximise the reflected intensity, using successive height and phi scans.

2.4.2.1 Data Analysis

Data reduction was performed by removing the noisy data at the extremes of Q, from the raw data. Specular *R(Q)* became indistinguishable from background at Q>0.3 $Å^{-1}$. The data collected from both incident angles was then rebinned then combined into a single ASCII file. Analysis of neutron reflectivity data is usually performed by a process of proposing layered models from which exact reflectivity profiles can be calculated and fits obtained by altering various parameters. First the specimen is divided into a number of layers of defined thickness and composition, and the reflectivity of this lamella stack is calculated by the exact optical matrix methods and compared by a least squares method to the experimental reflectivity. In this model the instrument resolution was incorporated, 5%, a roughness of 5 Å at the air polymer and polymer-substrate interfaces, and a silicon oxide layer of 25 Å.

2.5 Bulk Properties

2.5.1 Quasielastic Neutron Scattering (QENS)

Quasielastic neutron scattering is a form of inelastic scattering where the energy of scattered neutrons is measured relative to their incident energy. The energy transfer peak is located around transfer energy, E=O. In practise the peak width is always finite due to the instrumental energy resolution. The incident neutron beam is monochromated and collimated, but before detection can take place the energy of the scattered neutron is analysed. The analysis requires a crystal analyser (or a time-of-flight method) in order to resolve the energy transfer during scattering, figure 2:8.

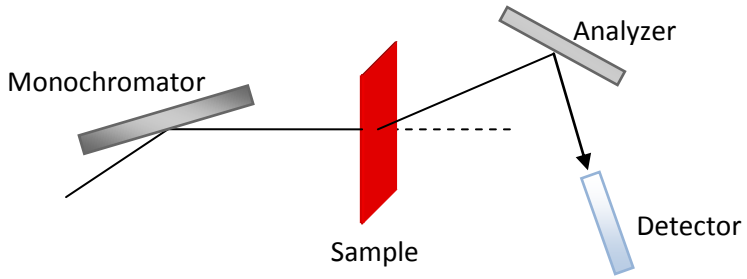

Figure 2:8 Schematic neutron beam set-up used during QENS

Both *Q* and E are resolved. QENS corresponds to the energy transfer around zero (elastic scattering) and may be used to investigate dynamic processes, such as diffusion modes. IRIS, figure 2:9, is a time-of-flight inverted-geometry crystal analyser spectrometer designed for quasi-elastic and low-energy high resolution inelastic spectroscopy (low wavelength diffraction capabilities). By altering the chopper frequency the energy transfer range (inelastic) or d-spacing range (elastic) can be changed. During both quasielastic and inelastic neutron scattering the energy of scattered neutrons are analysed by means of Bragg scattering from a large array of single crystals (pyrolytic graphite and muscovite mica) in close to backscattering geometry. Only those neutrons with correct energy or wavelength to satisfy the Bragg condition are directed towards the detector bank. By recording the time-of-arrival of each analysed neutron in a detector relative to t_0, the energy loss or gain process occurring within the sample can be investigated. By then measuring the total time-of-flight and having an accurate knowledge of the time-of-arrival of each analysed neutron, the flight path of the analysed neutrons and the primary neutrons then the energy exchange within the sample can be determined.

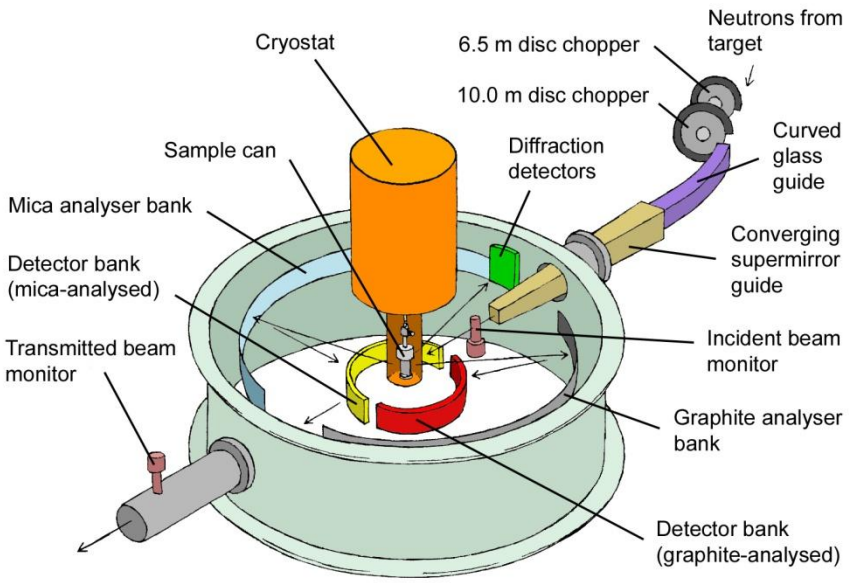

Figure 2:9 IRIS instrument used at RAL[17]

Samples prepared for QENS analysis were prepared as follows, table 2:5, and melt pressed to form 30×65mm rectangles that were either 0.1 mm (required 0.3 g of material) or 0.2 mm (required 0.6g material) thick.

SAMPLE	dPE /g	hPEa20 /g	hPE20 /g	Thickness /mm	%Additive
1	0.201	0.051	0	0.1	20
2	0.172	0.074	0	0.1	30
3	0.261	0.260	0	0.2	50
4	0.201	0	0.051	0.1	20
5	0.175	0	0.075	0.2	30
6	0.206	0	0.202	0.2	50

Table 2:5 Samples prepared for QENS measurements of blends of additives and matrices

The three different materials used were a control sample, hydrogenated PE20 (20 $kgmol^{-1}$ polyethylene), hydrogenated PEa20 (20 $kgmol^{-1}$ polyethylene with end-group A) and deuterated polyethylene, supplied by Polymer Source (Canada).

2.5.1.1 Data Analysis

The data was reduced by converting the measured time-of-flight data into S(Q,ω) by summing the spectra into groups and converting from detector angle to Q-value. The reduced data were then analysed by performing a Fourier Transformation of S(Q,ω) to *I(Q,t)* and fitting scattering functions to stretched exponential decays. Two programs, MODES[18] developed by ISIS and DAVE[19] developed by NIST were used to analyse the data.

2.5.2 Small angle Neutron Scattering (SANS)

Small angle neutron scattering is another bulk technique used for determining structural dimensions in the nanometre range, up to ~200 mn. These instruments measure in the low-Q region, which can be realized either through the use of small angles or long wavelengths (or both). In order to obtain small angles, good collimation and good resolution area detectors are needed. Good collimation is achieved through the use of long neutron flight paths before and after the sample. SANS2D provides enhanced signal to noise and/or shorter collection times compared to other SANS instruments e.g. LOQ. It exploits the time-of-flight techniques and by using multiple position-sensitive detectors, claims unsurpassed simultaneous data collection across the entire range of length scales (0.002 $Å^{-1}$ < Q < 3.0 $Å^{-1}$). By moving the detector away from the sample the resolution is increased but the intensity decreases[20].

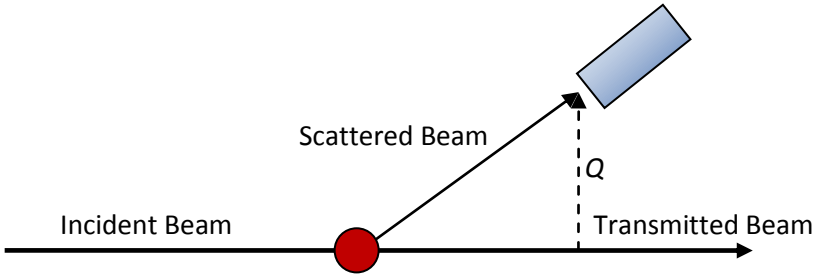

Figure 2:10 Beam direction and *Q* measured during SANS

The cell used for SANS measurements was a 7-position heating block made out of aluminium, transparent to neutrons. The diameter of each sample was 1.5 cm and is characterized by a sample thickness of 1 mm. Samples were placed between 2 aluminium windows and sealed using o-rings and tightening retainers on each side, figure 2:11.

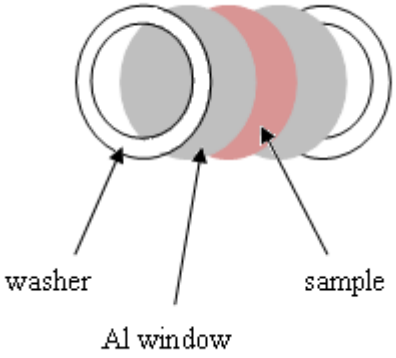

Figure 2:11 SANS sample holder

Samples used for SANS analysis were prepared as follows. A polymer blend was made by co-dissolving an additive with a perdeuterated matrix (deuterated PE, supplied by Polymer Source) in xylene and precipitating into methanol. Once dried the polymer blend was pressed into ~1 mm thick, x15 mm diameter discs. This required ~0.15 g of total polymer for each sample. The same molecular weight of additive was used, but each had a different end-group. This allowed the study of the end-group, on aggregation. The reason the matrix was deuterated was this gives the best contrast and lowest background. The additives used were PEb5 and PEc5 in the following ratios:

Additive %	Matrix %
1	99
2	98
4	96
8	92
12	88
16	84

Table 2:6 Polymer blends used for SANS

2.5.2.1 Data Analysis

In order to obtain a complete set of SANS measurements the runs required are

- Transmission from the sample
- Scattering from the sample
- Scattering from empty cell (estimates the incoherent scattering which is performed just in case there is anisotropy in the data)
- Transmission from the empty cell
- Scattering from the blocked beam
- Transmission from the empty beam
- Detector sensitivity from the plexiglass (only needed when the small-angle approximation is not valid) providing a correction to the detector efficiency.

Once this data has been obtained it needs to be reduced and rescaled to form the absolute differential scattering cross section $d\Sigma/d\Omega$ (units of inverse length). Data reduction involves calculating the various transmissions, subtracting the empty cell and the blocked beam, rescaling the 2D data to an absolute cross section, masking the unwanted detector cells, and radially averaging to obtain 1D data.

Data analysis methods for SANS involve either rapid interpretation using standard linear plots e.g. Guiner or Porod, or non-linear least-squares fitting to a model scattering function. Examples include the “Random Phase Approximation” (RPA) used to describe compatible macromolecular

blends with a small interaction parameter, whereas "Ornstein-Zernike" (OZ) is used to describe particulate scattering such as microphases in block polymers[21]. Analytical solutions for the OZ method include the Percus-Yevick equation, a simple analytical form for hard sphere interaction potential between spherical particles, the Mean Spherical Approximation, for charged particulate systems and the Zero Average Contrast method which uses deuterated and non-deuterated mixtures to isolate the single chain form factor[22].

2.5.3 Differential Scanning Calorimetry

Differential scanning calorimetry (DSC) is a type of thermal analysis. It is a technique that measures heat flow into or out of a material as a function of time or temperature thus measuring the thermal transitions of a polymer. DSC measures the differences in energy required to maintain the sample and a reference sample at the same temperature whilst raising the temperature of both at a fixed rate.

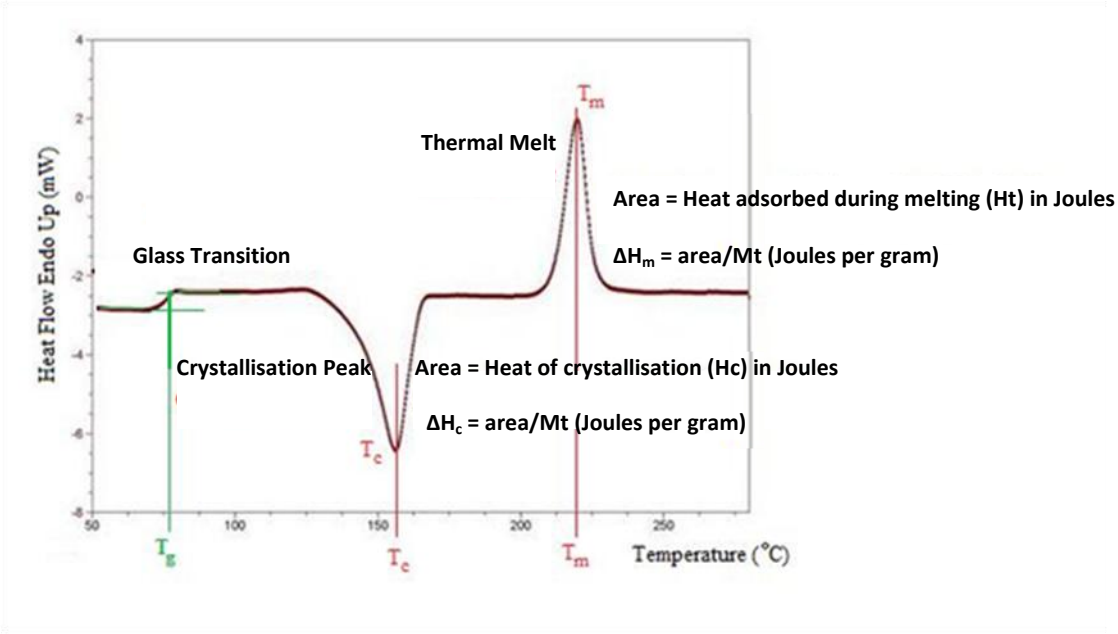

Figure 2:12 Sketch of a typical DSC isotherm illustrating the information that can be obtained.

DSC plot explained:

- At low temperatures molecular motion is restricted to molecular vibration – *glassy state* (polymer is hard rigid and brittle). On heating segments of the entangled chain can move and the amorphous glassy state becomes *rubbery*, soft and flexible. At the "Glass Transition Temperature" (which takes place over a temperature range) there is an increase in the heat capacity of the polymer. The

middle value is usually taken as the T_g. (This is a *second order transition* whereas melting and crystallisation are *first order*)

- Above the glass transition polymers have much more mobility and diffusion can take place. Once they have gained enough energy they may form very ordered arrangements – crystals. Large amounts of heat are given off when forming a crystalline arrangement. Only semi crystalline or crystalline samples have a latent heat of crystallisation as amorphous samples do not crystallise.

- As a polymer melts the crystals formed on crystallisation melt and again the polymer can move freely. As crystallisation is an exothermic transition, melting is an endothermic one and the temperature will only rise once all the polymer has melted. Only polymers which can form crystals will have a melting peak in a DSC isotherm.

2.5.3.1 Data Analysis

From a DSC isotherm a polymer's crystallinity can be determined by quantifying the heat associated with fusion (melting), ΔH_m, of the polymer and the theoretical heat of fusion, ΔH_m^*, for the polymer. The theoretical heat of fusion is that of 1 g of 100% crystalline polymer. The ΔH_m^* literature value for PE used during this study was 289 J/g[23].

Equation 2:3

Another way is to divide ΔH_m by ΔH_m^* which would give the amount of crystallinity after crystallisation.

Equation 2:4

Above the crystallisation temperature a polymer sample is effectively amorphous. The latent heat of crystallisation represents the heat given off when a certain amount of the sample forms crystalline regions and makes the sample semi-crystalline. Looking to below the crystallisation temperature the polymer forms both crystalline and amorphous regions. The latent heat of melting tells us the heat required to break all the intermolecular bonds formed on crystallisation.

2.5.4 Thermogravimetric Analysis (TGA)

TGA measures changes in the weight of a sample as a function of temperature and/or time. TGA is used to determine polymer degradation temperatures, residual solvent levels, absorbed moisture content, and the amount of inorganic (non-combustible) filler in polymer or composite material compositions. In the samples analysed by TGA the temperature at which 98% of the polymer remained was quoted as the decomposition temperature. All the materials were analysed by TGA, also the several blended additives PEa5, PEb5 and PEc5 in three polymer source matrices were analysed in following ratios:

% Additive	% Matrix	PEa5 Matrix M_w	PEb5 Matrix M_w	PEc5 Matrix M_w
1	99	79000	79000	82000
2	98	79000	79000	82000
4	96	79000	79000	82000
8	92	79000	79000	82000
12	88	79000	79000	79000
16	84	79000	82000	79000

Table 2:7 Samples prepared for TGA Analysis

2.5 Atomic Force Microscopy (AFM)

AFM is a powerful surface imagining technique which uses a fine probe to scan the sample surface. Deflections of the probe are detected by a laser reflected from the back surface of the probe tip and are used to characterise the surface topography of the sample. The instrument used was a Digital Instruments Nanoscope IV scanning probe microscope and tapping mode was used[24].

Blended samples, 12%, were used for all measurements and five different cooling conditions were explored and AFM images and NRA data collected.

2.5.1 Data Analysis

Using the data software "Nanoscope v6.13" the images were smoothed and the roughness value obtained. Secondly a surface section was taken creating a surface profile and using the angle of an imaginary line drawn, the angle of the height deviations with each sample were obtained.

2.6 References

1. Porath, J.; Flodin, P., *Nature* **1959,** *183* (4676), 1657-1659.
2. Narrainen, A. L.; Hutchings, L. R.; Ansari, I. A.; Clarke, N.; Thompson, R. L., *Soft Matter* **2006,** *2* (2), 126-128.
3. Cardoen, G.; Breitenkamp, K.; Emrick, T.; Coughlin, E. B., *Macromolecules* **2006,** *39* (20), 7170-7173.
4. Uhrig, D.; Mays, J. W., *Journal of Polymer Science Part a-Polymer Chemistry* **2005,** *43* (24), 6179-6222.
5. Hadjichristidis, N.; Iatrou, H.; Pispas, S.; Pitsikalis, M., *Journal of Polymer Science Part a-Polymer Chemistry* **2000,** *38* (18), 3211-3234.
6. Sugiyama, K.; Nemoto, T.; Koide, G.; Hirao, A., *Macromolecular Symposia* **2002,** *181*, 135-153.
7. Narrainen, A. P.; Hutchings, L. R.; Ansari, I.; Thompson, R. L.; Clarke, N., *Macromolecules* **2007,** *40* (6), 1969-1980.
8. Hadjichristidis, N.; Xenidou, M.; Iatrou, H.; Pitsikalis, M.; Poulos, Y.; Avgeropoulos, A.; Sioula, S.; Paraskeva, S.; Velis, G.; Lohse, D. J.; Schulz, D. N.; Fetters, L. J.; Wright, P. J.; Mendelson, R. A.; Garcia-Franco, C. A.; Sun, T.; Ruff, C. J., *Macromolecules* **2000,** *33* (7), 2424-2436.
9. Rachapudy, H.; Smith, G. G.; Raju, V. R.; Graessley, W. W., *Journal of Polymer Science Part B-Polymer Physics* **1979,** *17* (7), 1211-1222.
10. Hillmyer, M. A.; Bates, F. S., *Macromolecules* **1996,** *29* (22), 6994-7002.
11. Donkers EHD, W. R., Klumperman B, *Journal of Polymer Science Part A-Polymer Chemsitry* **2005,** *43* (12), 2536-2545.
12. Owens, D. K.; Wendt, R. C., *Journal of Applied Polymer Science* **1969,** *13* (8), 1741-&.
13. Hollas, J., *Modern Spectroscopy*. 3rd Edition ed.; John Wiley and Sons, NY.
14. Brown, J., *Molecular Spectroscopy*. Oxford University Press: 2003; Vol. 55.
15. Mayer, M. *SIMNRA User's Guide*; 9/113; Max-Planck-Institut für Plasmaphysik: Garching, 1997, 1997.
16. Barradas, N. P.; Jeynes, C.; Webb, R. P., *Applied Physics Letters* **1997,** *71* (2), 291-293.
17. http://www.isis.stfc.ac.uk/images/instruments/iris-/iris-schematic4923.jpg, QENS, last accessed March 2010
18. http://www.isis.stfc.ac.uk/instruments/iris/data-analysis/sotware-for-iris/osiris-data-analysis4697.html MODES.
19. http://www.ncnr.nist.gov/dave/ DAVE, last accessed March 2010
20. Lodge, T., *Mikrochimica Acta* **1994,** *116* (1-3), 1-31.
21. Hammouda, B., *Polymer Reviews* **2010,** *50* (1), 14-39.
22. Higgins, J.; Benoit, H., *Polymers and Neutron Scattering*. Clarendon Press - Oxford Science Publications: 1996.
23. Brandrup, J.; Immergut, E. H., *Polymer Handbook*. 3rd ed.; John Wiley & Sons, NY: 1989.
24. Butt, H. J.; Cappella, B.; Kappl, M., *Surface Science Reports* **2005,** *59* (1-6), 1-152.

3 Polymer Synthesis- Results and Discussion

This chapter discusses the synthesis of the polymers used in this study. Firstly the synthesis of polybutadiene is discussed, followed by the synthesis of the end-capping agents and end capped polybutadiene. Finally the results of the polymer saturation reactions will be reviewed.

The three types of polymers that were made were unfunctionalised high molecular weight hydrogenous polyethylene, functionalised low molecular weight deuterated polyethylene and unfunctionalised low molecular weight deuterated polyethylene. The higher molecular weight hydrogenous polymers were used as matrix polymers and the functionalised low molecular weight deuterated polymers as additives. By deuterating polymers they may be easily identified separately from hydrogenated polymers when using specific characterisation techniques. The additives were designed so that they undergo surface segregation and moreover, because the polymer backbone is the same as the matrix it increases compatibility and ensures that the additive is anchored securely at the surface through chain entanglements with the bulk.

Finally, identical lower molecular weight unfunctionalised deuterated polyethylene was synthesised so the effect of functionalisation on surface segregation could be isolated from the effect of deuteration upon diffusion/segregation at the surface.

3.1 Synthesis of Polybutadiene

Polybutadiene was prepared via living anionic polymerisation of butadiene in a non polar solvent, hexane, with *sec*-butyllithium as the initiator, using standard high vacuum techniques. The use of a lithium initiator and a non polar solvent was chosen to produce a polymer with a microstructure that was predominantly 1,4-enchainment rather than 1,2-enchainment. A high 1,4 content in polybutadiene results in a polymer which resembles linear low density polyethylene following saturation of the double bonds with either hydrogen or deuterium. Figure 3:1 illustrates the routes by which different microstructures are obtained during butadiene polymerisations.

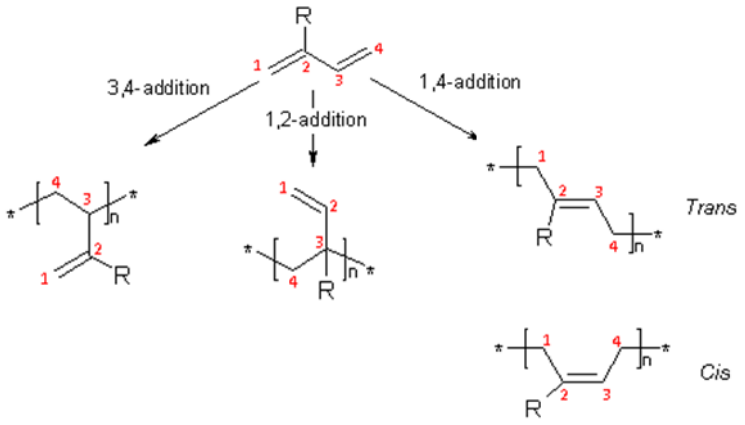

Figure 3:1 Diagram to illustrate the possible microstructures of diene addition

During the polymerisation of butadiene there can only be either 1,2 or 1,4 addition. This is because if the "R" group is replaced with a hydrogen, 3,4 becomes the same as 1,2. Secondly, if one of the hydrogen's is replaced with an alkyl group, e.g. isoprene, then there can also be (3,4-addition).

When using anionic polymerisation, the molecular weight of the resulting polymers can be carefully controlled. In this study, a range of molecular weights from 5– 200 $kgmol^{-1}$ were synthesised. Molecular weights and polydispersity values were obtained by size exclusion chromatography (SEC) and the microstructure obtain by ^{1}H-NMR – the details of which are given in table 3:1. In all but one case the resulting polymers had the narrow molecular weight distributions associated with a living polymerisation but in some cases, especially at higher molecular weights, there was a discrepancy between the target and experimental molecular weight. The final column in table 3:1 shows the % error in this discrepancy.

Sample Code	Target M_n	M_n (SEC) / $gmol^{-1}$	M_w (SEC) / $gmol^{-1}$	% 1,4-PB	% 1,2-PB	M_w/M_n	% Error
PB5	5000	4900	5000	91	9	1.02	2
PB10	10000	10700	11000	93	7	1.03	7
PB20	20000	23700	25400	93	7	1.07	19
PB50	50000	59500	60500	94	6	1.02	19
PB50	50000	56600	58900	93	7	1.04	13
PB100	100000	113000	117000	93	7	1.04	13
PB200	150000	135000	200000	93	7	1.48	10
	Fraction	205000	210000			1.02	37
	Fraction	223000	236000			1.06	49

Table 3:1 Summary of results of polybutadiene synthesis

In most cases the experimental molecular weight is slightly higher than the target molecular weight, the most being 15%, however this is still more than acceptable for an anionic polymerisation. If this error was constant it would be correct to presume that the concentration of the initiator was incorrect, however, as the % error tends to be higher as the target molecular weight increases a more likely explanation is the presence of traces of impurities. In section 1.3.2.3 there is a general discussion regarding the affect that impurities have on a living polymer system. In this section it was put to the reader that it is practically impossible to eliminate all traces of impurity. The reason for this is as the molecular weight of a polymer increases the amount of initiator decreases thus the effect that trace amounts of impurities has becomes more pronounced. Therefore, increasing the molecular weight makes the polymerisation harder to control.

The polydispersity in all cases (bar one) fell within the acceptably narrow range for anionic polymerisations. However, the PDI for PB200 was much broader than expected. The magnitude of the PDI and the increased molecular weight suggested that there were slow reacting impurities in the system resulting in propagation competing with termination, e.g. a leak in the vessel. Since a narrow polydispersity was desired this sample was fractionated into two low polydispersity fractions, fraction 1 and fraction 2. Fraction 1 was consequently used as it had the lowest PDI. The SEC trace of PB200, figure 3:2 and 3:3, illustrates a bump, at the high molecular weight side, which could be the results of a slow leak or coupling and the long tail at the low molar mass side is due to either the concentration of the initiator being lower or impurities being introduced terminating the polymer before all the monomer had been consumed.

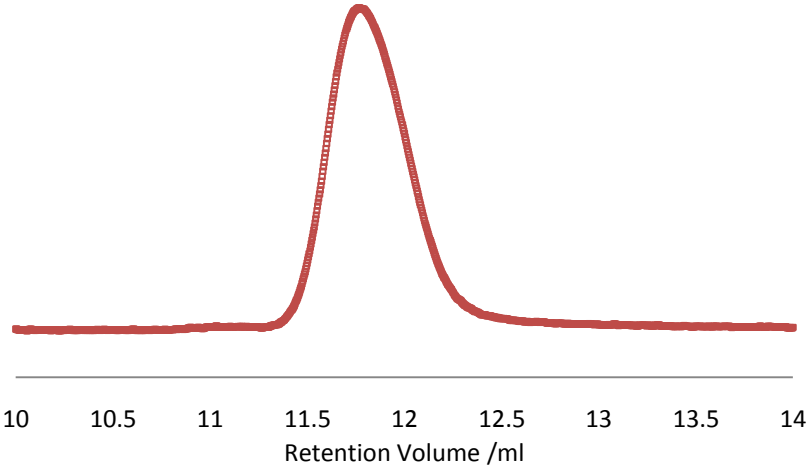

Figure 3:2 GPC trace of PB200 before fractionation showing broad PDI and baseline

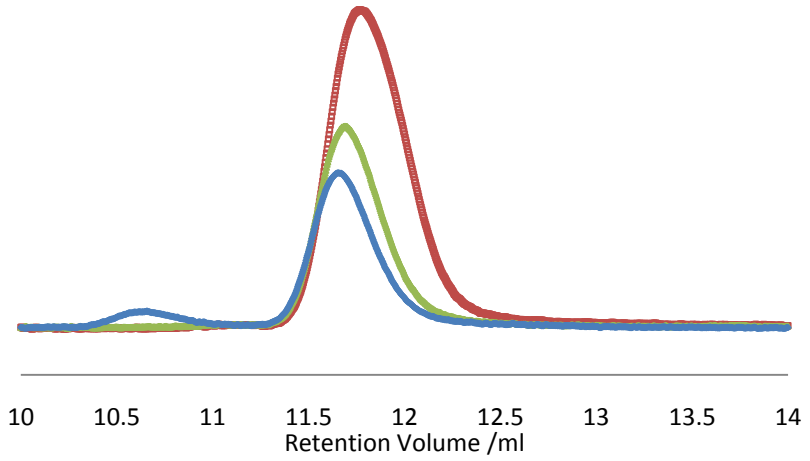

Figure 3:3 GPC trace of PB200 of Δ PB200 O PB200 fraction 1 and □ PB200 fraction 2

By examining the H^1 NMR (700MHz, $CDCl_3$) the microstructure of the synthesised polybutadiene can be calculated. Figure 3:4 shows an example of the procedure used to calculate microstructure for PB50, which was calculated to be 7% 1,2-polybutadiene and 93% 1,4-polybutadiene. This is consistent with ratios obtained when using hexane as a solvent.

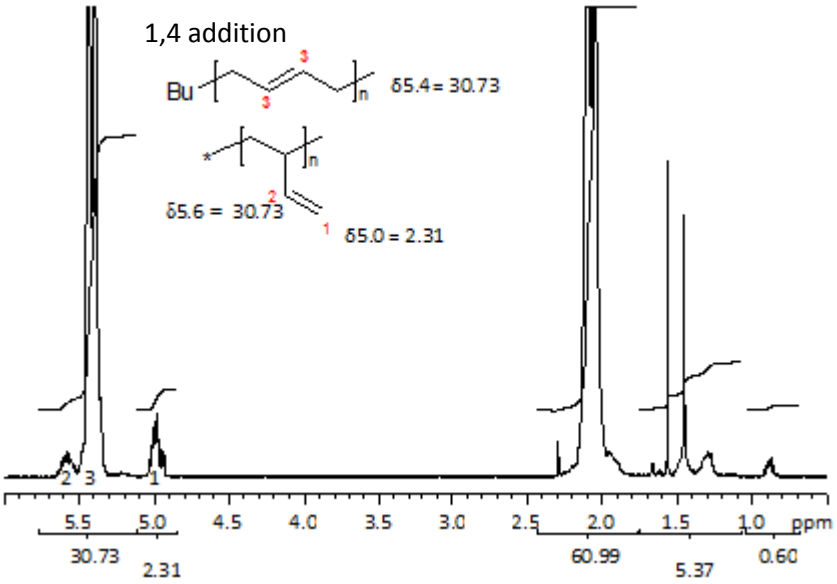

Figure 3:4 NMR spectrum illustrating the Microstructure of polybutadiene

CH_2 at δ5.0 has an integral of 2.31 (which is for 2H) – so the integral for 1H = 1.155

CH at δ5.6 is for 1H so its integral would be 1.155

HC=CH at δ5.4 is for 2H = 30.73 – 1.16 = 29.57, so 1H = 14.79

1,4 : 1,2

14.79 : 1.16

1,4 = 14.79/ (14.79+1.16) ~ 93%

1,2 = 1.16/ (1.16+14.79) ~ 7.0%

3.2 Synthesis of Fluoroalkylbromide End-capping Agents

Following the synthesis previously reported by Narrainen et al[1] a series of fluoroalkyl end capping agents were prepared, figure 3:5.

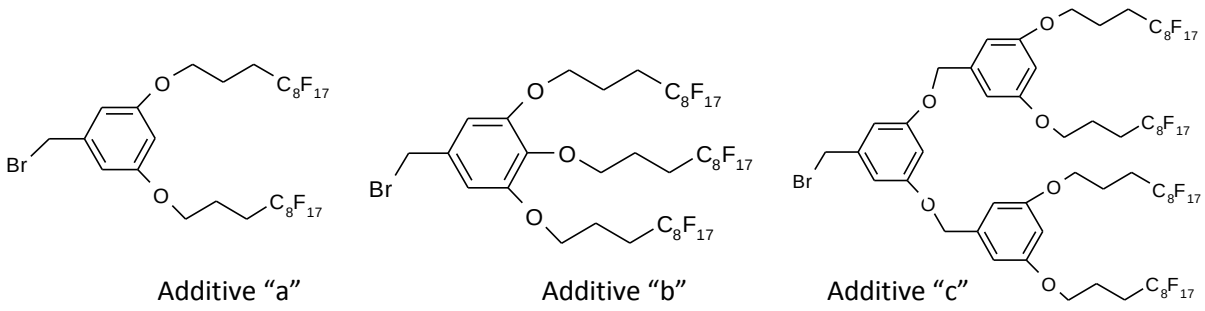

Figure 3:5 Illustration of synthesised end capping agents with 2CF groups (additive "a"), 3CF groups (additive "b") and 4CF groups (additive "c")

Synthesis of Type "a" End-capping agent. Type "a" end-capping agents were made in three steps via the Appel reaction between 3-(perfluorooctyl)-1-propanol, triphenyl phosphine and carbon tetrabromide followed by a Williamson coupling reaction between 3-(perfluorooctyl)propyl bromide and 3,5-dihydroxybenzyl alcohol. Finally, the alcohol functionality in the resulting product was then converted to the desired bromide functionality by reaction with CBr_4/PPh_3 according to the reaction scheme below, figure 3:6.

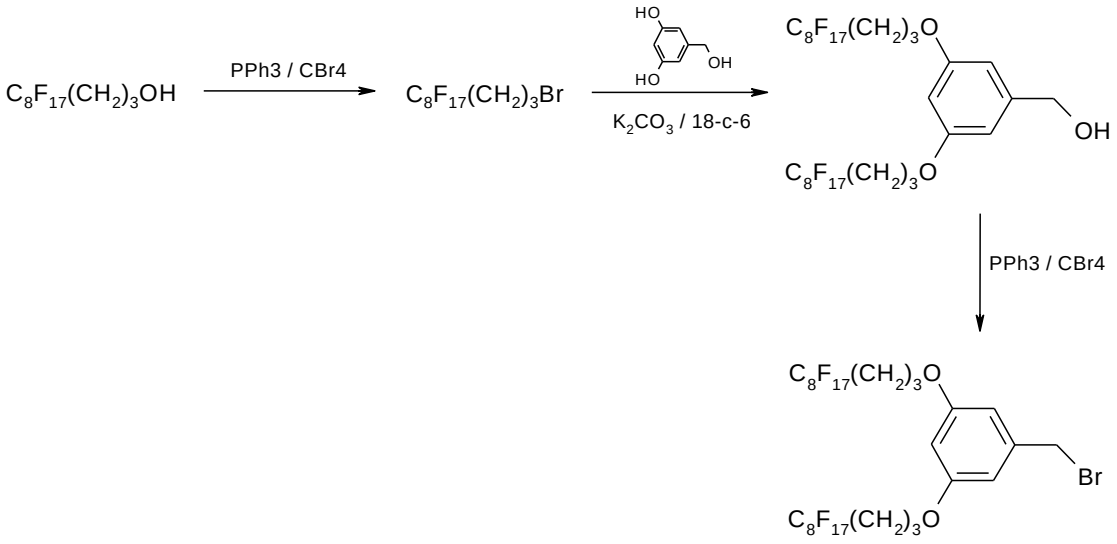

Figure 3:6 Synthesis of Type "a" End-Capping Agents

When preparing 3-(perfluorooctyl)propyl bromide from 3-(perfluorooctyl)-1-propanol NMR analysis revealed at peak at 3.6ppm (t, 2H, CH_2OH), indicating the presence of a small amount of the unreacted alcohol as the reaction had not gone to completion. However, it was decided not to attempt to remove this impurity from the product since it could play no part in the subsequent reaction. The yield for the first stage was 68%. The Williamson coupling reaction had a yield of 66%. The final Appel reaction had a yield of 76% but was complicated by the removal of triphenyl

phophineoxide. I discovered that stirring the recrystallised crude product in methanol for several hrs removed any remaining phosphine impurities.

Synthesis of Type "b" End-Capping Agent. Type "b" end-capping agents, were made (by a fellow group member, William Bergius) via the Appel reaction between 3-(perfluorooctyl)-1-propanol, triphenyl phosphine and carbon tetrabromide followed by a Williamson coupling reaction between followed by an Appel reaction according to the reaction scheme below, figure 3:7.

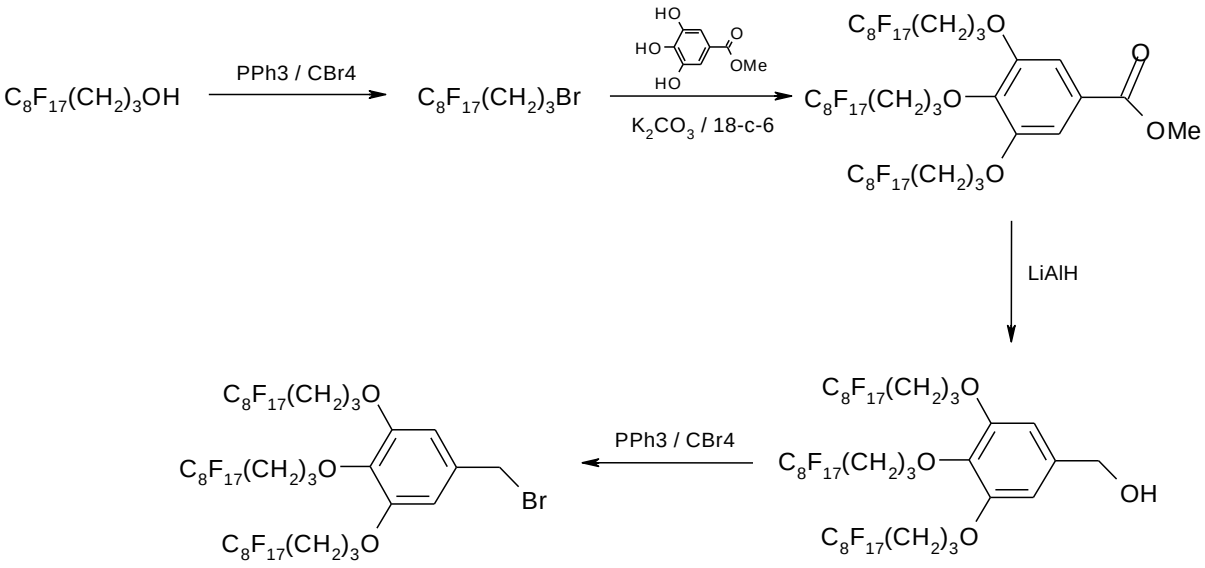

Figure 3:7 Synthesis of Type "b" End-Capping Agents

Synthesis of Type "c" End capping agent. Type "c" end-capping agents are G1 dendrons and can be made in two steps from the G0 Dendron (type "a" end capping agent). A Williamson Coupling reaction between end-capping agent "a" and 3,5-dihydroxybenzyl alcohol resulted in the production of G1 alcohol. By performing an Appel reaction the alcohol was converted to the desired functionality according to the reaction scheme below, figure 3:8.

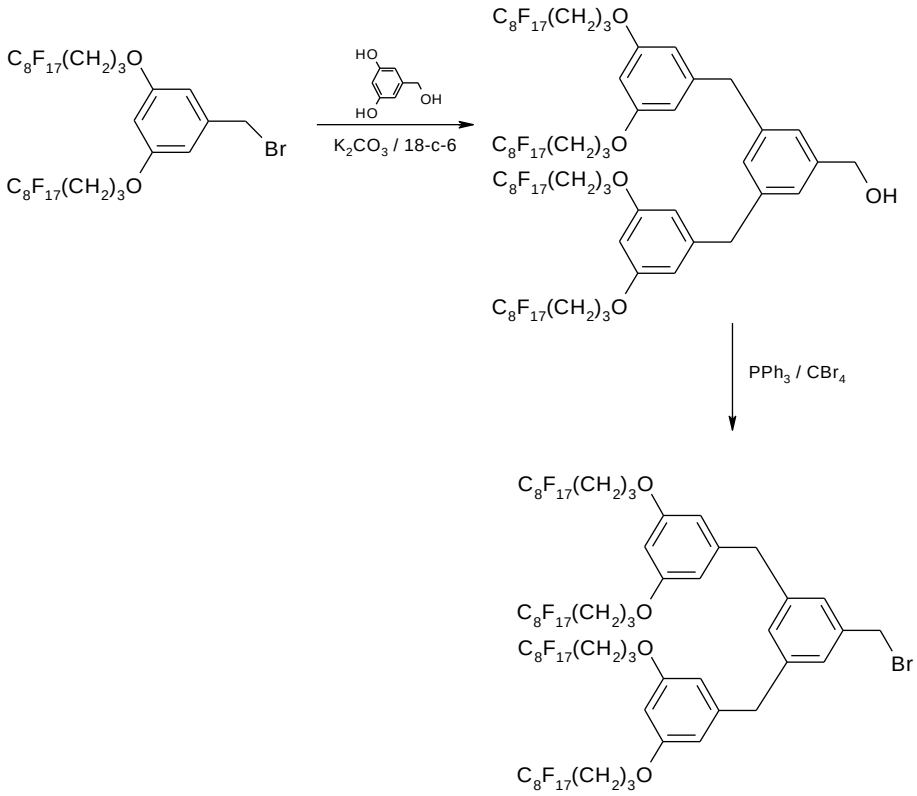

Figure 3:8 Synthesis of Type "c" End-Capping Agents

The synthesis of each of the end capping agents described above involves two key reactions; the conversion of an alcohol to a bromide functionality and a Williamson coupling reaction. The conversion of the alcohol to a bromide group can be achieved by the reaction of triphenylphosphine and tetrabromomethane commonly known as the Appel Reaction [2 3, 4]. The reaction mechanism proceeds by the activation of PPh_3 by the reaction with CBr_4, followed by the alcohol attacking the phosphorous to generating an oxyphosphonium intermediate. The oxygen is then transformed into a leaving group, and an S_N2 bromide displacement takes place. The mechanism below, figure 3:9, illustrates the many steps involved in the reaction scheme.

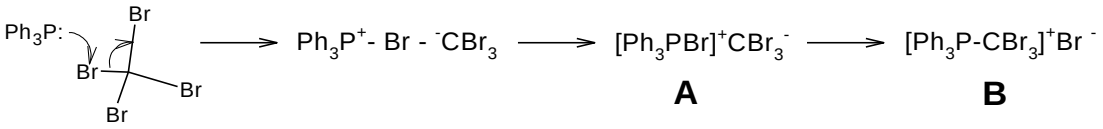

A + ROH

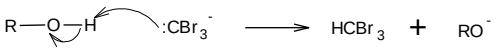

A + RO$^-$

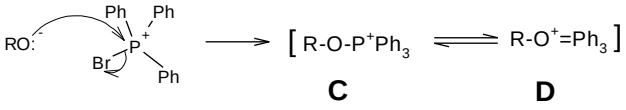

B + C

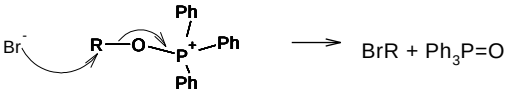

B + D

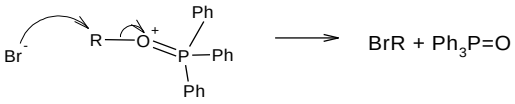

B + H_2O (to quench the reaction)

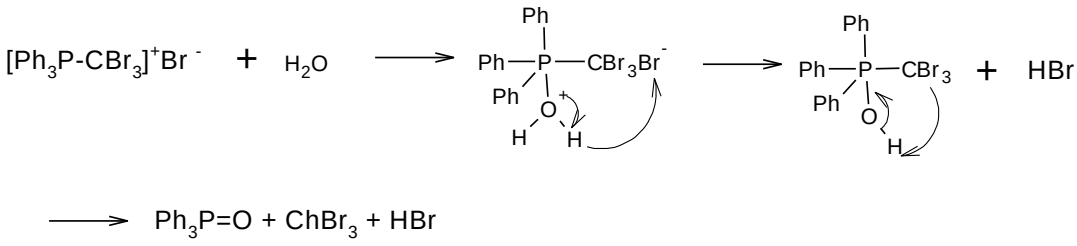

Figure 3:9 Appel Reaction Scheme

During the Appel reaction, triphenylphospine oxide is produced in large quantities. This is very difficult to remove as it is only sparingly soluble in many solvents. However, by continuous stirring of the product in methanol, over time the triphenylphospine oxide is dissolved and the alkylbromide can be removed by filtration.

The fluoroalkyl groups were attached to the phenolic alcohols via a Williamson ether coupling reaction. Firstly the alcohol is deprotonated by the base potassium carbonate to form a phenoxide:

$$2ROH + K_2CO_3 \rightarrow 2KOR + CO_2 + H_2O$$

Then via a Williamson ether synthesis the product is formed:

To facilitate this reaction crown ethers are required. Therefore, the potassium needs to be transported into the organic solvent where the reaction is taking place. They are based on repeating $-OCH_2CH_2-$ units, derived from ethylene glycol: $HOCH_2CH_2OH$. These compounds are very important and can be used as phase-transfer catalysts and agents to promote solubility of inorganic salts in organic solutions. So a metal ion inside the cavity can be "carried" into an organic solvent. This allows ionic systems such as K_2CO_3 to be dissolved in organic solvents and used as reagents. The crown ether dissolves in the organic solvent, the potassium ion complexes with the crown ether, and the carbonate is forced to dissolve in the organic solvent in order to ion-pair with the potassium ion. This also makes the anion quite reactive as it is unsolvated.

3.3 Synthesis of Polybutadiene end-capped with Fluoroalkylbromides

The chain end of 1,4-polybutadienyllithium is a primary carbanion and as such is unhindered and this plays an important role in the post-polymerization end capping reactions which can be affected by:-

- Reaction temperature;
- Polymeric chain stiffness/steric hinderance;
- Concentration;
- Solubility of the polymer;
- and the nucleophilicity/basicity of the anion.

The reaction of carbanions with alkyl halides[5, 6] are complicated because of important side reactions such as dehydrohalogenation, metal-halogen exchange (leading to Wurtz coupling), electron transfer and LiH elimination and these side reactions frequently lead to the formation of by products[7-10], section 3.3.1.

The side reactions are so apparent in polybutadiene end-capping reactions because as the amount of 1,4-addition units increases[11] the amount of primary carbanion chain ends increase and as such there is little or no steric hindrance. Some people have argued that stability of the propagating chain end decreases as the amount of 1,4 units increases and have suggested the addition of Lewis acids to reduce the activity aiding the control of the polymerisation e.g. addition of LiCl[6, 12-14], see section 3.3.5. However, there are some that believe coupling reactions, where the living chains react together, are independent of the chain end reactivity and are solely dependent on the steric requirements of the active chain end[11, 15, 16]. The addition of DPE[7, 11, 17, 18] to the chain ends or by increasing the concentration of 1,2 chain ends increases the chain end steric restrictions, see section 3.3.6. The effects of increased steric bulk of the propagating species and decreased coupling is demonstrated[11] by comparing the amount of coupling for the end-capping of polystyrenyllithium, poly(1,2)butyllithium and poly(1,4)butyllithium. *Quirk et al* found that as the vinyl content (of polybutadiene) increases the amount of coupling decreases. However, as the desired products in the current work must be an analogue of LLDPE increasing the vinyl (1,2) content would not be desirable.

Figure 3:10 illustrates the reactions that are possible when end-capping with a halo alkane[19]. It is clear that by direct nucleophilic substitution the desired product is formed, route "A", but there are two other side reactions. Route "B" results in chain coupling through lithium halogen exchange or by Wurtz coupling and route "C", although less likely, is the result of unfunctionalised polybutadiene undergoing E_2 elimination of HBr from the RBr by hydrogen transfer to the living polybutyllithium ion, figure 3:11.

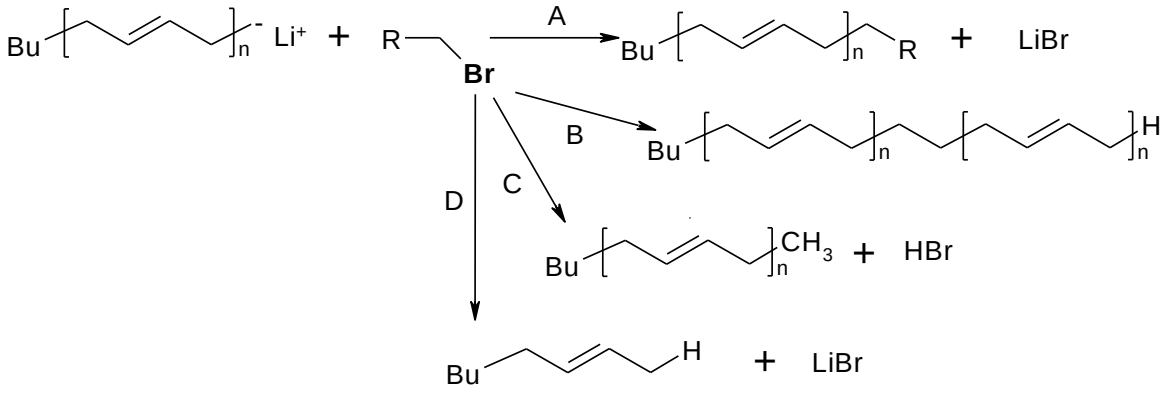

Figure 3:10 Scheme to illustrate possible reactions during end-capping a) end-capping reaction with alkyl bromide, b) coupling reaction, c) hydrogen abstraction followed by elimination and d) hydrogen abstraction

Route "C" is less likely when using benzyl bromide (as in our case) since a double bond would have to be created with a phenyl carbon, which is extremely unlikely as the carbon would have to be pentavalently bonded.

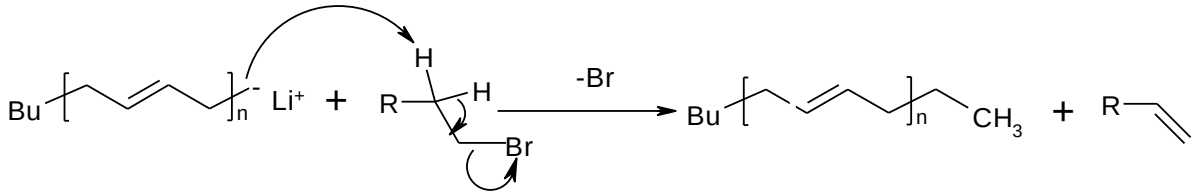

Figure 3:11 Mechanism Illustrating E_2 Elimination

3.3.1 Specific Coupling Associated with Polydiene Polymerisations

Living polybutadienes have good stability in hydrocarbon solvents at room temperature, however, at elevated temperatures and/or when stored for prolonged periods their stability is limited and they tend to be deactivated. An indication of deactivation is the polymers colour. Solutions of living dienes are colourless/yellow but upon heating their colour changes to dark yellow/amber. This colour change is an indication of active centres being destroyed by coupling, forming higher molecular weight products, where the rate of decomposition increases with increasing chain end concentration. Specifically polybutadienyllithium is the more stable towards thermal decomposition but least stable when stored[20] where metalation of the backbone can occur by elimination of lithium hydride[21] or by in chain metalation[22].

If LiH elimination occurs, the resulting molecular weight can be several times the predicted molecular weight. Elimination of LiH occurs via either intra or intermolecular elimination[11, 23]. In intramolecular elimination the polydienyllithium is deactivated and during intermolecular elimination of LiH a coupled product of two macromolecules which could continue to form a star like branched polymer, figure 3:12.

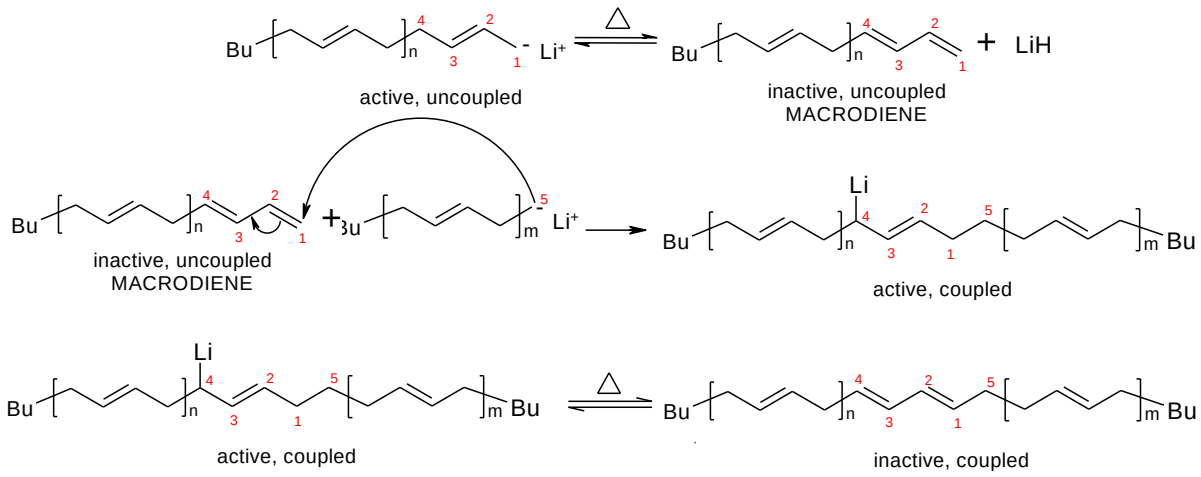

Figure 3:12 Mechanism Illustrating Coupling as a result of Intermolecular Elimination of LiH

In-chain metalation, figure 3:13, coupled with elimination of lithium hydride would lead to in-chain diene units that would have even more reactive allylic hydrogens for further metalation-elimination-coupling sequences. This would promote thermal decomposition, branching and ultimately gel formation, as well as colour formation in polymers.

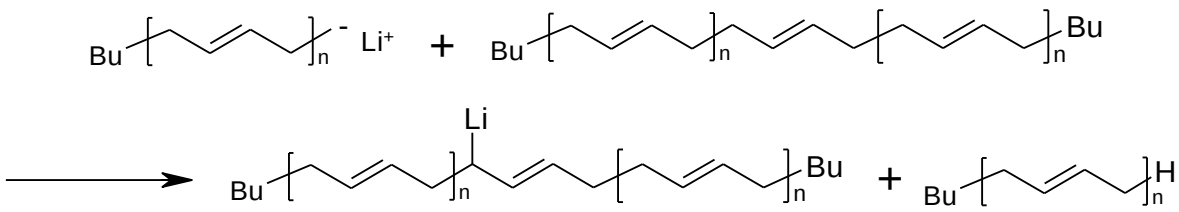

Figure 3:13 Mechanism Illustrating Coupling as a result of in-chain metalation

Another type of coupling that arises is the result of lithium halogen exchange. The mechanism for coupling by lithium halogen exchange involves the lithium counterion being exchanged for the bromide on the alkyl bromide. This results in the production of alkyl lithium by nucleophilic substitution with the brominated polymer and a coupled product is formed, figure 3:14.

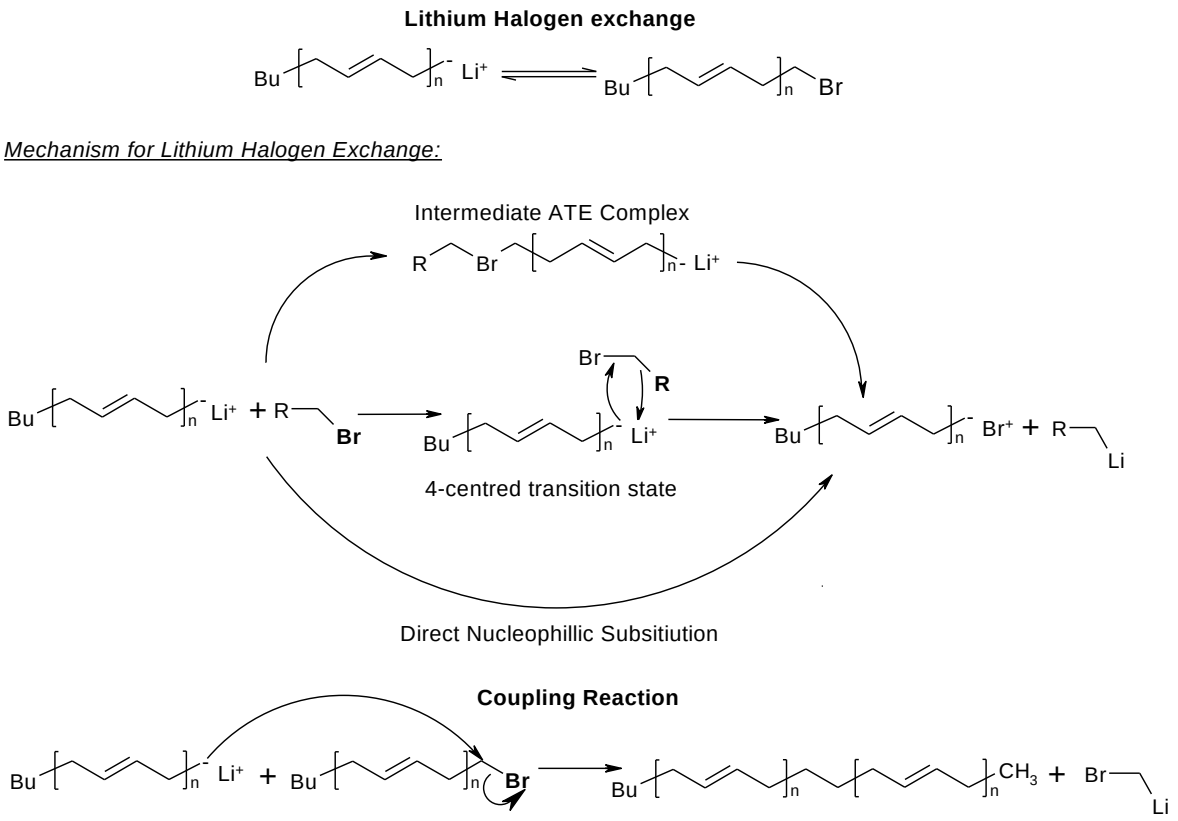

Figure 3:14 Mechanism Illustrating Coupling as a result of lithium halogen exchange

The final example of a coupling reaction that can occur is the Wurtz reaction[5, 6, 8, 9], named after Charles-Adolph Wurtz. It is a coupling reaction whereby alkyl halides react to form new carbon-carbon bonds, figure 3:15, due to the formation of radicals during a single electron transfer.

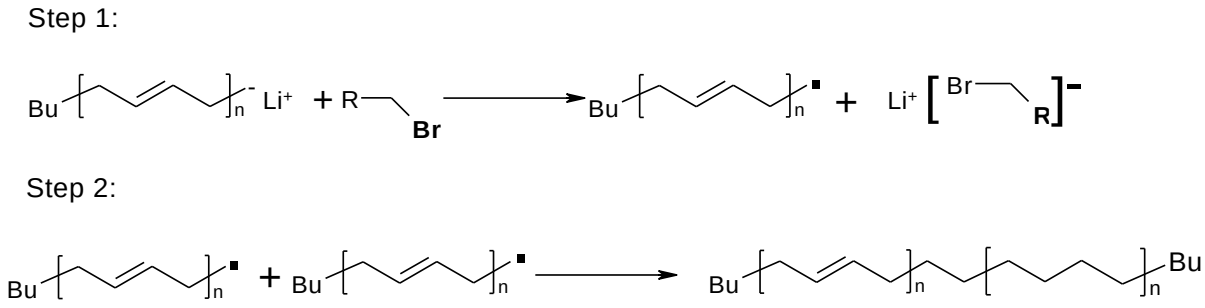

Figure 3:15 Mechanism Illustrating Coupling as a result of Wurtz reaction

All of these side reactions can be avoided but in order to do so extra reaction steps in the synthesis are required which increases both cost and time. It would be more advantageous to synthesise end-capped polybutadiene in a one step process. As such several different methods were tried to avoid any additional synthetic steps, section 3.3.2 – 3.3.4. However, the synthesis of

these polymers proved to be much more complicated than originally anticipated. Benzyl bromide was used as a model end capping agent in the trial reactions due to it being a cheaper and commercially available analogue to the synthesised end capping agents. When the process had been optimised using benzyl bromide, a series of polybutadiene polymers with varying molecular weights were synthesised and the living polymers end capped with one of three fluoroalkylbromides in a controlled termination reaction.

3.3.2 Attempted synthesis of polybutadiene end capped with benzyl bromide

Polybutadiene was synthesised by living anionic polymerisation with *sec*-butyllithium as the initiator and hexane as the solvent using standard high vacuum techniques as described earlier in section 2.2.3.1.2. The polymerisation was allowed to proceed for 24 hrs at 50 ^{o}C at which point a sample was collected for molecular weight analysis and terminated with nitrogen sparged methanol. The reaction flask was then cooled to -78 ^{o}C with an acetone/dry ice bath and THF was distilled into the reaction flask (to give approximately 20% THF by volume) – the reaction flask was maintained at this temperature for the duration of the reaction. The reaction had to be maintained at 78 ^{o}C for the duration of the reaction to reduce the number of unwanted side reactions and eliminate the possibility of reaction between THF and the living polymer chain end. Meanwhile, THF (2 ml) was distilled under vacuum into a completely separate round bottomed flask, to which was injected benzyl bromide (1.2 mole equivalents with respect to butyllithium). Flask A was then raised to atmospheric pressure with dry nitrogen before the contents of flask A were cooled to -78 ^{o}C at which point the benzyl bromide solution was injected into the living polymer solution. The end capping reaction was allowed to proceed at -78 ^{o}C for 3 hrs and then raised to room temperature over 2 hrs. Nitrogen sparged methanol was then added to the polymer solution to terminate any residual living chains and 1 ml of BHT antioxidant in toluene added. The polymer solution was poured into a large excess of stirred methanol containing BHT causing the polybutadiene to precipitate as a sticky solid. The polymer was allowed to settle, and the supernatant solvent decanted to waste. The polymer was then collected, dried in vacuo to constant mass and stored in a freezer.

The possibility of side reactions during the end capping reaction has been discussed above, however the results of previous studies involving the end capping of polystyryllithium with benzyl bromide[24, 25] led us to believe that the addition of THF and a reduced temperature would circumvent these side reactions. However, ^{1}H NMR analysis coupled with SEC analysis showed that this was not the case. SEC analysis, figure 3:17, showed that 20% of the polymer chains had coupled. The target molecular weight was 10 kgmol^{-1} and the molecular weight obtained was significantly higher, 27 kgmol^{-1} (uncoupled) and 57 kgmol^{-1} (coupled). The NMR analysis, figure

3:18, indicated an extent of end capping of approximately 51% - signals at 7.2 ppm in the NMR spectrum correspond to the 5 protons of the benzyl end group. However, this end-capping result is misleading as the molecular weight is much higher than estimated so the benzylbromide would have been added in a very high excess and so it is likely that the NMR is representing a large proportion of the unreacted benzyl bromide. The integration value of 1H, calculated from the signals at 5.4ppm and 5.0ppm, was 0.023. The excess benzyl bromide peak for 2H, 4.5ppm, was 0.04, therefore the 5H associated would give an integration value of 1. These protons account for all the phenyl protons detected between 7.1-7.4ppm therefore the amount of end-capping must be negligible. As a result of these findings, modifications to the described end capping reaction were explored to try to reduce the coupling.

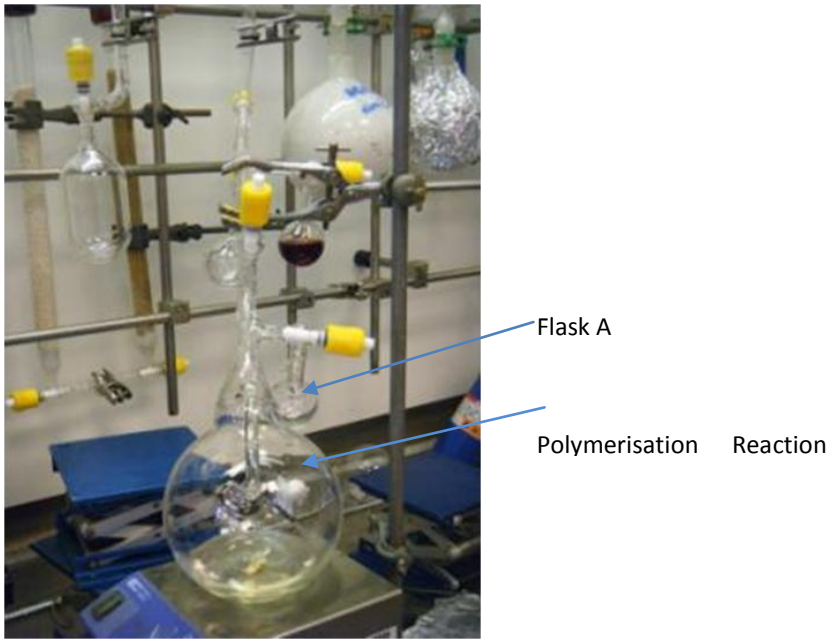

Figure 3:16 Reaction Vessel 1 and Flask A

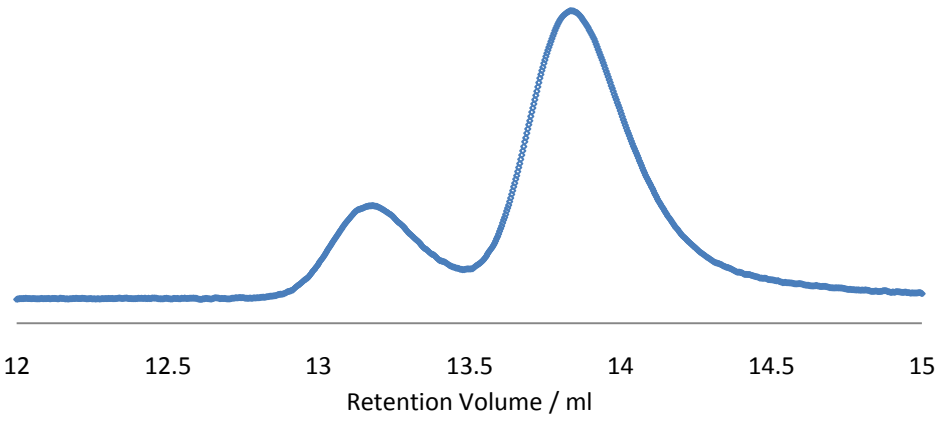

Figure 3:17 SEC Analysis for the end-capping of polybutadiene with benzyl bromide showing 20% coupled polymer, lower retention volume, and 80% uncoupled polymer

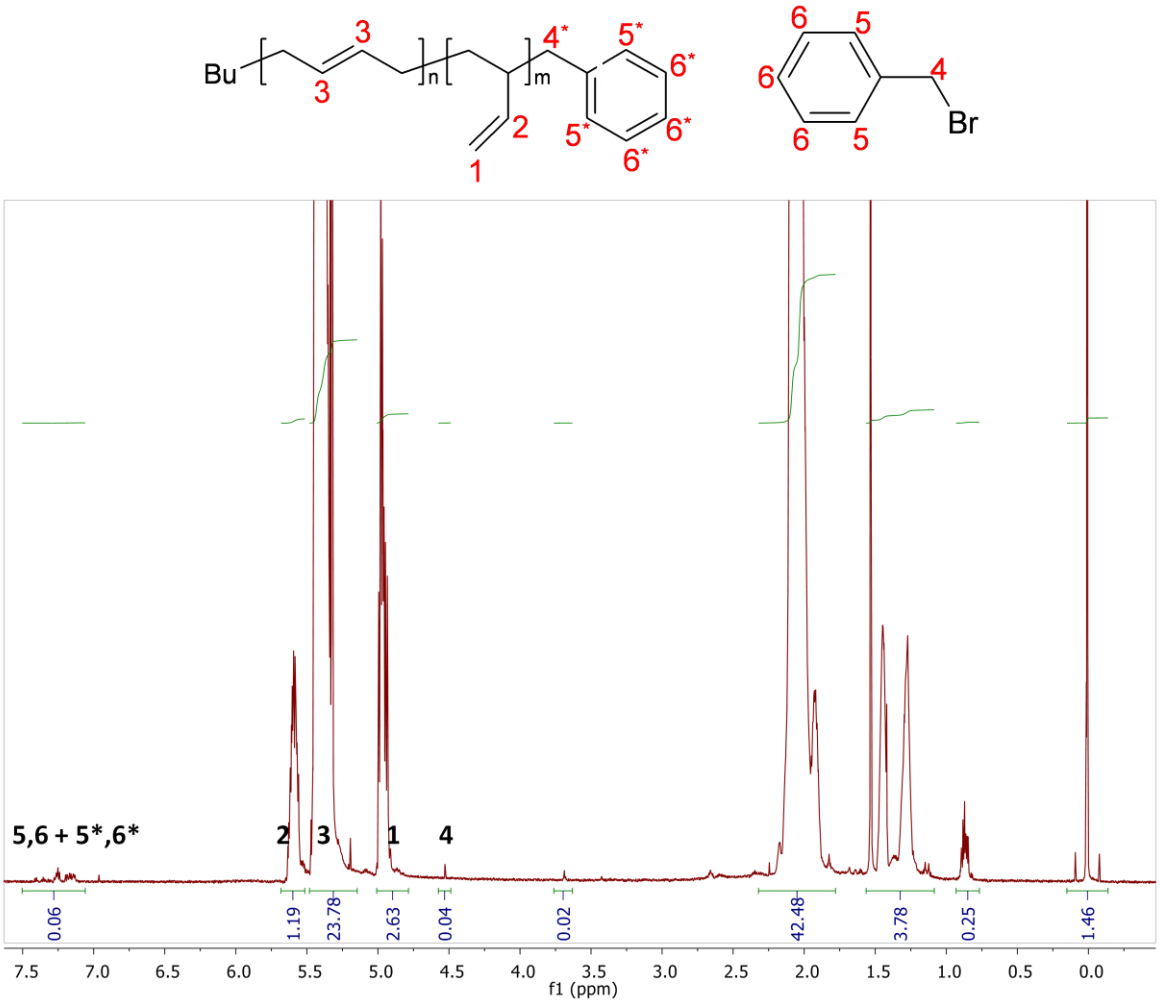

Figure 3:18 NMR spectrum for the end-capping of polybutadiene with benzyl bromide

3.3.3 Modified procedure for the end capping of polybutadiene with benzyl bromide – decanted addition of benzyl bromide.

In the previous reaction it was observed that the poor extent of end capping was due in part to polymer-polymer coupling (approximately 20%) but it was deduced that to a large extent the living chains had been terminated by some other method – possibly by the introduction of environmental impurities accompanying the injection of the benzyl bromide solution. It had been necessary to raise the flask containing the benzyl bromide solution to atmospheric pressure with nitrogen gas to allow injection and this process is clearly a possible source of impurities. In order to obviate the need for this process a new reaction vessel, figure 3:19, was commissioned so that benzyl bromide could be injected into flask 3 and decanted across into the living polymer solution, flask 1, without the need to introduce nitrogen gas. Secondly a sample of the living polymer was

collected before end-capping, by decanting a sample into flask 2, to try to deduce when coupling occurred. In the sample there was no coupling.

The polymerisation was carried out as described in section 3.3.2 except that THF (2mL) was distilled into flask 3 of the new reaction vessel, figure 3:19, to which benzyl bromide was injected. Flask 3 was then cooled to -78 ^{o}C at which point the chilled benzyl bromide solution was decanted into the living polymer solution. The end capping reaction was allowed to proceed at -78 ^{o}C for 3 hrs and then raised to room temperature over 2 hrs.

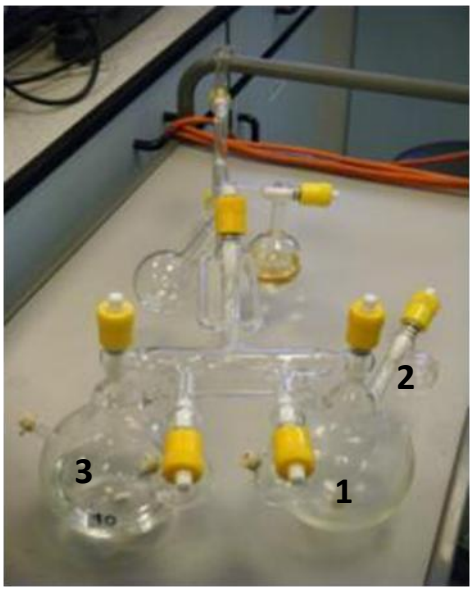

Figure 3:19 Reaction Vessel 2

By decanting the end-capping agent into the living polymer solution it was hoped any unwanted impurities would be eliminated. From the results it would appear that although the coupling has not been eliminated. SEC analysis, figure 3:20, again showed a much higher degree of polymer-polymer coupling, 67%, but the NMR analysis, figure 3:21, indicated that again there was some unreacted benzyl bromide and by subtracting the integration value for the unreacted benzyl bromide phenyl protons from the end-capped protons the degree of end-capping was 42%. Although this method did not improve the amount of coupling it did eliminate any environmental impurities so the polymer could be either coupled or end-capped.

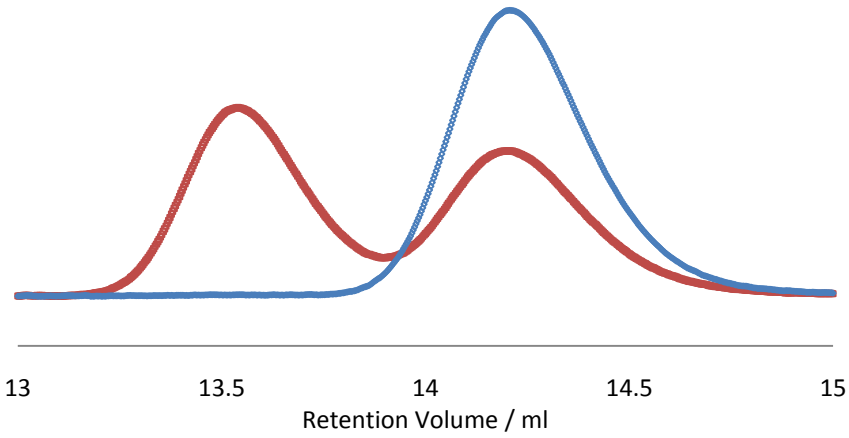

Figure 3:20 SEC Analysis NMR for □ the end-capping of polybutadiene with benzyl bromide– decanted addition of benzyl bromide and ◊ sample taken before endcapping, terminated with MeOH

As a result of these findings further modifications to the described end capping reaction were explored to try to eliminate coupling.

3.3.4 Modified procedure for the end capping of polybutadiene with benzyl bromide – inverse decanted addition of benzyl bromide.

In the previous reaction it was suggested that termination by environmental impurities was eliminated, but as a consequence the coupling (67%) had been increased as more polymer is available to couple. However, the remaining living chains had mostly terminated by end-capping. In previous attempts, the end-capping agent was added to the living polymer solution, and as such the polymer was always in excess compared to the end capping agent. By reversing the mode of addition and adding the living polymer to the end-capping agent it the end-capping agent would always be in excess and statistically more likely to end-cap the living polymers before coupling could occur. In this reaction the same reactor was used as in the previous experiment, figure 3:19.

The same procedure was followed as described in section 3.3.2 however, after Flask 3 was cooled to -78^{o}C, the living polymer solution was decanted into the benzyl bromide solution. This alternative method did not significantly reduced the amount of coupling, SEC analysis (figure 3:21) shows both attempts at this method, and the NMR analysis indicated that only 22% of the uncoupled polymer had been end capped by the benzyl bromide by comparing the signals at 2.2ppm and calculating the integration value for one proton using the signals from polybutadiene. As a result of these findings it was repeated and the % of uncoupled polymer that had been end-

capped remained low, 18%. From the consistently low extent of end capping, it was decided that although a 1-step synthesis would have been ideal it was apparent that further chain-end modifications would be required to achieve greater end-capping.

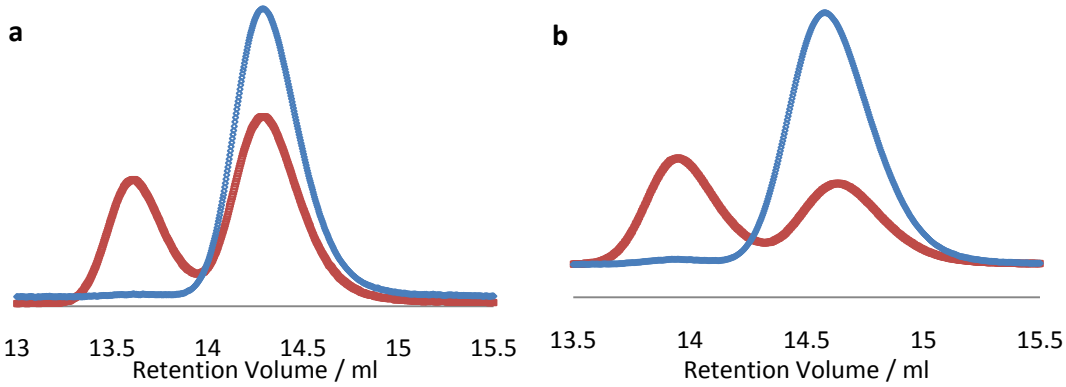

Figure 3:21 SEC trace for □ the for the end capping of polybutadiene with benzyl bromide – inverse decanted addition of benzyl bromide A) attempt 1 and B) attempt 2 and ◊ sample taken before endcapping, terminated with MeOH for attempt 1 and 2

3.3.5 Modified procedure for the end capping of polybutadiene with benzyl bromide – addition of Lithium Chloride to increase chain end stability

LiCl was added to the polybutyllithium ions to make μ-ligands, figure 3:22, thus increasing the stability and lowering the reactivity, of the chain ends. The optimal result of this is that the amount of coupling will be decreased the coupling reaction of alkylhalides with living polymers will be promoted. The susceptibility of organic halides towards Wurtz-coupling is in the order RI>RBr>RCl[5]. The cross-associated aggregates of RLi and LiCl generally have decreased reactivity and higher selectivity towards the end-capping agent compared to the uncomplexed RLi[9, 12 14, 26, 27]. Also by adding LiCl there is a marked decrease in the rate of a polymerization as the living end is stabilized by strongly aggregating to the salt leading to the formation of μ-complexes[28-31].

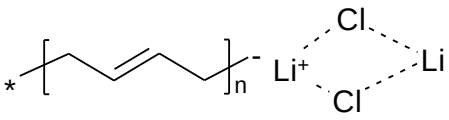

Figure 3:22 Example of a μ-ligand with polybutadienyl lithium

To establish whether LiCl has a positive beneficial effect upon the coupling reaction, a polymerisation was carried out according to the same procedure described in section 3.3.3. However, before the living polymer solution was decanted into the benzyl bromide solution in a separate flask (indicated A, figure 3:19), a suspension of LiCl (10× excess with respect to butyllithium) in hexane (2 ml) was injected and freeze pumped thawed twice. Flask A was then raised to atmospheric pressure with dry nitrogen before its contents were cooled to -78 ^{o}C at which point the LiCl solution was injected into the living polymer solution and the reaction left to proceed for 1hr. THF was then distilled into the living polymer solution (to give approximately 20% THF by volume) – the reaction flask was maintained at this temperature for the duration of the reaction. After benzyl bromide solution was cooled to -78 ^{o}C the living polymer solution was decanted into it.

Unfortunately even though Wurtz coupling was eliminated it was evident from the NMR that the polymer had not reacted with the benzyl bromide. LiCl is very hygroscopic so water may have been introduced to the polymerisation which would result in the polymer terminating through hydrogen abstraction. Secondly as the LiCl did not dissolve in hexane there would be an issue with the reaction proceeding as the mixture was not homogeneous. This conclusion would account for the SEC analysis, figure 3:23, showing no polymer-polymer coupling and the NMR analysis, figure 3:24, indicating the uncoupled polymer had not been end capped by the benzyl bromide.

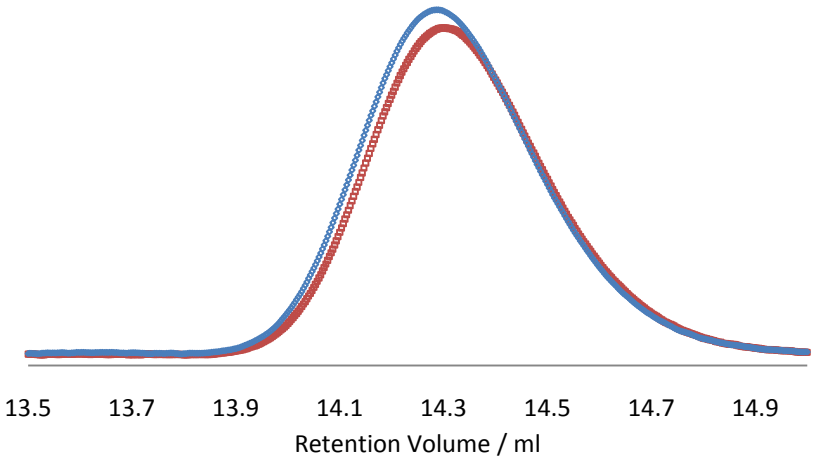

Figure 3:23 SEC Trace for □the end capping of polybutadiene with benzyl bromide – using Lithium Chloride to increase chain end stability and ◊ sample taken before endcapping, terminated with MeOH

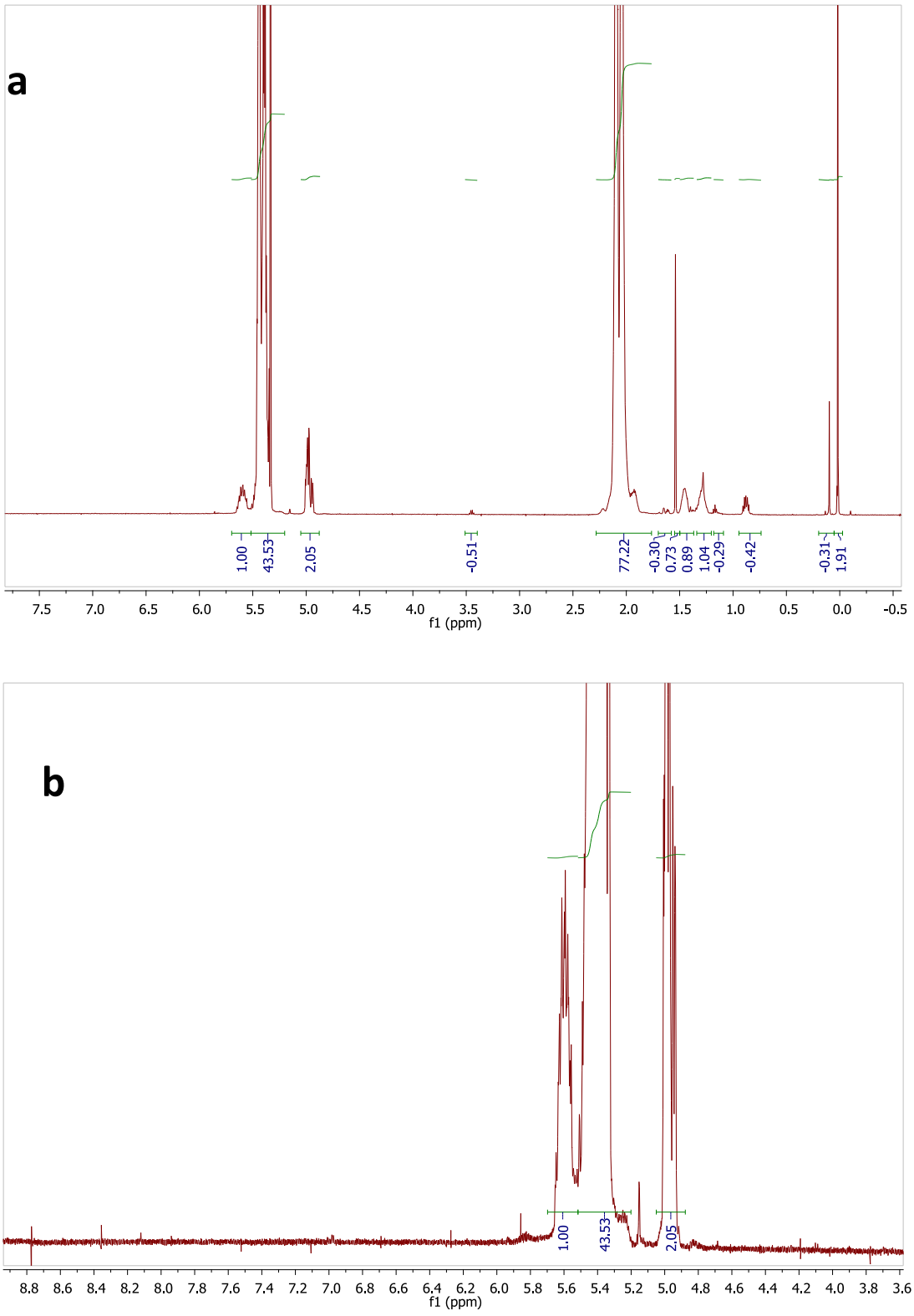

Figure 3:24 NMR for the end capping of polybutadiene with benzyl bromide – using lithium chloride to increase chain end stability a) full NMR and b) phenyl proton region

3.3.6 Modified procedure for the end capping of polybutadiene with benzyl bromide – using diphenylethylene (DPE)

Adding DPE to the end of a living polymer chain decreases the nucleophilicity of the end group resulting in side reactions B,C and D, illustrated in figure 3:10, not being possible, thus coupling could not occur. In this situation the only termination reactions possible are by impurities or by nucleophilic substitution with an alkyl bromide1,1-diphenylalkyllithium species are reported to be associated into dimers in hydrocarbon solvents[32], however because DPE increases the steric hindrance at the living chain ends the strength of the dimeric association is decreased. If radicals are still formed by Wurtz coupling they are unlikely to couple because of the steric hindrance; however, the decreased nucleophilicity of the end group reduces radical formation. Figure 3:25 illustrates the mechanism for DPE addition to a living chain end[8].

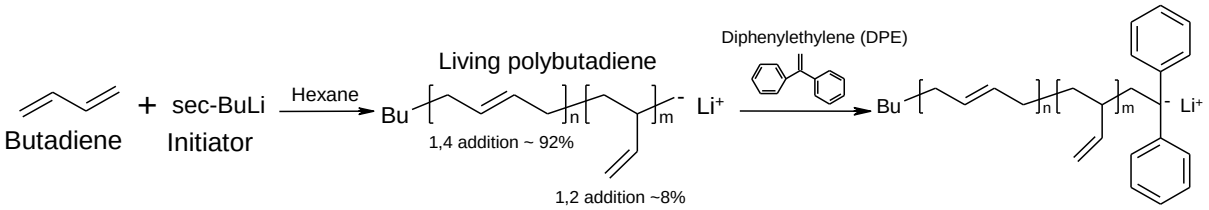

Figure 3:25 Mechanism to show DPE addition

Hence, a polymerisation was carried out using the same procedure as described in section 3.3.3. However, before the living polymer solution was decanted into the benzyl bromide solution, in a separate flask (indicated A, figure 3:19), a solution of DPE (1.5 moles with respect to butyllithium) in THF (2 ml) was injected into flask A and freeze pumped thawed twice. At this point *sec*-BuLi, 0.2 mole with respect to living polybutadiene, was added drop wise into Flask A to purify the DPE and remove any impurities. This is apparent by the permanent colour change from colourless to deep red. Flask A was then raised to atmospheric pressure with dry nitrogen at which point DPE solution was withdrawn, injected into the living polymer solution and the reaction left to proceed for 24 hrs at 50 ^{o}C. At this point, a sample was collected for molecular weight analysis and terminated with nitrogen sparged methanol. The colour of the polybutadiene-diphenyllithium was uncharacteristically dark orange, rather than dark red, which might be interpreted as being a sign of low concentration or incomplete reaction. THF was then distilled into the living polymer solution at -78 ^{o}C (to give approximately 20% THF by volume) – the reaction flask was maintained

at this temperature for the duration of the reaction. After benzyl bromide solution was cooled to -78 ^{o}C the living polymer solution was decanted into it. When end-capped the characteristic colour of dark orange of the RDPE^{-}Li^{+} vanishes [7].

The SEC results showed that from the sample taken after DPE was added there was a tiny bit of coupling (4%) whereas the rest (96%) remained uncoupled and the NMR results showed that 87% of the uncoupled polymer had been successfully end-capped with DPE. Following the addition of benzyl bromide the extent of coupling only increased slightly, 8% of the polymer was coupled which could be owing to impurities or by to Wurtz coupling, figure 3:27. NMR analysis showed that of the 87% of the polymer that had been end-capped with DPE, 49% had been successfully end-capped with benzyl bromide, figure 3:27.

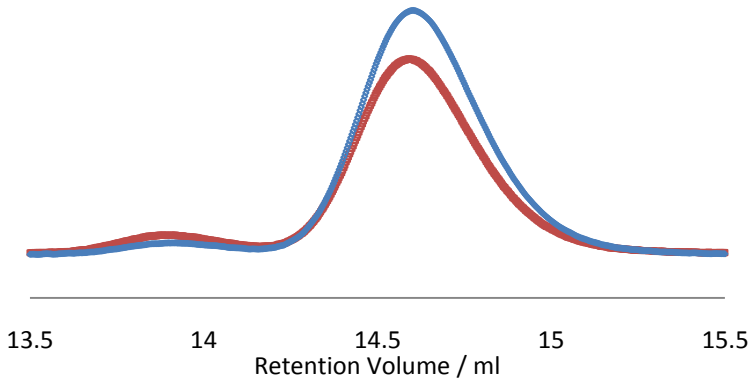

Figure 3:26 SEC chromatogram for □ the end capping of polybutadiene with benzyl bromide – using diphenylethylene to increase chain end hindrance and ◊ sample taken before endcapping, terminated with MeOH

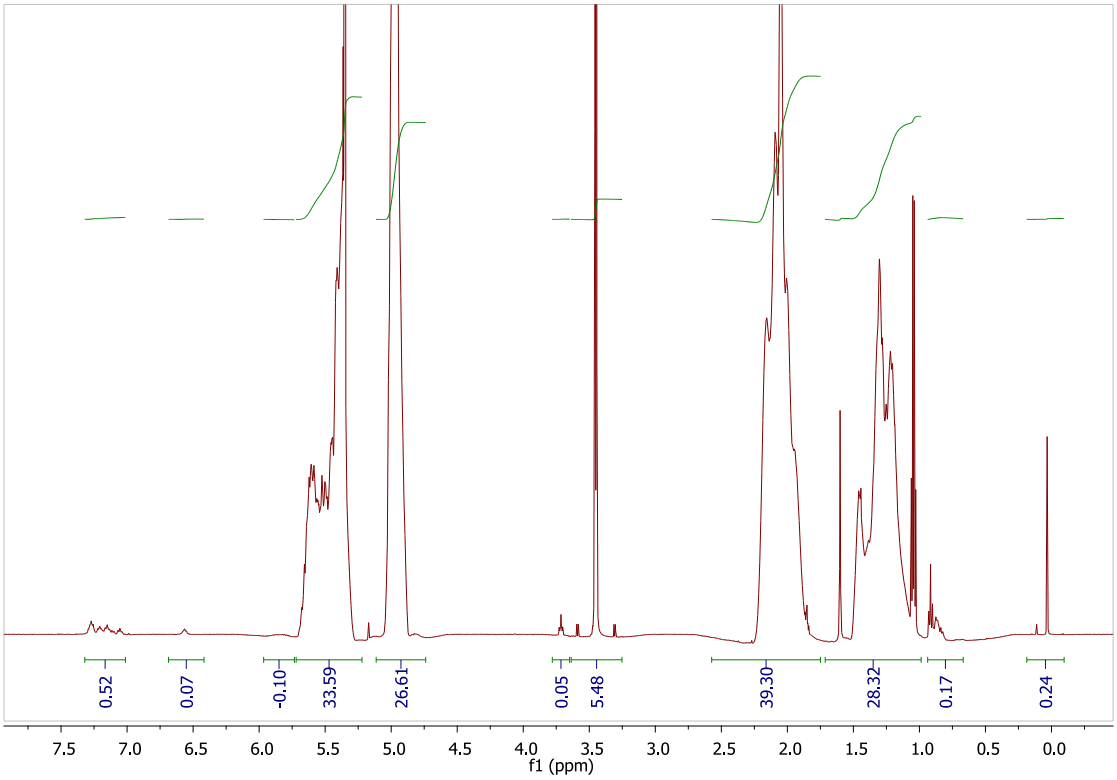

Figure 3:27 NMR the end capping of polybutadiene with benzyl bromide – using diphenylethylene to increase chain end hindrance

From the GPC result 96% of total polymer is uncoupled and the NMR showed that 87% was end-capped with DPE and 47% was end-capped with DPE and benzyl bromide. Therefore if only the uncoupled polymer is considered 90% was end-capped with DPE and 49% was end-capped with both DPE and benzyl bromide. This could be improved so the next step was to add TMEDA to try to decrease the number of aggregates.

3.3.7 Modified procedure for the end capping of polybutadiene with benzyl bromide – using diphenylethylene and tetramethylethylenediamine (TMEDA)

All alkyl lithiums aggregate in hydrocarbon solvents. Adding 20% THF to the reaction solvent should completely destroy the aggregates, but by replacing with TMEDA, which is also a base, will have the additional benefit of speeding up the rate of reaction. Secondly, THF reacts with Li^+ leading to undesired side products. TMEDA is a Lewis base (σ-ligands) and has the reverse effect that adding a Lewis acid has (e.g. LiCl). Electron donors, such as ethers (THF) or amines (Tetramethylethylenediamine, TMEDA), are able to solvate lithium ions, figure 3:28.

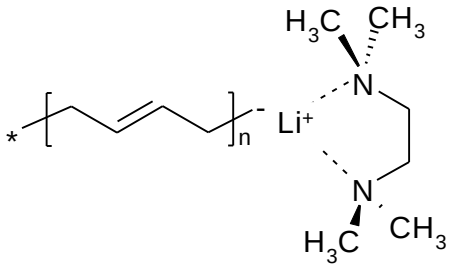

Figure 3:28 Illustration of an σ-ligand

Lewis bases stabilise the electronic charges through intermolecular association, which leads to the formation of aggregates in non-polar solvents, thus TMEDA reduces the formation of aggregates. Also depending on the concentration, tertiary amines (TMEDA) can lead to an increase or decrease in the rate of the polymerisation owing to the fact that the reaction order is 0.5 in the absence of TMEDA whereas 1 in its presence[33, 34]. However, if added before the monomer has been consumed they will increase the amount of 1,2-addition as they have an effect on the stereochemistry of diene polymerisations [35, 36].

The same procedure was followed as described previously in section 3.3.5 however, in Flask A purified DPE (4.5mole equivalents with respect to the moles of living polybutadiene) and TMEDA (2 mole equivalents with respect to DPE) were injected. The molar excess of DPE used was accidental, however, this mistake alerted us to the possibility that more than one DPE unit was attached to the end of the living chain as unreacted butadiene was still present. The target molecular weight for this experiment was 5 $kgmol^{-1}$ but unfortunately 20 $kgmol^{-1}$ was synthesised. This is most likely due to error in calculating the amount of *sec*-BuLi required.

SEC analysis of the MeOH terminated sample collected after the addition of DPE showed a monomodal peak with no evidence of polymer-polymer coupling, figure 3:29. NMR analysis, figure 3:30a, of the sample indicated that the polymer chain had approximately 4 DPE units on the chain end.

SEC analysis of the final product, figure 3:29, indicated that coupling, 16%, occurred after benzyl bromide was added. However, following from the NMR of the sample, which had 4DPE units on the chain end, showed the percentage of end-capping with 4DPE units and one benzyl bromide (45 protons) was 97%, figure 3:30b. The error associated with NMR is normally quite low however for these results to be significant the error would have to be less than 10%, which is high for NMR, so although these results should be approached with caution they are still significant.

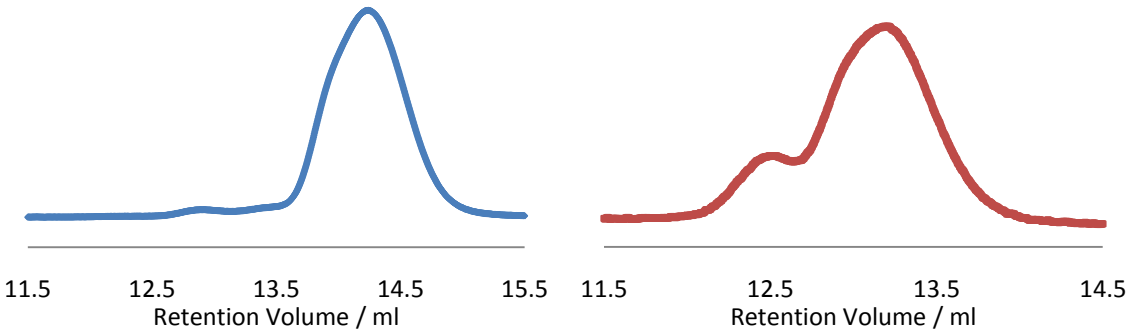

Figure 3:29 SEC trace for □ the end capping of polybutadiene with benzyl bromide – using diphenylethylene and tetramethylethylenediamine and ◊ sample taken before endcapping, terminated with MeOH

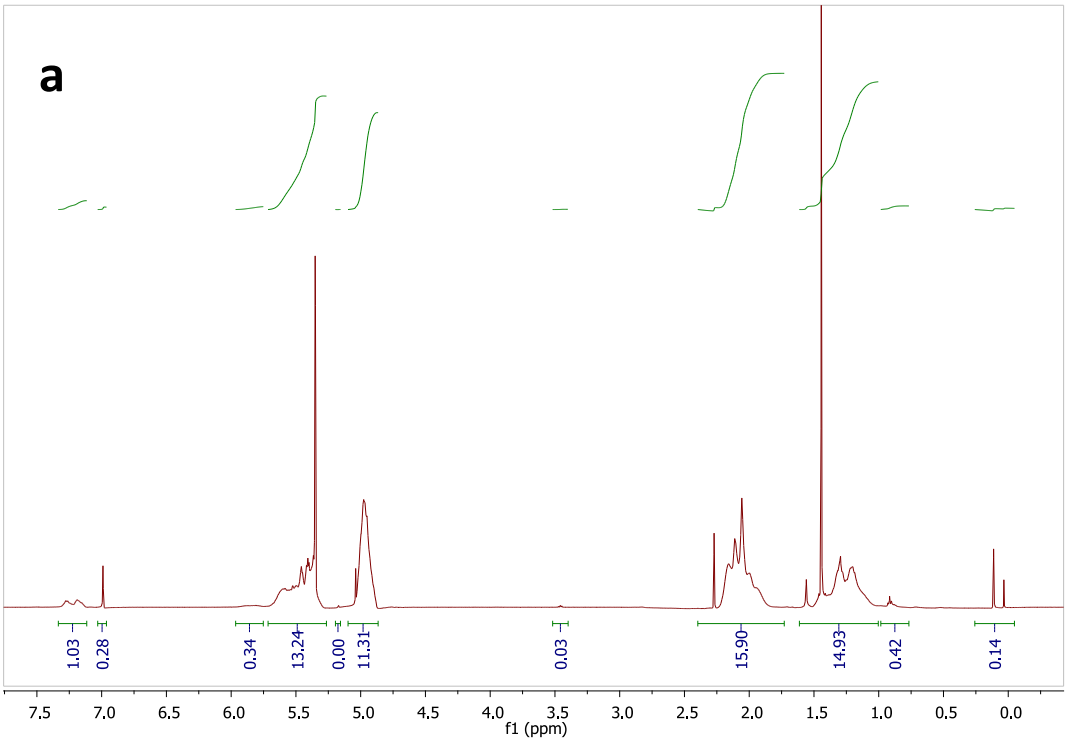

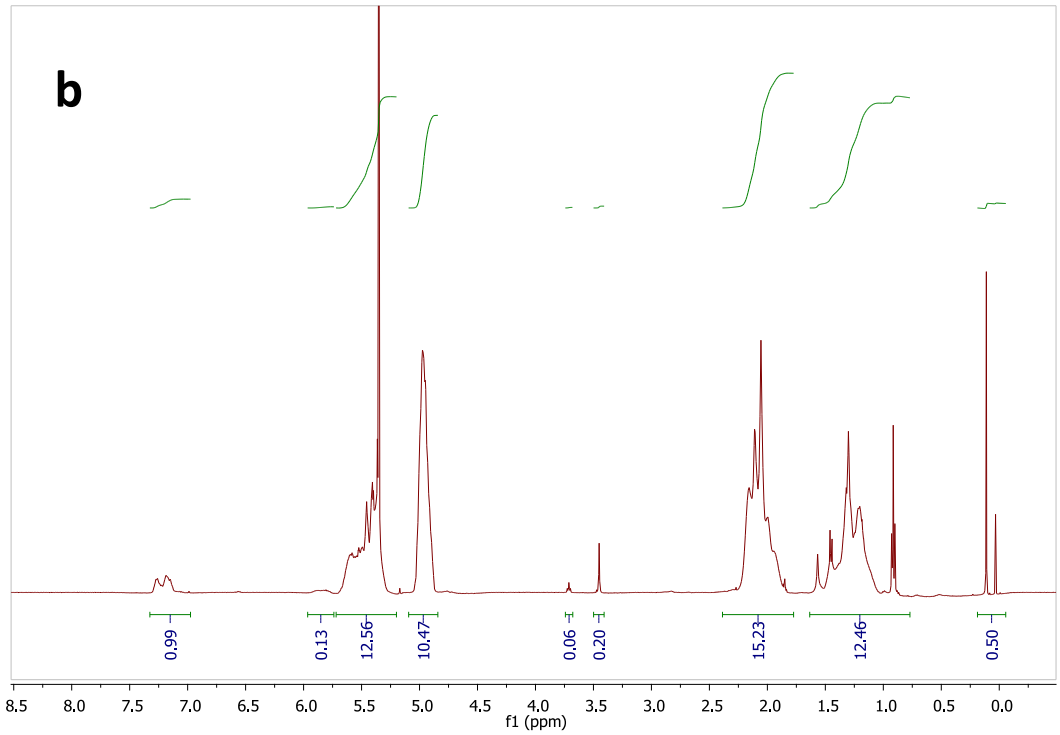

Figure 3:30 NMR for the end capping of polybutadiene with benzyl bromide – using Diphenylethylene and N,N,N I , N /-Tetramethylethylenediamine a) MeOH terminated sample and b) benzyl bromide terminated ample

An early indication that there was unreacted butadiene in the reaction vessel was the colour of the mixture. Normally polybutadiene-diphenyllithium is dark red but this solution was dark orange colour. The reason for the dilution of the colour was some polybutadienyl-lithium chain ends were present. The NMR results also showed that there was considerable amount of DPE incorporated into the polymer. As DPE cannot homopolymerise[17] the chain end must be alternating between butadiene and DPE. This suggests that the polymerisation of butadiene has not gone to completion before the addition of DPE. Another indication that there were butadiene monomers in the reaction vessel was the high proportional of 1,2 content, 39%. TMEDA increases the probability of 1,2 chain ends and it was added at the same time as DPE.

Although the kinetics of copolymerisation in non polar solvent are not favourable, when in a subsequent reaction any possible unreacted butadiene was removed, section 3.3.9, the end-capping was successful. So if there is any unreacted monomer remaining at the point of addition of DPE it is likely that in many cases the terminal repeat unit in the polymer will be a butadiene unit which upon addition of benzyl bromide may result in the undesirable side reactions discussed earlier, figure 3:31.

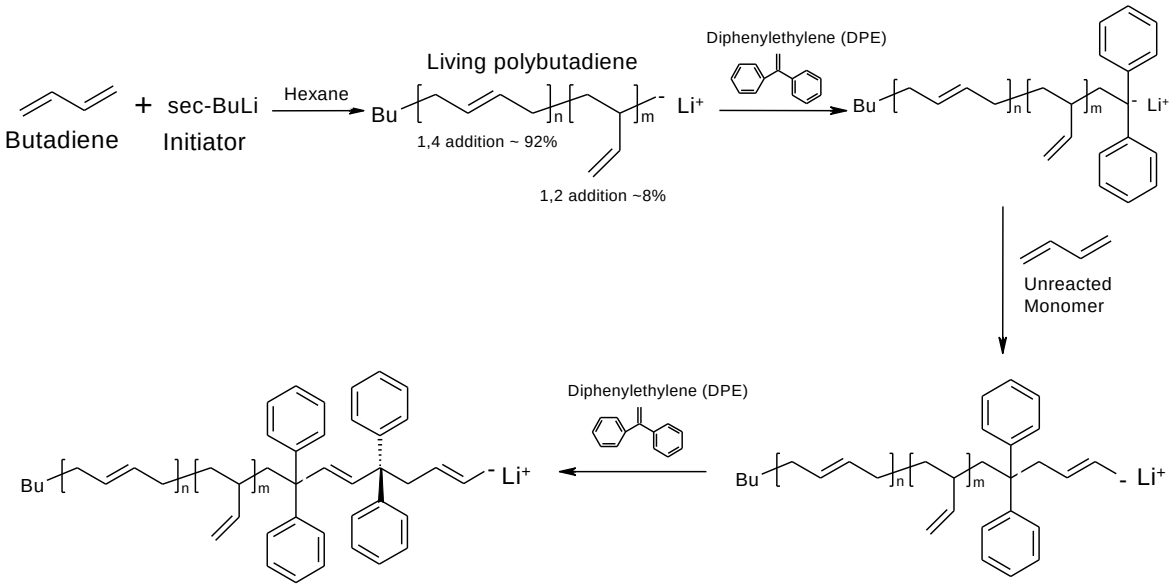

Figure 3:31 Mechanism of DPE addition in the presence of unreacted monomer

3.3.8 Modified procedure for the end capping of polybutadiene with benzyl bromide – using Diphenylethylene and Tetramethylethylenediamine and removing any unreacted butadiene

When DPE forms the terminal repeat unit at a polymer chain end, it can stabilise active centre through resonance. Thus a polymer with DPE on the chain end will be more stable than one with 1,2 butadiene and considerably more stable than 1,4 butadiene. Therefore if any polybutadiene-diphenylethyllithium is present in the presence of unreacted butadiene and polybutadienyllithium it is more likely that:

- The unreacted butadiene will react with polybutadiene-diphenylethyllithium which would lead to coupling upon addition of benzyl bromide
- The polybutadienyllithium will react with DPE, and then the polybutadiene-diphenylethyllithium will again react with the unreacted butadiene, leading to coupling.

A qualitative representation of a mixture of polybutadienyl-lithium with some polybutadiene-diphenylethyllithium is represented by the diluted red, figure 3:32a, where only polybutadiene-diphenylethyllithium gives a dark red colour, figure 3:32b.

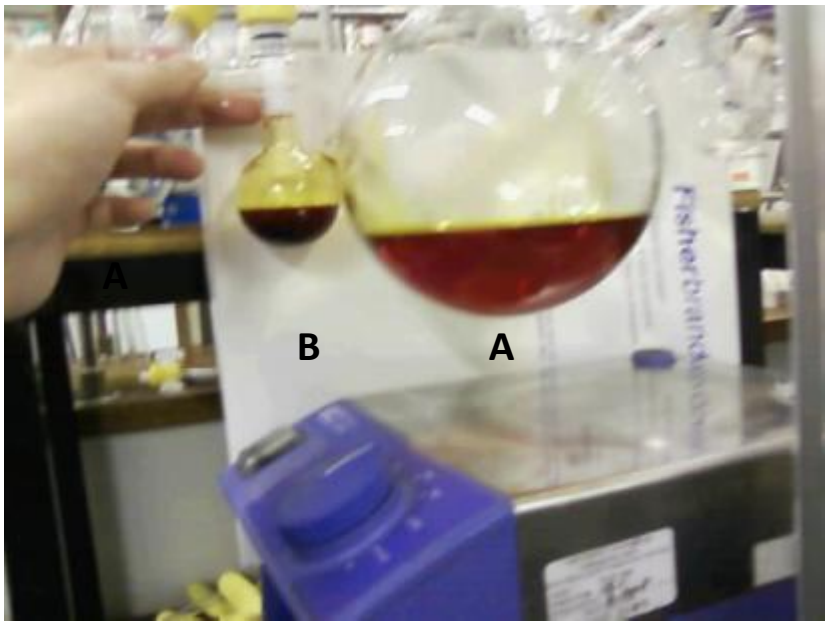

Figure 3:32 Illustration of the colour difference between a) diluted polybutadiene-diphenylethyllithium and b) pure polybutadiene-diphenylethyllithium

The same procedure was followed as previously described in section 3.3.7 however, before the DPE+TMEDA mixture was decanted into the living polymer solution (NB the amount of DPE used was 1.5× moles with respect to polybutadiene), the solvent from the living polymer solution was removed and replaced three times. First the living polymer solution was heated gently and the solvent distilled into a separate round bottom flask that was cooled. Upon removal of the solvent the living polymer solution was cooled to -78 ^{o}C and fresh, purified hexane distilled in. The process of removing the solvent was carried out to remove any unreacted butadiene, which dissolves in hexane. After the addition of DPE, the living polymer solution immediately turned dark red and continued to intensify in colour over the course of the reaction, qualitatively indicating that DPE had reacted with the chain ends. On this occasion, Flask A contained 10 molar excess of DPE, with respect to polybutadienyllithium, rather than 1.5 molar excess as used previously to ensure that the chain ends were granted to react with DPE. After the reaction with DPE had finished, a sample was collected for molecular weight and NMR analysis and terminated with nitrogen sparged methanol. THF was then distilled into the living polymer solution (to give approximately 20% THF by volume) – the reaction flask was subsequently maintained at -78 ^{o}C for the duration of the reaction. After the benzyl bromide solution was cooled to -78 ^{o}C, the living polymer solution was decanted into it, and the polymerisation continued as previously reported.

Using the NMR signals at 7.2ppm, figure 3:34, the extent of DPE end-capping was calculated to be 74% and on adding benzyl bromide 80% of the polybutadine-diphenylethyllithium chain ends

were terminated with benzyl bromide. SEC analysis, figure 3:33, shows there was no coupling upon addition of benzyl bromide.

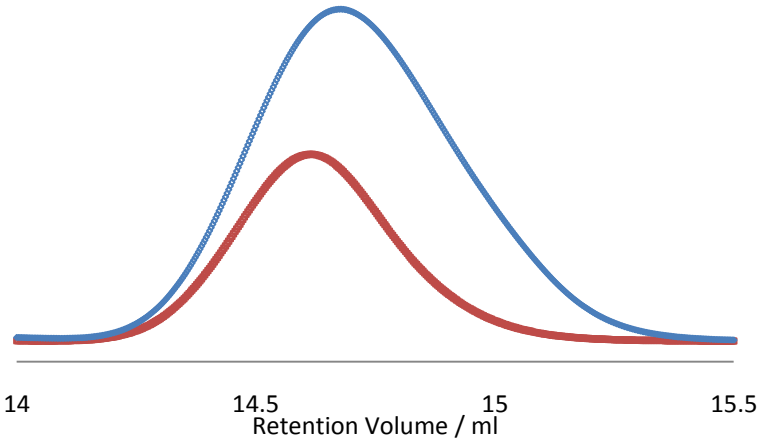

Figure 3:33 SEC trace for □ the end capping of polybutadiene with benzyl bromide – using Diphenylethylene and Tetramethylethylenediamine and removing any unreacted polymer and ◊ sample taken before endcapping, terminated with MeOH

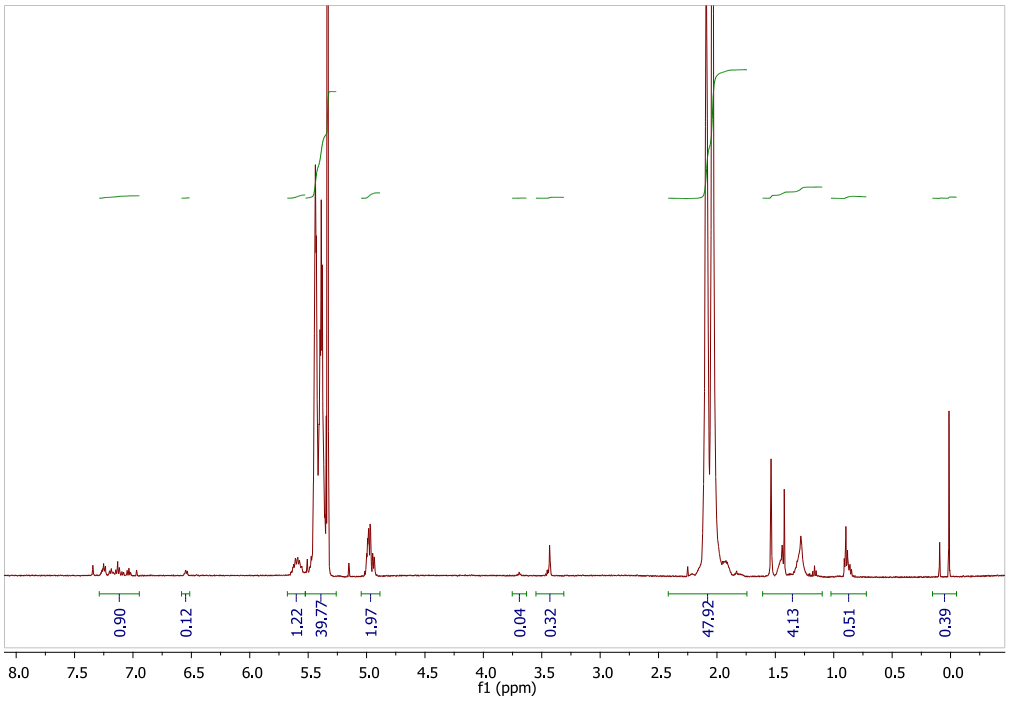

Figure 3:34 NMR for the end capping of polybutadiene with benzyl bromide – using Diphenylethylene and Tetramethylethylenediamine removing any unreacted monomer

From these results it is clear that polymer-polymer coupling and side reactions had been eliminated and the end-capping with benzyl bromide was reaching acceptably high levels, figure 3:35.

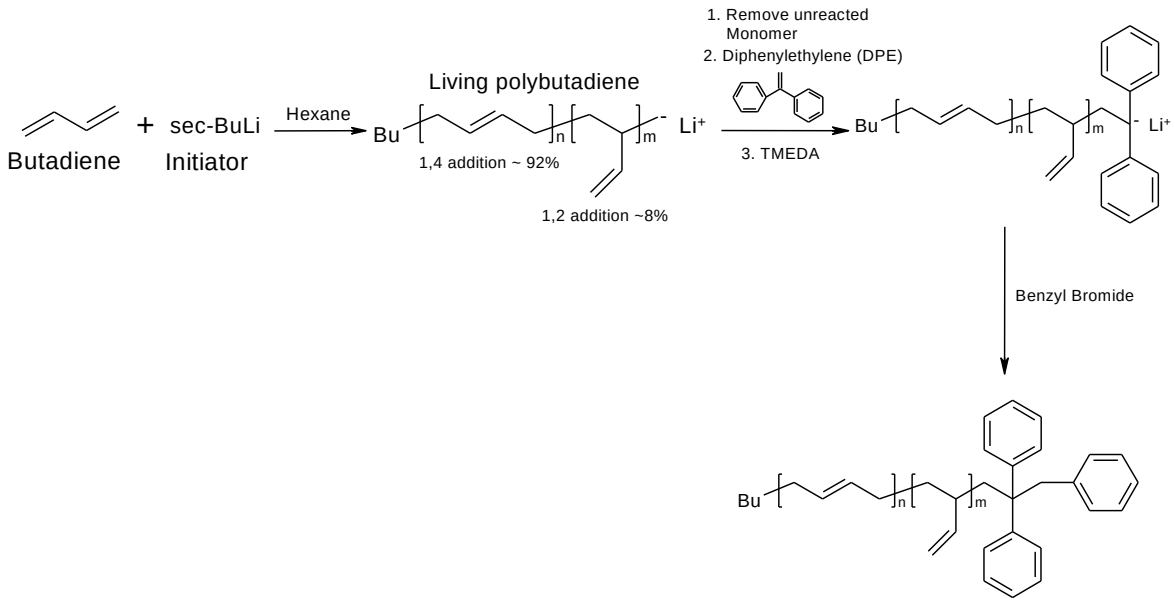

Figure 3:35 Mechanism of Optimal End-capping with Benzyl Bromide

3.3.9 Polybutadiene end-capped with Fluoroalkylbromides

As a result of carrying out a series of end capping reactions with benzyl bromide, an optimal methodology was established and this method was used for the end capping of polybutadiene with the fluoroalkylbromides end capping agent. However, to further enhance the chances of success and to further minimise the possible impact of environmental impurities a modified reaction vessel was commissioned, figure 3:36. The main polybutadiene polymerisation was carried out in flask D. Flask B was used to collect a sample for molecular weight analysis. DPE and TMEDA were injected into flask C and subsequently decanted into the main reactor D. Finally the flask A was used to purify the end capping agent before addition into D.

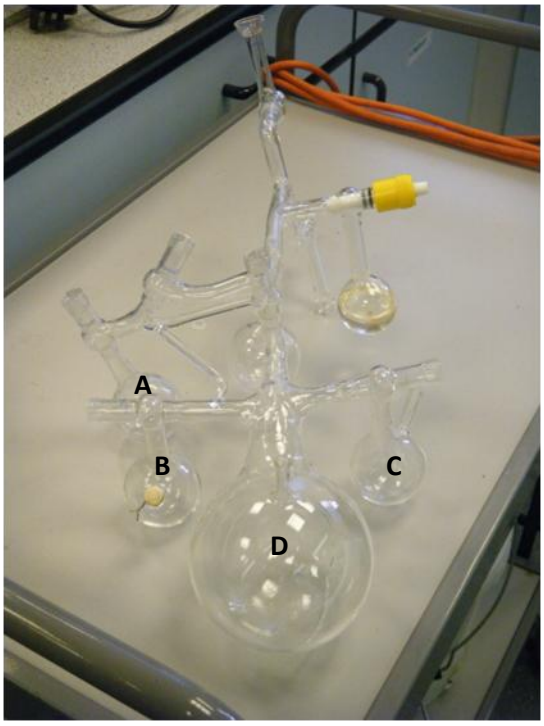

Figure 3:36 Reaction vessel used for end-capping polybutadiene with fluoroalkylbromides

A typical end-capping reaction using a fluoroalkylbromide end capping agent was carried out as follows. Polybutadiene was synthesised by living anionic polymerisation with *sec*-butyllithium as the initiator and hexane as the solvent using standard high vacuum techniques as described earlier in section 2.2.3.1.2. Before the polymerisation was carried out, hexane was decanted into flask C using Schlenk techniques from previously dried hexane in a separate round bottomed flask. The purpose of this was to act as a solvent when injecting DPE, TMEDA and BuLi into flask C. Following this, the polymerisation carried out in the flask labelled D. The polymerisation was allowed to proceed for 24 hrs at 50 ^{o}C at which point the solvent from the living polymer solution was removed and replaced three times, to remove any unreacted butadiene. At this point in flask C purified DPE, (1.5×moles with respect to polybutadienyllithium), TMEDA (2x moles with respect to DPE) and sec-BuLi (0.2 x moles with respect to DPE) was injected into the hexane. The contents of flask C was then decanted into the living polymer solution and the DPE end capping reaction left to proceed for 24 hrs at 50 °C after which a sample was collected and terminated with nitrogen sparged methanol. The sample taken was used for molecular weight analysis and to calculate the degree of DPE end-capping. Meanwhile in flask A the fluoroalkylbromide, (1.2 equivalents with respect to polybutadienyllithium), was evacuated and azeotropically dried with benzene three times. Reaction flask D was then cooled to -78 ^{o} C with an acetone/dry ice bath and THF distilled into the reaction flask (to give approximately 20% THF by volume) and 5ml into flask A. The contents of flask A was then decanted into flask D, which was maintained at -78 ^{o}C for the

duration of the reaction. The end capping reaction was allowed to proceed at -78 ^{o} C for 3 hrs and then raised to room temperature over 2 hrs. Nitrogen sparged methanol was then added to the polymer solution to terminate any residual living chains and 1 ml of BHT antioxidant (in toluene) added. The polymer solution was poured into a large excess of stirred methanol containing BHT causing the polybutadiene to precipitate as a sticky viscous liquid. The polymer was allowed to settle, and the supernatant solvent decanted to waste. The polymer was then collected, dried in vacuo to constant mass and stored in a freezer.

SEC analysis was performed on all the materials and the results detailed in the tables below. ^{1}H NMR, ^{19}F NMR ^{13}C NMR were also used to quantify the degree of end-capping. ^{19}F NMR and ^{13}C NMR were performed since during end-capping the proton signals from the fluoroalkylbromides moved considerably when attached to the end of a polymer. The signal at 4.2ppm from the CH_2O proton signal shifted to 3.76ppm in the proton spectrum after end-capping. As the polymer backbone masks the CH_2 multiplet at 1.85ppm, a ^{13}C NMR was required to establish that the peak was indeed the end group and not THF as in a ^{1}H spectrum they appear at the same point. The ^{13}C-NMR of THF in $CDCl_3$ has two signals for CH_2 at 25.62ppm and CH_2O at 67.97ppm and the NMR taken proved that THF was not present in the end product. Secondly, a ^{19}F NMR was performed to make sure that the same fluorine shifts were present on the polymer as in the fluoroalkylbromide.

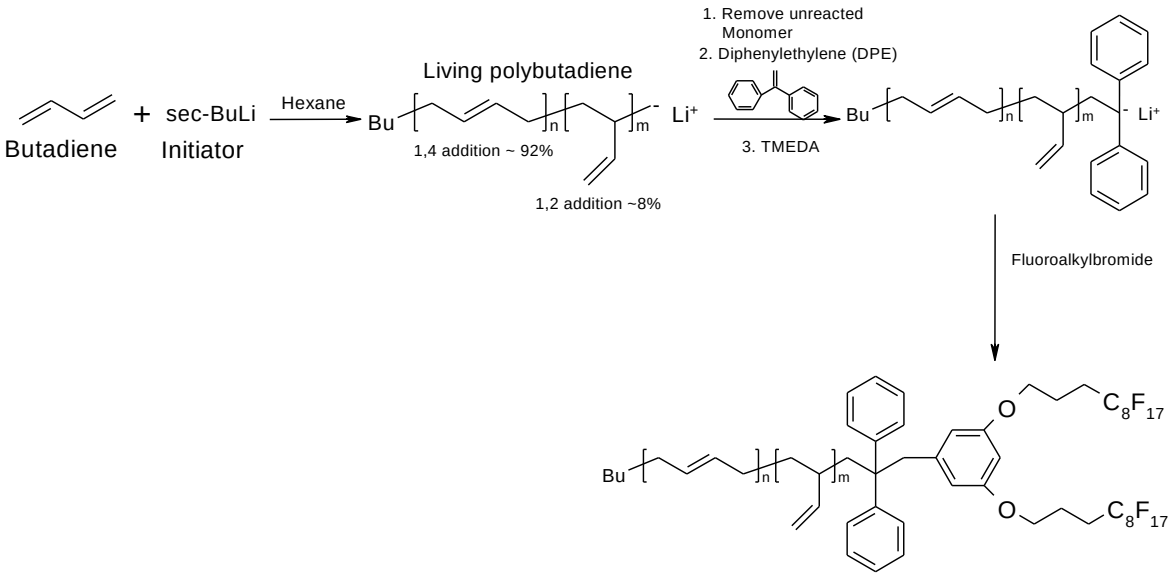

Figure 3:37 End-capping Mechanism using Type “a” Fluoroalkylbromides

3.3.9.1 Synthesis of Polybutadiene end-capped with Type "a" Fluoroalkylbromides

The procedure outlined above was followed except that type "a" fluoroalkylbromides were used instead of benzyl bromide. Three end capped polybutadiene additives were synthesised with different molecular weights. Molecular weights and the % end-capping is summarised in table 3:2.

Sample Code	**M_n gmol^{-1}**	**% End-capping**
PBa5	7100	84
PBa10	15400	86
PBa20	26800	81

Table 3:2 Table of % end-capping for eolybutadiene end-capped with type "a" fluoroalkylbromides from NMR integrations

The extent of end-capping obtained using this method was in each case greater than 80% which is more than satisfactory, when considering the number of side reactions that could occur. The reason that the end-capping was not 100% is almost certainly due to the introduction of traces of environmental impurities such as water, oxygen or carbon dioxide, all of which may react with and terminate the living carbanionic chain ends.

Below is an example of an NMR obtained from a typical type "a" end-capping. From figure 3:38 it is clear that proton signals shift when attached to a polymer end. This is due to their new environments. The amount of end-capping was quantified using the peaks at δ3.65, which were for 4H, and compared with the peaks at δ3.25, which were for 2H.

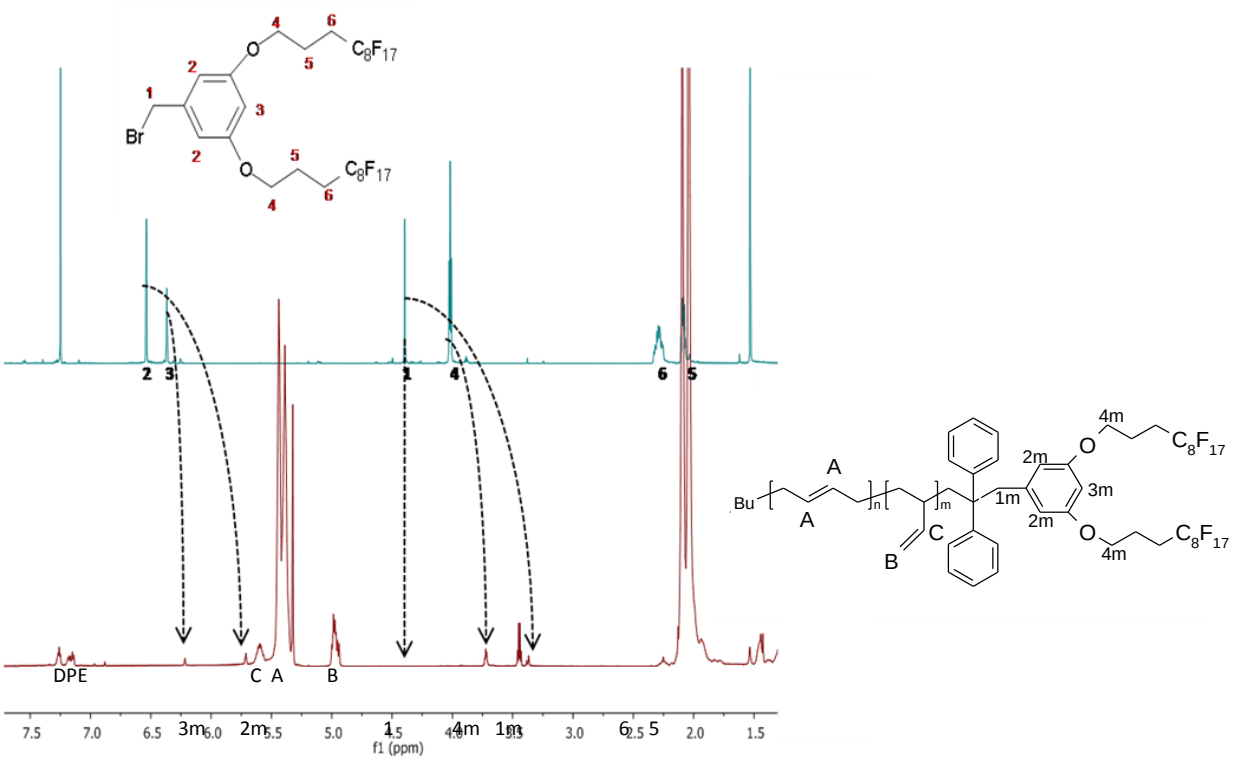

Figure 3:38 NMR of a typical type "a" end-capping

The peaks labelled A, B, C and at 2ppm can be assigned to the polymer backbone. When the polymer is end-capped most of the end-capping peaks (1-6, excluding 5) and the polymer backbone can still be separately seen, however, the CH_2 peak from the additive that was at 4.4ppm has moved to 3.4ppm as it is attached to the polymer. The end-capped polymer NMR no longer has a peak at 4.4ppm as no unreacted brominated additive is present. .

3.3.9.2 Synthesis of Polybutadiene end-capped with Type "b" Fluoroalkylbromides

Again the procedure outlined above was followed except that type "b" fluoroalkylbromides were used. Only one polymer, M_n 7000 UNITS, was synthesised and the extent of end-capping was 75%. The amount of end-capping was quantified using the peaks at δ3.65, which were for 4H and compared with the peaks at δ3.29, which were for 2H. The extent of end-capping is slightly lower than for the previous alkylbromides but still more than sufficiently high enough to be used in further studies. Below is the NMR obtained from a type "b" end-capping. From figure 3:39 it is clear that proton signals shift when attached to a polymer end. This is due to the new environments.

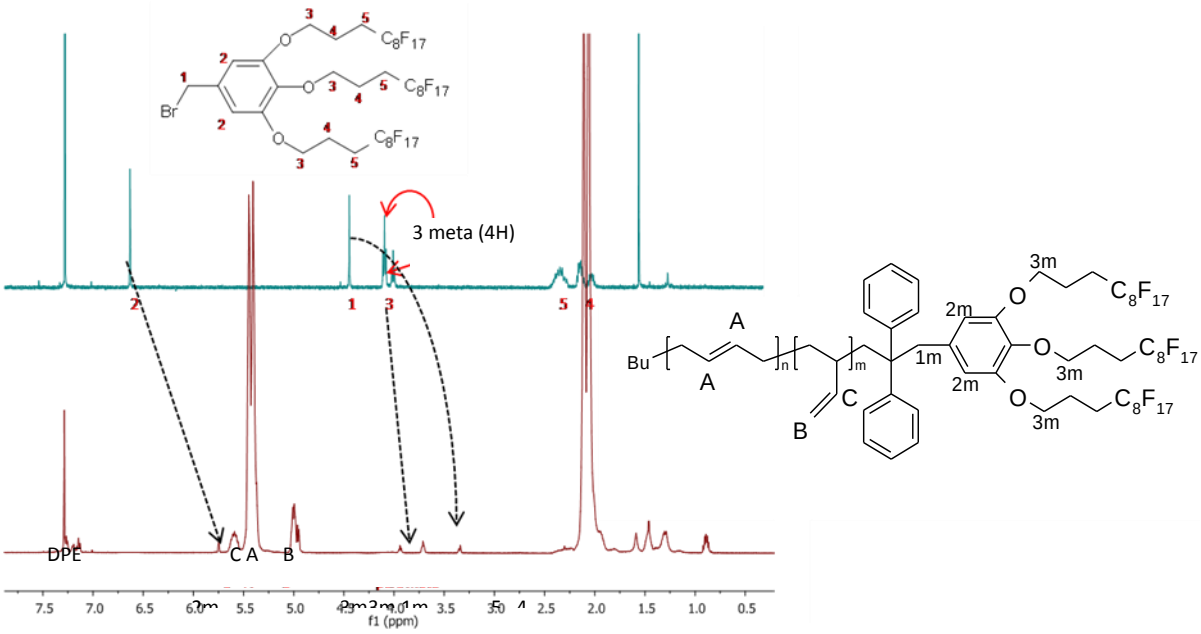

Figure 3:39 NMR of a typical type "b" end-capping

3.3.9.3 Synthesis of Polybutadiene end-capped with Type "c" Fluoroalkylbromides

Again the procedure outlined above was followed except that type "c" fluoroalkylbromides were used. The extent of end-capping is summarised in table 3:3.

Sample Code	M_n / gmol^{-1}	% End-capping
PBc5	4200	86
PBc10	13500	99
PBc20	24200	79
PBc50	78300	65

Table 3:3 Table of % end-capping for polybutadiene end-capped with type "c" fluoroalkylbromides

The extent of end-capping is excellent for all the polymers; however the extent of end-capping for PBc50 is slightly lower than desired. This could be because the higher molecular weight makes measuring out accurately the required amount of alkylbromide difficult and the reduced amount of chain ends increases the reaction time increasing the chance of termination by impurities. Nevertheless all were used for further studies.

Below is an example of an NMR obtained from a typical type "c" end-capping. From figure 3:40 it is clear that proton signals shift when attached to a polymer end. This is due to the new

environments. The amount of end-capping was quantified using the peaks at δ4.05, which were for 8H.

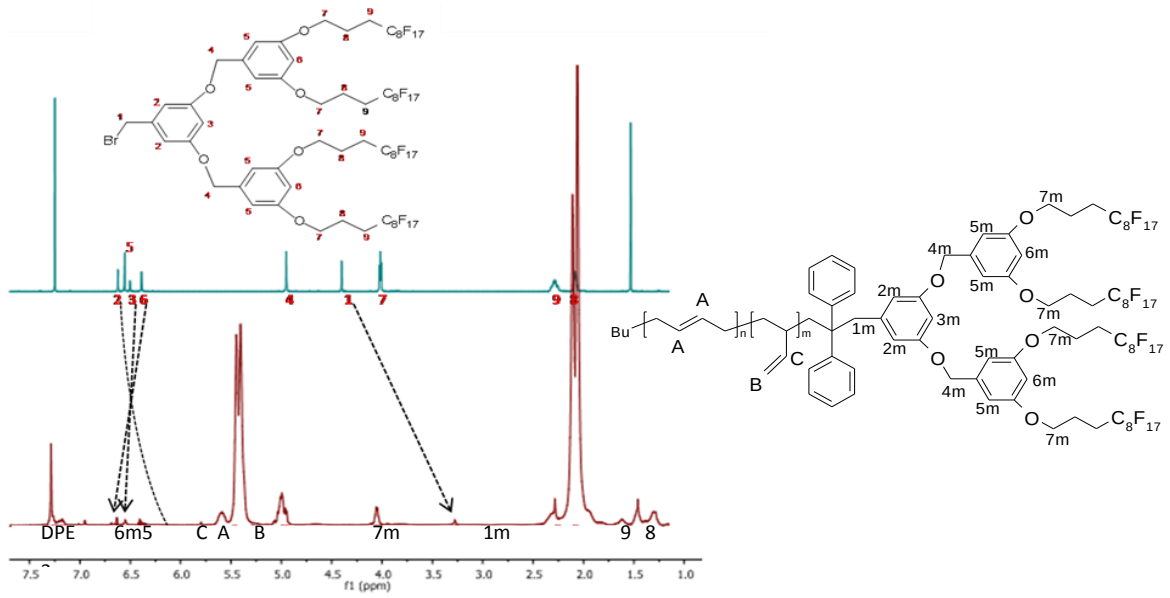

Figure 3:40 NMR of a typical type “c” end-capping

3.4 Synthesis of polyethylene-co-butene by the catalytic hydrogenation of polybutadiene

There are many methods to hydrogenate the backbone of polybutadiene and form polyethylene-co-butene, a polymer analogous in structure to LLDPE. Generally, high temperature, pressures and a transition metal catalyst are used. Many hydrogenations are carried out using homogenous catalysis. These catalysts are formed by reaction between a metal alkyl and an organic salt of a transition metal[37, 38]. The benefits of homogenous catalysis are milder reaction conditions, whereas the disadvantages are that often hydrogenations are incomplete and separating the catalyst from the product is problematic. Therefore, often heterogeneous catalysis is used [37, 39-46] but there are also problems with such systems such as leaching, catalyst selectivity and activity. Despite possible problems with heterogeneous catalysis, in this study a Pd catalyst supported on $CaCO_3$ was chosen owing to the ease of work up.

The overall reaction for the saturation of end-capped polybutadiene follows the scheme in figure 3:41 where deuterium or hydrogen gas was used to saturate the double bonds of the polybutadiene using a palladium catalyst, on a calcium carbonate support, at 500psi and 95°C.

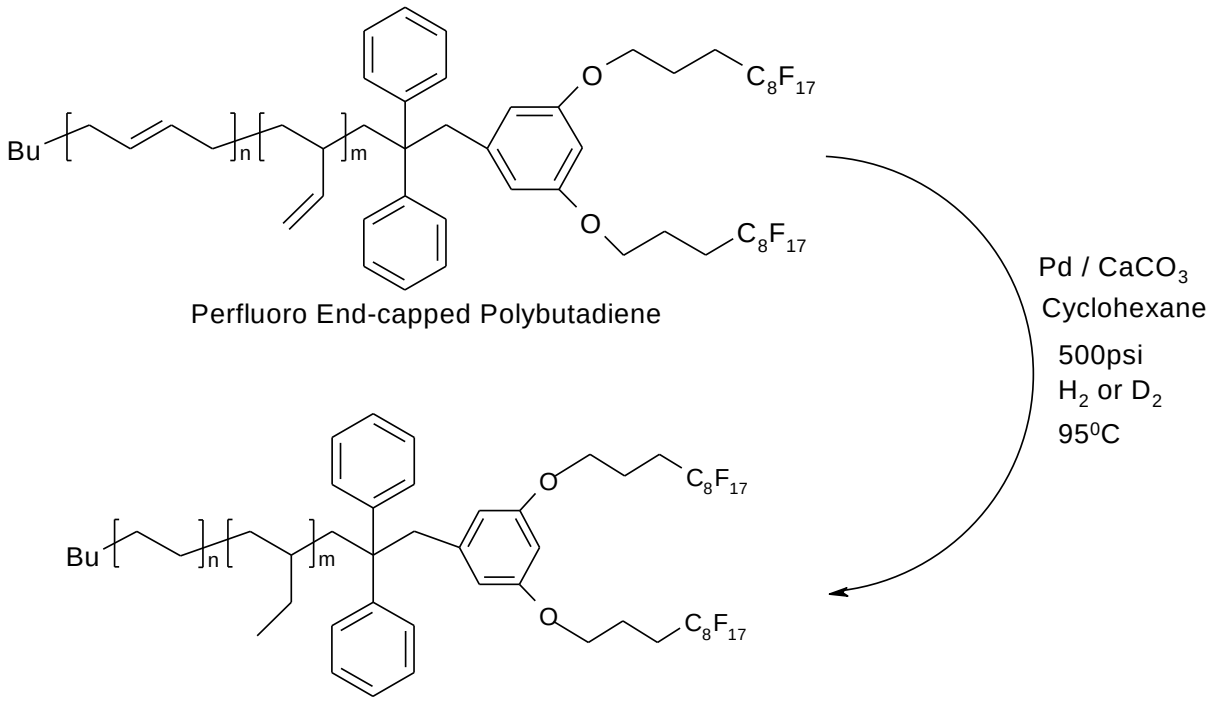

Figure 3:41 Hydrogenation mechanism

The percentage conversion of double bonds to single bonds via hydrogenation of polybutadiene to polyethylene was determined by ^{1}H NMR using TCE-d_2 at 100^0C, figure 3:42. Moreover, FT-IR spectroscopy confirmed the disappearance of C=C, confirming the successful saturation process. In the IR spectrum of polybutadiene, which has characteristic C=C peaks at ~960cm^{-1} for *trans*, at 735cm^{-1} for *cis* and one at 910cm^{-1} for *vinyl*, whereas upon saturation the strong and sharp[47] *trans, cis* and *vinyl* bands disappear when the PB is converted to PE.

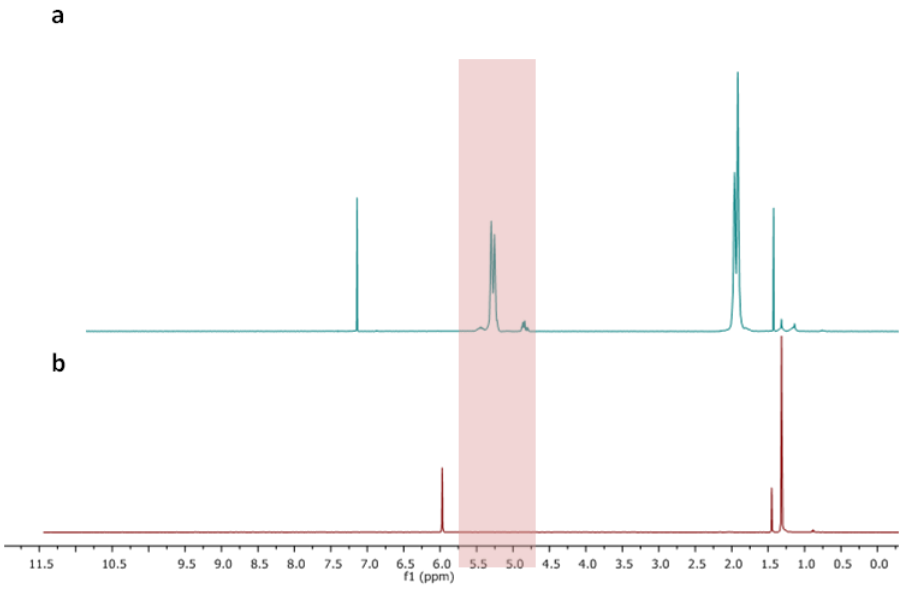

Figure 3:42 Typical NMR for the saturation of polybutadiene with hydrogen a) PB50 and b) hPE50 illustrating the disappearance of the C=C hydrogens

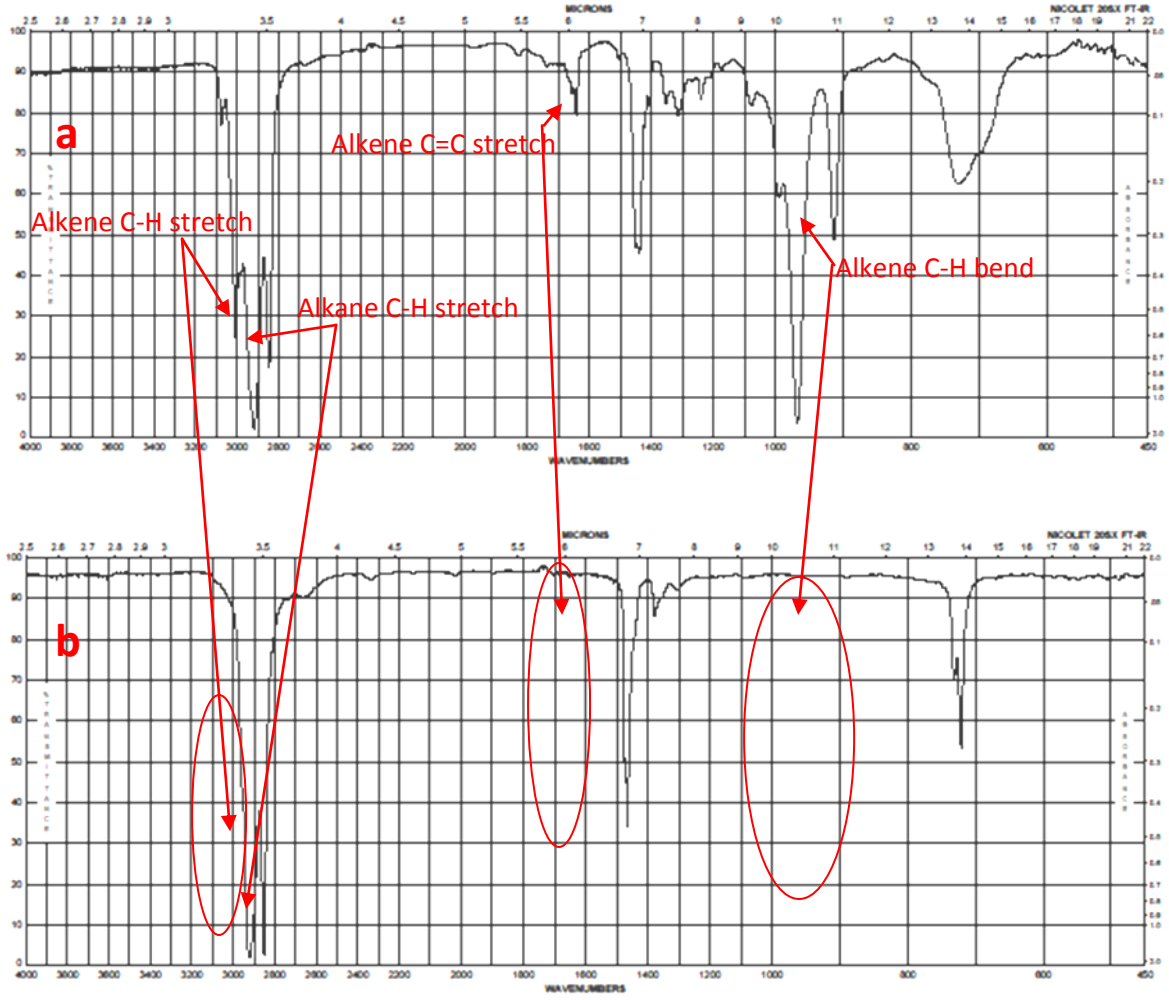

Figure 3:43 IR of a) polybutadiene and b) polyethylene

3.4.1 Hydrogenation of unfunctionalised Polybutadiene

The hydrogenations of the unfunctionalised polybutadiene achieved 100% saturation on the 2nd attempt, where the temperature was increased from 70°C to 100°C. From the Ideal gas equation, PV=nRT, if the temperature, T, is increased and the volume kept constant the pressure will rise to balance the equation. This will result in the molecules having more kinetic energy, thus more likely to react in a given time. Table 3:4 summaries the extent of hydrogenation estimated from NMR.

Sample Code	M_n ($gmol^{-1}$)	Hydrogenation %
hPE50	56600	99.7
	56600	100.0
hPE100	113000	98.6
	113000	100.0
hPE200	203000	99.4
	203000	100.0

Table 3:4 Results of hydrogenations of unfunctionalised polybutadienes

3.4.2 Deuteration of end capped Polybutadiene

Deuteration, rather than hydrogenation, enables contrast matching so the additives can be detected using techniques such as nuclear reaction analysis and neutron scattering where the matrix polymers were hydrogenated. The deuteration of the functionalized polymers were more problematic owing to the presence of the fluorinated end-group. Both a hydrogenation and deuteration was carried out on the functionalised polymers and in both cases the highest saturation achieved was 97%, after several attempts. A possible reason for this could be that the bulky fluorine groups at the end of the polymer chain are forming unimolecular micelles thus shielding the C=C from the reaction and the larger the end-group the more likely the polymers are to form micelles. Therefore, it is most likely that the unsaturated C=C bonds are directly behind the fluoro-dendrimer head group, but further investigation is required for a definitive conclusion to be drawn. A second explanation for the lower saturation is that the bulky end groups, especially for the “c” polymer are too large to bind the catalyst surface so some double bonds remain unsaturated.

The deuterations of the unfunctionalised low molecular weight polybutadienes, used to determine the effect of deuterium on surface segregation, proceeded to 100%. This further suggests that the end-groups on the polymers having a limiting effect on the deuteration process. The deuteration results are listed in table 3:5 below.

Sample Code	Deuteration %
dPE5	99.0
PEa5	99.0
PEa10	99.0
PEa20	99.0
PEb5	99.0
PEc5	73.0
PEc10	99.8
PEc20	98.0
PEc50	81.0

Table 3:5 Results of deuterations of functionalised polybutadienes

3.5 Summary

A range of both functionalised and unfunctionalised polymers were made successfully with very high end-capping yields. The percentage of *1,4* and *1,2*-polybutadiene microstructure (93% and 7% respectively) were consistent with what is expected from polymerisations carried out in hexane. These microstructures were ideal for making analogues to LLDPE via hydrogenation.

Hydrogenating polybutadiene prepared by anionic polymerisation yields a random copolymer of ethylene and 1-butene which is important as the composition of the final polymer depends on the 1,4 and 1,2 microstructure of the polybutadiene precursor. The hydrogenation and deuteration reactions of the unfunctionalised polymers went to 100% saturation but these quantitative conversions could not be achieved for the functionalized polymer. This is potentially an issue since the residual C=C bonds could result in cross-linking in the polymer blends which could ultimately undermine the maximum amount of surface segregation that is achievable. This is discussed in greater detail in section 6.3.

3.6 References

1. Narrainen, A. P.; Hutchings, L. R.; Ansari, I.; Thompson, R. L.; Clarke, N., *Macromolecules* **2007,** *40* (6), 1969-1980.
2. Hagiwara, H.; Morohashi, K.; Sakai, H.; Suzuki, T.; Ando, M., *Tetrahedron* **1998,** *54* (22), 5845-5852.
3. Appel, R.; Wihler, H. D., *Chemische Berichte-Recueil* **1976,** *109* (10), 3446-3449.
4. Baughman. T.W., S. J. C., Wagener. K.B., *Tetrahedron* **2004,** *60*, 10943-10948.
5. Ueda, K.; Hirao, A.; Nakahama, S., *Macromolecules* **1990,** *23* (4), 939-945.
6. Quirk, R. P.; Lee, Y., *Journal of Polymer Science Part a-Polymer Chemistry* **2000,** *38* (1), 145-151.
7. Huckstadt, H.; Gopfert, A.; Abetz, V., *Macromolecular Chemistry and Physics* **2000,** *201* (3), 296-307.
8. Gauthier, M.; Moller, M., *Macromolecules* **1991,** *24* (16), 4548-4553.
9. Takaki, M.; Asami, R.; Kuwata, Y., *Polymer Journal* **1979,** *11* (5), 425-428.
10. Halasa, A. F.; Adams, H. E., *Journal of Polymer Science Part C-Polymer Symposium* **1970,** (30), 169-&.
11. Cho, J. C.; Kim, K. H.; Kim, K. U.; Kwak, S.; Kim, J.; Jo, W. H.; Chun, M. S.; Lee, C. H.; Yeo, J. K.; Quirk, R. P., *Journal of Polymer Science Part a-Polymer Chemistry* **1998,** *36* (11), 1743-1753.
12. Novak, D. P.; Brown, T. L., *Journal of the American Chemical Society* **1972,** *94* (11), 3793-&.
13. Glaze, W. H.; Chaudhur.J; Hanicak, J. E.; Moore, M., *Journal of Organometallic Chemistry* **1972,** *44* (1), 39-&.
14. Waack, R.; Doran, M. A., *Chemistry & Industry* **1964,** (12), 496-497.
15. Stavely, F. W.; Dunbrook, R. F.; Forman, L. E.; Foster, F. C.; Stearns, R. S.; Talcott, T. B.; Wakefield, L. B.; Alliger, G.; Russell, J. R.; Smith, S.; Smith, W. A.; Willis, J. M.; Binder, J. L.; Forster, M. J.; Hanson, E. E.; Liska, J. W.; Ransaw, H. C.; Barzan, M.; Gates, R. D.; Johnson, B. L.; Downing, J. P.; Hammond, C. H.; Hanson, E. S.; Mayes, C. G.; Para, A.; Smith, F. M.; Brock, M. J.; Eberly, K. C., *Industrial and Engineering Chemistry* **1956,** *48* (4), 778-783.
16. Morton, M. a. L. J. F., *Rubber Chemistry and Technology 48*, 359-409.
17. Yuki, H.; Hotta, J.; Okamoto, Y.; Murahash.S, *Bulletin of the Chemical Society of Japan* **1967,** *40* (11), 2659-&.
18. Hirao, A.; Hayashi, M.; Matsuo, A., *Polymer* **2002,** *43* (25), 7125-7131.
19. Hirao, A.; Sugiyama, K.; Yokoyama, H., *Progress in Polymer Science* **2007,** *32* (12), 1393-1438.
20. Hsieh, H. L., Quirk, R.P, *Anionic Polymerization: Principles and Practical Applications*. Marcel Dekker Inc: 1996.
21. Pennisi, R. W.; Fetters, L. J., *Macromolecules* **1988,** *21* (4), 1094-1099.
22. Antkowia.Ta, *Abstracts of Papers of the American Chemical Society* **1971,** (NSEP), 63-&.
23. Nentwig, W.; Sinn, H., *Makromolekulare Chemie-Rapid Communications* **1980,** *1* (2), 59-63.
24. Ryu, S. W.; Asada, H.; Watanabe, T.; Hirao, A., *Macromolecules* **2004,** *37* (17), 6291-6298.
25. Hirao, A.; Haraguchi, N., *Macromolecules* **2002,** *35* (19), 7224-7231.
26. Glaze, W.; West, R., *Journal of the American Chemical Society* **1960,** *82* (16), 4437-4437.
27. Boutillier, J. M.; Favier, J. C.; Hemery, P.; Sigwalt, P., *Polymer* **1996,** *37* (23), 5197-5203.
28. R.H.Crabtree, *The Organometallic Chemsitry of the Transition Metals*. 3rd ed.; Wiley: New York, 1994; p p2.

29. Wang, J. S.; Warin, R.; Jerome, R.; Teyssie, P., *Macromolecules* **1993,** *26* (25), 6776-6781.
30. Teyssie, P.; Fayt, R.; Hautekeer, J. P.; Jacobs, C.; Jerome, R.; Leemans, L.; Varshney, S. K., *Makromolekulare Chemie-Macromolecular Symposia* **1990,** *32*, 61-73.
31. Zune, C.; Dubois, P.; Jerome, R.; Kriz, J.; Dybal, J.; Lochmann, L.; Janata, M.; Vleek, P.; Werkhoven, T. M.; Lugtenburg, J., *Macromolecules* **1998,** *31* (9), 2744-2755.
32. Fetters, L. J.; Young, R. N., *Anionic Polymerisation; Kinetics, Mechanisms and Synthesis*. American Chemical Society: Washington, DC, 1981.
33. Helary, G.; Fontanille, M., *European Polymer Journal* **1978,** *14* (5), 345-348.
34. Fontanille, M.; Helary, G.; Szwarc, M., *Macromolecules* **1988,** *21* (5), 1532-1533.
35. Halasa, A. F.; Lohr, D. F.; Hall, J. E., *Journal of Polymer Science Part a-Polymer Chemistry* **1981,** *19* (6), 1357-1360.
36. Stellman, J. M.; Woodward, A. E., *Journal of Polymer Science Part a-2-Polymer Physics* **1971,** *9* (1), 59-&.
37. Rachapudy, H.; Smith, G. G.; Raju, V. R.; Graessley, W. W., *Journal of Polymer Science Part B-Polymer Physics* **1979,** *17* (7), 1211-1222.
38. Ko, Y.; Kim, H.; Kim, J.; Row, K.; So, M. Process for removal of metal catalyst from polymer selectively hydrogenated unsing organotitanoum compound. 08/15/2001, 2002.
39. Dooley, K.; Knopf, C.; Nikitopoulos, D. *Heterogeneous Catalyzed Polymer Hydrogenation in Oscillating Systems*.
40. Okumura, M.; Akita, T.; Haruta, M., *Catalysis Today* **2002,** *74* (3-4), 265-269.
41. Sarkany, A.; Schay, Z.; Stefler, G.; Borko, L.; Hightower, J. W.; Guczi, L., *Applied Catalysis a-General* **1995,** *124* (2), L181-L187.
42. Jugnet Y; Sedrati R; JC, B., *JOURNAL OF CATALYSIS* **2005,** *229* (1), 252-258.
43. Hillmyer, M. A.; Bates, F. S., *Macromolecules* **1996,** *29* (22), 6994-7002.
44. Hadjichristidis, N.; Xenidou, M.; Iatrou, H.; Pitsikalis, M.; Poulos, Y.; Avgeropoulos, A.; Sioula, S.; Paraskeva, S.; Velis, G.; Lohse, D. J.; Schulz, D. N.; Fetters, L. J.; Wright, P. J.; Mendelson, R. A.; Garcia-Franco, C. A.; Sun, T.; Ruff, C. J., *Macromolecules* **2000,** *33* (7), 2424-2436.
45. *Platinum Metals Review* **1999,** *43* (4), 172-175.
46. Luo, Y. M., *Journal of Applied Polymer Science* **1995,** *56* (6), 721-737.
47. Rochefort, W. E.; Smith, G. G.; Rachapudy, H.; Raju, V. R.; Graessley, W. W., *Journal of Polymer Science Part B-Polymer Physics* **1979,** *17* (7), 1197-1210.

4 Surface Analysis

Surface properties are important when discussing the applications of polymers. To date this is the first study of the influence of multi end functional polyethylene on surface composition and surface properties. In this chapter the influence of small quantities of multi-end functional additive on the surface property is determined by direct measurement (hydrophobicity) and chemical analysis (XPS) using the experimental techniques described in chapter 2. A more detailed theoretical basis of each technique is briefly outlined along with how the data were analysed. The results obtained will be discussed in terms of molecular structure, i.e. the influence of functional group, additive molecular weight and matrix molecular weight.

4.1 Contact Angles

The shape of a droplet formed on the surface of a sample is determined by the Young-Laplace equation and is the most common method of measuring a solid's surface energy.

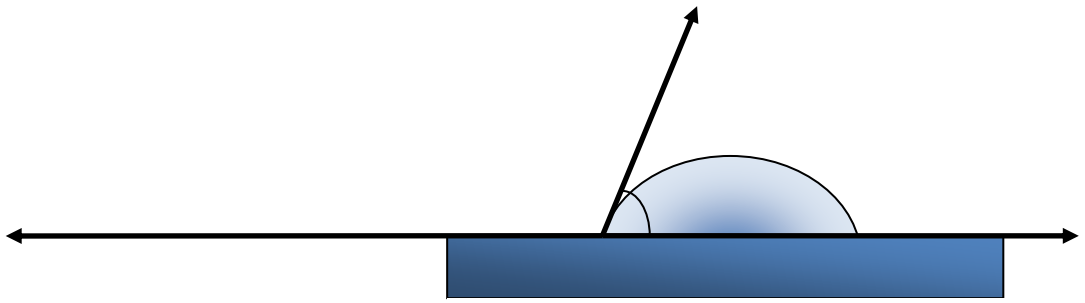

Figure 4:1 Illustration of surface an interfacial components contributing to equilibrium contact angle

Contact angle is a result of the thermodynamic equilibrium of the surface free energy at the solid-liquid-vapour interface and was developed for the case of an ideal solid surface, where the surface is smooth, rigid, chemically homogenous, insoluble and non-reactive. During equilibrium and when the driving force for spreading is the minimisation of the interfacial free energy [1].

There are two ways of measuring a contact angle:

(1) Static contact angle: obtained by sessile drop measurements, where the drop is deposited on the surface and a value is obtained by a goniometer.

(2) Dynamic contact angle: measured during the growth (advancing contact angle) and shrinkage (receding contact angle) of a water droplet. The difference between the advancing and receding contact angle is referred to as the contact angle hysteresis. Many surfaces show a large $\Delta\theta$ due to surface roughness and chemical heterogeneity[2].

Because most surfaces are rough two models have been developed for the behaviour of liquid droplets on surfaces. In either case a much higher contact angle is observed than those obtained from smooth surfaces.

(1) Wenzel Model describes how a liquid droplet penetrates into a rough surface and becomes pinned so it cannot easily roll off when tilted. A roughness factor (r) used in this model can be determined from a height map on an AFM[3] micrograph.
(2) Cassie-Baxter Model utilises the idea that there are air-pockets in the cavities of rough surfaces which suspend the liquid droplet so it can easily roll off when tilted.

Contact angle measurements yield data which reflects the thermodynamics of the liquid/solid interaction and characterises the wetting behaviour. Penetration of the contact fluid into the solid, swelling of the solid by the liquid and chemical reactions can all play a role in the difference between the experimentally observed and the apparent contact angle[4]. The contact angle of an ideal solid is referred to as the "ideal contact angle" (ICA). This becomes apparent when dealing with rough surfaces where there is no ICA instead the "apparent contact angle" (APCA). This is the angle between the tangent to the liquid-fluid interface and the line that represents the nominal surface.

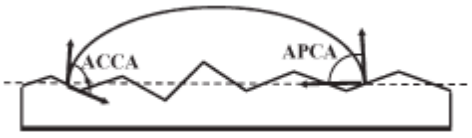

Figure 4:2 Diagram to show the difference between the actual contact angle(ACCA) and the apparent contact angle(APCA)[5]

On rough surfaces there is both chemical and physical hysteresis, whereas on ideal surfaces there is no hystersis[4, 6], where the molecules at the interface may relax or change their configuration

when the surfaces come into contact, arriving at time in an equilibrium configuration which may differ from the start. This reorganisation may take various forms involving interdiffusion, reorientation[7, 8], or exchange of chemical species from the bulk to surface or vice versa [3, 9].

4.1.1 Analysis and Results

The contact angles for all the films span from 103° to 115° for water, 1° to 55° for dodecane and 80° to 115° for glycerol, figure 4:3 illustrates the general trends each contact fluid gives on the films. Table 4:1 lists the polar and dispersive contributions to the surface tension from the contact fluids and table 4:2 lists the average contact angles for PTFE and each of the matrix polymer films.

Contact Fluid	γ^D	γ^P	γ
Glycerol	34	30	64
Water	21.8	51	72.8
Dodecane	25.4	0	25.4

Table 4:1 Surface free energies for contact fluids used

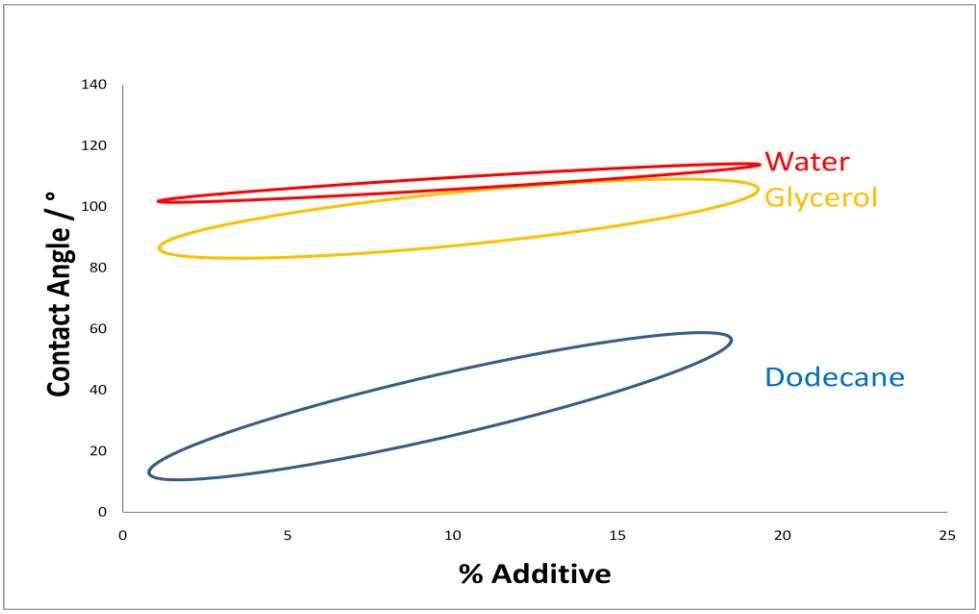

Figure 4:3 Trends of obtained contact angle values for three different contact fluids

Polymer Film	Average Water CA /°	Average Glycerol CA /°
PTFE	108.67 ± 3.44	112.17 ± 5
hPE50	92.50 ± 3.99	95.10 ± 2
hPE100	97.75 ± 6.02	90.82 ± 1
hPE200	98.42 ± 0.58	86.67 ± 1

Table 4:2: Average contact angles for matrices and PTFE

The values of the water CAs on the hPE film surfaces are different but agree within the errors bars. The literature values for the water CAs of LLPDE and PTFE are 89° and 108° respectively[10, 11]. The LLDPE results are higher than expected and could be owing to surface roughness. However, the glycerol CA values on hPE are significantly different from one another which is unusual all the polymer films are essentially PE and of sufficiently high molecular weight for end groups to be insignificant. Roughness could be an important parameter adding to the inconsistency of the results. A greater variation in surface roughness can not only add to the variation in the CAs measured but also to the absolute value obtained.

The water contact angle results for blend films containing multi-end-capped additives are presented by firstly comparing the effect of additive molecular weight on surface segregation, then the effect of matrix molecular weight and finally the effect of the number of fluorocarbon groups. Each of the films had six measurements taken on the surface, from which a standard deviation was calculated and plotted as error bars. The nominal uncertainty in solution concentration given by the precision of weighing out the polymers is much smaller than the width of the points presented. However, the difficulty in transferring hot xylene solutions to the photoresist spinner may be increasing this uncertainty somewhat.

4.1.1.1 Effect of Additive Molecular weight on Surface Segregation

The additives used were always one of four different molecular weights: 5; 10; 20 or 50 $kgmol^{-1}$. From figure 4:4 it is obvious those additives that have molecular weight higher than 20 $kgmol^{-1}$ are not as effective at reducing surface wettability compared to those of lower molecular weight. However there is significant uncertainty and overlapping data in each series which suggests that hydrophobicity is not very sensitive to molecular weight of additive. This is partly due to the fact that PE is already quite hydrophobic so there is only limited scope for increasing hydrophobicity.

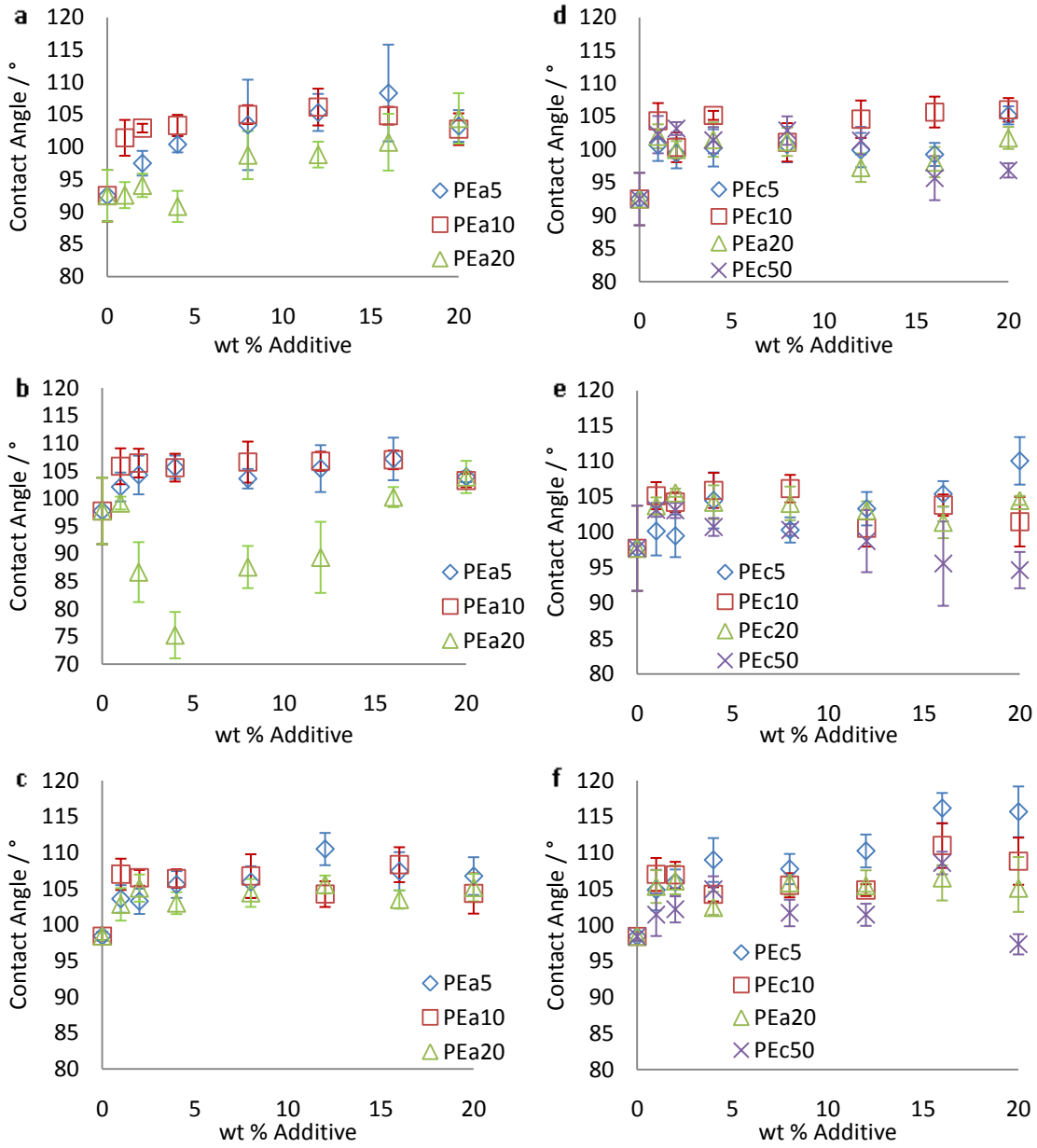

Figure 4:4 Water contact angles data comparing the effect of additive molecular weight on surface segregation for a) deuterated additives of type "a" in hPE50, b) deuterated additives of type "a" in hPE100, c) deuterated additives of type "a" in hPE200, d) deuterated additives of type "c" in hPE50, e) deuterated additives of type "c" in hPE100 and f) deuterated additives of type "c" in hPE200

4.1.1.2 Effect of Matrix Molecular weight on Surface Segregation

Following from section 4.1.1.1 the additives that were most effective at reducing the surface wettability (additives with a molecular weight of 10 $kgmol^{-1}$ and below) were further investigated by comparing the effect of matrix molecular weight. These additives were blended into one of three different matrices with a molecular weight of either 50 $kgmol^{-1}$; 100 $kgmol^{-1}$or 200 $kgmol^{-1}$. The water contact angle data are shown below for additives of type "a", figure 4:5, additives of type "b", figure 4:7 and additives of type "c", figure 4:9.

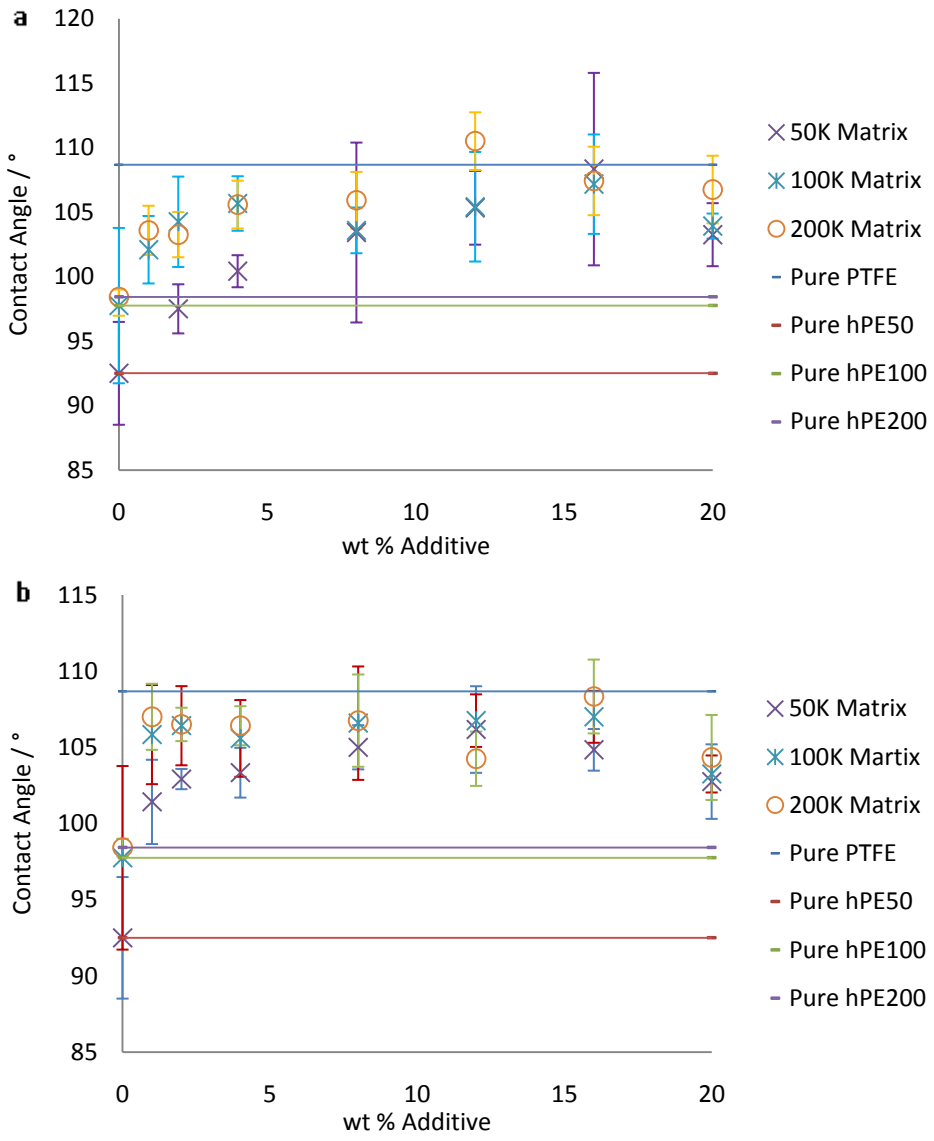

Figure 4:5 Water CA for a) PEa5 in hPE50, hPE100 and hPE200 matrix and b) PEa10 in hPE50, hPE100 and hPE200 matrix

For every blend, adding a small amount of any additive increases the contact angle from that of the pure homopolymer towards that of PTFE. This basic trend is seen for every combination of additive and matrix although there is some variation in the concentration of additive required to achieve this for each system. At the lower percentage additive concentrations the additives behave very similarly except 5 $kgmol^{-1}$ additive "a" in 50 $kgmol^{-1}$ matrix which has a lower CA. As the percentage of additive increases it becomes more apparent that the 5 $kgmol^{-1}$ additive "a" in 200 $kgmol^{-1}$ matrix is the most efficient at increasing the water CA. By considering the increase in contact angle in terms of the pure polymer, table 4:2, which increases with molecular weight, it is apparent that fluorine has a dramatic effect on the water contact angle.

For the 50 kgmol^{-1} matrix, irrespective of the additive molecular weight, the CA increases the most, compared to pure matrix. For the 100 kgmol^{-1}and 200 kgmol^{-1} matrix the increases in contact angle compared to the pure matrix is about the same, figure 4:6.

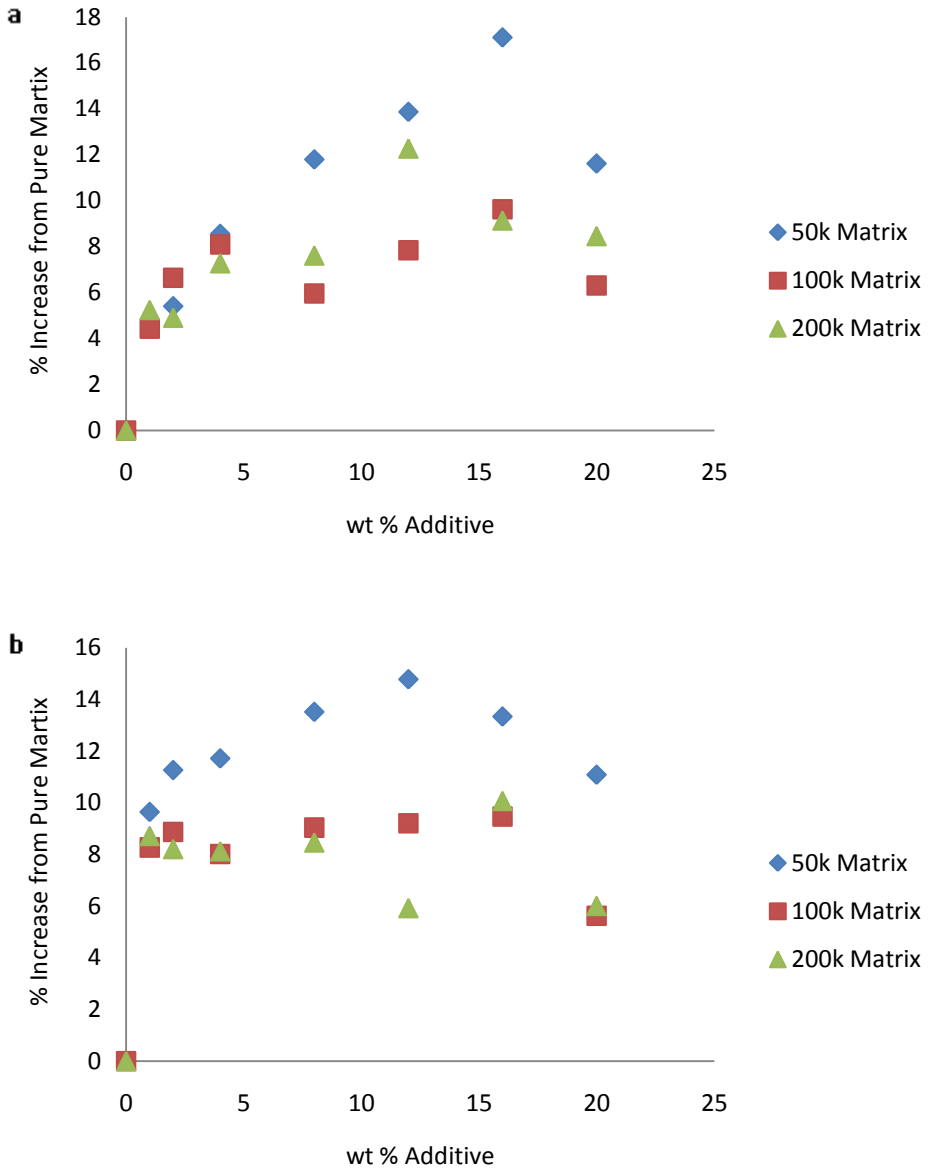

Figure 4:6 Percentage in Water CA increase for a) PEa5 in hPE50, hPE100 and hPE200 matrix and b) PEa10 in hPE50, hPE100 and hPE200 matrix where the error is $\pm$ 5%

The water contact angle data for additives of type “b”, figure 4:7, illustrates that within error this additive gave near identical increases in hydrophobicity in 50 kgmol^{-1} and 100 kgmol^{-1} PE matrices. In contrast in the 200 kgmol^{-1} there is greater modification for a given concentration of PEb5 until

the highest concentration of additive where its ability to increase the water CA is similar for the other matrices.

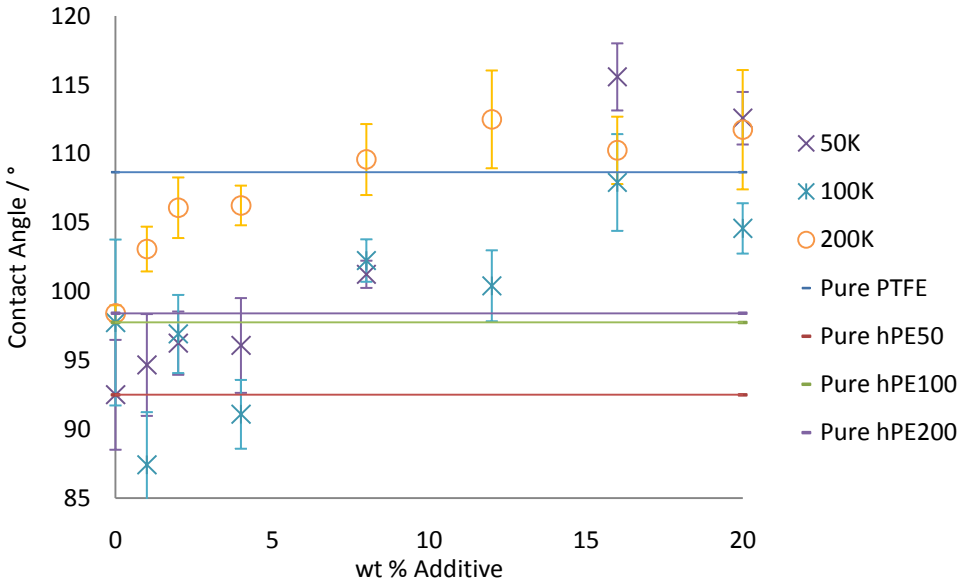

Figure 4:7 Water CA for PEb5 in hPE50, hPE100 and hPE200 matrix

From figure 4:8 it is apparent again that the increase in contact angle, relative to the pure polymer, increases as more fluorinated additive is added. The 50 and 200 $kgmol^{-1}$matrices behave very similarly until the highest concentration of additive, where the 50 $kgmol^{-1}$ matrix is the most hydrphobic. Surprisingly, in the 100 $kgmol^{-1}$ matrix the contact angle after PEb5 is added appears to have decreased from the pure component at low concentrations before increasing at higher concentrations.

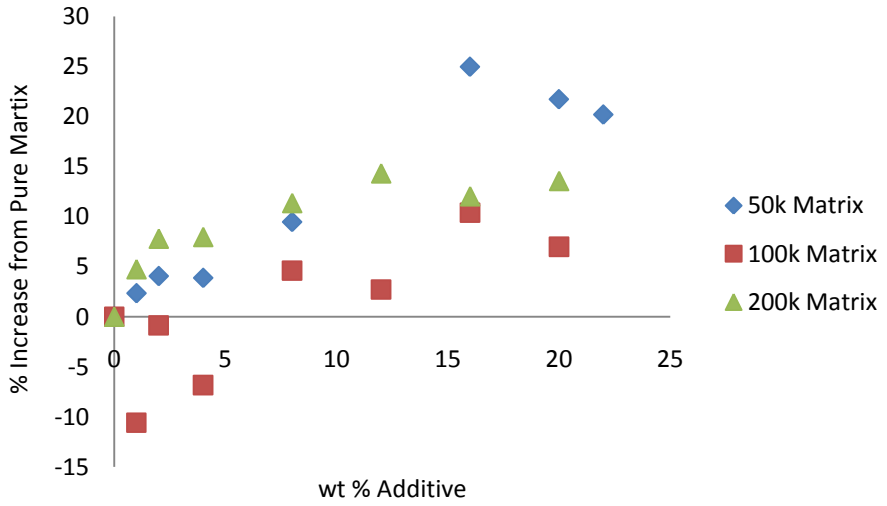

Figure 4:8 Percentage water CA increase for PEb5 in hPE50, hPE100 and hPE200 matrix where the error is $\pm$ 5%

Additives of type "c" show the clearest surface modification behaviour according to matrix molecular weight, where the highest matrix molecular weight tends towards the highest CA. Blends containing additive PEc5 have the greatest hydrophobicity, which could be taken to indicate greater surface segregation. As the concentration of additive increases it becomes more apparent that the lowest molecular weight additive (PEc5) in the highest molecular weight matrix (200 $kgmol^{-1}$) is the most efficient at increasing the water CA which is followed by the 10 $kgmol^{-1}$ additives of type "c" in 200 $kgmol^{-1}$ matrix. This is a clear indication that the greater the difference between additive molar mass and matrix molar mass the greater the efficiency of surface modification.

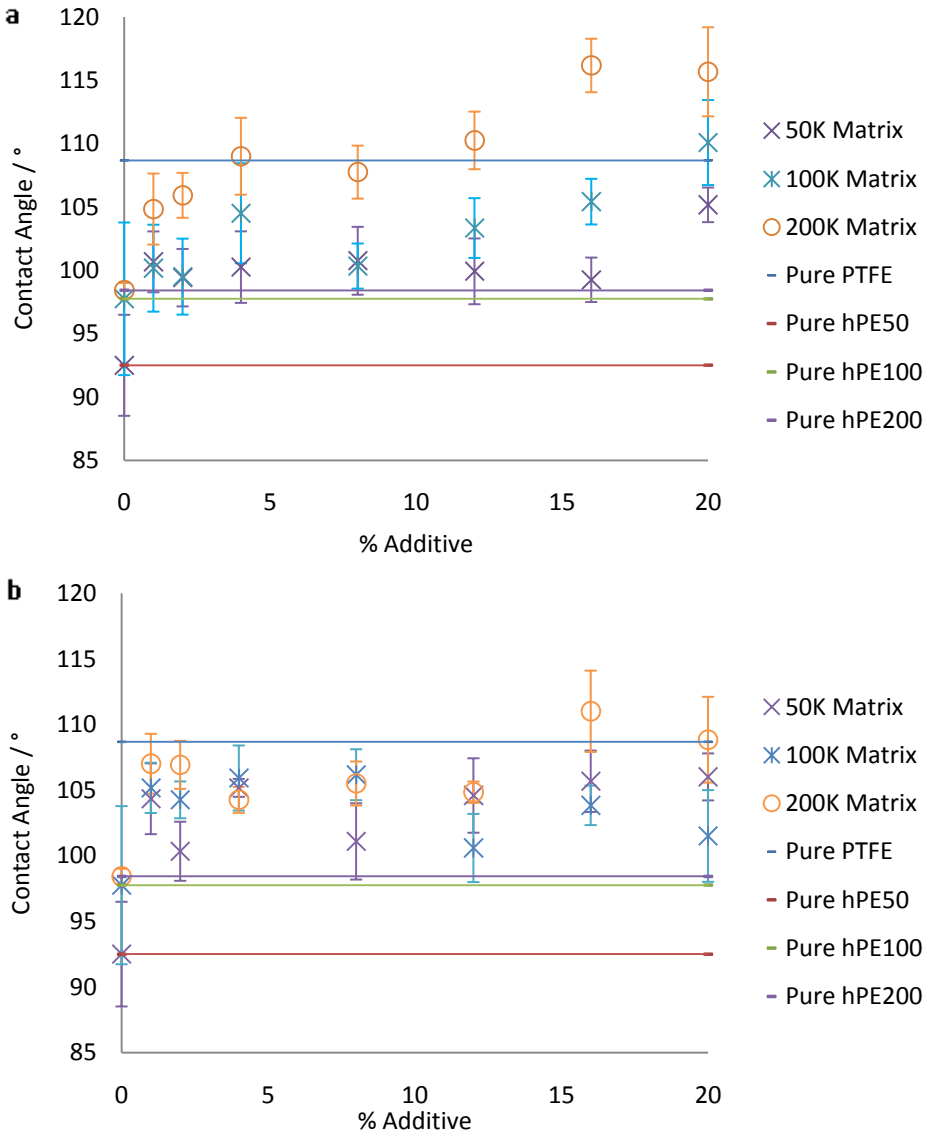

Figure 4:9 Water CA for a) PEc5 in hPE50, hPE100 and hPE200 matrix and b) PEc10 in hPE50, hPE100 and hPE200 matrix

By comparing the increase in contact angle, in terms of pure polymer, for additives of type "c", figure 4:10, for PEc5 the increase follows the concentration of additive with the 200 kgmol-1 matrix the most altered. However, for PEc10 regardless of the matrix molecular weight, the increase in hydrophobicity of PE is similar when PEc10 is added.

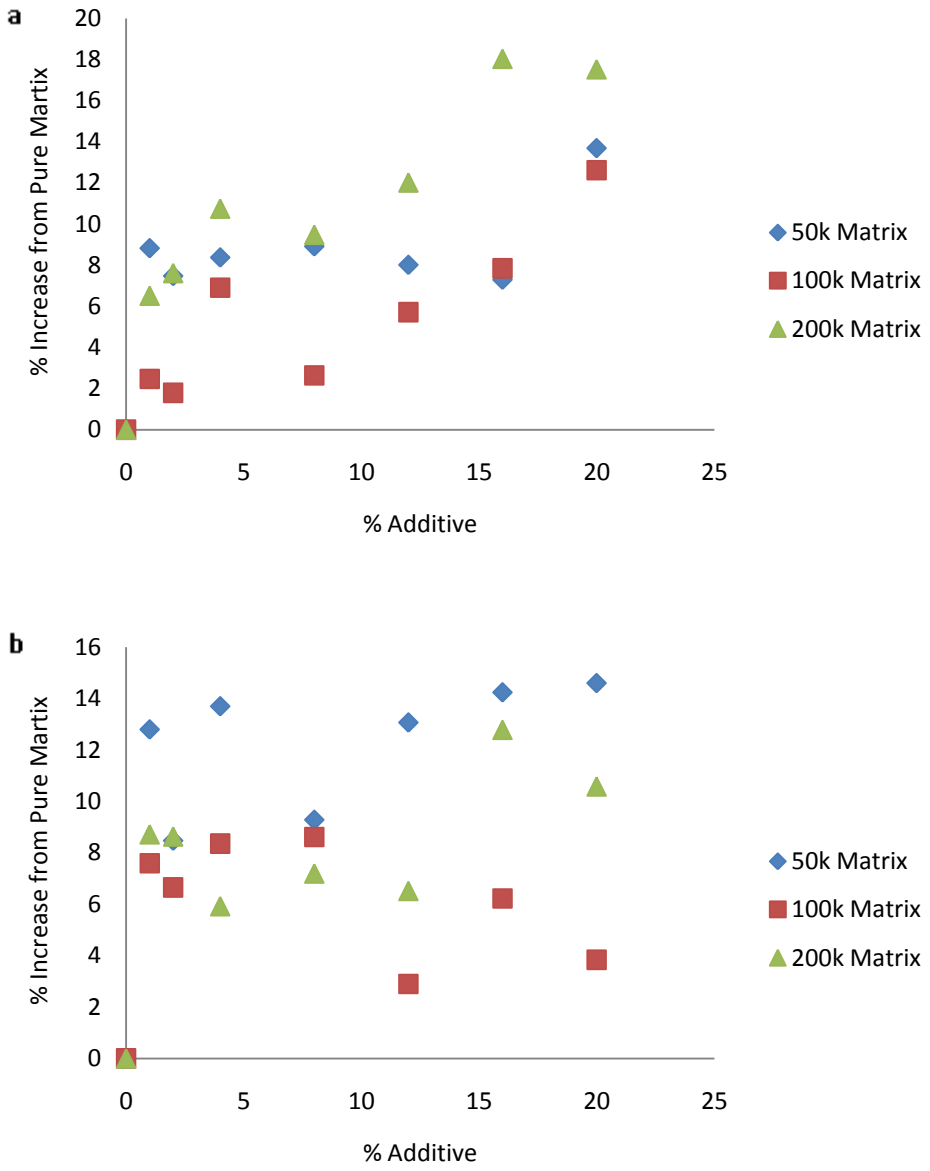

Figure 4:10 Percentage water CA increase for a) PEc5 in hPE50, hPE100 and hPE200 matrix and b) PEc10 in hPE50, hPE100 and hPE200 matrix where the error is $\pm$ 5%

A control experiment was performed based on these results using a non-end-capped deuterated additive that was 5 kgmol^{-1} mixed in 200 kgmol^{-1} matrix, figure 4:11. These results show that a low molecular weight deuterated additive does have some effect on raising the water CA, by ~ 4°, however, this may not be due to the deuterium, and in fact it could be owing to the surface roughness as adding a little low molecular weight additive could increase the crystallinity, so increasing the roughness.

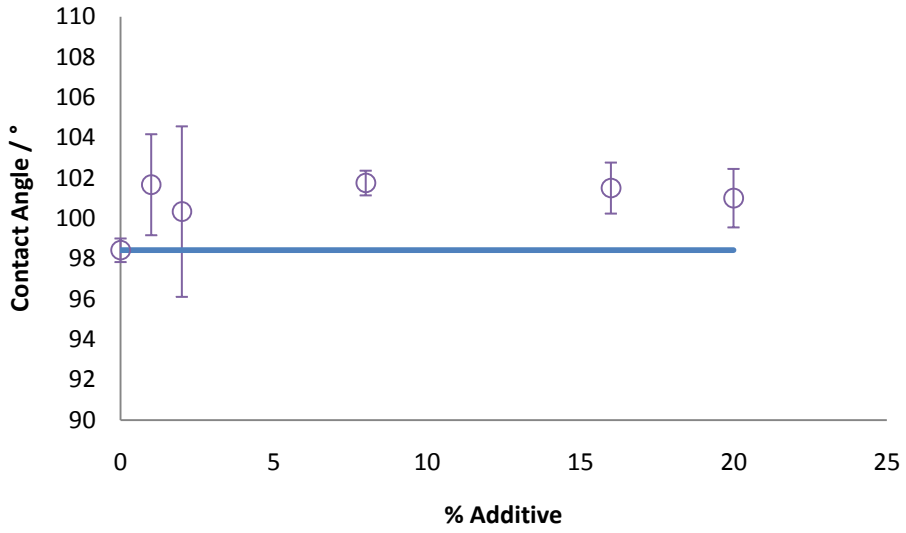

Figure 4:11 Water CA for 5 kgmol^{-1} deuterated unfunctionalised control additive (dPE5) in hPE200 matrix (blue line)

4.1.1.3 Effect of Type of Additive on Surface Segregation

Since the previous results show quite subtle variations in behaviour as a function of additive functionalisation and matrix molecular weight it is easier to see overall trends in terms of the extremes of these parameters. Figure 4:14 illustrates which additive, “a”, “b” or “c”, is the most efficient as increasing the surface wettability. It is clear that the higher the fluorine content of the end group the greater the additive’s ability to increase the contact angle.

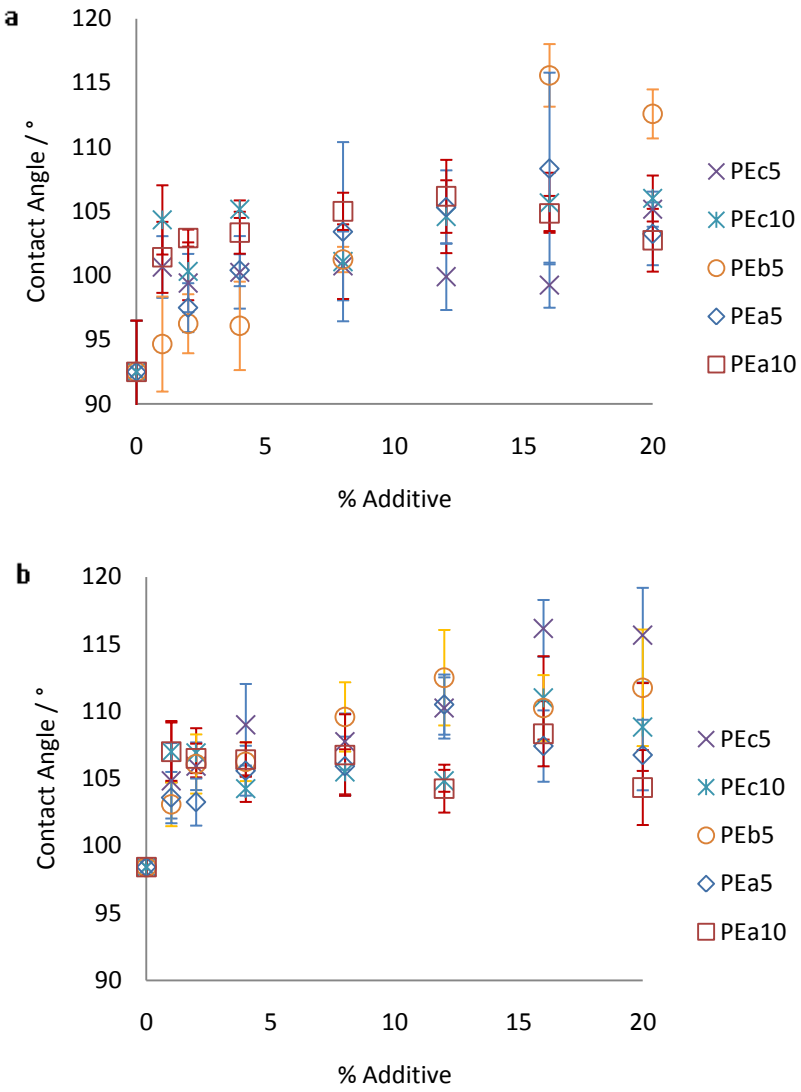

Figure 4:12 Water CA for different deuterated additives in a) hPE50 and b) hPE200 matrix

In most cases an initial increase in hydrophobicity with additive concentration followed by a broad plateau is visible. This is similar to results found for related amorphous blends[12]. For semicrystalline additives in 200 $kgmol^{-1}$ matrices much higher CAs are achieved than the lower molar mass matrices where, the highest CA is about 105° for the lower molar mass matrix, whereas in the higher molar mass matrix the average is about 105°. In either matrix additive PEb5 gives on average the highest CA.

4.2 Surface Free Energies

The contact angle of a surface can be directly used to determine the surface free energy of a solid. The surface free energy can be regarded as the surface tension of a solid[13] which is the energy required to create a unit of surface area. Surface tension measurements yield data which directly reflects the thermodynamic characteristics of the liquid being tested, therefore to characterise the thermodynamics of a solid surface fully the solid needs to be tested against a series of liquids, as there are two unknowns in the Young Laplace equation, figure 4:1. Calculations based on these measurements produce a parameter which quantifies the characteristics of the solid. There are 5 models commonly used to calculate the surface tension of a solid and they are discussed below in chronological order.

(1) Critical Surface Tension (Zisman along with Fox[14, 15]) – Empirical method for determining the wettability of low energy solid surfaces. By using several different non-polar liquids and plotting the relationship between $cos\vartheta$ and γ_L the data will form a straight line. The intercept with the line $cos\vartheta=1$ was defined as γ_c, which shows the wettability of solid surfaces[16].

(2) Girifalco and Good[16-18] furthered Zismanns work by suggesting that when the liquid and solid phases have the same molecular volume and interact through van der Waals forces, whose constants obey a geometric mean, the interaction between a solid and a liquid is given by:

Equation 4:1

where φ= function of the molecular properties of the two phases

(3) Fowkes[16, 18, 19] then considered the attractive forces at interfaces and proposed that the total free energy at the surface is the sum of the contributions from the different intermolecular forces. By assuming that the dispersive force is the only, or predominant, contribution and Young's equation becomes,

Equation 4:2

which is an approximation of the dispersive component of the sold surface energy, which can be made from a single contact angle measurement.

(4) Owens and Wendt extended the Girifalco-Good-Fowkes idea[16, 18, 20, 21] by adding a polar interaction term. This approach divides the surface tension into two components, dispersive and polar, and uses a geometric mean approach to combine their contributions:

Equation 4:3

Equation 4:4

Dispersive energy contributions are built up from a single interaction, which is generated by the movement of an electron around an atom or molecules. The difference in dispersive contributions can be explained in part by the difference in the density of the films, the higher the density the lower the dispersive contribution to the surface energy. The polar contribution is built up from different forces or interactions like hydrogen bonds, covalent bonds and dipole-dipole interactions. The larger the polar contribution to the surface free energy the more a surface attracts polar liquids and the higher the wettability of the surface by water.

Because the surface properties of a polymeric material are determined by the surface configuration in the top surface region[22-24], the overall effect of fluorinating a surface is a decrease in the surface tension[25, 26]. The existence of surface polarity strongly influences the interfacial properties leading to increased wettability as a function of surface polarity. Fluorocarbons have weak dispersive interactions and low polarity, therefore the more C-F bonds at a surface the lower its wettability[27]. The Owens-Wendt equation was used to calculate the surface energies and has been applied to relate systems previously[28, 29].

4.2.1 Analysis and Results of Surface Free Energies

The interactions of molecules in the bulk are balanced by equally attractive forces in all directions. Molecules at the surface experience an imbalance of forces and the net effect of this situation is the presence of free energy at the surface, the wettability of a surface directly relates to the surface energy[30]. Using the contact angle data measured for PTFE and the matrix polymer films the surface free energy was calculated and listed in Table 4:3. These measured values were much lower than the literature values[31]. This could be due to surface roughness and that the two contact fluids are quite similar in terms of polar and dispersive components, thus making the simultaneous equation that must be solved to obtain the surface energy ill-conditioned. AFM

measurements confirmed that the surfaces of the spun films were very rough, ~6.5nm, which results in a significant contact angle hysteresis, ~10°. As such caution has to be taken when interpreting the results from surface energies and should only be used as a guide to the surface behaviour rather than a definitive value.

Polymer Film	**Surface Energy / mNm^{-1}**	
	Literature Values[32]	**Calculated Values**
PTFE	16-17.9	8.95
LLDPE	31-33	25.76
hPE50	Not available	25.38
hPE100	Not available	25.77
hPE200	Not available	22.34

Table 4:3 Calculated surface free energies using CA measurements and the literature values for PTFE and LLDPE

In section 4.1.1.3 it was concluded that greater hydrophobicity of polymer blends occurs to the greatest extent with highly fluorinated, low molecular weight additives. Figure 4:13 illustrates their calculated surface energies derived from contact angle measurements with water and glycerol.

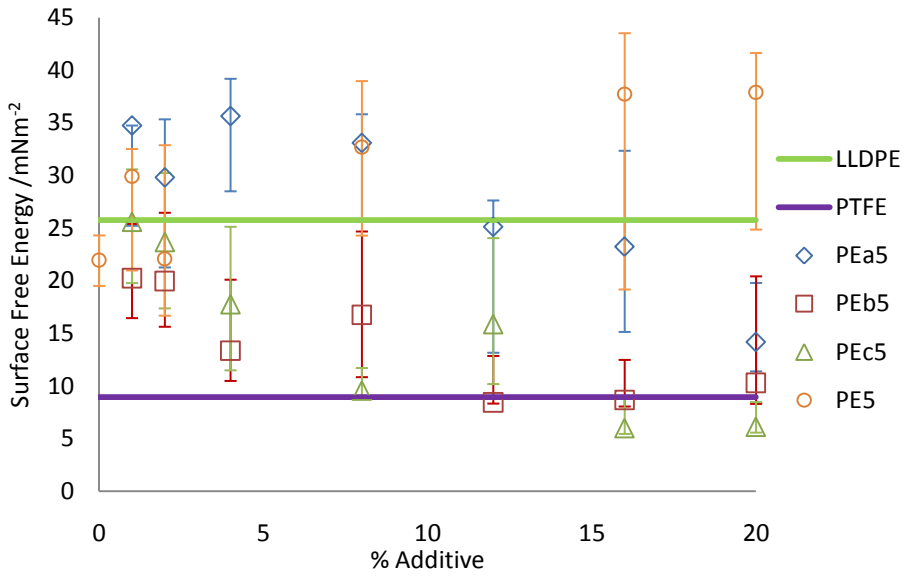

Figure 4:13 Calculated Surface Free Energies of most efficient mixtures (5 $kgmol^{-1}$ deuterated additive in hPE200 matrix)

The control additive, dPE5, shows that deuterium has no effect on lowering the surface free energy, compared to the fluorinated additives. This is in contrast to previous observations where the deuterated component will preferentially segregate to the surface and lower the surface energy[33] however, the errors in these measurements are significantly owing to surface roughness and similarity in contact fluids. The surface energy results typically follow the trend that PEc5 blends have the lowest surface energy and PEa5 the highest. As the concentration approaches 8% surface energies similar to PTFE are obtained and possibly surpass PTFE at concentrations. A contact fluid that has a much smaller polar component, such as oil, but is not soluble, should be used to reduce the errors associated with the surface energy calculations. Unfortunately, time did not permit further work therefore surface energy calculations errors were very large.

Interestingly although additive PEa5 does not reach surface energies as low as PTFE, in the range of concentration that were covered in the experiment, the results suggest that at high enough concentration, surface energies as low as PTFE would be obtained. So by extrapolating from figure 4:13 one could speculate that PEa5 might be able to reach comparable surface energies as the others at 20-25% blends.

4.3 X-ray Photoelectron Spectroscopy (XPS)

When an incident photon of certain energy (E_{photon}) from a monochromatic x-ray beam hits a surface it results in photoemission from the sample surface. This is the basis of the photoelectric effect, explained by Einstein in 1905, and utilises Rutherford equation,

Equation 4:5

which defines the binding energy as the energy of the X-ray photons being used, E_{photon}, minus the characteristic kinetic energy of the photoemitted electron, (E_K), as measured by the instrument plus *w*, the work function of the spectrometer.

XPS relies on the ionisation of core electrons by an incident beam of x-rays and the resulting emitted photoelectrons are detected and their energy analysed[34]. The surface sensitivity of XPS arises from the fact that the energy of the emitted electrons are such that they strongly interact with matter resulting in a short escape depth in solids, therefore almost all observed signal in polymer XPS arises from the top 30 Å[35]. Because the atomic orbitals of an element, in different chemical environments, possess slightly different binding energies the measured kinetic energy can reveal information about the types of chemical bonds within the sample e.g. C-O or C=O. Differences in oxidation state, molecular environment and co-ordination number all provide

different chemical shifts. Chemical shifts arise because of the variations in electrostatic screening experienced by the core electrons as the valence and conduction electrons are drawn towards or away from the specific atom[36].

Photoelectrons arising from insulating samples experience a shift in energy due to charging[35]. The reason for this shift is that escaping photoelectrons cause an overall positive charge on the polymer surface resulting in a retardation of electrons from the surface, the net effect being a shift to lower kinetic energy. Because of this some of the peaks in the high resolution scans are distorted slightly so accurate chemical analysis cannot be performed. However this does not hinder quantification of elemental composition since the peaks arising from different elements are still normally well resolved from each other.

4.3.1 Analysis and Results

Figures 4:15 and 4:16 illustrate the data obtained from the measurements and plotted in CasaXPS[‡‡], following from the samples submitted for analysis, section 2.3.4. The fluorine counts per seconds were plotted against the binding energy and to make the plots clearer only the F 1s peaks have been shown, figure 4:14. All the plots show a clear trend of the amount of fluorine on the surface increasing as the concentration of additive increases. Figure 4:15 illustrates the intensity change as the concentration of additive increases from 4-20% for PEa5 and PEc5 in different matrixes and figure 4:16 illustrates the intensity change as the % of additive increases from 1-20% for PEb5 for all threes matrixes.

[‡‡] CasaXPS Version 2.3.15 © 2005 CasaXPS Manual 2.3.15

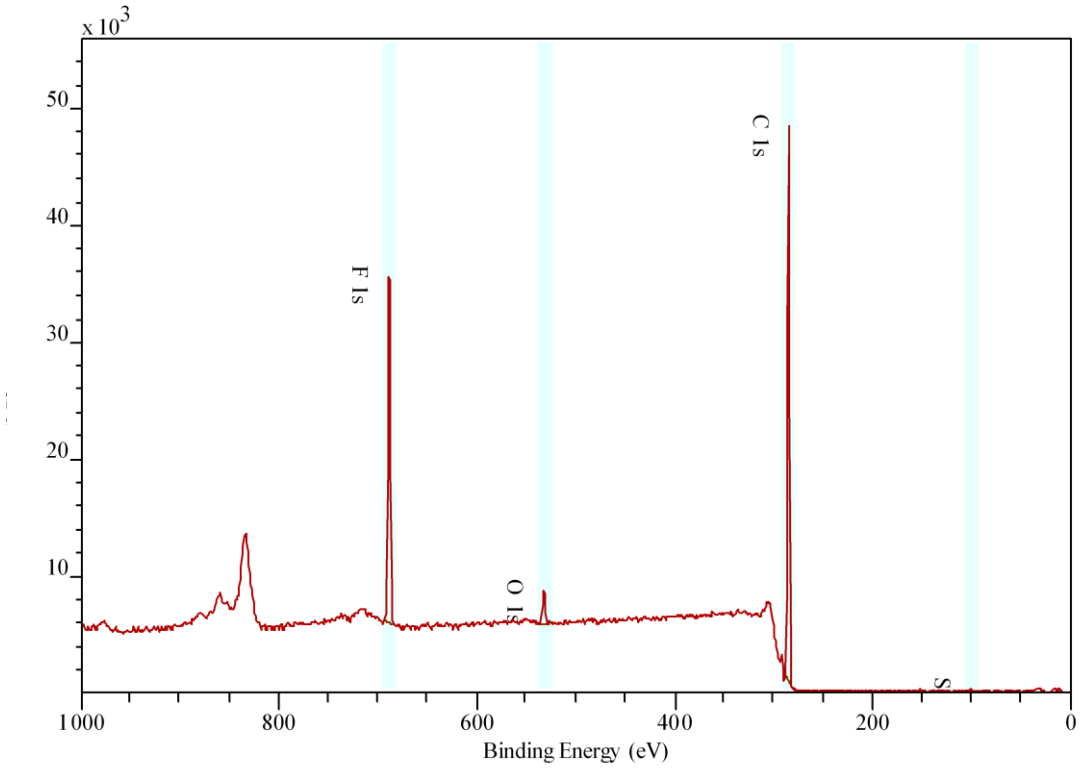

Figure 4:14 Typical XPS spectrum showing photoelectron yield versus binding energy where the elemental markers indicate the envelopes characteristic for each ionisation event recorded.

Using the data obtained, the atomic percentage of fluorine at the surface can be calculated and used to rationalise the effect additive structure has on surface segregation, the effect of the matrix and the adsorption efficiency. These samples similar to the contact angle samples, and roughly 120nm thick. These measurements were carried out by Emily Smith in Nottingham and the following analysis performed by the author. Four measurements were taken for each sample and the major source of error arose from the integration of the fluorine peak because the carbon peak was very large in comparison. A standard deviation was taken and the errors were typically less than or equal to 6% of the fluorine peak integration value. The vertical scale in figures 4:16 and 4:17 is arbitrary and is only the size relative to C (1s) that is important

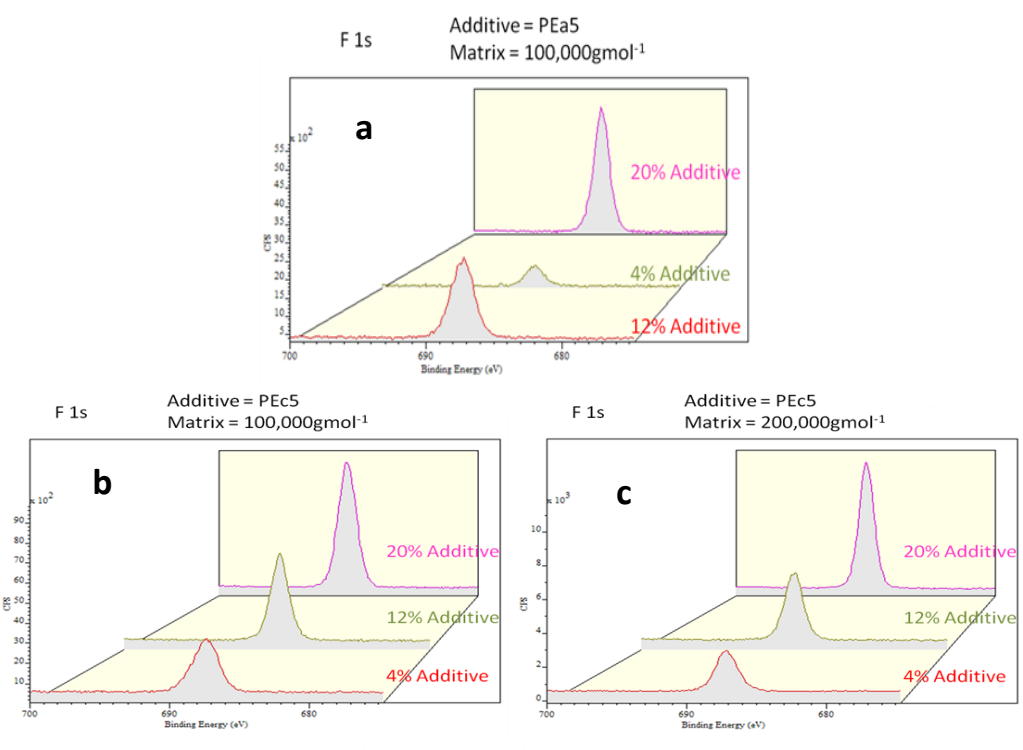

Figure 4:15 CasaXPS graphs of fluorine counts per second compared to percentage PEa5 and percentage PEc5 additive, a) PEa5 when matrix is hPE100, b) PEc5 when matrix is hPE100 and c) PEc5 when matrix is hPE200

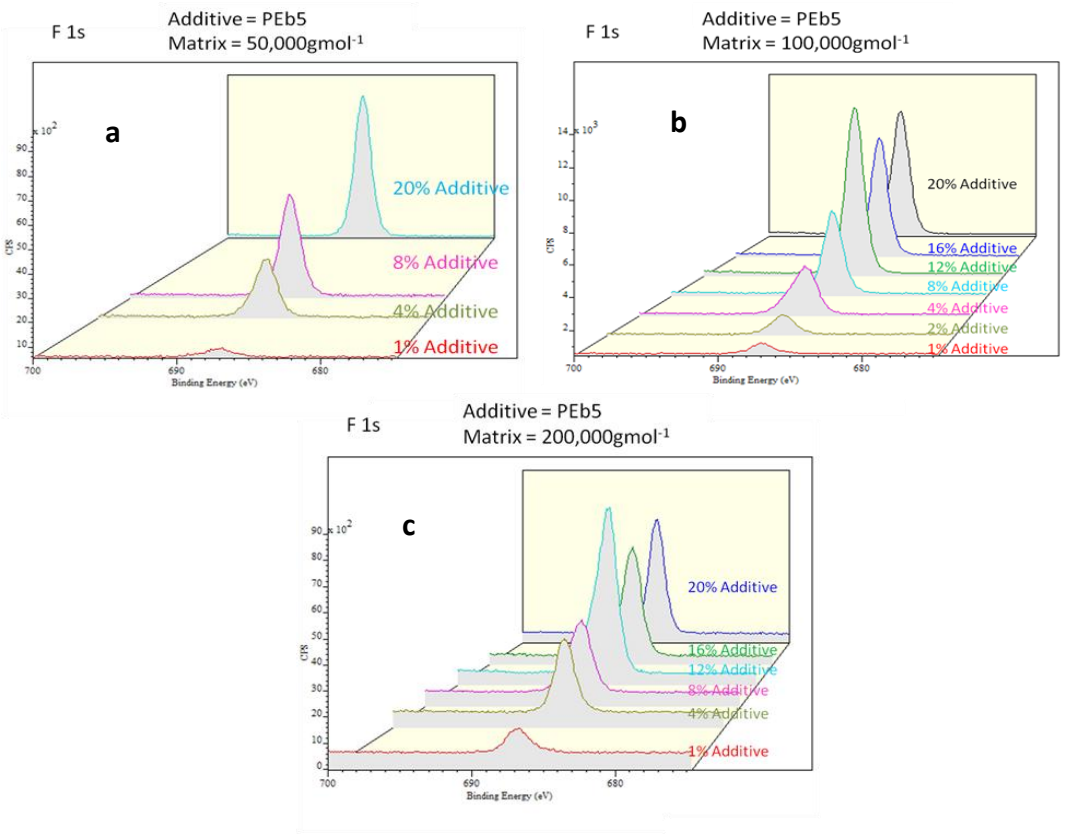

Figure 4:16 CasaXPS graphs of fluorine counts per second compared to percentage PEb5 additive, a) when matrix is hPE50, b) matrix is hPE100 and c) matrix is hPE200

4.3.1.1 Effect of Matrix Molecular weight on Surface Segregation

Fluorine was successfully measured at the surface for the first time for these new molecules and the amount of fluorine generally increased with increasing additive concentration for all systems. However, there are some fluctuations suggesting that behaviour is more complex than simple amorphous analogues that have been the subject of earlier studies. The values obtained are also likely to be lower than the actual amount of fluorine present at the surface. This is because the depth range of XPS is 1-10nm and from crude C-C bond length calculations all CF groups should be with the first 1nm.

By plotting the PEb5 and PEc5 data recorded using different matrices, figure 4:17, there appears to be no overall matrix effect on surface segregation, figure 4:17. The surface of the 100 $kgmol^{-1}$ blend is most successfully fluorinated by PEb5 whereas PEc5 has the greatest effect on 200 $kgmol^{-1}$ blend surfaces. By examining very carefully the PEb5 data there is a recurrent trend at each concentration of additive that the higher the matrix molecular weight the more surface segregation, but the overall difference is very small. As each fluorine is associated with a carbon (C_8F_{17}) figure 4:17 illustrates the surface composition of fluorocarbon groups instead of fluorine atoms.

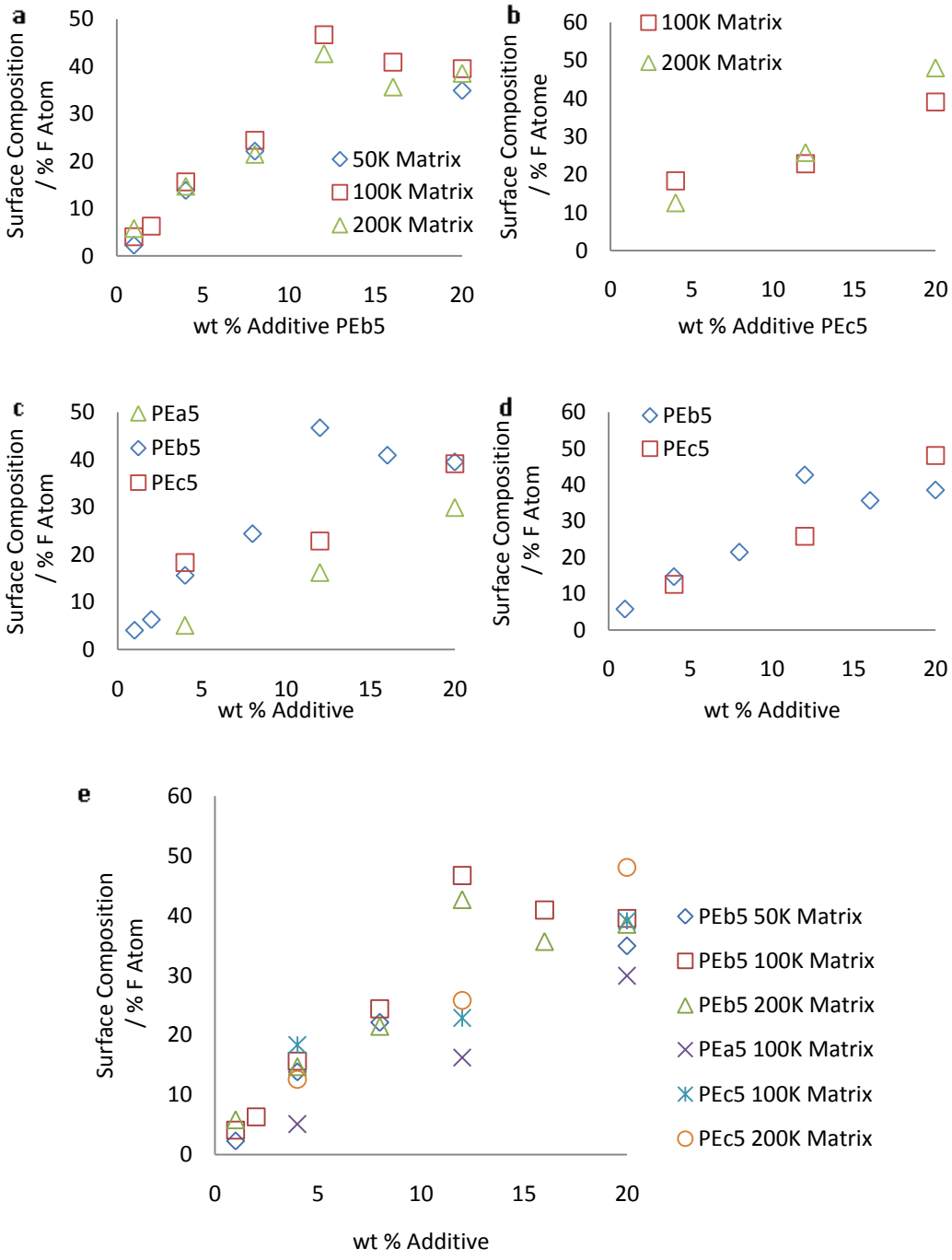

Figure 4:17 Graphs illustrating the a) effect of additive/matrix on the surface segregation of C_8F_{17} groups from additive PEb5, b) effect of additive/matrix on the surface segregation of C_8F_{17} groups from additive PEc5, c) effect of additive/matrix on the surface segregation of C_8F_{17} groups from hPE100, d) effect of additive/matrix on the surface segregation of C_8F_{17} groups from hPE200 matrix and e) combined results

The absolute surface fluorine concentration in 200 $kgmol^{-1}$ matrix (figure 4:17d) can be directly compared, and should correlate, with the CA results and the resulting surface energies, figure 4:13. There appears to be no difference in the absolute surface fluorine concentration measured by XPS but the surface energy calculations indicate that blends containing PEc5 yield the lower

surface energies. Again this could be an indication that surface roughness is critical when measuring and interpreting CA results.

4.3.1.2 How Efficient is Adsorption?

By quantifying the magnitude of fluorocarbon groups at the surface compared to the bulk an estimate of how efficient the adsorption process is can be determined. In all cases the efficiency of surface adsorption decreases as the amount of additive increases. This could be because of surface saturation or that equilibrium between the energy required to moved a group to the surface versus the energy gain from it being at the surface is established. As with figure 4:17, figure 4:18 shows that very similar results were obtained for each additive, regardless of the molecular weight of matrix in which it was dispersed.

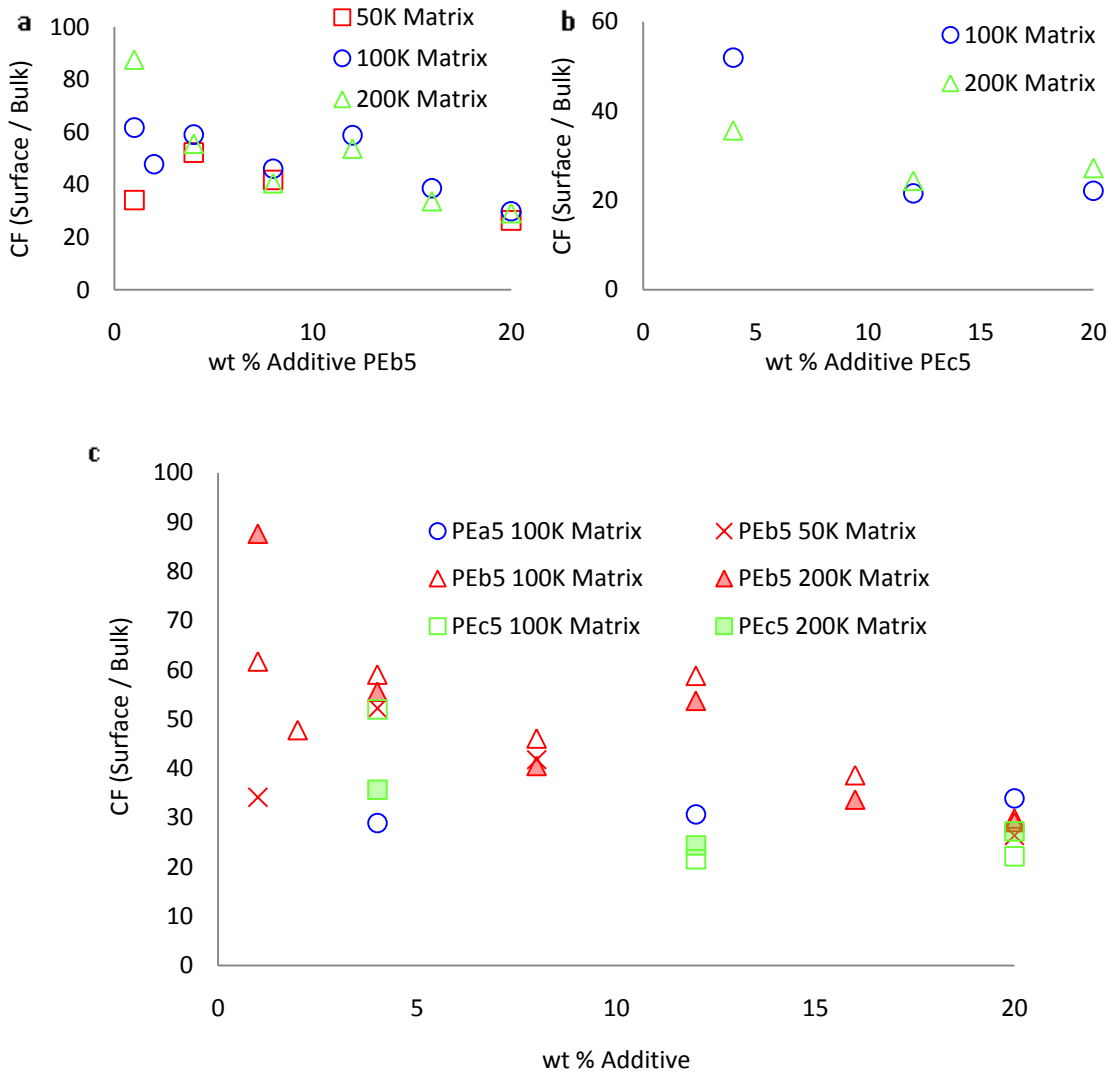

Figure 4:18 XPS adsorption efficiency comparing a) the effect of matrix molecular weight for additive PEb5, b) the effect of matrix molecular weight for additive PEc5 and c) the combined results

Figure 4:19 illustrates the effect that the number of fluorocarbon groups has on adsorption efficiency, which does not always agree with the CA results, section 4.1.1.3 (figure 4:12). Additives of type "a" give the least fluorinated blend surfaces, agreeing with CA results. However, additives of type "b" and "c" have very similar surface concentrations of fluorine, but differing CA values. Additives of type "b" are much more efficient at surface adsorption than additives of type "c", even though they have approximately the same percent of fluorines at the surface.

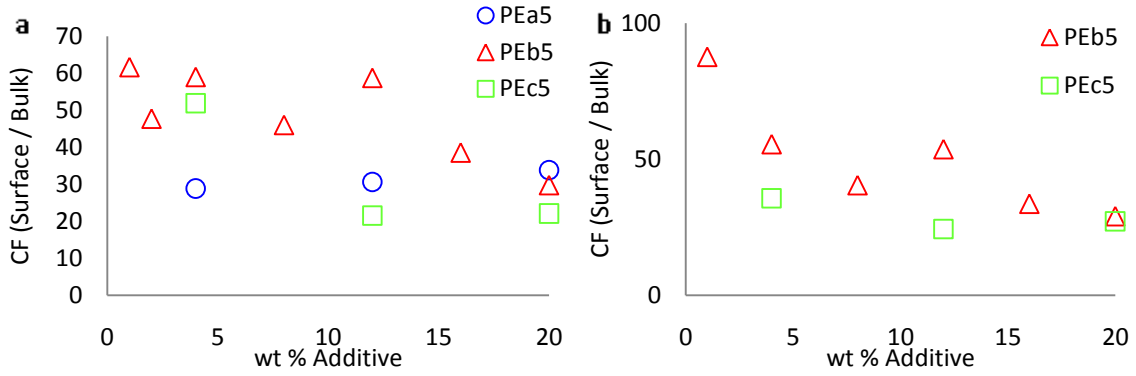

Figure 4:19 Effect of additive on adsorption efficiency in a) 100 $kgmol^{-1}$ matrix and b) 200 $kgmol^{-1}$ matrix

4.4 Roughness Discussion using AFM

Following from the XPS results AFM images were taken to compare the surface roughness for different samples that underwent standard annealing (annealing to 110°C for 1 hr, then cooling on the bench - cooling rate 14°C/min) and no annealing. For unannealed samples, figure 4:20, shows that as the number of fluorocarbons increases the size of the crystals increases and the roughness increases. Comparing the roughness to standard annealing conditions, figure 4:21, the same trend is observed irrespective of the matrix used.

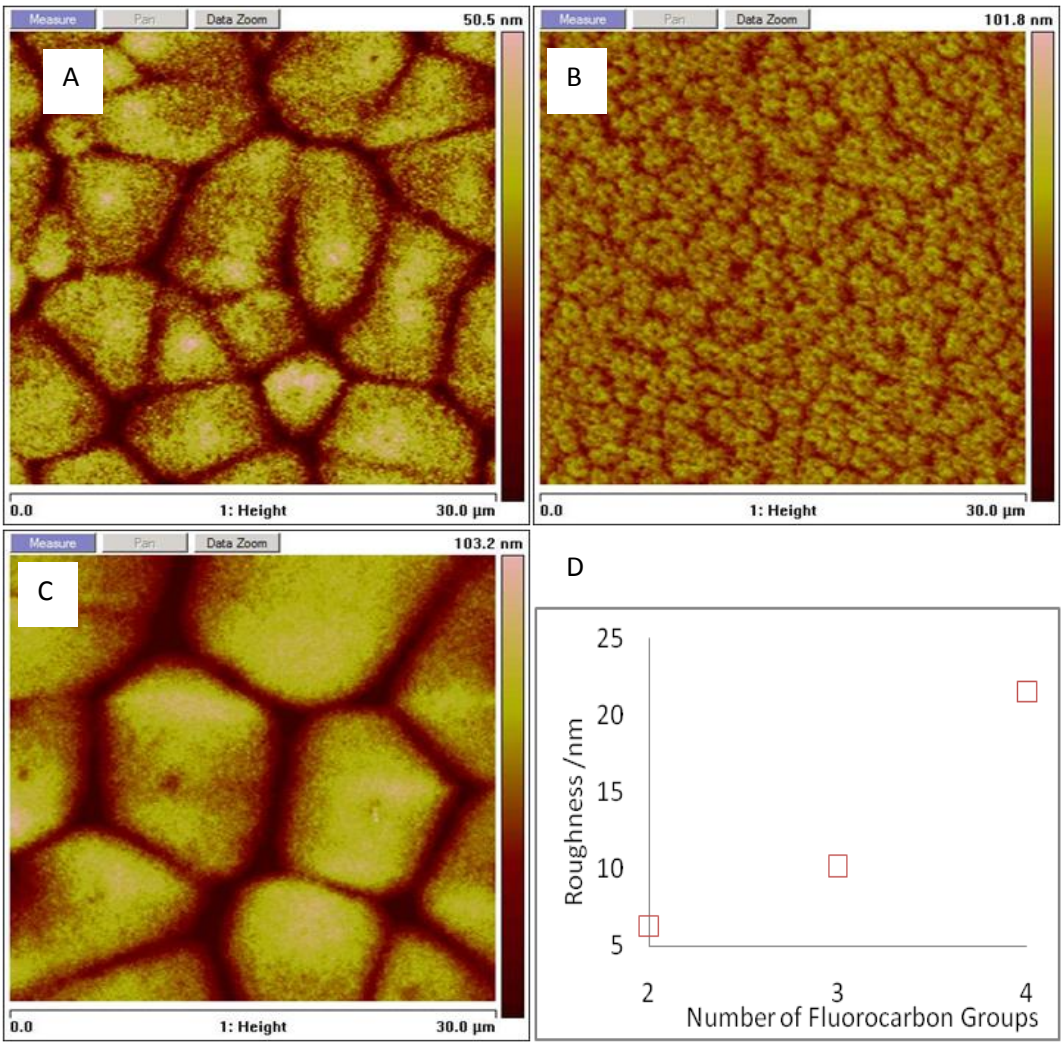

Figure 4:20 AFM images for no annealing a) 12% PEa5 in hPE100, b) 12% PEb5 in hPE100, c) 12% PEc5 in hPE100 and d) graph representing the effect of the number of fluorocarbon groups on surface roughness

Without annealing crystallisation effectively occurs from solution, therefore better crystals are formed, compared to annealed films which crystallise from the melt. This gives rougher surfaces due to greater crystallinity in spin cast films, figure 4:21.

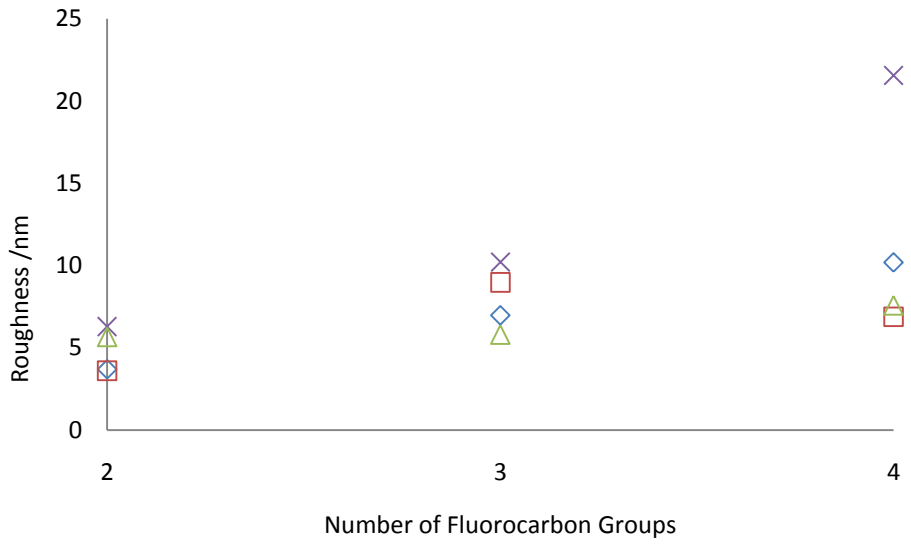

Figure 4:21 Effect of the number of fluorocarbon groups (additive always 12%wt) on surface roughness in ◊ hPE200, □hPE100 and Δ hPE50 matrix when bench cooled after standard annealing and the effect on the number of fluorocarbon groups (additive always 12%wt) in 100 $kgmol^{-1}$ matrix (x) when no annealing occurs

The effect that the matrix molecular weight has for different additives is as follows. For additives of type "a" the CA data show that the 50 $kgmol^{-1}$ matrix has the highest increase in contact angle as more fluorinated additive is added, whereas for the 100 $kgmol^{-1}$ and 200 $kgmol^{-1}$ matrix the increase in contact angle compared to the pure matrix is about the same, figure 4:6. The AFM data obtained complements these data as the surface roughness is slightly higher for 50 $kgmol^{-1}$ matrices than for either of the larger molecular weight matrices. For additives of type "b" the CA data shows that in terms of the pure polymer there is little difference between matrices, figure 4:8. Again the AFM data complements this as the increase in roughness is minimal as the matrix decreases. Finally, additives of type "c" were the only systems which illustrated clear surface adsorption dependence on the matrix where the 200 $kgmol^{-1}$ matrix exhibited the greatest hydrophobicity, figure 4:10. However, from the XPS results little effect of matrix molecular weight on surface fluorination was seen; the AFM results, figure 4:22, again confirm that the surface roughness is playing an important role in hydrophobicity.

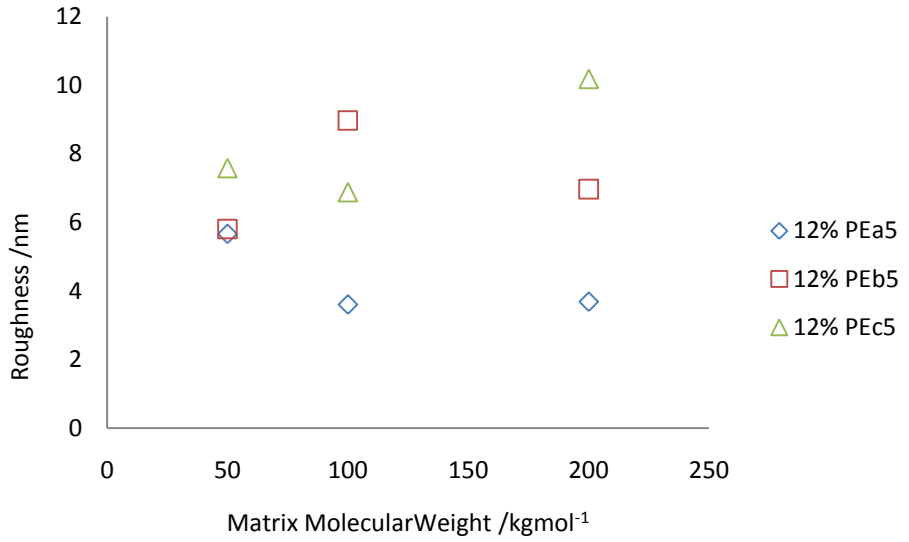

Figure 4:22 Effect of the matrix molecular weight on surface roughness when bench cooled after standard annealing

4.5 Conclusions

Anionic polymerisation produces low polydispersity polymers which enables a clear comparison of the influence of distinct well-defined molecular weights of additive and matrix. Following this the results obtained from the XPS and the CA data conclude that the amount of fluorine at the surface increases as the percentage of additive added increases. Following from this the ability of the additives to reduce the surface wettability increases as the percentage of additive added increases. However, in all cases the efficiency of surface adsorption decreases as the amount of additive increases.

Section 4.1.1.1 describes the effect of additive molecular weight on surface segregation and the conclusions that can be drawn from this are that the additives that have a molecular weight of 10 $kgmol^{-1}$ and lower are more effective at reducing the surfaces wettability and do this by roughly the same amount.

Section 4.1.1.2 describes the effect of matrix molecular weight on surface segregation and the conclusions that can be drawn from this are from the CA results are that additives of type “a” and “b” show that for these two additives the segregation is essentially independent of matrix molecular weight over the range explored, whereas additives of type “c” showed clear segregation behaviour according to matrix molecular weight. This is not particularly surprising since adsorption is not expected to be a strong function of molecular weight when the matrix is larger than additive. Previously described in section 1.4.2.5 when for constant additive molar

mass of the additive where molar mass of the matrix is large the tendency of the additive to adsorb to the surface increases.

The contact angle results for additives of type "a", figure 4:5, show that as the percentage of additive increases the 5 $kgmol^{-1}$ additive in the 200 $kgmol^{-1}$ matrix is the most effective system at increasing the water CA. However, by considering the increase in contact angle in terms of the pure polymer the 50 $kgmol^{-1}$ matrix has the most significant increase in contact angle as more fluorine as added, whereas for the 100 $kgmol^{-1}$ and 200 $kgmol^{-1}$ matrix the increase in contact angle compared to the pure matrix is about the same. However, this may only be an artefact of the lower contact angle for hPE50.

The contact angle results for additives of type "b" again show that as the percentage of additive increases the water CA increases. However, by considering the increase in contact angle in terms of the pure polymer with error there is little difference between matrices which agrees with the XPS data showing that no overall matrix that is better in promoting surface segregation irrespective of additive concentration.

The CA results for additives of type "c" are the only system which illustrated clear surface hydrophobicity according to it's matrix molecular weight. Blends containing additive PEc5 in 200 $kgmol^{-1}$ matrix exhibit the greatest hydrophobicity, which could be taken to indicate greater surface segregation.. However, from the XPS results there was no clear influence of matrix molecular weight on surface fluorination.

Section 4.1.1.3 describes the effect of additive structure and concentration on its surface segregation and from the CA results the higher the fluorine content of the end group the greater the additive's ability to decrease the contact angle, implying that either there is more fluorine present at the surface or the surface is roughest for the additive with more fluorocarbon groups.

From the XPS at lower additive concentrations the amount of fluorine present at the surface is very similar irrespective of the type of additive. As the additive concentrations increase the efficiency of adsorption is greatest for additives of type "b", irrespective of matrix and there is little difference between the absolute amounts of fluorine at the surface between, contradicting the CA results. This suggests that as the amount of fluorine increases, either at lower additive concentrations but with different additives, or by increasing the concentration of additive fluorine makes the surface rougher. Thus the XPS results suggest that roughness is a major contributing factor to the higher CA's recorded as by XPS there is not that much fluorine at the surface at low concentrations. However, the XPS results may be grossly underestimating the fractional fluorocarbon coverage by virtue of the penetration range exceeding the F-chain dimensions (i.e.

averaging over 10nm when CF coverage is only in the first 1nm). An example of this is that for apparently low fluorocarbon coverage by XPS the surface may still be substantially fluorinated, hence CA results hit a plateau whilst XPS results continue to rise with increasing concentration. That is putting more fluorinated additive in the blend forces more molecules to the surface. To accommodate this some F-chains may stand on end but does not in practice much alter the fluorocarbon surface which is already close to saturation, hence the CA results plateau whilst the XPS keep rising.

The efficiency of the additives fluorinating the surface was generally found to decrease as the concentration of the additive increases. Figure 4:17 showed that the additives “b” or “c” have very similar surface concentrations of fluorination, however, additives of type “b” are overall more efficient at surface adsorption than additives of type “c”, since the bulk CF concentration is lower. This could be due to the bulky fluorocarbon-head groups at the end of the polymer reducing the ability for the polymer to diffuse to the surface as it is sterically constrained, or that the surface has become saturated. Additives of type “a” are the least efficient at surface modification because of the lower driving force to the surface, which is consistent with earlier work on related amorphous polymers[37].

Finally, as the matrix molecular weight increases the CA increases due to roughness not extra fluorine groups. Overall when the matrix is changed for the same additive, figure 4:22, the roughness mirrors the trends observed from the CAs, figure 4:17, measured and provides a clear indication that surface roughness is a contributing factor on surface hydrophobicity.

4.6 References

1. Cassie, A. B. D., *Transactions of the Faraday Society* **1948,** *44* (3), 11-16.
2. Li, X. M.; Reinhoudt, D.; Crego-Calama, M., *Chemical Society Reviews* **2007,** *36* (8), 1350-1368.
3. Packham, D. E., *International Journal of Adhesion and Adhesives* **1996,** *16* (2), 121-128.
4. Kwok, D. Y.; Gietzelt, T.; Grundke, K.; Jacobasch, H. J.; Neumann, A. W., *Langmuir* **1997,** *13* (10), 2880-2894.
5. Marmur, A., *Soft Matter* **2006,** *2* (1), 12-17.
6. Kwok, D. Y.; Lam, C. N. C.; Li, A.; Leung, A.; Wu, R.; Mok, E.; Neumann, A. W., *Colloids and Surfaces a-Physicochemical and Engineering Aspects* **1998,** *142* (2-3), 219-235.
7. O'Rourke-Muisener, P. A. V.; Koberstein, J. T.; Kumar, S., *Macromolecules* **2003,** *36* (3), 771-781.
8. Koberstein, J. T., *Journal of Polymer Science Part B-Polymer Physics* **2004,** *42* (16), 2942-2956.
9. Yoshizawa, H.; Chen, Y. L.; Israelachvili, J., *Journal of Physical Chemistry* **1993,** *97* (16), 4128-4140.
10. Riekerink, M. B. O.; Terlingen, J. G. A.; Engbers, G. H. M.; Feijen, J., *Langmuir* **1999,** *15* (14), 4847-4856.
11. Yao, Z. H.; Yin, J. H.; Song, Y. X.; Jiang, G. W.; Song, Y. C., *Polymer Bulletin* **2007,** *59* (1), 135-144.
12. Clarke, N.; Colley, F. R.; Collins, S. A.; Hutchings, L. R.; Thompson, R. L., *Macromolecules* **2006,** *39* (3), 1290-1296.
13. Johnson, R. E., *Journal of Physical Chemistry* **1959,** *63* (10), 1655-1658.
14. Fox, H. W.; Zisman, W. A., *Review of Scientific Instruments* **1948,** *19* (4), 274-274.
15. Zisman, W. A., *In Advances in Chemistry*. American Chemical Society: Washington, DC, 1964.
16. Saito, M.; Yabe, A., *Textile Research Journal* **1983,** *53* (1), 54-59.
17. Good, R. J.; Girifalco, L. A., *Journal of Physical Chemistry* **1960,** *64* (5), 561-565.
18. Nguyen, T.; Johns, W. E., *Wood Science and Technology* **1978,** *12* (1), 63-74.
19. Fowkes, F. M., *Industrial and Engineering Chemistry* **1964,** *56* (12), 40-&.
20. Owens, D. K.; Wendt, R. C., *Journal of Applied Polymer Science* **1969,** *13* (8), 1741-&.
21. Tamai, Y.; Makuuchi, K.; Suzuki, M., *Journal of Physical Chemistry* **1967,** *71* (13), 4176-&.
22. Fox, H. W.; Hare, E. F.; Zisman, W. A., *Journal of Colloid Science* **1953,** *8* (2), 194-203.
23. Miyama, M.; Yang, Y. X.; Yasuda, T.; Okuno, T.; Yasuda, H. K., *Langmuir* **1997,** *13* (20), 5494-5503.
24. Langmuir, I., *Science* **1938,** *87*, 493-500.
25. Dutoit, F. J.; Sanderson, R. D.; Engelbrecht, W. J.; Wagener, J. B., *Journal of Fluorine Chemistry* **1995,** *74* (1), 43-48.
26. Chaudhury, M. K.; Whitesides, G. M., *Science* **1992,** *255* (5049), 1230-1232.
27. Lee, S.; Park, J. S.; Lee, T. R., *Langmuir* **2008,** *24* (9), 4817-4826.
28. Hutchings, L. R.; Narrainen, A. P.; Eggleston, S. M.; Clarke, N.; Thompson, R. L., *Polymer* **2006,** *47* (24), 8116-8122.
29. Thompson, R. L.; Narrainen, A. P.; Eggleston, S. M.; Ansari, I. A.; Hutchings, L. R.; Clarke, N., *Journal of Applied Polymer Science* **2007,** *105* (2), 623-628.
30. Cherry, B. M., *Polymer Surfaces*. **1981**.
31. Brandrup, J. a. E. H. I., *Polymer Handbook*. 3rd ed.; John Wiley & Sons, NY: **1989**.

32. Brandrup, J.; Immergut, E. H., *Polymer Handbook*. 3rd ed.; John Wiley & Sons, NY: **1989**.
33. Harton, S. E.; Stevie, F. A.; Griffis, D. P.; Ade, H., *Applied Surface Science* **2006,** *252* (19), 7224-7227.
34. Jones, R. A. L.; Richards, R. W., *Polymers at Surfaces and Interfaces*. Cambridge University Press.
35. Feast, D. C. a. W., *Polymer Surfaces*. John Wiley and Sons, NY.
36. Brown, J., *Molecular Spectroscopy*. Oxford University Press, London: 2003; Vol. 55.
37. Ansari, I. A.; Clarke, N.; Hutchings, L. R.; Pillay-Narrainen, A.; Terry, A. E.; Thompson, R. L.; Webster, J. R. P., *Langmuir* **2007,** *23* (8), 4405-4413.

5 Surface Organisation

In this chapter the results of nuclear reaction analysis (NRA) and neutron reflection (NR) experiments, used to understand the surface organisation of end functionalised polyethylenes and their blends, are described. By using both NRA and NR the surface composition of semi-crystalline samples can be compared with melt samples, where no crystalline regions exist, and thus the effect of crystallinity on surface composition examined.

Firstly the surface organisation, examined by NRA shall be discussed in terms of molecular structure, i.e. the influence of functional group, additive molecular weight and matrix molecular weight. Following from this the results obtained from the study of the surface organisation under melt conditions will be discussed for one additive in two molecular weight matrices. Finally, the effect that the amount of crystallinity within the sample has on surface segregation and surface hydrophobicity is discussed, with a combination of differential scanning calorimetry, AFM and NRA used to quantify the effects of crystallinity.

5.1 Ion Beam Analysis

A more detailed theoretical basis NRA is described in Appendix 1 and the experimental procedure used were as described in section 2.4.1. The samples used were identical to those used for CA analysis.

5.1.1 Results and Discussion

NRA data reduced to volume fraction *versus* depth appear as follows, figure 5:1a, where the additive is found to enrich the top 10 nm and the bulk concentration is comparable to the amount added. The result of there being a certain amount of additive in the bulk is the potential for the additive to migrate to the surface in the event of the surface layer being damaged[1]. However, in certain systems a secondary excess in the bulk was observed which corresponds to the substrate interface, figure 5:1b and 5:1c. The average volume fraction is a little inaccurate which is due to the uncertainty in charge collection.

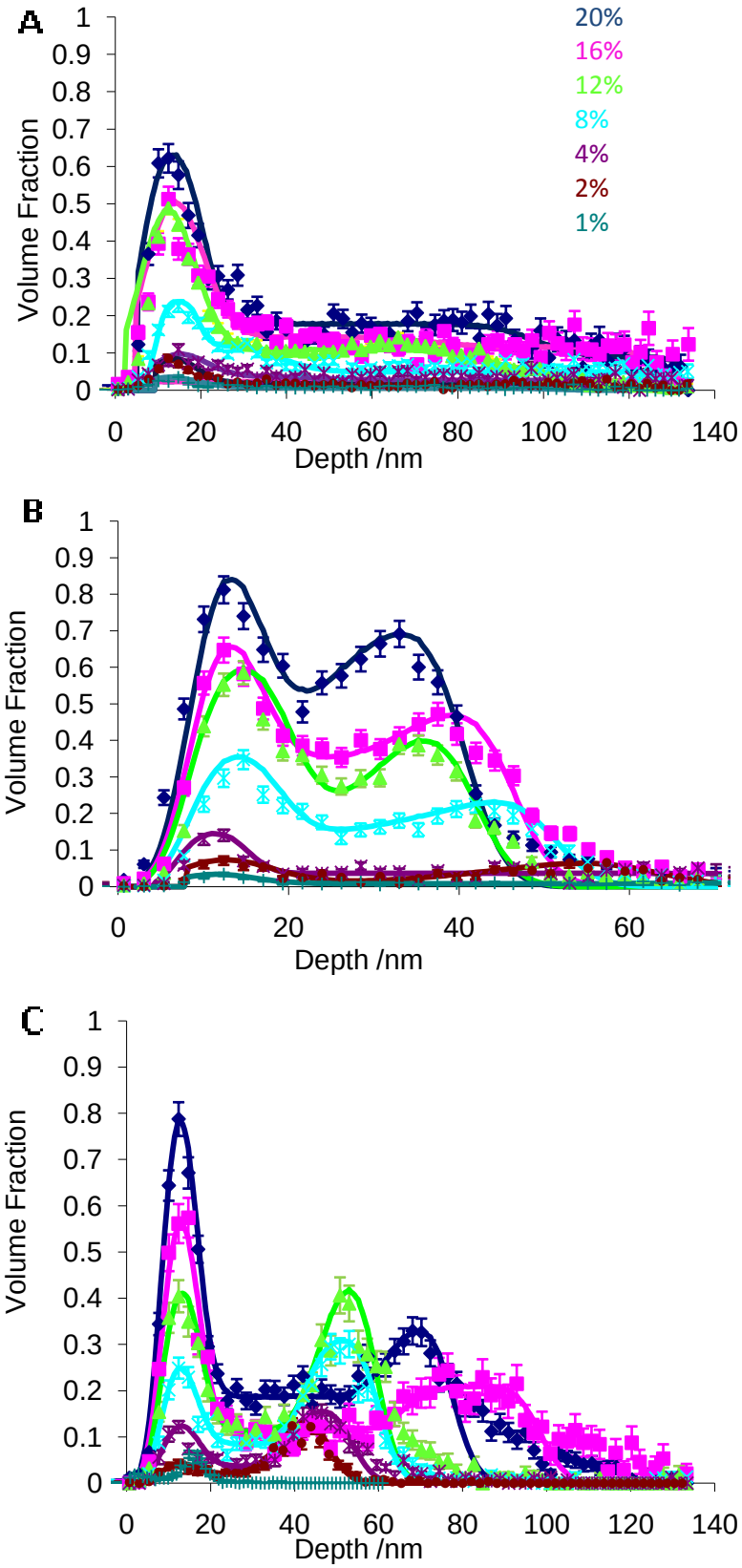

Figure 5:1 NRA data and fits illustrating the two blend compositions, perpendicular to the surface, A), PEa5 in hPE100 matrix showing volume fraction of additive as a function of depth normal to the film surface, B) PEa20 in hPE200 matrix showing volume fraction of additive as a function of depth normal to the film surface and C) PEc20 in hPE200 matrix showing volume fraction of additive as a function of depth normal to the film surface

A CF group has low surface energy so is attracted to the air surface and previous studies on similar materials do not usually show a CF excess at the substrate[2]. Silicon has a relatively high surface energy thus an excess at its surface is unexpected, and in general only polymers with polar functional groups such as NH_2[3], COOH[4] form an excess at the substrate interface. This excess could be an effect of crystallisation or phase separation as seen previously by Ansari *et al*[5] in amorphous systems. In those systems they observed that the excess, formed at the air surface of the spin cast film was associated with a depletion in the adjacent bulk layer (figure 5:2). Under spinodal decomposition (phase separation) the concentration fluctuations between 1, 2 and 3 grow in size, so annealing the sample causes $\phi 1$ and $\phi 3$ to increase at the expense of $\phi 2$.

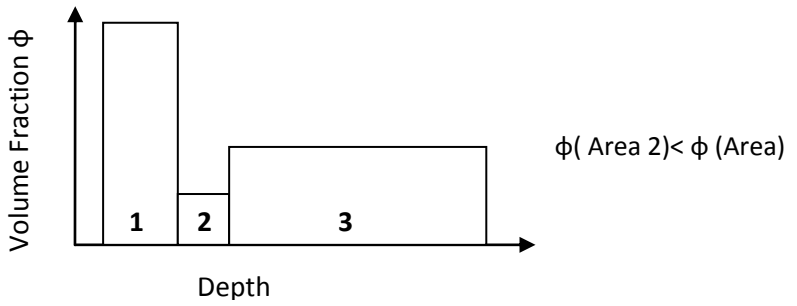

Figure 5:2 Illustration of the influence of phase separation on film composition *vs* depth[5]

The lack of segregation at the substrate, figure 5:1a, could indicate that this additive is miscible with the matrix, or that phase separation was not seen due to the film thickness exceeding the range of the measurement. The final observation regarding figures 5:2b and 5:2c is that the surface peak is significantly sharper than the substrate peak. Although some loss of resolution is usually apparent in ion beam analysis due to energy straggling, this effect is normally marginal, as seen in amorphous films of similar thickness[6]. However, for semi-crystalline polymer films the surface roughness gives rise to the variation in the thickness of the polymer that the ion beam must traverse in order to reach the substrate. This adds to the uncertainty in the location of the substrate illustrated in figure 5:3 and consequently a smearing of the substrate excess peak. Occasionally it was observed that at the highest concentration of additive there was a slight decrease in the *z** value. This was due to an increase in bulk concentration from which the *z** value was calculated. The surface excess, *z**, is as defined in section 2.4.1.1, where the *z** value was then corrected so the average volume fraction of the model agrees with the actual value of the blend. This compensates for any error in charge integration in each experiment.

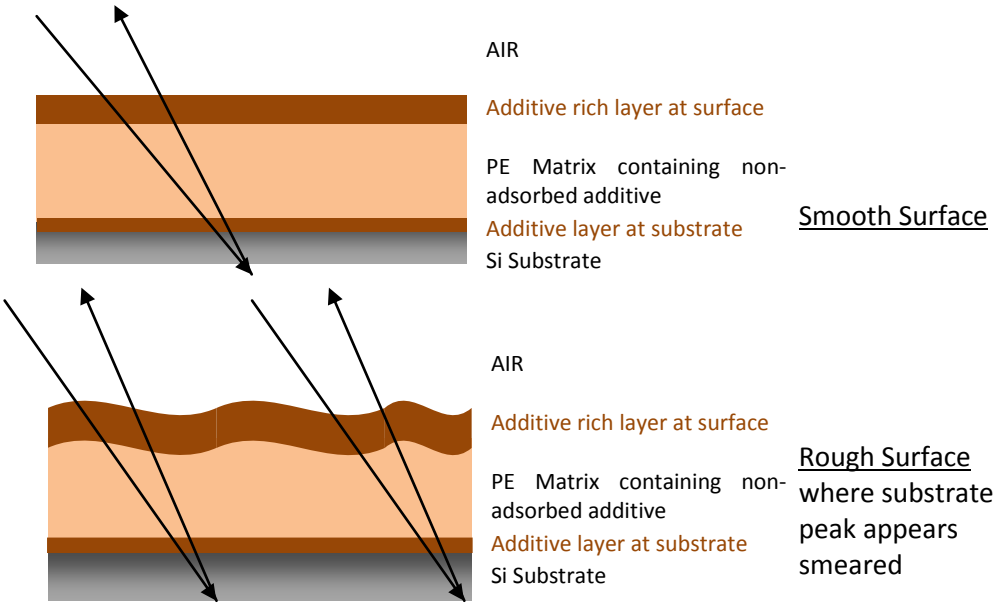

Figure 5:3 The depth traversed in both smooth and rough surfaces by a beam during NRA

The anchor blocks of the additives used in this study were repeat units of $C_4H_6D_2$ where the matrix was C_4H_8. It is well understood that deuterated polymers spontaneously segregate to the surface when blended in a non-deuterated matrix[7]. Figure 5:4 shows results for NRA measurements of the surface excess of the deuterated additive, with no CF end-groups, in a non-deuterated matrix. It should be stressed that this combination of high matrix molecular weight and low deuterated additive molecular weight is expected to give the greatest surface excess of a deuterated additive.[8] However, this effect is normally only significant for high molecular weight fully deuterated blends close to their phase boundary, which can be detected with ion beam methods. In some cases surface segregation is clearly apparent, and this result is therefore surprising, and points to a greater incompatibility between the polymers than might be expected from deuteration alone. A possible reason for this incompatibility is the small differences in microstructure (1,2 vs 1,4) enchainment. For other combinations of lower matrix molecular weight and higher additive molecular weight, the surface excess would be expected to be even lower.

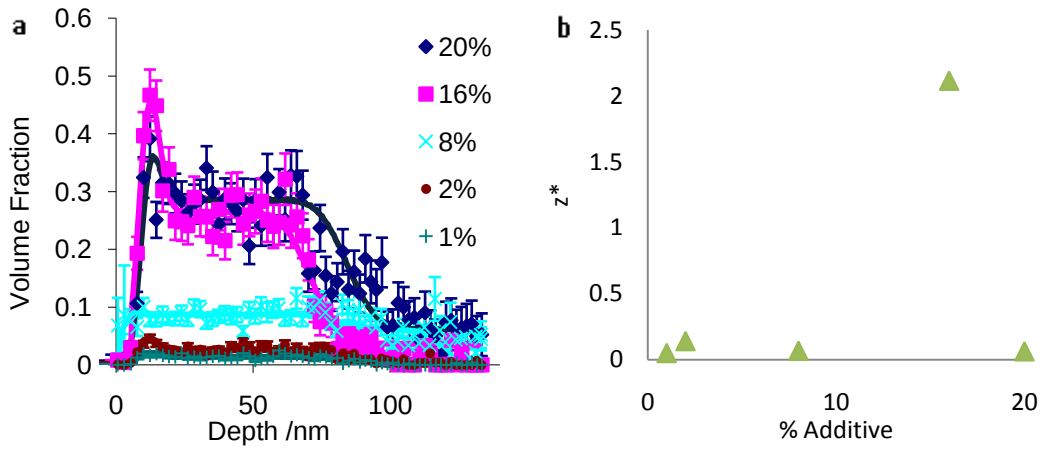

5:4 NRA data and fits of dPE5 in hPE200 a) the volume fraction *vs* depth, b) the calculated z* values for different concentrations of additives

In most cases deuteration alone gives rise to a small surface excess when compared to the corresponding functionalised additives. For the 16% additive there was a relatively large surface excess, which could be an anomalous result, or due to errors accrued during measurement.

5.1.1.1 Effect of Matrix and Additive molecular weight on Surface Segregation

The surface excess, z*, increases with increasing concentration, broadly consistent expected behaviour and in agreement with CA and XPS. However there is some uncertainty in the z* values where a typical standard deviation in results in 0.86 and in similar systems[9] the errors was reported to be 15%. Figures 5:5a-c and 5:6a-c illustrates the effect that the matrix molar mass has on surface segregation. In general, the surface excesses are much larger for all of the fluorocarbon functionalised additives than for the unfunctionalised control sample data shown in figure 5.4. This is the first evidence (directly comparable with previous studies) that multi-end functional polymers can be used to modify surfaces of semi-crystalline polymers. Furthermore, it is evident that increasing additive concentration, leads to a systematic increase in surface excess, which is not clearly apparent for the unfunctionalised blends. Generally for additives of type “a” as the additive molecular weight increases the z* values become more scattered, figure 5:5d-f, but for PEa5 very little matrix effect is observed, figure 5:5a. Conversely, for additives of type “c” the matrix appears to have no overall effect on surface segregation, figure 5:6d-f, for any additive molar mass, however there is some scatter increase as the additive molar mass increases.

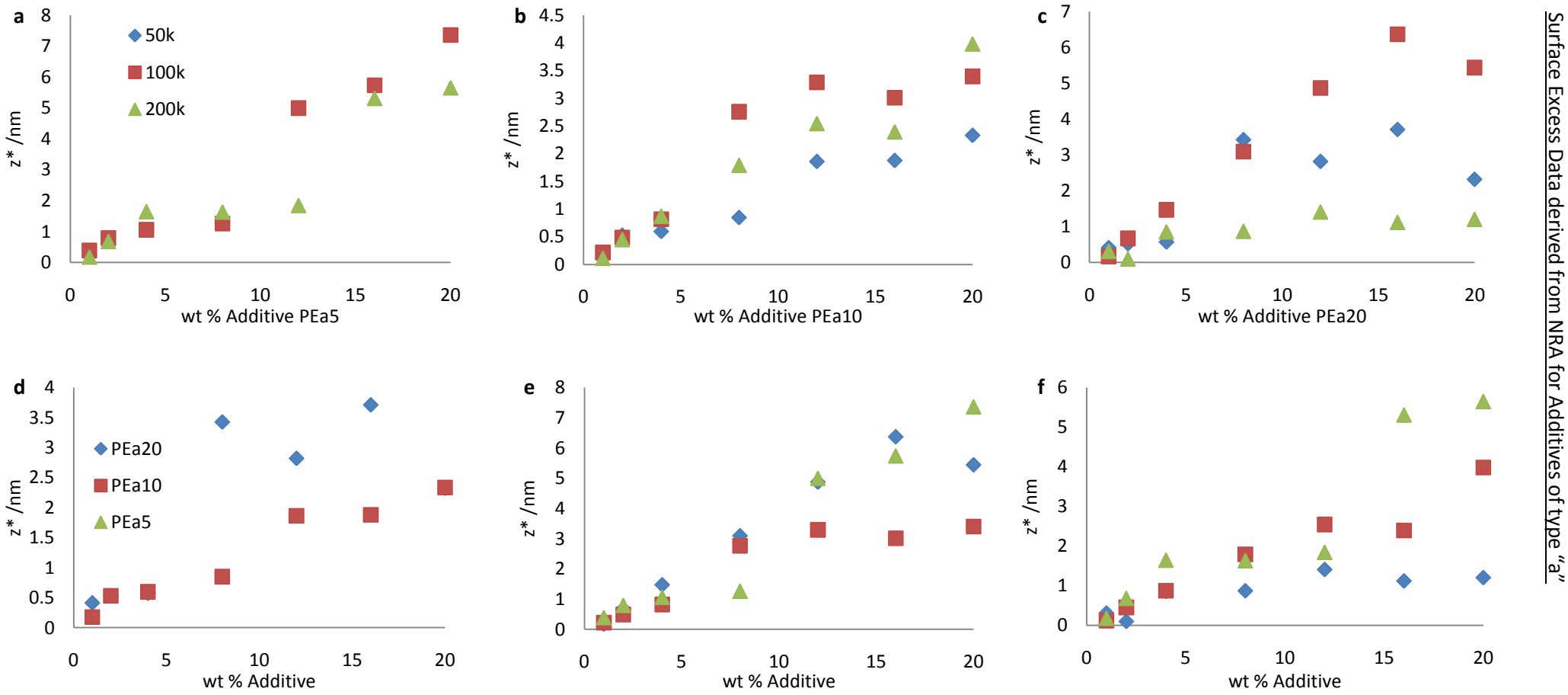

Figure 5:5 Surface excess values extracted from NRA measurements for additives of type "a" where for graphs a-c the key is in graph a and for d-f the key is in graph d a) PEa5 different molar mass matrices, b) PEa10 in different molar mass matrices, c) PEa20 in different molar mass matrices, d) hPE50 matrix with different molar mass deuterated additives, e) hPE100 matrix with different molar mass deuterated additives, f) hPE200 matrix with different molar mass deuterated additives.

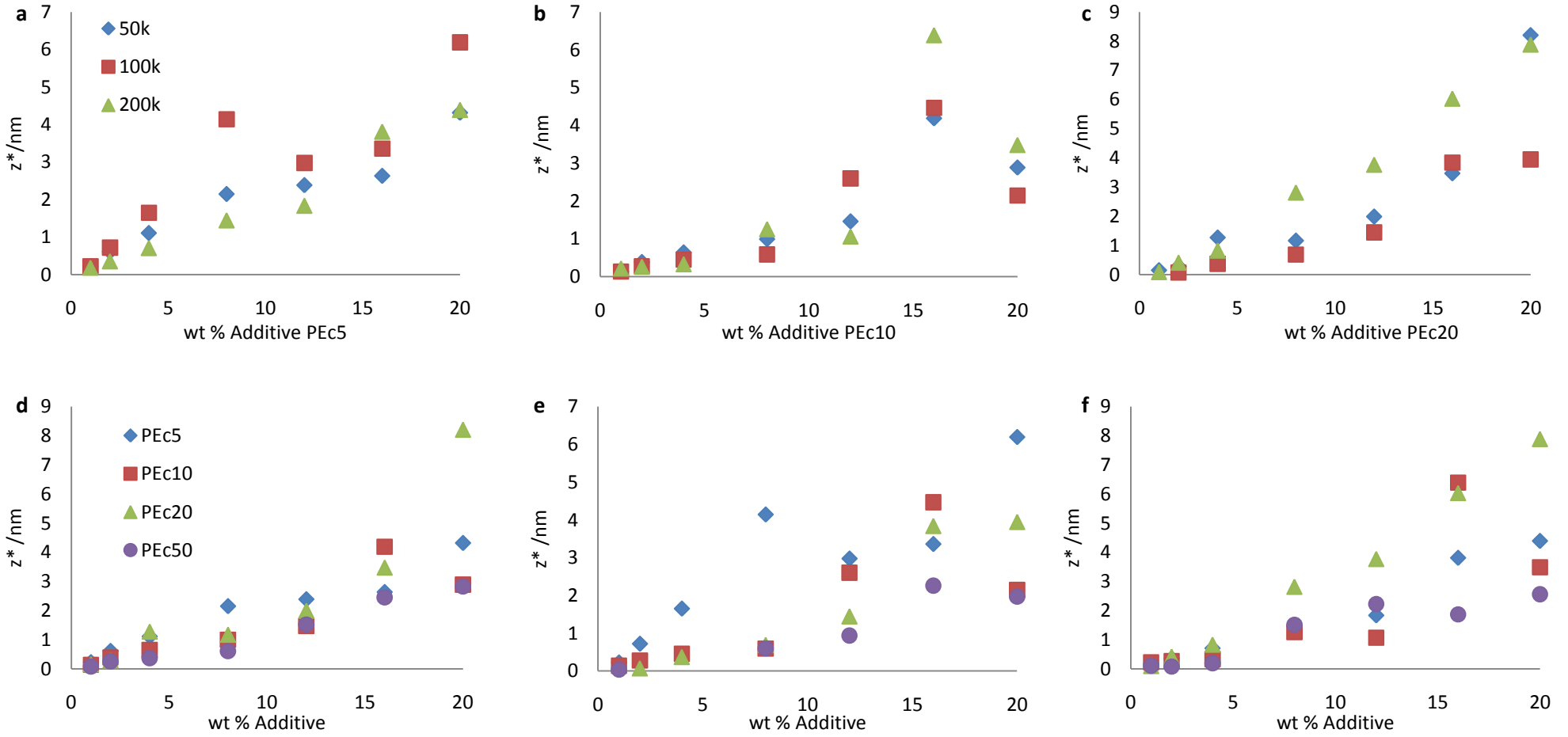

Figure 5:6 Surface excess values extracted from NRA measurements for additives of type "c" where for graphs a-c the key is in graph a and for d-f the key is in graph d a) PEc5 in different molar mass matrices, b) PEc10 in different molar mass matrices, c) PEc20 in different molar mass matrices, d) hPE50 matrix with different molar mass deuterated additives, e) hPE100 matrix with different molar mass deuterated additives, f) hPE200 matrix with different molar mass deuterated additives.

Another effect that was observed was that there appears to be a critical concentration of additive where the *z** values dramatically increase, this was only observed for additives of type ”a”. This occurs for 5 blends, table 5:1. An example of this behaviour can be clearly seen in the volume fraction versus depth data presented in figure 5.1.

Additive	**Matrix M_w /kgmol^{-1}**	**Wt % of Additive**
PEa10	50	12
PEa20	50	8
PEa5	100	12
PEa10	100	8
PEa5	200	16

Table 5:1 Critical concentrations of additive and matrix blends

From table 5:1 the following trends were observed. The critical concentration decreases slightly as the additive molecular mass increases in the same matrix, and there is no clear trend with matrix molecular mass. Although this behaviour is not seen universally, even for all of the type “a” additives, the occurrence at all is of interest, since it has never been seen for comparable amorphous systems. In general amorphous blends with multi-end functional additives show very efficient surface segregation at low concentrations and relatively little effect in increasing concentration beyond a few percent of additive.[10] Two possibilities could explain this phenomenon that is apparently unique to semicrystalline polymer blend films. Firstly the additive may be partially miscible with the matrix in the crystalline form, and therefore a fixed fraction of the additive tends to be incorporated into crystallites upon cooling. With increasing additive concentration beyond this miscibility limit, substantially more additive is available to form an excess layer.

Secondly, there could be a kinetic effect due to the slightly lower melting point of the additives than the matrix polymers. Care was taken with the thin films to anneal them at 110°C, which is only just above the melting point of the matrix, in order to preserve the integrity of the film. It may be that this annealing regime was not quite sufficient to ensure equilibration in all cases, but for the films with high proportions of relatively miscible type “a” additive, the melting point was suppressed, enabling better equilibration.

Figures 5:5d-f and 5:6d-f illustrates the effect of the additive molar mass on surface segregation. As z* is a measure of the amount of material adsorbed, the number of adsorbed C_8F_{17} groups, per unit area, can be calculated by dividing the *z** value by the additive molecular volume thus enabling better comparison to XPS data which are sensitive to CF groups, not deuterium. This eliminates the additive molar mass variable thus allowing the effect of matrix molar mass to be

directly compared. Figure 5:7 illustrates the effect that the matrix has on surface segregation, independent on additive molar mass. In the lowest matrix, figure 5:7a, 10 $kgmol^{-1}$ and 20 $kgmol^{-1}$ additive behave very similar, in the 100 $kgmol^{-1}$ matrix again the 10 and 20 $kgmol^{-1}$ additive behave similar, figure 5:7b, however the 5 $kgmol^{-1}$ does not. Once the concentrations of additive reaches a critical amount for PEa5 the surface excess increases, however as the critical concentration was not reached for the other additives the same excess was not achieved. In the 200 kgmol-1 matrix, figure 5:7c, there is a clear trend that the lower the additive molar mass the greater its tendancy to segregate[§§]. Again in figure 5:7c the critical concentration required to reach higher surface excesses can be seen for PEa5, at 16%, and PEa10, at 20%.

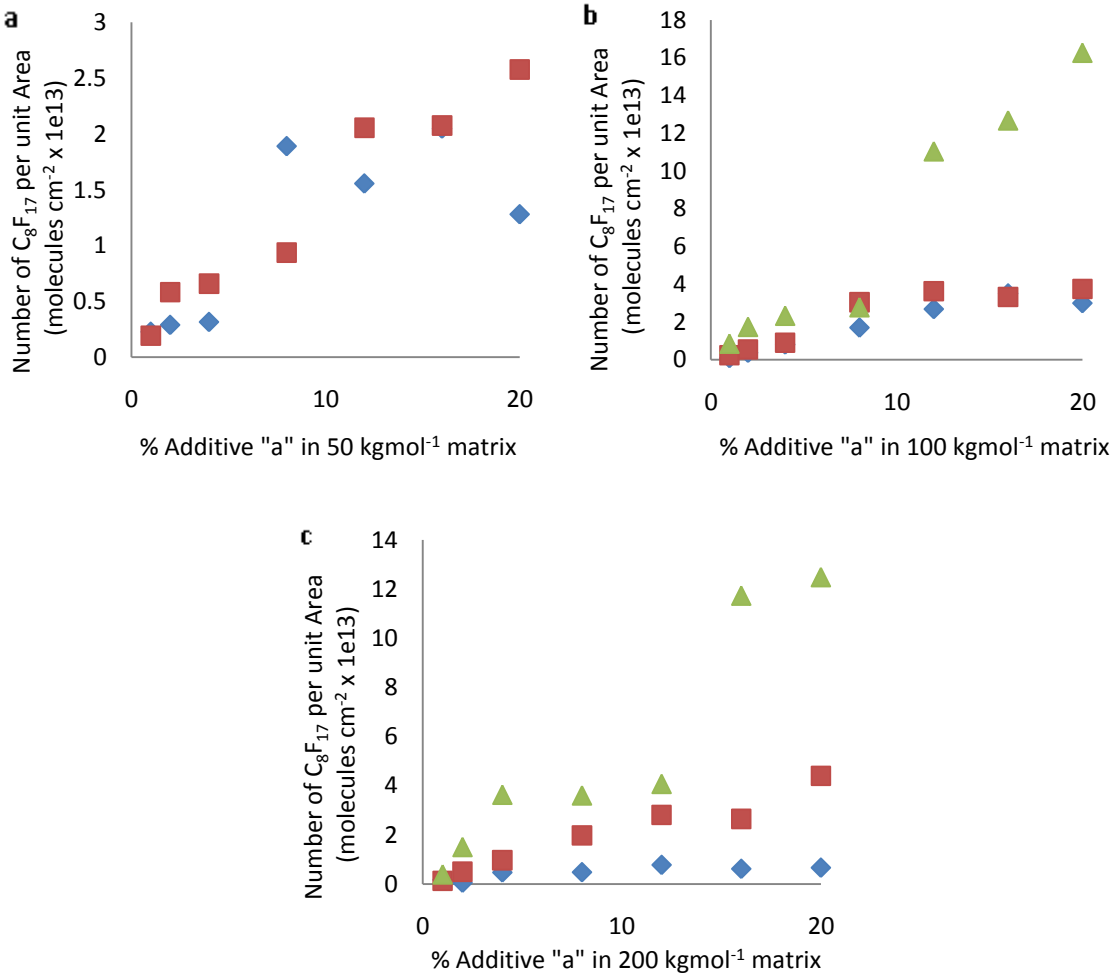

Figure 5:7 Number of chains per unit area, independent of additive molar mass, for additives of type "a" in a) hPE50, b) hPE100, c) hPE200, where ◊ is PEa20, □ PEa10 and Δ PEa5

When these results are combined for additives of type "a" the lowest molar mass additive in either 100 or 200 $kgmol^{-1}$ matrix has the most chains per unit area figure 5:8. This is consistent with theoretical and experimental prediction for unfunctionalised additives of disparate

[§§] Number of chains per unit area = [(z*/molecular weight of additive) × density] × N_A) × number of C_8F_{17} groups, where the density used for PE was 0.918g/mL

molecular weight[8], however in this case the effect is greatly enhanced by the presence of fluorocarbon groups. The additive molecular weight effect is also qualitatively consistent with amorphous systems[10].

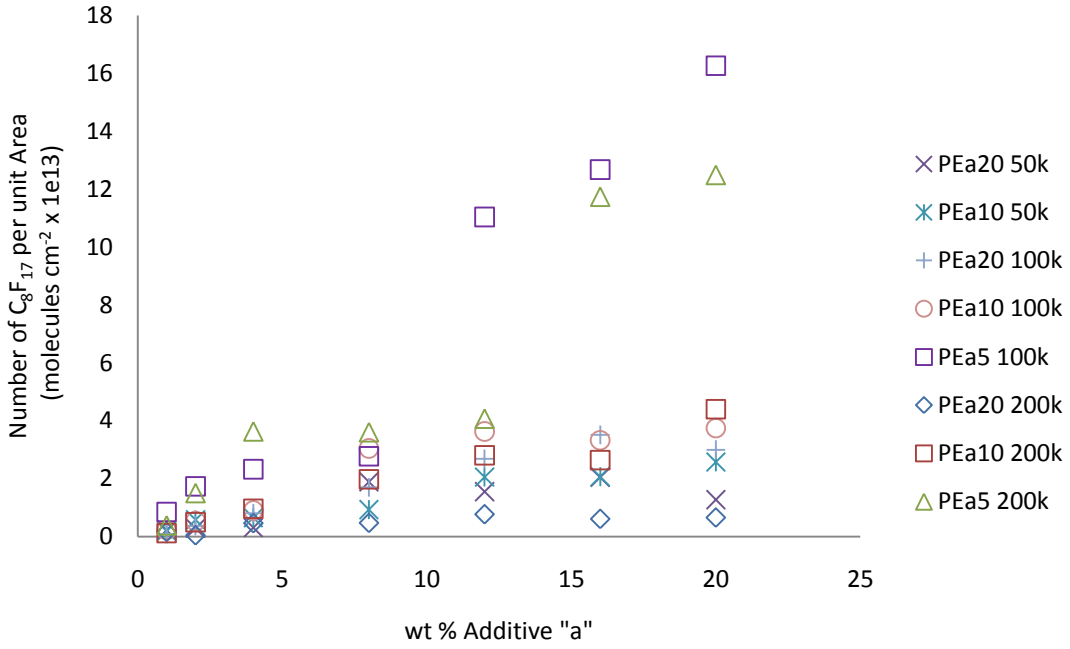

Figure 5:8 Combined results for the number of chains per unit area for deuterated additives of type “a”

Figure 5:9 illustrates the effect that the additive structure in each matrix has on surface segregation, independent on additive molar mass for additives of type “c”. For all blends there is a clear trend that the lower the additive molar mass the greater its ability to segregate with PEc5 the most surface active additive.

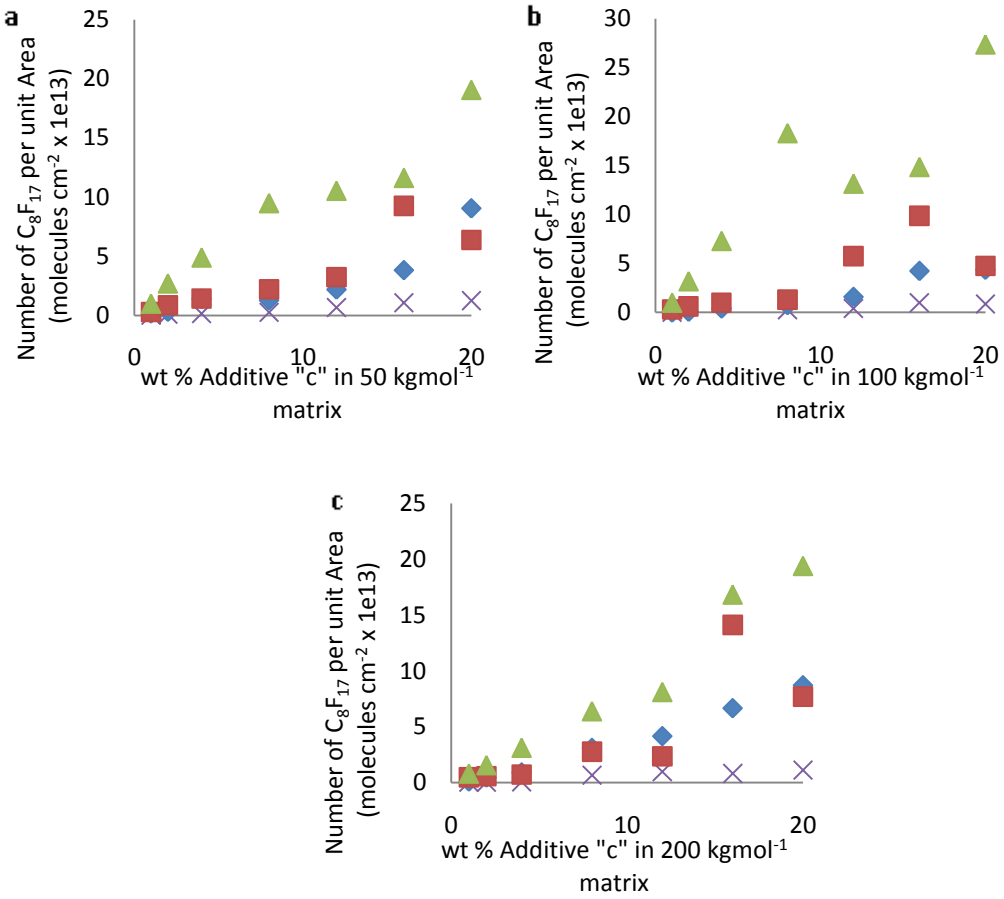

Figure 5:9 Number of chains per unit area, independent of additive molar mass, for additives of type "c" in a) hPE50, b) hPE100, c) hPE200, where × is PEc50 ◊ PEc20, □ PEc10 and Δ PEc5

The findings for additives of type "c" are consistent for those found for additives of type "a" where again the lowest molar mass additives, PEc5, in, any matrix have the greater tendency towards surface segregation, and are combined in figure 5:10.

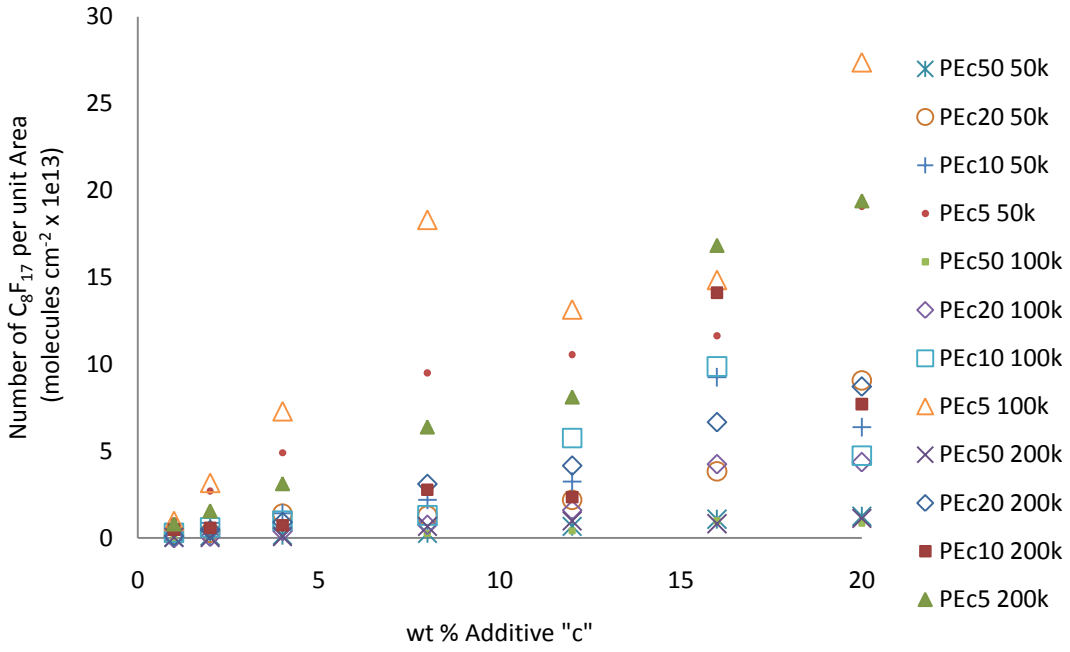

Figure 5:10 Combined results for the number of chains per unit area for deuterated additives of type “c”

Finally for additive PEb5 as the concentration of additive increases the results become increasingly scattered. Whilst the reason for this is not apparent, it should be noted that this is consistent with the other additives, figure 5:11.

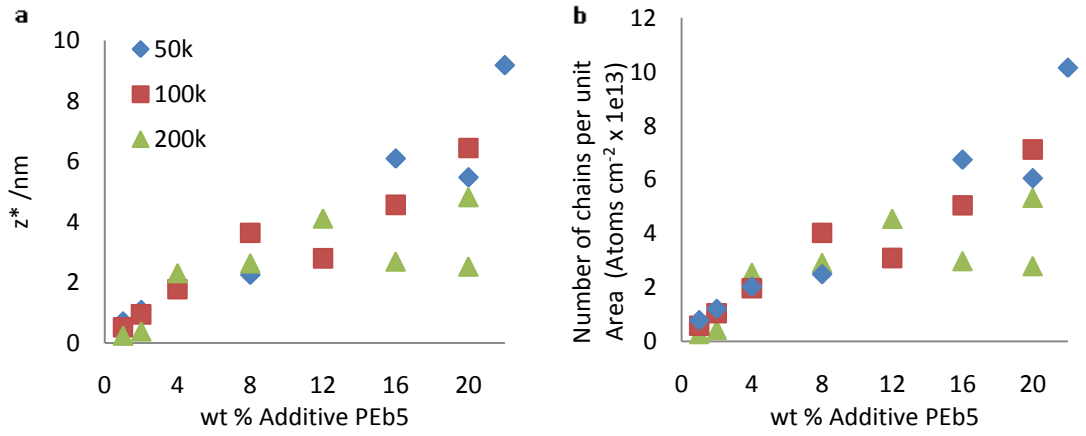

Figure 5:11: The effect of matrix molar mass on PEb5 a) surface excess values extracted from NRA measurements for additives of type “b” and b) number of chains per unit area, independent of additive molar mass

The repeated measurements showed more scattering than the statistically expected uncertainty therefore the effect of crystallinity was explored through controlled cooling rates, section 5.1.2.

5.1.1.2 The Effect that the Number of Fluorocarbons per Polymer Chain has on Surface Segregation

By comparing the *z** values with the contact angle (CA) results, which are sensitive to the amount of fluorine per unit area, the hydrophibicity of the surface can be compared to that owing to CF groups, and that owing to surface roughness. Figures 5:12a-c, 5:13a-c, 5:14a-c summarise the *z** values obtained for each type of CF, where the only variable is the type of CF group. Figures 5:12d-f, 5:13d-f, 5:14d-f show the corresponding water CA results. The graphs g-j in figure 5:12 correspond to the XPS data for the appropriate matrix molar from Chapter 4 figure 4:18 related to the z* values.

For the 5 $kgmol^{-1}$ additives in the 50 $kgmol^{-1}$ matrix, figure 5:12a, additives of type "b" has generally the highest *z** value. In the 100 $kgmol^{-1}$ matrix, figure 5:12b, there is no discernible difference between additives of type "b" additives of type "c", but at higher concentrations of additives of type "a" has the highest *z** value. Surprisingly, this trend is not observed in either the XPS or CA results. Finally, in the 200 kgmol-1 matrix, figure 5:12c, additives of type "b" generally have the highest *z** value and the spread in results increases as more additive is added. The CA results suggest that depending on the additive concentration both additives of type "b" and "c" are highly effective at increasing hydrophobicity whereas additives of type "a" has less influence on surface properties. In general, the XPS results agree with the CA, figure 5:12g-j. This is the opposite trend to that observed by NRA. A possible reason for this is that CA and XPS is sensitive to the amount of fluorine at the surface, whereas NRA is sensitive to the amount of deuterium. At any given molecular weight of additive, the F:D ratio is lowest for additives of type "a" and highest for additives of type "c", therefore additives of type "c" brings less deuterium to the surface, but the most fluorine. This can explain why NRA experiments tend to suggest relatively little surface activity for additives of type "c" in comparison to additives of type "b". This may be further exasperated by the partial deuteration of PEc5 as this was not taken into account.

For the 10 $kgmol^{-1}$ additives in the 50 $kgmol^{-1}$ matrix, figure 5:13a, additives of type "a" behaves very similarly to additives of type "c", apart from at the highest concentrations. The CA results follow the same trend and tendency to spread at higher additive concentrations, where PEc10 has a higher CA than PEa10, complementing the NRA results. As there is a factor of two between the F:D ratio for polymers PEa10 and PEc10 the CA and NRA results can be compared directly and as PEc10 has more CF groups than PEa10 it should segregate more strongly to the surface, thus have a higher *z** value.

In the 100 $kgmol^{-1}$ matrix, figure 5:13b, additives of type "a" has generally the highest z* value, again CA results do not follow the same trend. The reason for this unexpected result could again

be that each type "c" chain at the surface delivers more fluorocarbon to the surface than type "a" of equivalent molecular mass.

Finally, in the 200 $kgmol^{-1}$ matrix additives of type “a” behaves very similar to additives of type “c”, as in the 50 $kgmol^{-1}$ matrix. The CA results loosely follow this trend and exhibit the same deviation at 12% and 16% that the NRA *z** values do, which could be owing to surface roughness.

For the 20 $kgmol^{-1}$ additives in the 50 $kgmol^{-1}$ matrix, figure 5:14a, again additives of type “a” behaves very similarly to additives of type “c”, apart from at the highest concentrations. The CA results follow the same trend. In the 100 $kgmol^{-1}$ matrix, figure 5:14b, additives of type “a” generally has a higher *z** value then additives of type “c”. Again this could be owing to the larger dendrimers aggregating and the surface roughness could explain the higher CA’s for additives of type “c”. Finally, in the 200 $kgmol^{-1}$ matrix additives of type “c” has the highest *z** values and the CA results are similar for either additive.

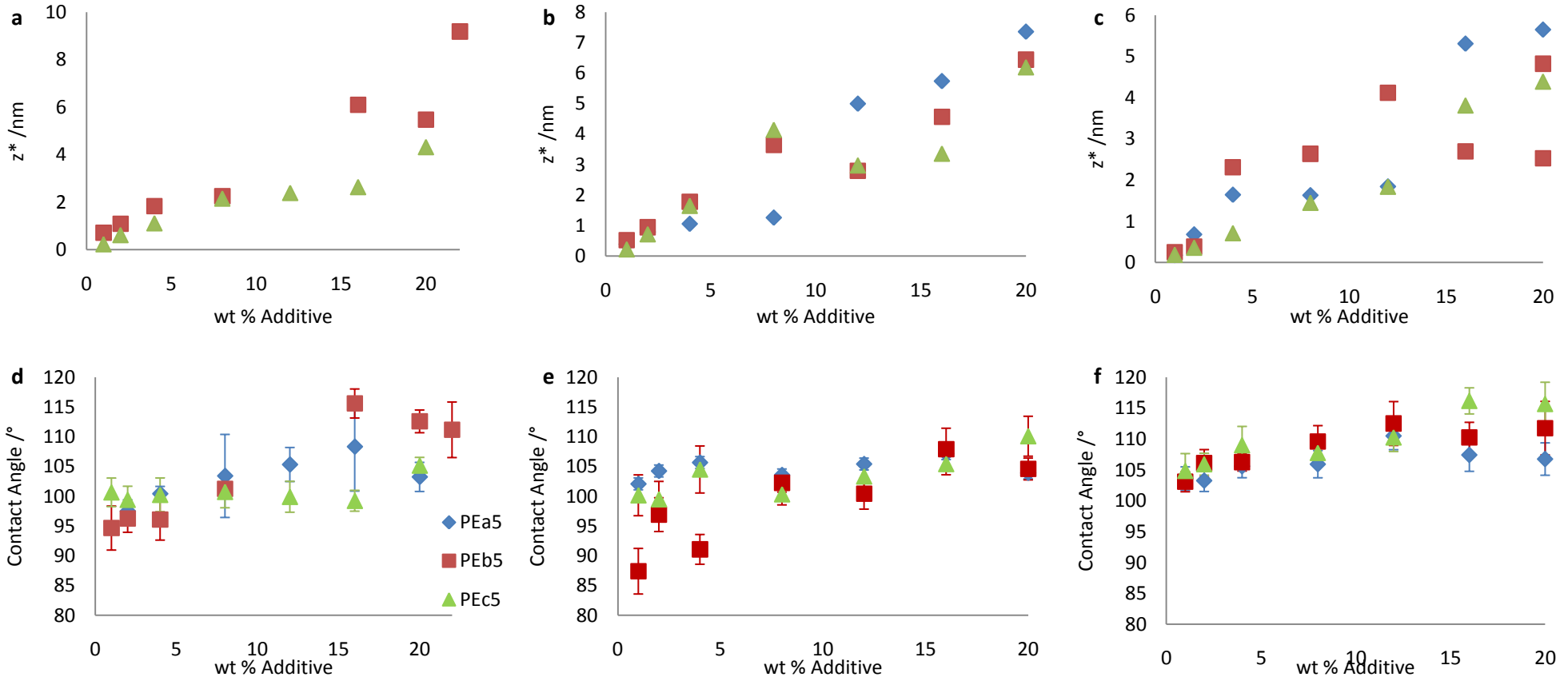

Figure 5:12 Surface excess values extracted from NRA measurements for 5 kgmol^{-1} additive and the corresponding CA measurements where ◊ represents additives of type "a", □ represents additives of type "b" and Δ represents additives of type "c" for graphs a-c and for d-f the key is in graph d. a) 5 kgmol^{-1} deuterated additives in hPE50, b) 5 kgmol^{-1} deuterated additive in hPE100, c) 5 kgmol^{-1} deuterated additive in hPE200, d) 5 kgmol^{-1} deuterated additives in hPE50 CA measurements, e) 5 kgmol^{-1} deuterated additive in hPE100 CA measurements, f) 5 kgmol^{-1} deuterated additive in hPE200 CA measurements

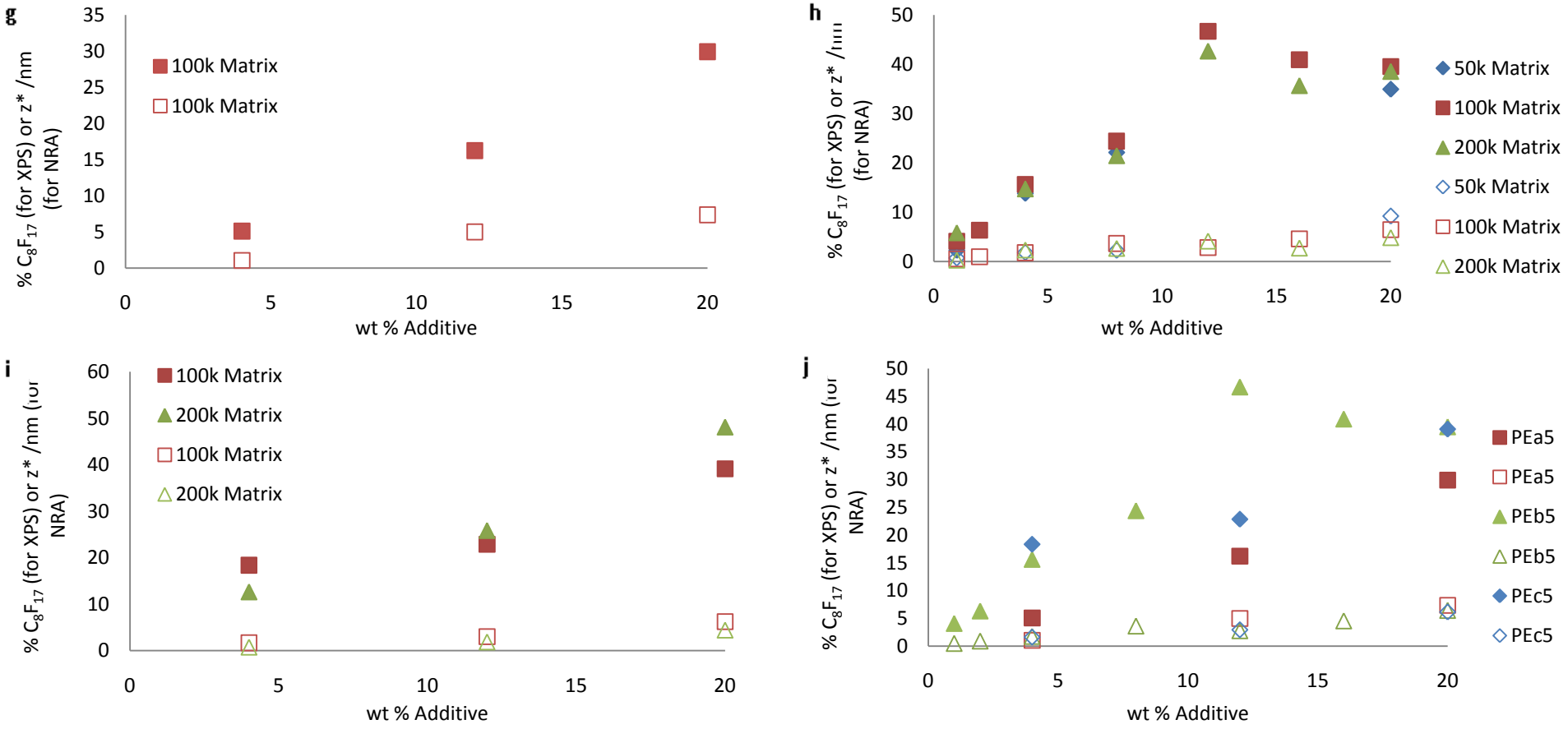

Figure 5:13 Surface excess values extracted from NRA measurements of the top 10nm (phiTOP region) compared to the XPS for g) PEa5 in 100kg mol^{-1} matrix, h) PEb5 in 50kg mol^{-1}, 100kg mol^{-1} matrix and 200kg mol^{-1} matrix, i) PEc5 in 100kg mol^{-1} matrix and 200kg mol^{-1} matrix and j) combined results for all 5kgmol^{-1} additives in 100kgmol^{-1} matrix, where solid markers represents XPS % C_8F_{17} in top 10nm and open markers represent the NRA z* surface excess values for the phiTOP region.

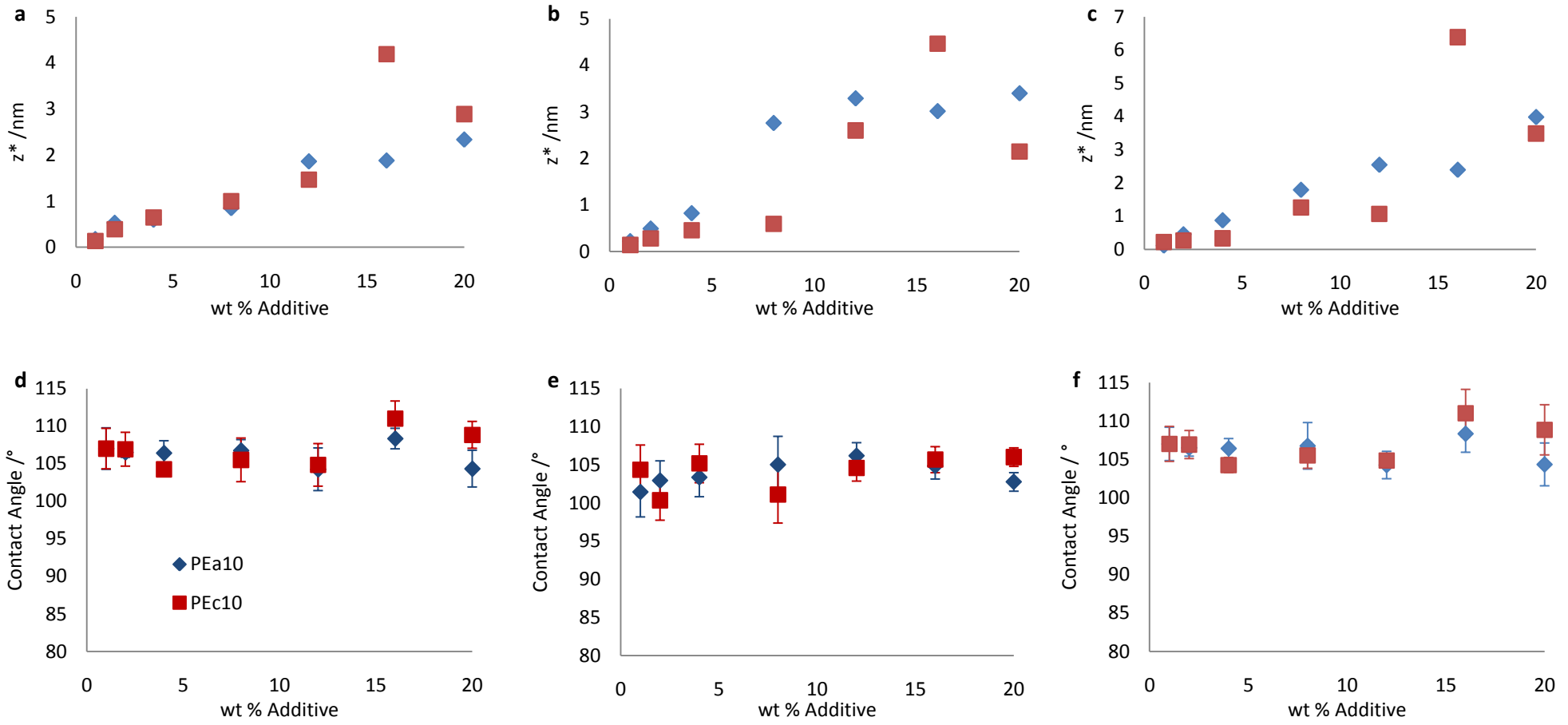

Figure 5:14 Surface excess values extracted from NRA measurements for 10 kgmol^{-1} additive and the corresponding CA measurements where ◊ represents additives of type "a", □ represents additives of type "b" and Δ represents additives of type "c" for graphs a-c and for d-f the key is in graph d, a) 10 kgmol^{-1} deuterated additives in hPE50, b) 10 kgmol^{-1} deuterated additive in hPE100, c) 10 kgmol^{-1} deuterated additive in hPE200, d) 10 kgmol^{-1} deuterated additives in hPE50 CA measurements, e) 10 kgmol^{-1} deuterated additive in hPE100 CA measurements, f) 10 kgmol^{-1} deuterated additive in hPE200 CA measurements.

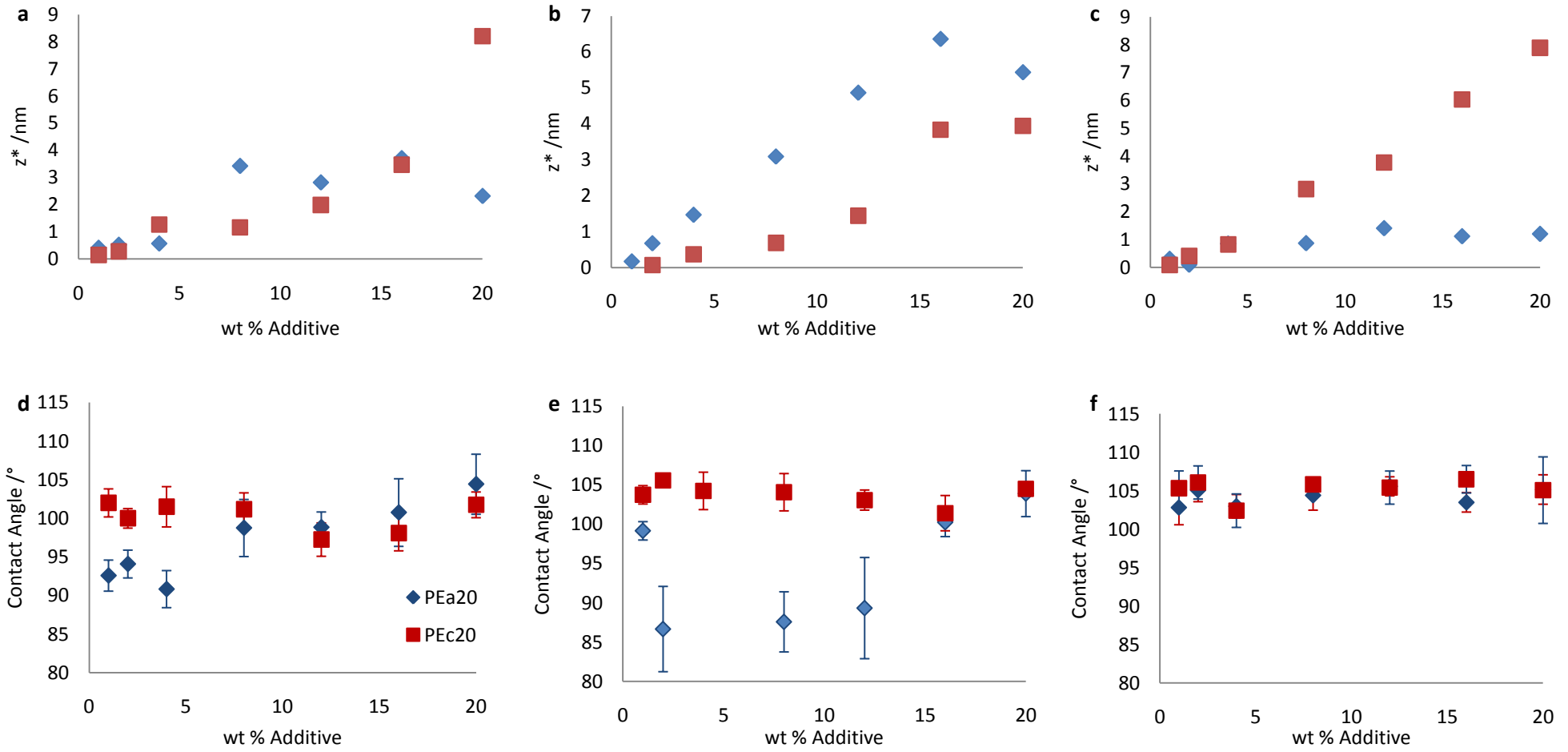

Figure 5:15 Surface excess values extracted from NRA measurements for 20 kgmol^{-1} additive and the corresponding CA measurements where ◊ represents additives of type "a", □ represents additives of type "b" and Δ represents additives of type "c" for graphs a-c and for d-f the key is in graph d. a) 20 kgmol^{-1} deuterated additives in hPE50, b) 20 kgmol^{-1} deuterated additive in hPE100, c) 20 kgmol^{-1} deuterated additive in hPE200, d) 20 kgmol^{-1} deuterated additives in hPE50 CA measurements, e) 20 kgmol^{-1} deuterated additive in hPE100 CA measurements, f) 20 kgmol^{-1} deuterated additive in hPE200 CA measurements.

5.1.2 Effect of Cooling Rate on Crystallinity

The cooling rate used has a dramatic effect on the degree of crystallinity so sufficient time must be allowed for the chains to diffuse into the correct orientation required for crystallite formation. The amount of crystallinity regions in the blend is directly affected by thermal history. Rapid cooling from the melt usually prevents the development of significant crystallinity, and leads to the formation of many small, imperfect crystallites with a relatively low melting temperature

Five different cooling rates were used, where the samples, 12% 5 $kgmol^{-1}$ additive in 100 $kgmol^{-1}$ matrices, were cooled from annealing at 110 °C for 1 hour. The cooling rates were measured by taking temperature measurements every 10 seconds using a temperature probe, and estimated from the gradient of a temperature versus time graph. In reality the cooling rate is not constant so the rate was only measured until the crystallising temperature.

The cooling rates were:

- No annealing – cooling rate 0°C/min
- Annealing to 110°C for 1 hr, then cooling in vacuum oven with the vacuum on - cooling rate 0.53°C/min
- Annealing to 110°C for 1 hr, then cooling in vacuum oven with the vacuum off- cooling rate 0.7°C/min
- Annealing to 110°C for 1 hr, then cooling on the bench - cooling rate 14°C/min
- Annealing to 110°C for 1 hr, then quenching in liquid nitrogen - cooling rate 94.5°C/min

The roughness value obtained by AFM, R_q, is the root mean square roughness. The measurements obtained from each point of a height map, resulting in a root mean square average of height deviations, equation 5:1, where n is the number of points averaged, z is the height at each point and z_{mean} is the average height.

$$\text{–} \qquad \text{Equation 5:1}$$

Using these data the effect that the number of CF groups has on the crystallinity was explored, using the standard cooling rate – bench cooling.

5.1.2.1 AFM and NRA Results

AFM images were taken of the films prepared under different cooling conditions and the roughness calculated. The results show as the cooling rate increases the surface roughness decreases, irrespective of the type of additive used, figure 5:15. This is likely to be owing to a

kinetic effect where the time required to form crystalline structures is reduced upon rapid cooling, thus the roughness decreases and is consistent with the idea that roughness, in semicrystalline polymer films, is dominated by the crystallinity or the size of the crystallites formed.

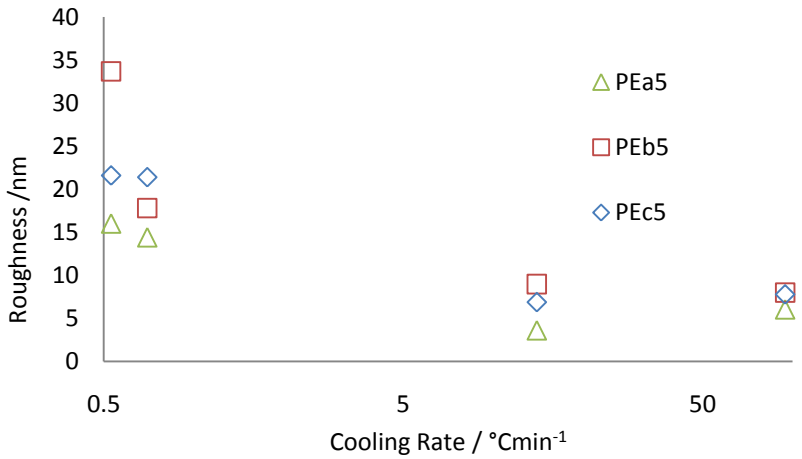

Figure 5:16 Effect of cooling Rate on the surface roughness for three different deuterated additives (12% in hPE100)

Using the data obtained from the AFM images of additives of type “a”, figure 5:16a-d, it was clear that the roughness decreased as the cooling rate increased. For additives of type “a” the blended film containing the additive was the smoothest could account for the overall lower CAs. The NRA measurements carried out on each of these films, after cooling at different rates, showed remarkably little difference in the surface concentration profiles obtained.

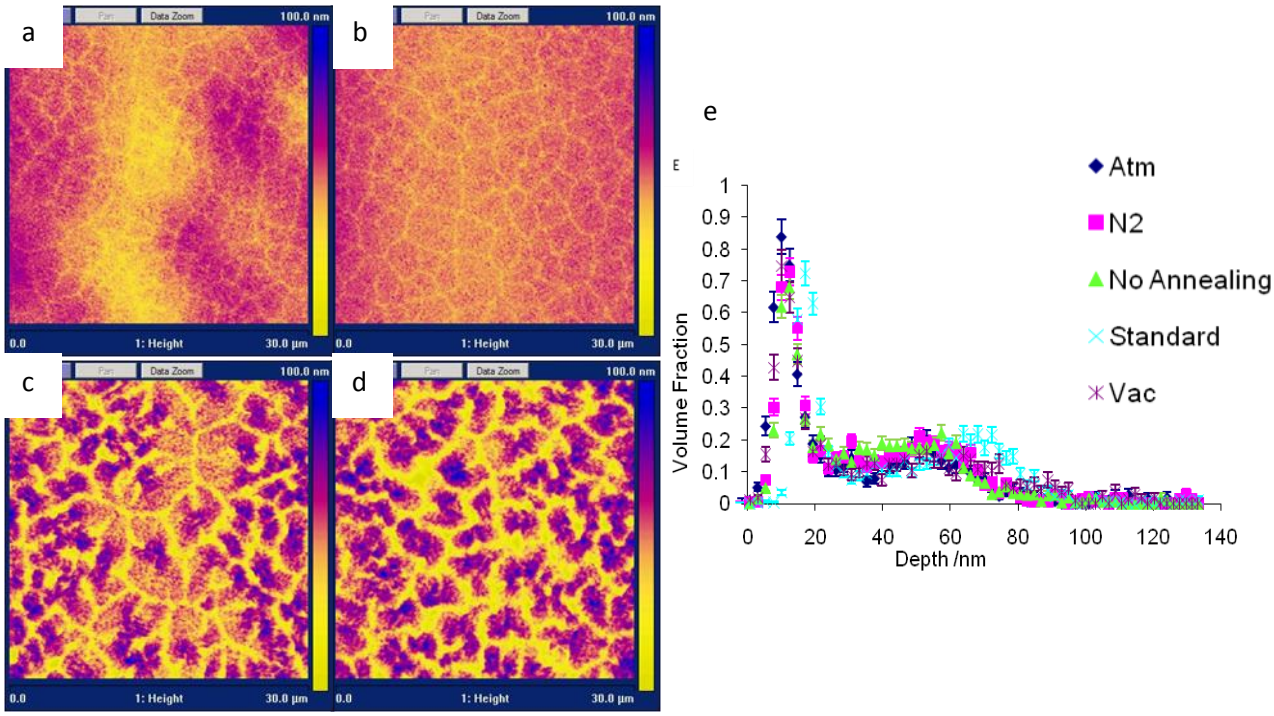

Figure 5:17 AFM images (height map) of sample surface after cooling from the melt to below T_c at different rates a) liquid N_2, b) bench cooling, c) vacuum off (ATM), d) vacuum on (Vac) and e) surface excess data derived from NRA for 12% PEa5 in hPE100

Additives of type “b” produced generally the roughest surfaces, which is illustrated in the AFM images taken, figure 5:17a-d. However like additives of type “a” the NRA volume fractions profiles obtained were remarkably similar showing little dependence on cooling rates. For additives of type “c”, figure 5:18, again the NRA volume fractions obtained are not dependant on cooling rate.

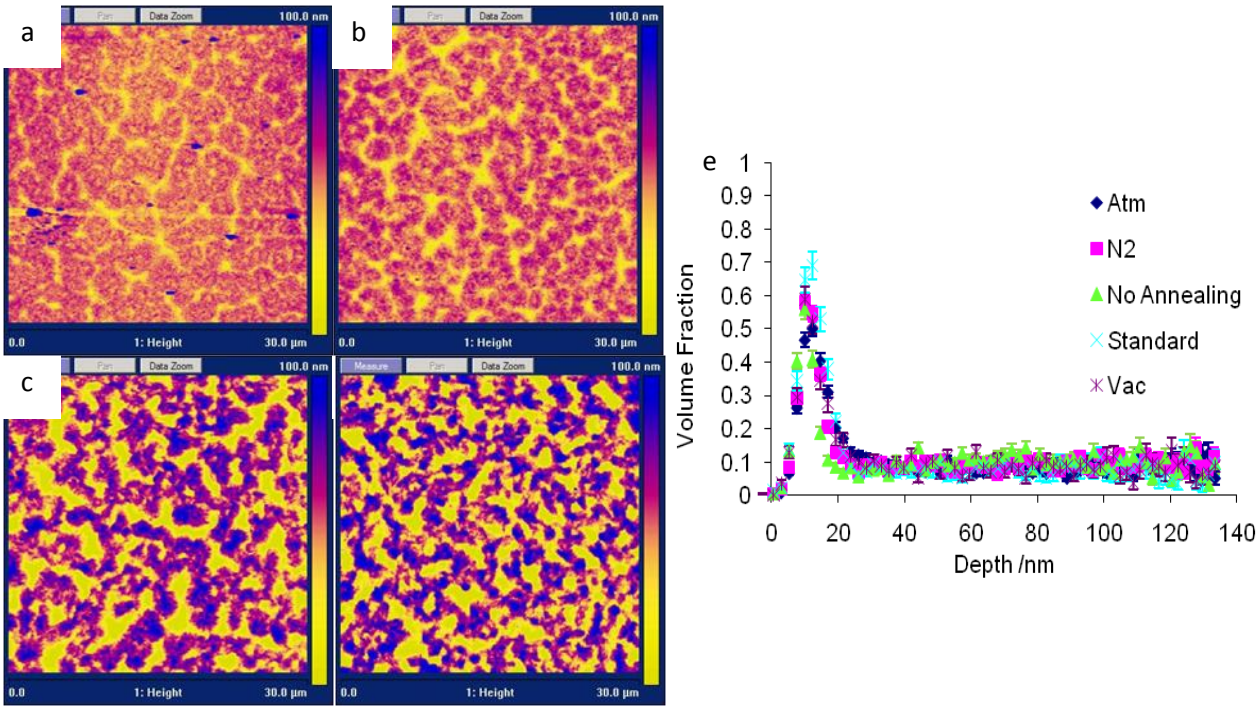

Figure 5:18 AFM images (height map) of sample surface after cooling from the melt to below T_c at different rates a) liquid N2, b) bench cooling, c) vacuum off (ATM), d) vacuum on (Vac) and e) surface excess data derived from NRA for 12% PEa5 in hPE100

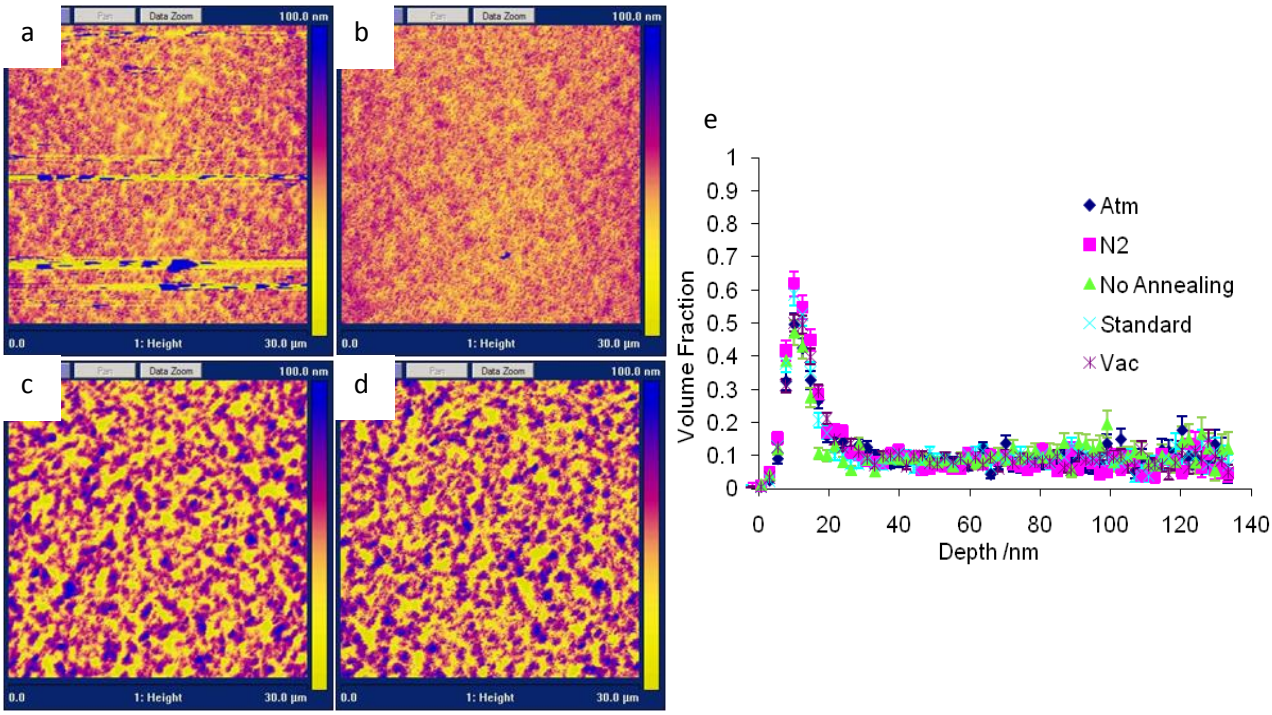

Figure 5:19 AFM images (height map) of sample surface after cooling from the melt to below T_c at different rates a) liquid N2, b) bench cooling, c) vacuum off (ATM), d) vacuum on (Vac) and e) surface excess data derived from NRA for 12% PEc5 in hPE100

Surface excess data derived from NRA was compared for each for each of the additives at the different cooling rates, figure 5:19. When cooled extremely slowly there is no difference between the *z** values, but there is a significant variation in roughness, figure 5:15. When cooling faster additives of type "b" have the lowest surface volume fraction and additives of type "a" the highest, where additives of type "b" have the roughest surface and additives of type "a" the smoothest.

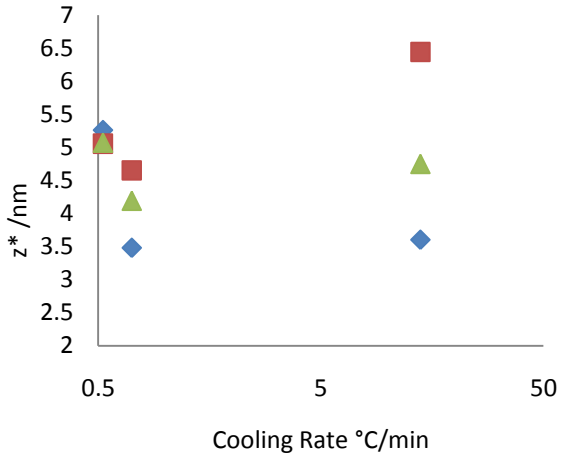

Figure 5:20 Surface excess values extracted/derived from NRA measurements/experiments for the effect that the type of CF group has on the degree of surface segregation where ◊ represents additives of type "a", □ represents additives of type "b" and Δ represents additives of type "c"

By combining all these results, figure 5:20, the *z** values and the surface roughness mirror each other whereas the roughness increases the *z** value increases, going from 2-4 CF groups on the chain end. However the CA results contradict which could be because RMS roughness is not directly sensitive to gradients in slope and functionality in the modified surface, which will affect CA hysteresis. This leads to the conclusion that CA measurements are an unreliable technique for measuring surface functionalities.

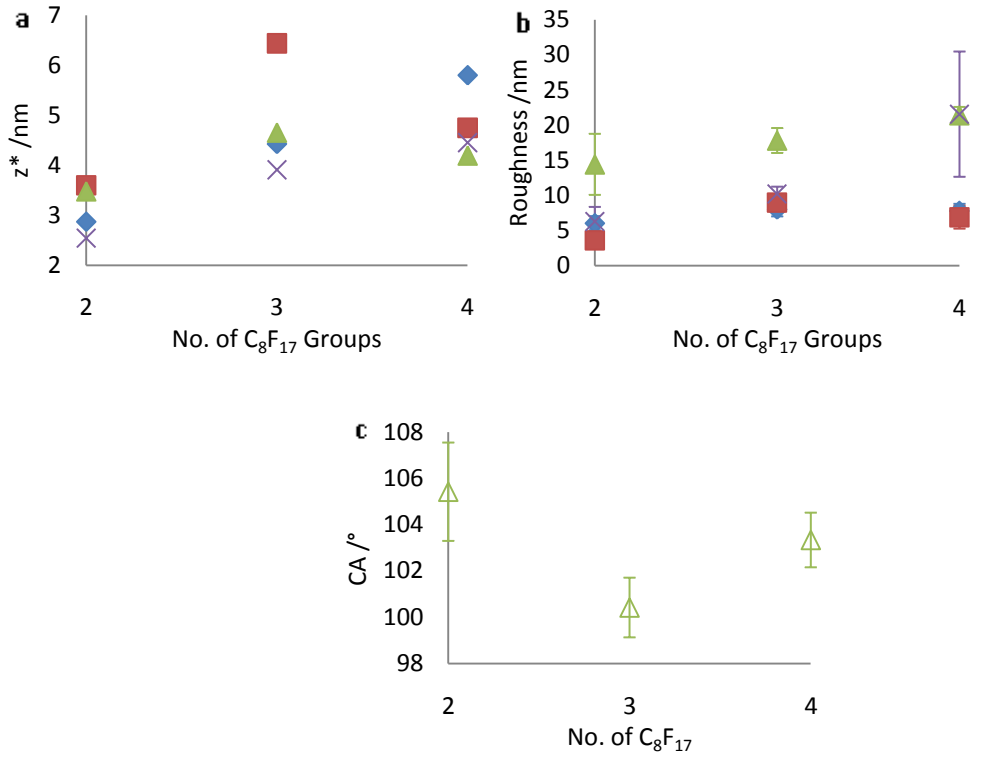

Figure 5:21 12% additive in hPE100 combined results for a) surface excess values extracted from NRA measurements, b) roughness at different cooling rates where ◊ is rapid cooling in N_2, □ is standard bench cooling, Δ is vacuum on and × is no annealing and c) CA at standard cooling rates

5.2 Neutron Reflectivity

Neutron reflectivity (NR) is a technique that provides a detailed description of the depth composition profile of thin planar samples, thus providing information about layer thickness, surface and interfacial width and profiles[11-13]. Specifically to polymers it provides information about the surface coverage and area per molecule. Interfacial tension, diffusion coefficients and χ can also be extracted from NR data. The reflectivity of neutrons is dependent on their wavelengths, the angle of incidence and the chemical composition gradient, normal to the interface (which manifests itself through the neutron scattering lengths of the constituent atoms).

The essence of a NR experiment is a measure of the specular reflection as a function of Q, perpendicular to the reflecting surface, when a neutron beam is incident on a smooth surface at any angle greater than the critical angle. Neutrons are reflected as waves at the surface and buried interfaces[14]. The measurement of reflectivity can be obtained by varying either λ or Q, which is related to the angle of incidence, θ, by the following equation:

— Equation 5:2

The *Q* dependent reflectivity, *R(Q)*, is simply a ratio of the reflected to incident beam intensities. The reflectivity profile *R(Q)* is determined by the near surface composition depth profile of the specimen. *R(Q)* is represented by:

Equation 5:3

where $I_{ref}(Q)$ is the reflected and $I_{inc}(Q)$ the incident beam intensity.

The reflective properties of neutrons are analogous to that of light, thus the same rules of optics apply where the refractive index of a material, n_i, is expressed as:

Equation 5:4

where N_a is the atomic number density, λ is the neutrons wavelength (typically 0.05-20 Å) and b_{coh} is the scattering length of the atom. For many materials $n_i > n_{air}$ ($\simeq 1.0$) which facilitates total external reflection from a surface, figure 5:21.

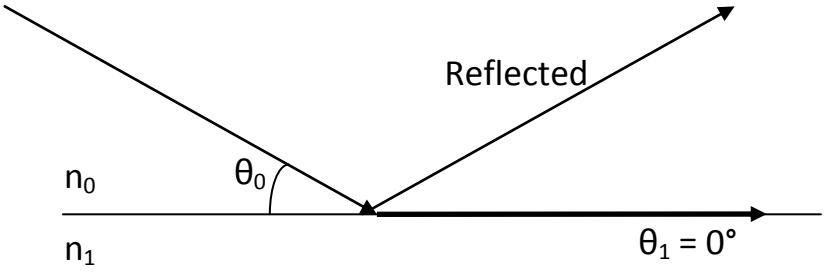

Figure 5:22 The paths that a neutron beam takes during reflection

If the neutron refractive index of the material normal to the surface is a quantity varying with depth, then the refracted beam will be specularly reflected in a manner determined by this neutron refractive index variation. The neutron refractive index at any point in the thin film is determined by the scattering length density at that point, which is controlled by the volume fraction composition of the sample[15].

Reflectometry involves higher order terms in the Born Approximation and thus a completely different theoretical basis than all other (single) scattering methods. When a neutron beam hits an interface at a critical angle, θ_c, total reflection is observed. The critical angle for total reflection increases with neutron wavelength:

Equation 5:5

where,

Equation 5:6

This equation is derived from Snell's Law, where at total reflection $\theta_0=\theta_c$ and $\theta_1=0$. On silicon substrates there is always a critical edge where $R(Q)=1$ at sufficiently low Q (<0.01Å^{-1}). The Fresnel reflectivity, R_f, can be used to determine the size of a 'buried' interface from the reflection of a thin film (media 1) between two bulk media (media 0 and 2), figure 5:22. The scattering length density for each polymer is calculated in section A2.2.5 for C_4H_8 and section A2.2.6 for mixtures of $C_4H_4D_2$ and C_4H_8.

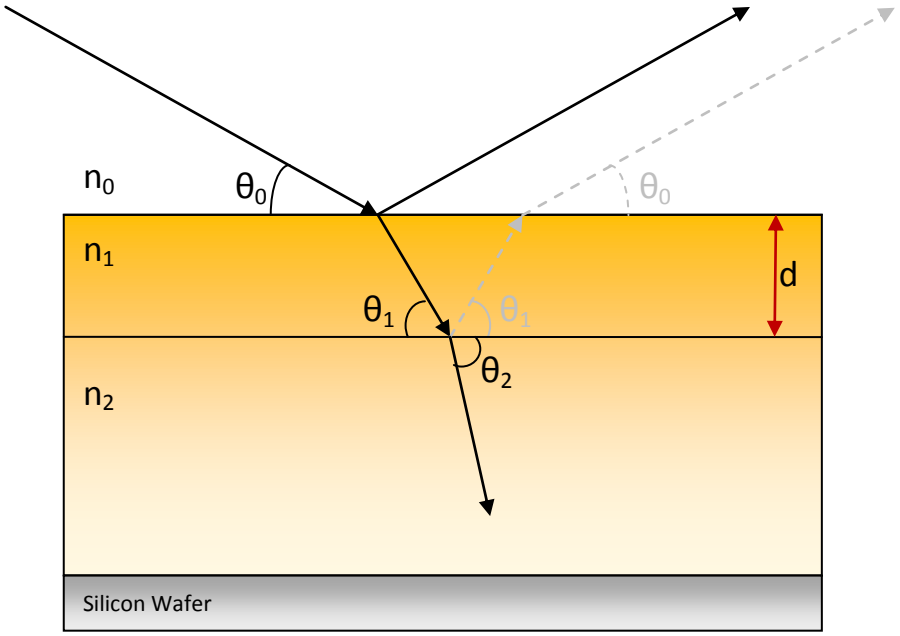

Figure 5:23 Illustration explaining Fresnel reflectivity (R_f) through layers and the corresponding mathematical expression

As the beam travels through the film it changes phase, thus a phase term, , needs to be introduced to the reflectivity equation. The phase term includes information about layer thickness, d, and can be used to determine the reflectivity for a thin film, R,

Equation 5:7

where r_1 and r_2 are the Fresnel coefficients for the respective interfaces given by

.

From this expression it is clear that the reflectivity obtained from a neutron reflectivity experiment is sensitive to both the thickness of the monolayer as well as the monolayer's composition.

5.2.1 Analysis and Results

A general introduction to neutron scattering is described in A2 and the experimental details used in section 2.4.2 where the same samples used in NRA and CA measurements were used. When there is a reflective surface at the air-polymer interface and a reflective surface at the polymer-substrate interface, that is a surface that has a SLD that is different to air, Kiessig fringes are observed in the *R(Q) vs Q* scattering plots. The amplitude of the fringes can reveal the surface excess concentration of the additive. Figure 5:23 illustrates the path of a neutron during reflection from two types of films. In figure 5:23a, no reflection occurs at the air surface as the SLD of PE is similar to that of air. The absence of Kiessig fringes is apparent when measuring the reflection from hPE50 and hPE100, figure 5:24 and *R(Q)* decays monotonically with Q^{-4}. Conversely if there is a layer at the surface which has a different SLD reflection occurs, figure 5:23b.

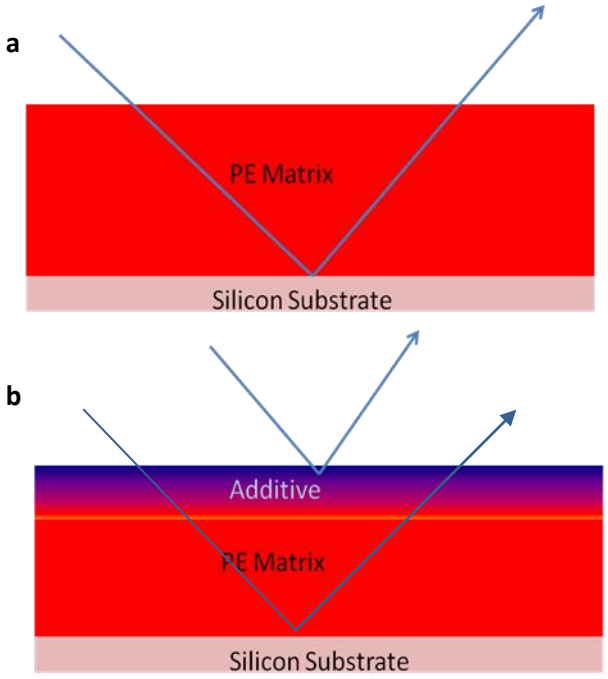

Figure 5:24 Path of neutron during reflection from different surfaces a) pure PE films and b) PE blend

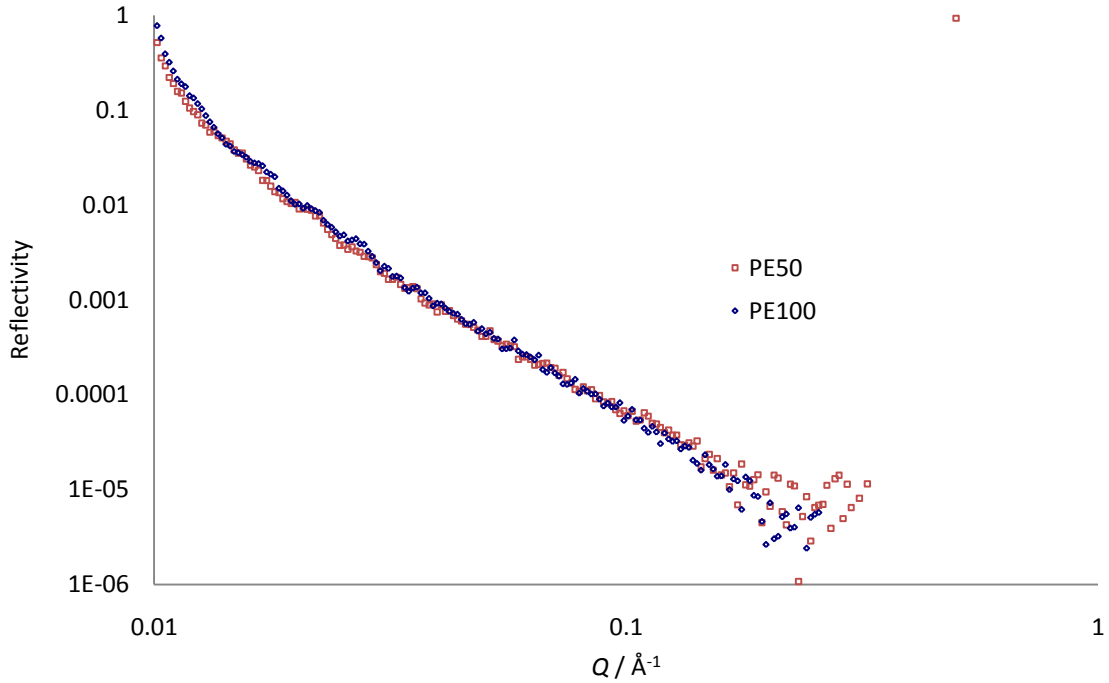

Figure 5:25 Neutron Reflection data for hPE50 and hPE100 matrix without any blended additive at 120 °C

5.2.1.1 Neutron Reflectivity Profile for PEa5 in hPE50 Matrix at room temperature, 120°C and during cooling from the melt

Figure 5:25a illustrates the raw reflectivity profiles for PEa5 in 50 kgmol^{-1} matrix. In this case the data and simulation are shown as RQ^4 versus Q which eliminates the Q^{-4} decay seen in all reflectivity data. This representation highlights variations in *R(Q)* due to adsorbed layers. The model used to generate simulation that is fitted to the data was analyzed by fitting the calculated reflectivity for a surface excess layer conforming to an error function profile of:

Equation 5:8

where *z* is depth, *w* is the width of the interface, *h* is the distance between the film surface and the centre of the interface, and ϕ_∞ is the bulk volume fraction of deuterated polymer[5]. The adjustable parameters in the fit were ϕ_s, *h*, and *w*. Figure 5:25 illustrates typical sample and fit data.

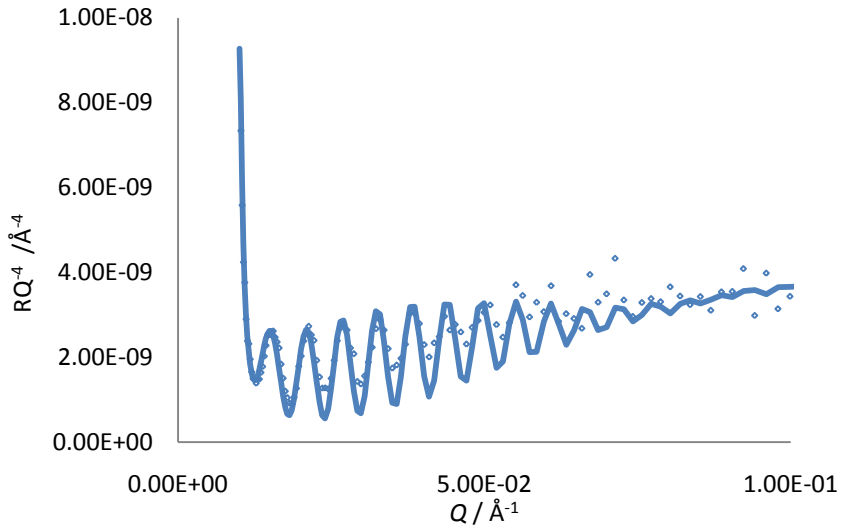

Figure 5:26 Typical neutron reflectivity sample and fit data for 8% PEa5 in hPE50 matrix at 120°C

The area under the curve in the SLD profiles, figure 5:26b, increases as the concentrations of additive increases. However higher concentrations of additive have much sharper profiles which could be owing to the films being thinner.

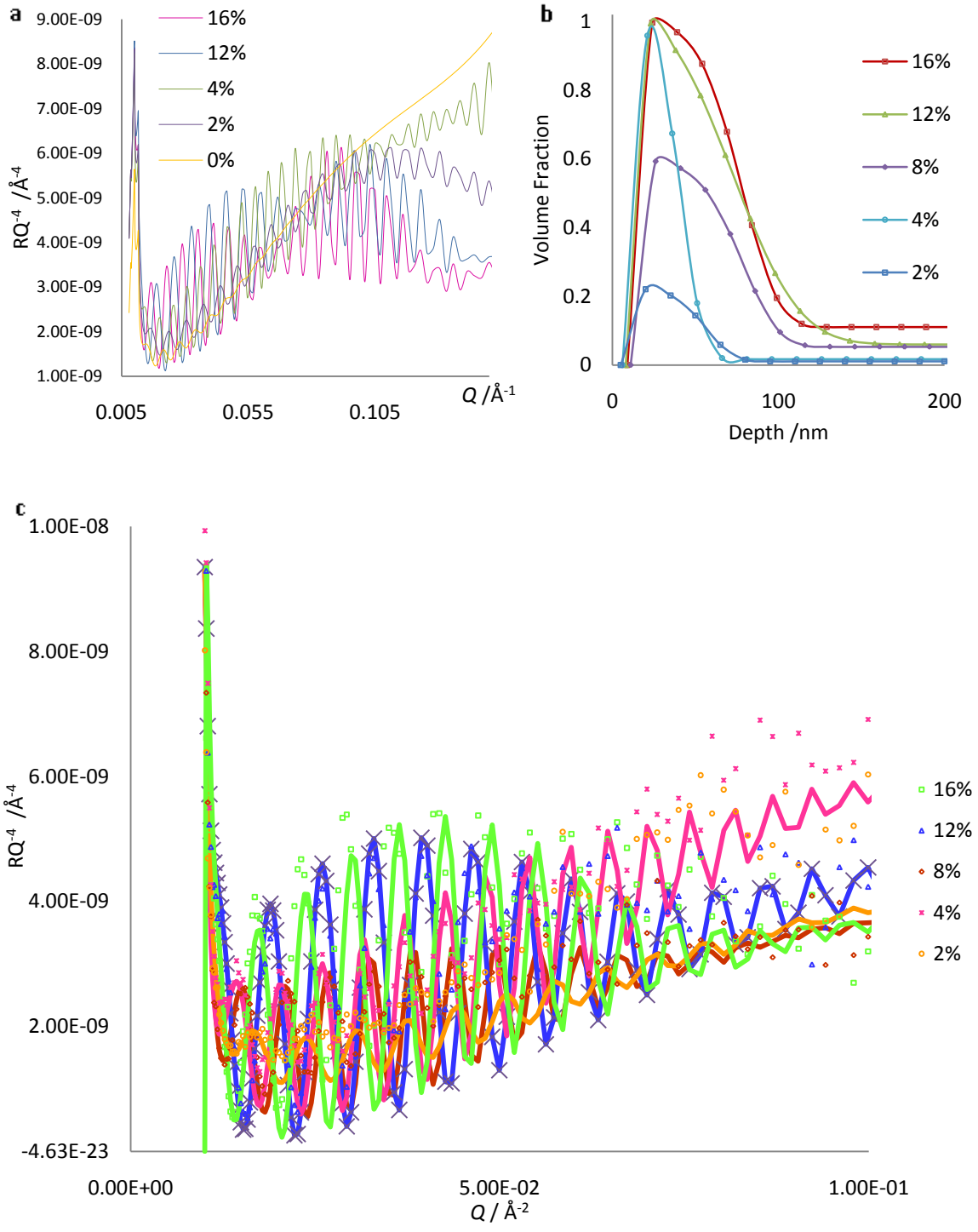

Figure 5:27 Neutron reflection data for different concentrations of PEa5 additive in hPE50 matrix at 120°C a) raw reflectivity, b) scattering length density (SLD) profile and c) reflectivity and fit data

The z* values determined by integration of the NR profiles agreed with the NRA z* values obtained for similar systems in that the values increased as the concentration of the additive increased, figure 5:27. For both NR and NRA the z* values at low concentrations appear to be low

and very similar, but at high concentrations, the large jump in z* seen by NRA below T_m is not apparent by NR in the melt. These results could be due to the incorporation of additive at low concentrations into crystals, restricting z*, which is not seen in NR as no crystals are present. The large excess in NRA at high concentrations indicates crystallisation drives the additive to the surface. Although the z*(NR) values are much smaller, there appears to be a leap in values between 8-12%. This could be due to the critical concentration required to saturate the surface, as seen in NRA data, suggesting that even in the melt that two polymers become incompatible above a certain concentration resulting in phase separation. This is interesting as the critical concentration, measured by NRA, occurs between 12-16% in hPE100 and between 16-20% in the hPE200. Although the critical concentration here is measured in the melt it follows a trend which decreases as the matrix molar mass increases. Suggesting that the smaller the matrix molar mass the more incompatible the system becomes.

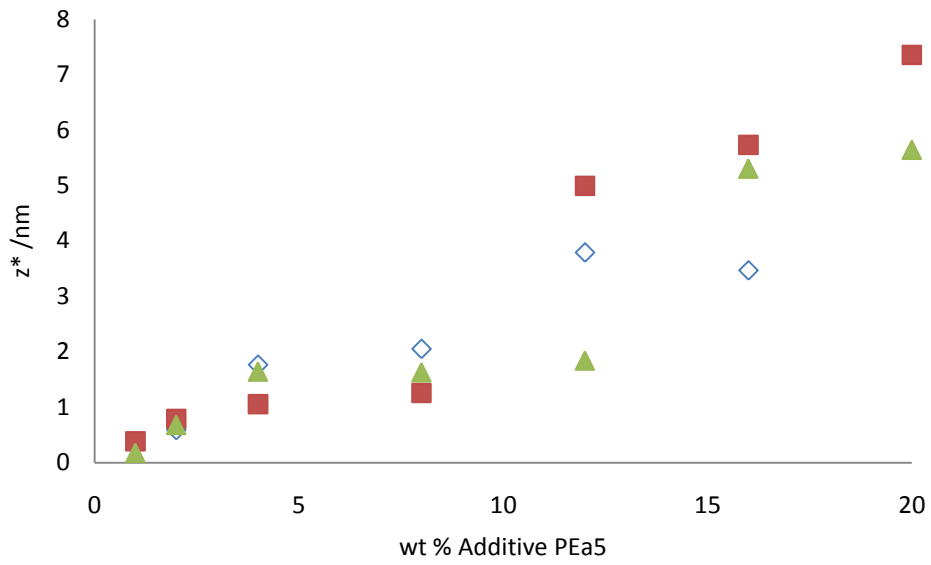

Figure 5:28 Surface excess values (z*) extracted from NRA and NR measurements (at 120 °C) for different concentrations of PEa5 additive measured where ◊ represents additive in hPE50, □ represents additive in hPE100 and Δ represents additive in hPE200 (NRA closed data points and NR open)

Due to time and beam time allocations it was not possible to repeat 50 $kgmol^{-1}$ matrix experiments by NRA, secondly the films dewetted and were extremely challenging to prepare. However, the AFM results obtained in section 5.1.2.1 allow us to presume that the matrix effects are usually small, so some comparison between the NRA on 100 $kgmol^{-1}$ matrix and NR on 50 $kgmol^{-1}$ matrix can still be made. Figure 5:28 compares the reflectivity measured at room temperature (RT) and in the melt (at 120 °C). The amplitude of the fringes are comparable but the frequency of the fringes in the melt are higher than those measured at room temperature, clearly indicating expansion of the film upon heating.

By comparing the depth of the films at room temperature and in the melt the expansion on heating can be calculated, figure 5:28d. The expansion is 15% ±5% which is indicative of the systems volume increasing. It also implies that, within error, either the amount of additive does not affect expansion, again suggesting that it is excluded from the crystalline regions in the matrix polymer, or that the additive experiences the same degree of expansion as the matrix. In either case, the crystallinity of the film is not greatly affected by the additive.

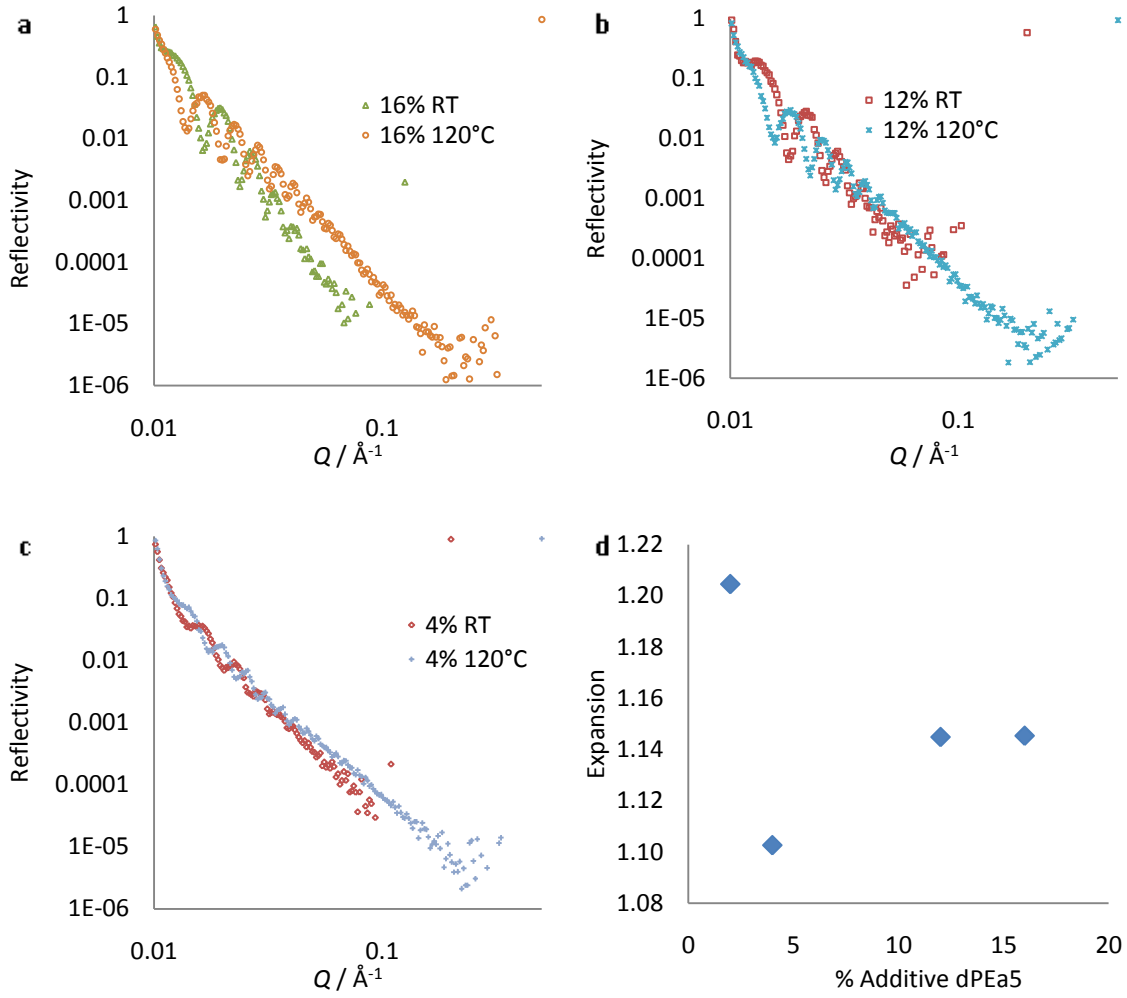

Figure 5:29 Neutron reflection data for different concentrations of PEa5 additive in hPE50 matrix cooling a) raw reflectivity for 16% of PEa5 at room temperature and 120°C, b) raw reflectivity for 12% PEa5 at room temperature and 120°C, c) raw reflectivity for 4% PEa5 at room temperature and 120°C and d) the expansion on heating

The specular reflectivity profile was also measured when cooling from 120 °C to 95 °C, figure 5:29a, for 8% additive blends. From the raw reflectivity it is clear that the system crystallises between 105-100 °C thus the amount of reflectivity diminishes as the surface becomes rough. Above the crystallisation temperature the SLD profiles and z* values are in excellent agreement

with each other, within experimental error, which was as expected as the same sample was used, figure 5:29b-c.

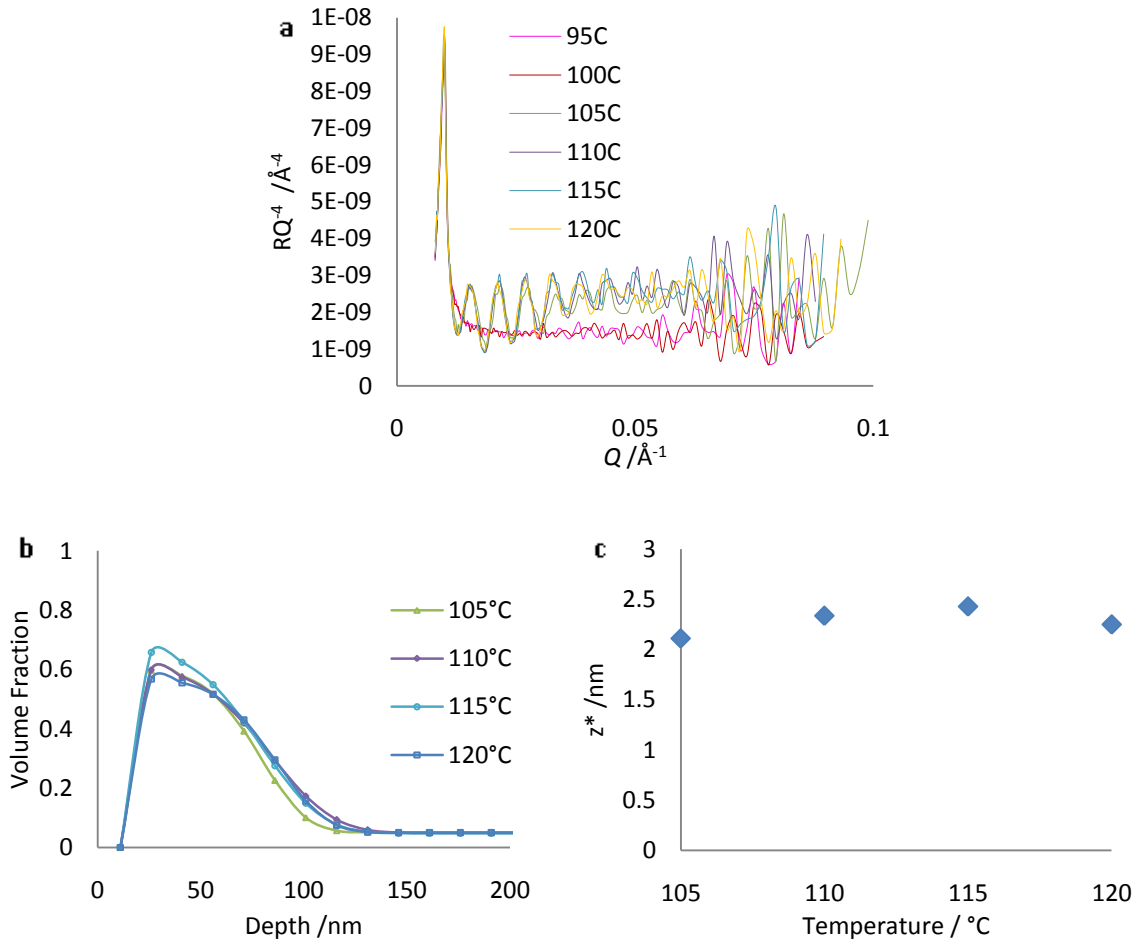

Figure 5:30 Neutron reflection data for different concentrations of PEa5 additive in hPE50 matrix cooling from 120°C a) raw reflectivity, b) scattering length density (SLD) profile and c) the calculated z*

5.2.1.2 Neutron Reflectivity Profile for PEa5 in hPE100 Matrix at 120°C

Figure 5:30 illustrates the raw reflectivity profiles for PEa5 in hPE100 matrix. It is clear from these figures that the fringes dampen earlier than for the hPE50 experiments or have no fringes. This is a clear indication that there is significant variation in thickness across the sample surface. Possible explanations for this are that the crystalline samples have not equilibrated during the measurement window owing to the crystalline regions not fully melting. Another explanation is that lateral phase separation has occurred. In either case it was not possible to extract a volume fraction versus depth profile for these samples that was consistent with the scattering length densities of the components.

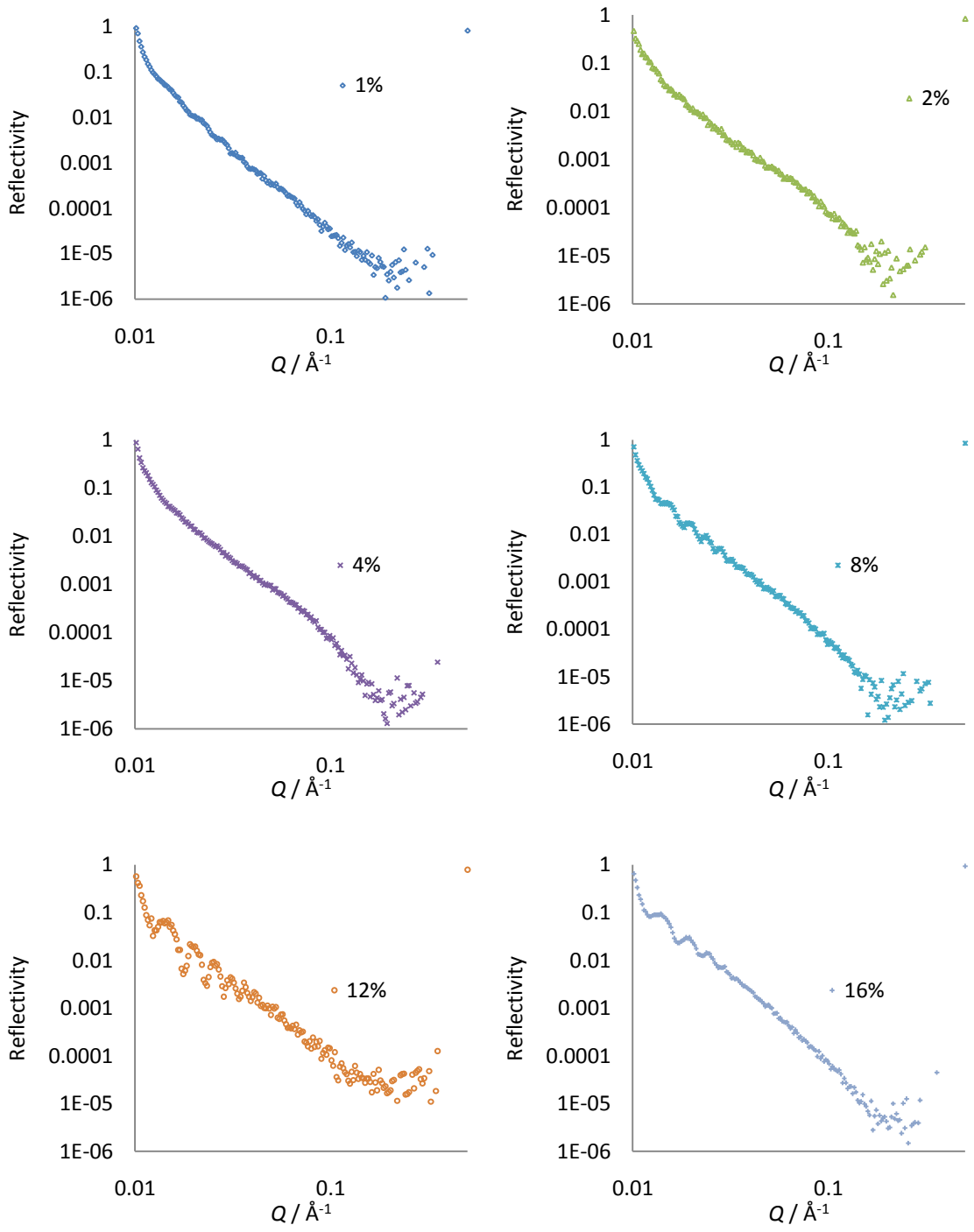

Figure 5:31 Neutron Reflection data for different concentrations of PEa5 additive in hPE100 matrix at 120°C a) raw reflectivity for 1% PEa5, b) raw reflectivity for 2% PEa5, c) raw reflectivity for 4% PEa5, d) raw reflectivity for 8% PEa5, e) raw reflectivity for 12% PEa5 and f) raw reflectivity for 16% PEa5

Figure 5:31 illustrates a schematic of the type of phase separation that could occur. It is known from the difference between the scattering length density of the additive and the matrix that the crystallinities are different, which impacts on specular reflection. Hence the additives would

occupy a greater volume in the film, if the matrix was not yet molten, thus creating a height variation. In this situation a surface excess would still be observed.

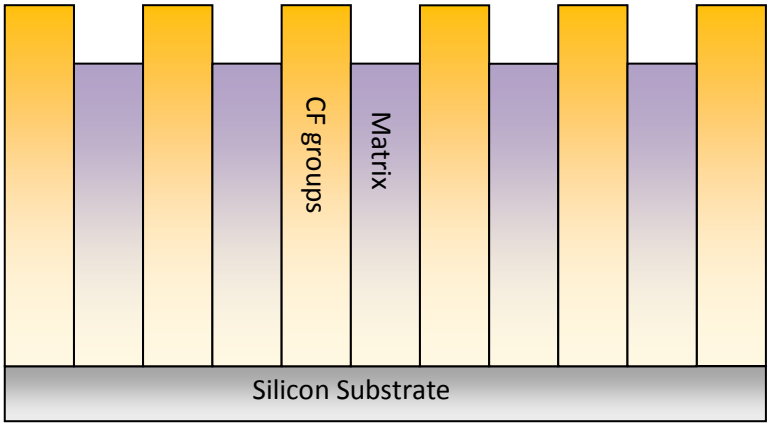

Figure 5:32 Schematic illustrating one possible type of lateral phase separation occurring during neutron reflection in 100 $kgmol^{-1}$ matrix

Owing to this drop in reflectivity several fitting programs were used. A layer model, which managed to account for the profile but not for the intensity, then Volfmem (a maximum entropy model) was used. Volfmem[16] either fitted the data and produced an unrealistic profile, or poorly fitted the data constrained to a more realistic profile. As this data could not be fitted more work is required and owing to this a neutron proposal using Off-spec was submitted, but could not be scheduled during the project time frame.

5.3 Conclusion

The main conclusions that can be drawn from these results are that as the additive concentration increases the surface excess of the additive increases whether in the melt or in the crystalline state. These results agree with the CA and XPS results described in the previous chapter. However as the roughness and/or surface heterogeneity has proven to be very important it can be concluded that at the lowest concentration of additives roughness dominates and the CA is higher than expected for a smooth homogeneous surface with the level of fluorination indicated by XPS. At higher additive concentrations the roughness is less critical and amount of fluorine at the surface dominates.

From the NRA data it was observed that the lowest additive molar mass in the highest matrix molar mass, leads to the highest surface excess, however matrix molar mass is not a very influential parameter, and it does not consistently control surface segregation. This was in agreement with the CA and XPS results from the previous chapter.

Finally, the most interesting conclusion that can be drawn from this chapter is that there appears to be a "critical concentration" required to reach the highest surface excesses. A possible explanation for this could be that either the CF groups are aggregating or that the CF groups are only excluded from the crystalline regions above a certain concentration. Although the maximum NR *z** values are somewhat smaller, the "critical concentration" is observed even in the melt suggesting that two polymers become incompatible above a certain concentration resulting in enhanced segregation. Phase separation could possibly explain the results observed in the 50 $kgmol^{-1}$ data and be a contributing factor for the lack of reflectivity in the 100 $kgmol^{-1}$ data, owing to the uneven surface which could be caused by lateral variation is scattering length density.

5.4 References

1. Thompson, R. L.; Narrainen, A. P.; Eggleston, S. M.; Ansari, I. A.; Hutchings, L. R.; Clarke, N., *Journal of Applied Polymer Science* **2007,** *105* (2), 623-628.
2. Narrainen, A. L.; Hutchings, L. R.; Ansari, I. A.; Clarke, N.; Thompson, R. L., *Soft Matter* **2006,** *2* (2), 126-128.
3. Hutchings, L. R.; Richards, R. W.; Thompson, R. L.; Bucknall, D. G.; Clough, A. S., *Eur. Phys. J. E* **2001,** *5* (4), 451-464.
4. Clarke, C. J.; Jones, R. A. L.; Clough, A. S., *Polymer* **1996,** *37* (17), 3813-3817.
5. Ansari, I. A.; Clarke, N.; Hutchings, L. R.; Pillay-Narrainen, A.; Terry, A. E.; Thompson, R. L.; Webster, J. R. P., *Langmuir* **2007,** *23* (8), 4405-4413.
6. Hutchings, L. R.; Douglas, C. J. R.; Rhodes, C. L.; Carswell, W. D.; Skoda, M. W. A.; Webster, J. R. P.; Thompson, R. L., *Langmuir* **2010,** *26* (19), 15486-15493.
7. Jones, R. A. L.; Norton, L. J.; Kramer, E. J.; Composto, R. J.; Stein, R. S.; Russell, T. P.; Mansour, A.; Karim, A.; Felcher, G. P.; Rafailovich, M. H.; Sokolov, J.; Zhao, X.; Schwarz, S. A., *Europhysics Letters* **1990,** *12* (1), 41-46.
8. Hariharan, A.; Kumar, S. K.; Russell, T. P., *J. Chem. Phys.* **1993,** *98* (5), 4163-4173.
9. Narrainen, A. P.; Clarke, N.; Eggleston, S. M.; Hutchings, L. R.; Thompson, R. L., *Soft Matter* **2006,** *2* (11), 981-985.
10. Hutchings, L. R.; Narrainen, A. P.; Eggleston, S. M.; Clarke, N.; Thompson, R. L., *Polymer* **2006,** *47* (24), 8116-8122.
11. Penfold, J.; Richardson, R. M.; Zarbakhsh, A.; Webster, J. R. P.; Bucknall, D. G.; Rennie, A. R.; Jones, R. A. L.; Cosgrove, T.; Thomas, R. K.; Higgins, J. S.; Fletcher, P. D. I.; Dickinson, E.; Roser, S. J.; McLure, I. A.; Hillman, A. R.; Richards, R. W.; Staples, E. J.; Burgess, A. N.; Simister, E. A.; White, J. W., *Journal of the Chemical Society-Faraday Transactions* **1997,** *93* (22), 3899-3917.
12. Zhou, X. L.; Chen, S. H., *Physics Reports-Review Section of Physics Letters* **1995,** *257* (4-5), 223-348.
13. Stamm, M.; Schubert, D. W., *Annual Review of Materials Science* **1995,** *25*, 325-356.
14. Hopkinson, I.; Kiff, F. T.; Richards, R. W.; Bucknall, D. G.; Clough, A. S., *Polymer* **1997,** *38* (1), 87-98.
15. Shull, K. R.; Kramer, E. J.; Hadziioannou, G.; Tang, W., *Macromolecules* **1990,** *23* (22), 4780-4787.
16. Penfold, J.; Webster, J. R. P.; Bucknall, D. G.; Sivia, D. S., *Colloids and Surfaces a-Physicochemical and Engineering Aspects* **1994,** *86*, 165-170.

6 Bulk Dynamics

In this chapter the bulk properties of the polymer blend used throughout this study shall be examined. Firstly the bulk dynamics, using quasielastic neutron scattering, will be discussed. Following from this the structural organisation will then be discussed using the results obtained from small angle neutron scattering. The samples used for SANS were blends of various weight percentage deuterated additive (PEa5, PEb5 and PEc5) in a deuterated matrix, again supplied by Polymer Source (Canada). Finally, the effect that the amount of crystallinity within the sample has on surface segregation and surface hydrophobicity is discussed. The combination of differential scanning calorimetry, AFM and NRA are used to quantify the effects of crystallinity.

6.1 Quasielastic Neutron Scattering (QENS)

Quasieleastic neutron scattering (QENS) can be used to study the dynamic properties of molecules which contain hydrogen atoms[1-4]. In a typical neutron scattering experiment an elastic scattering event appears as a peak in intensity at E=0 (i.e. the scattered neutron has the same energy as the incident neutron), with the scattering curve having a finite width, which corresponds to the instrument resolution. The width defines the time scale over which the diffusive motions are observable. If the diffusive motions are much slower than the instrument resolution then they cannot be distinguished from the elastic peak, whereas, if they are much faster the quasielastic component will be a very broad flat term. Therefore, the characteristic times of the samples diffusive motions have to be of the same order as the instruments resolution. QENS spectrometers cover timescales in the range approximately 10^{-13} – 10^{-9} s and length scales in the range of 1-30 Å (local scales around inter and intramolecular distances[5]). This allows the study of different dynamical processes, from fast modes (vibrations, rotations and localized motions) to slower modes (relaxation and diffusion).

Hydrogen atoms are ideally suited for study by QENS because of their large incoherent scattering cross-section. In general QENS is used to probe self dynamics and the intermediate incoherent scattering function, , gives the probability[6] of finding an atom at a time, t, at some distance, r, where $r=2\pi/Q$, from its original position at t=0.

When $I(Q, t=0) =1$ the particle has not moved from its initial position and thus the probability of finding it within a distance r from its starting position is 1. This can be clearly demonstrated at -230^{0}C, figure 6.1.

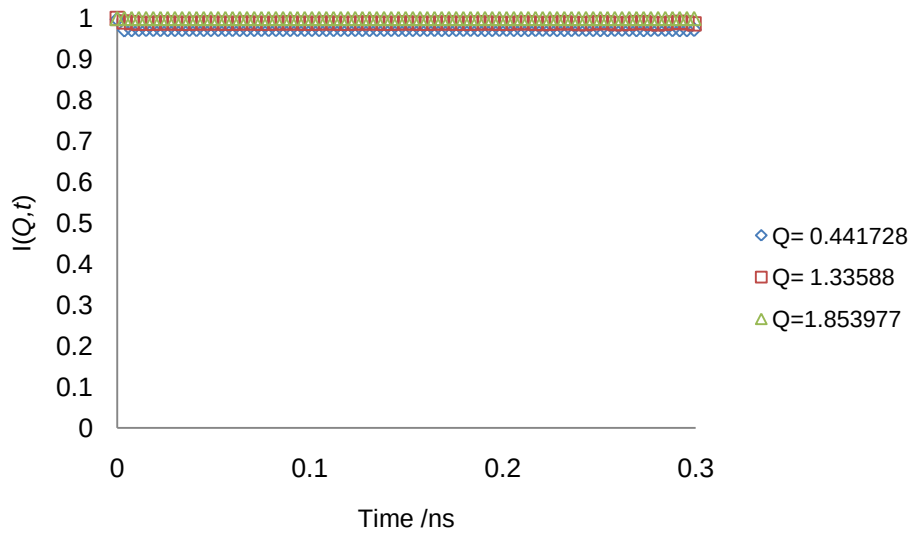

Figure 6:1 Representation of the degree of movement at very low temperature, -230°C, for 50% control additive (hPE20) in a deuterated matrix

The term includes the position vector, , of the scattered neutron which can be separated into two different components, depending on the type of motion. The position vector of scattered neutrons at a given time is represented by:

Equation 6:1

The first term on the RHS of equation 6:1 provides us with the location of the equilibrium position at a given time, with respect to an externally fixed point. The second term on the RHS is the displacement vector of the nucleus from equilibrium in a given time because of vibrations. This therefore describes the diffusive motions of the entire molecules and can be separated into two parts:

Equation 6:2

where the first term, , represents the translational motion. For a solid the centre of mass is restricted to well defined positions thus translational diffusion does not occur on a timescale relevant for experimental observations. However, small fluctuations around its centre of mass do occur owing to heating. In liquids translational diffusion can occur and is time dependant, but this is not considered here. For solids . Translational diffusion, , is not time dependent, whereas the thermal fluctuations, , occur in a given time.

The second term, , represents the rotational motion around its centre of mass. When a molecule rotates around its centre of mass it is very convenient to describe the rotation as instantaneous jumps between several equilibrium orientations. Between the jumps the molecule assumes an orientation where small amplitude rotational oscillations occur which depend on intermolecular interactions. So the rotational motion around its centre of mass can be represented by, , if several equilibrium orientations exist then the term is included, but if only one exists then is not time dependant. The deviation from the equilibrium position is represented by . It follows that the intermediate incoherent scattering function position vector, , of the scattered neutron equals:

Equation 6:3

If several equilibrium orientations exist then:

Equation 6:4

whereas, if one precise equilibrium orientations exist then:

Equation 6:5

Following from this the intermediate incoherent scattering function, , can be rewritten replacing $R_j(0)$ and $R_j(t)$ with the appropriate position vector. For example for a solid when several equilibrium orientations exist would equal the summation is over all scattering bodies, *N*:

Equation 6:6

Equation 6:7

When t=0 the time independent terms, in red, are ignored. The position vector, , ultimately describes three different types of motions, which occur on different time scales.

is proportional to where the Fourier Transform yields the incoherent dynamic structure factor, .

Equation 6:8

The quasielastic contribution originates from both the rotational diffusive motions and the translational diffusion. The rotational diffusive motions are described by . The lattice contribution, , produces broadening lines at relatively high energy which are connected to the vibrational levels within the molecule. The intramolecular vibrations, , lead to a broad band of scattered intensity in the surrounding area of the quasi elastic region and a small flat background in the quasielastic region. This is because they are much faster than the diffusive motions. The lattice contributions and the intramolecular vibrations produce the inelastic spectra outside the quasielastic region, figure 6:2.

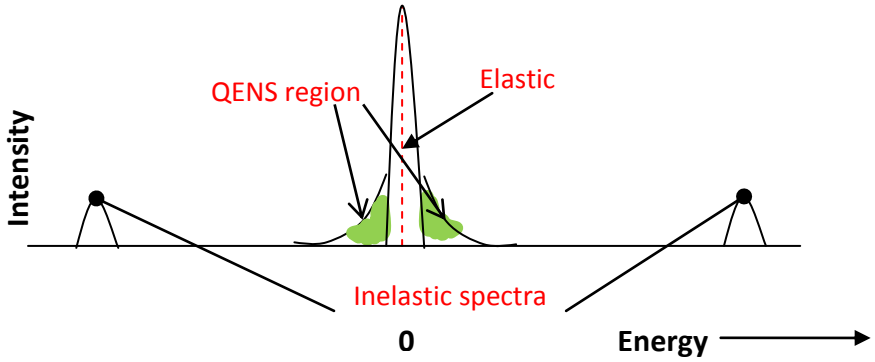

Figure 6:2 Intensity *vs* energy for elastic, inelastic and quasi-elastic scattering events

6.1.1 Analysis and Results

A control sample, containing 50% hPE20 (hydrogenated 20 kgmol^{-1} polyethylene) in a deuterated matrix, supplied by Polymer Source 78 kgmol^{-1}, and a 50% hPEa20 (hydrogenated 20 kgmol^{-1} polyethylene with end-group “a”) also in a deuterated matrix was used. If beam time were limitless, it would be preferable to study systems at a comparable concentration to earlier chapters. However, as beam time is not limitless high additive concentrations were used to get a signal in a reasonable time. Polyethylene is different from other polymers as it has an absence of side groups, therefore conformational transitions are not a fundamental motion[7]. So by comparing the dynamics of a control polymer (hPE20) and a polymer with a chain end (hPEa20), the influence of chain end-capping distribution on bulk dynamics can be explored.

6.1.1.1 Bragg Peaks

Bragg peaks, indicated by the red line in figure 6:3 and 6:4, occur from purely elastic scattering and appear only in crystalline samples. The existence of Bragg peaks are measured during a fixed

window scan, where the neutron scattered intensity is recorded within a narrow energy interval centred at E=O and only neutrons that are scattered elastically are counted. Elastic intensity of the Bragg Peaks is monitored as a function of temperature and Q. It measures the coherent scattering from the sample, from C and D. In crystallography, the intensities of the Bragg reflections allow determination of the lattice structure and the d-spacing, .

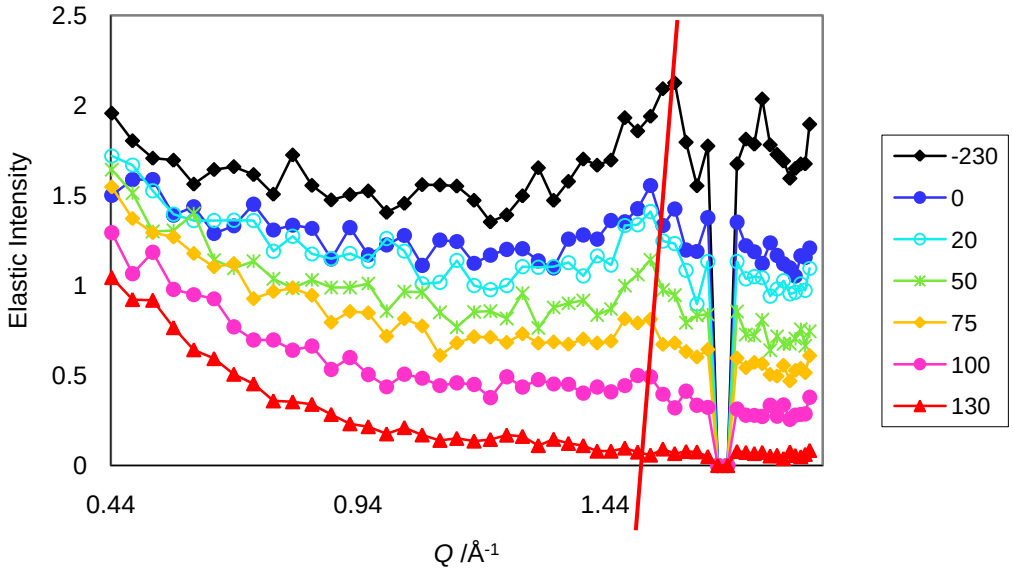

Figure 6:3 Elastic scan of 50% hPEa20 at constant temperature in 50% deuterated matrix with a red line indicating the Bragg peak

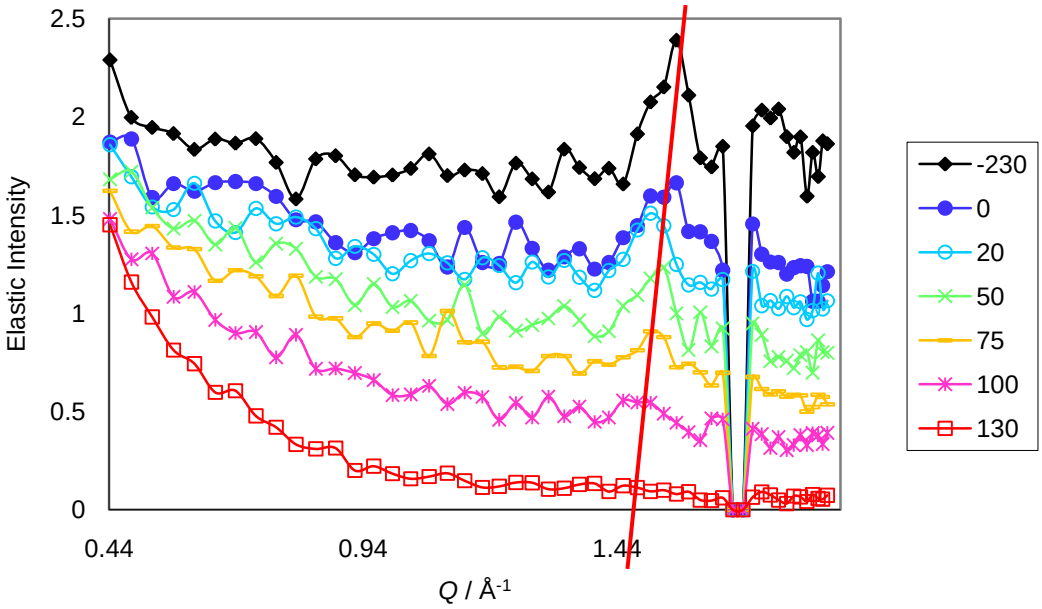

Figure 6:4 Elastic Scan of 50% hPE20 at constant temperature in 50% deuterated matrix with a red line indicating the Bragg peak

The Bragg peaks, clearly move towards lower *Q* values as the temperature is increases and eventually disappear at the highest temperature for both the control and the additive. As *Q* decreases it indicates that the lattice spacing, d, is increasing.

When Bragg peaks exist at certain temperatures or in certain *Q*-regimes, the QENS analysis in those regions has to be taken with care since they will be contaminated with extra elastic scattering. Normally the Bragg region in the QENS spectra is disregarded.

Secondly, the elastic intensity decreases as the temperature increases, as the Bragg condition is not satisfied for the *Q* values in figure 6:5. The elastic incoherent scattering intensity is dominated by H (i.e. the additive). In the absence of rotational or translational motion, molecular vibrations give rise to a decrease in the elastic intensity with increasing temperature. This is because as the temperature rises the width of the quasi-elastic component becomes larger compared to the width of the resolution function indicating there are more motions with timescales faster than or equal to those accessible in the QENS energy window.

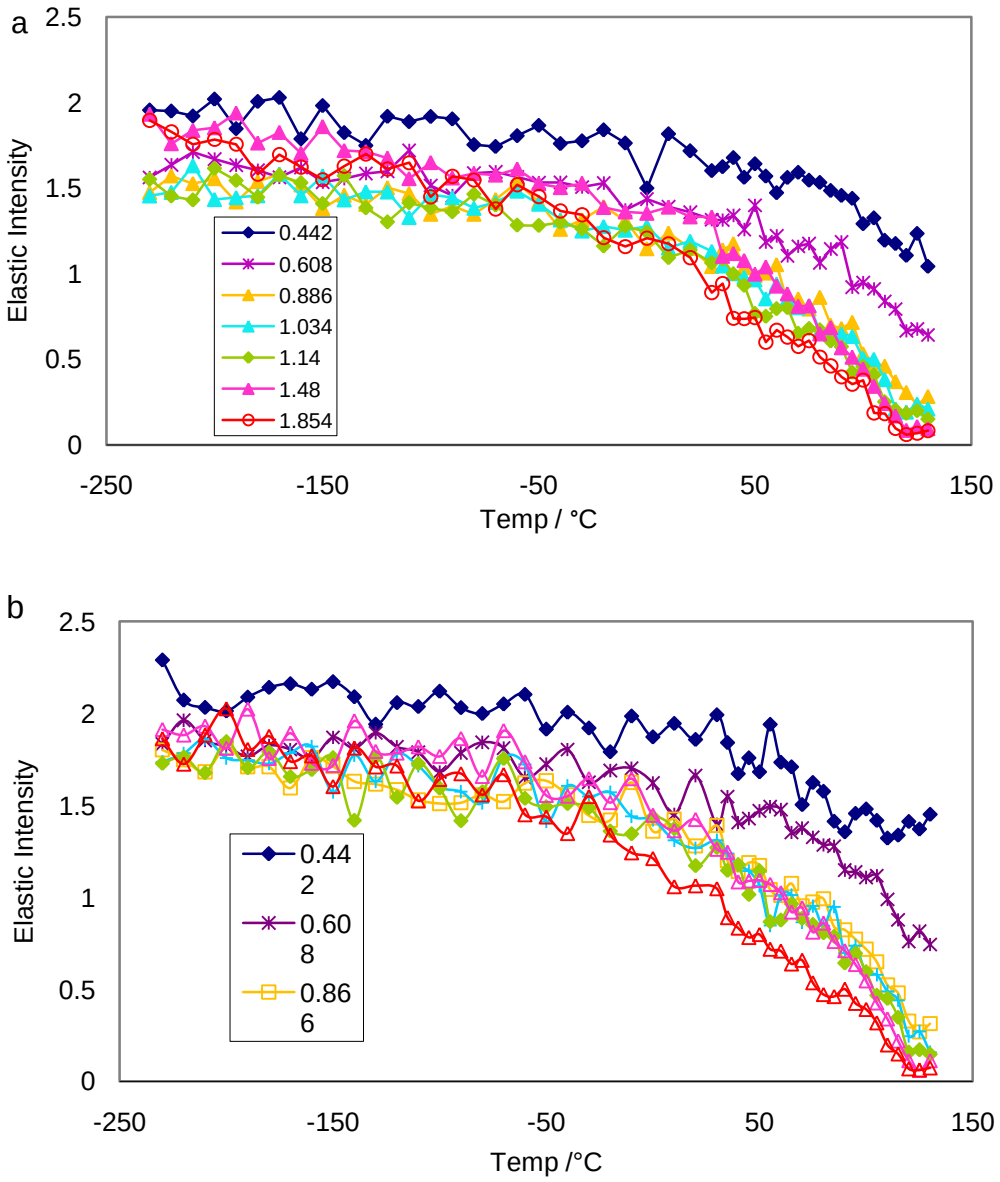

Figure 6:5 Elastic Scan at constant *Q* ($Å^{-1}$) for a) 50% hPEa20 and b) 50% hPE20 in a deuterated matrix at different temperatures

Normally fewer elastic events indicate more motion. By normalising the plots to a minimum intensity of 1 a comparison can be made between the additive and the control, figure 6:6. From figure 6:6d, where several *Q* values have been combined to reduce the scatter, it can be observed that on the whole the additive and the control have similar numbers of elastic events, thus it can be concluded that the two additives behave similarly in this matrix.

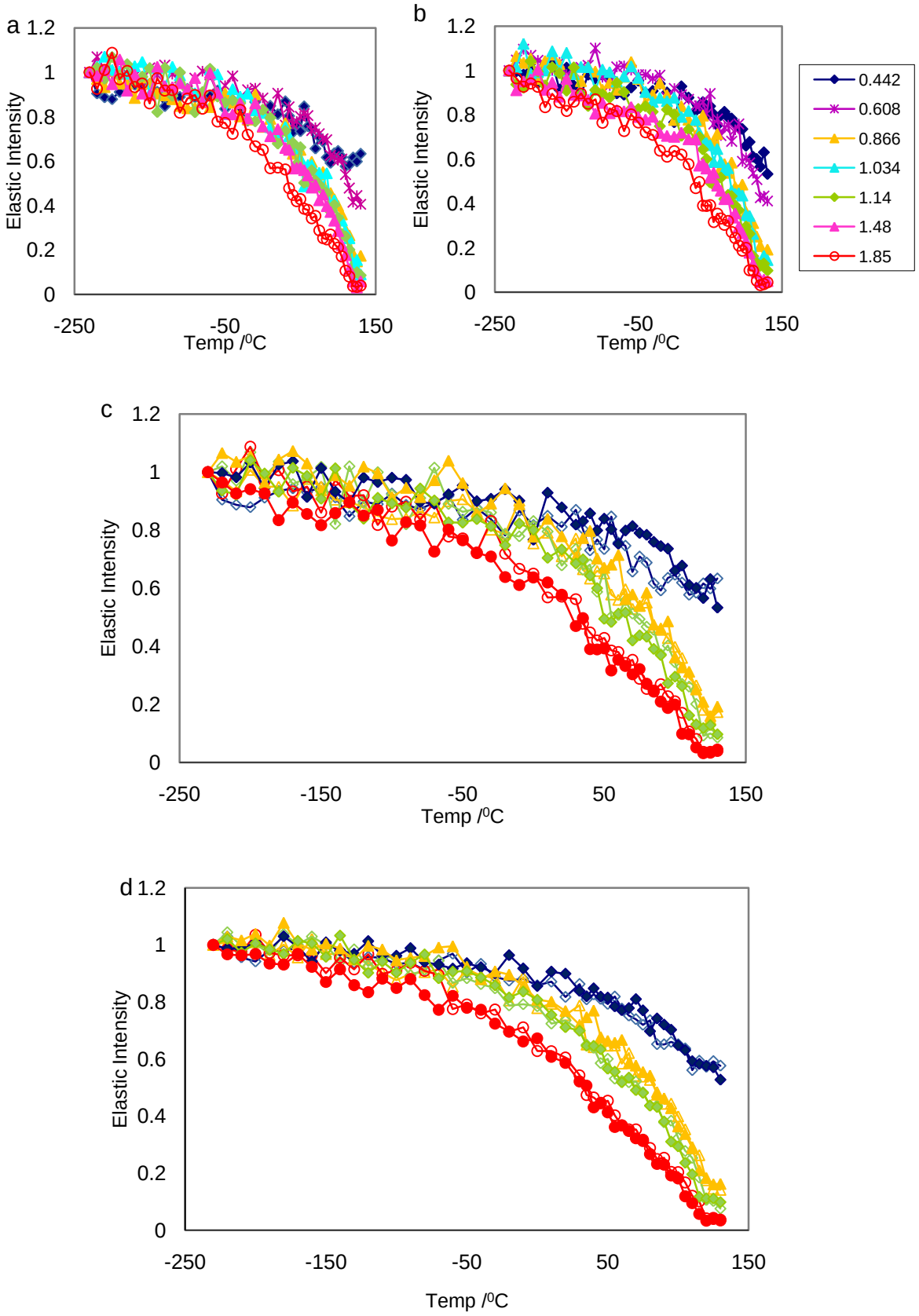

Figure 6:6 Normalised elastic intensity at constant Q (Å^{-1}) for a) 50% hPE20, b) 50% PEa20 in a deuterated matrix, c) combined results where open point are for hPE20 and closed for PEa10 and d) grouped detector combined results where open point are for hPE20 and closed for PEa10

6.1.1.2 I(Q,t) vs Time at constant Temperature

I(Q,t) describes how far something has moved from its origin in a given time. By fixing *Q* then *I(Q,t)* is a measure of the time taken to moved a distance corresponding to ~1/*Q*, where at the origin t=0 (I(*Q,t*)=1) and after movement so I(*Q,t*)<1. If an atom has moved a very long way from its origin it can no longer correlate to its original position therefore I(*Q,t*)=0. If *Q* is large, this represents a small lattice space, thus, "moving out of the box". When *Q* is large movement out of the "box" occurs on a quicker timescale then when *Q* is smaller. This is demonstrated by the gradient of the graphs below, figure 6:7, which gets steeper as *Q* increases, indicating that movement out of the "viewing window" increases as the "viewing window" reduces, increasing *Q*. Also these figures illustrate that mobility increases as temperature increases, which is the expected behaviour.

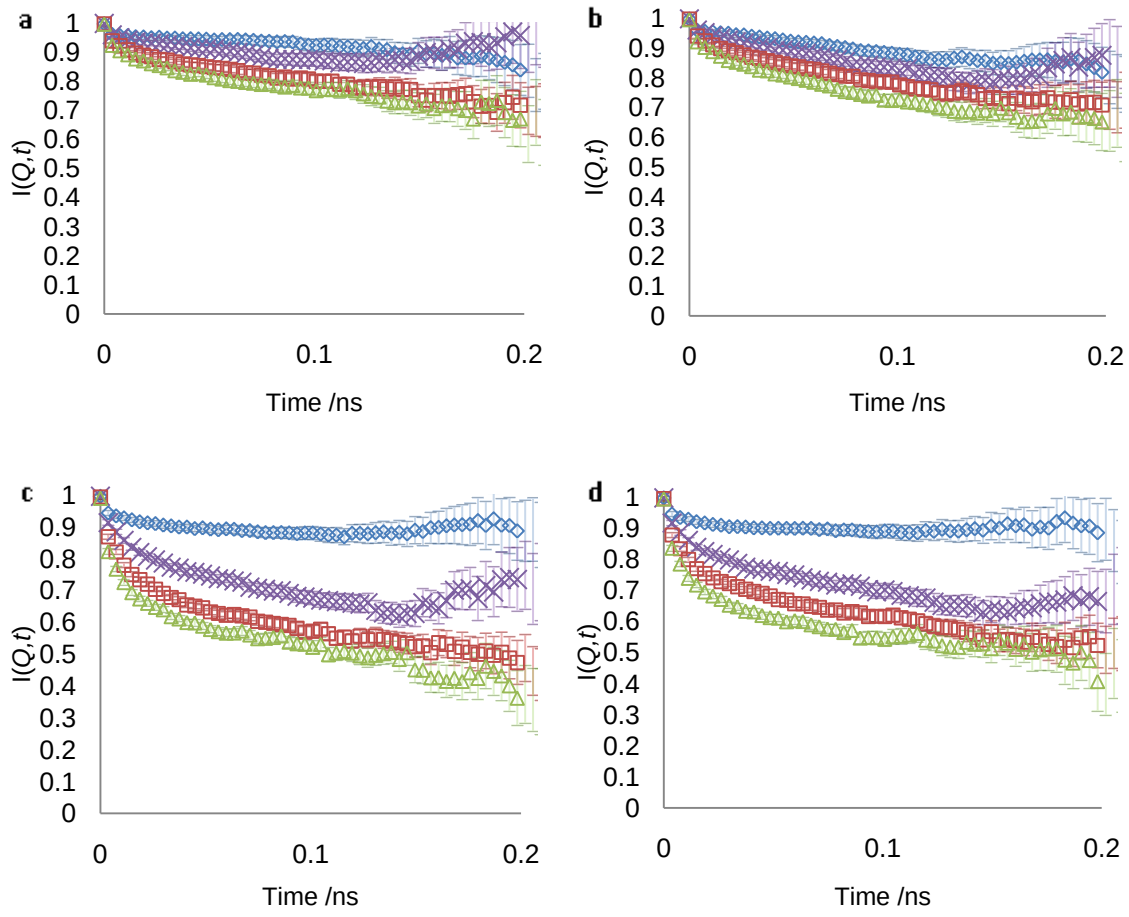

Figure 6:7 *I(Q,t)* versus time at constant *Q* (Å^{-1}) for three different temperatures where a) 0°C 50% hPEa20, b) 0°C 50% hPE20, c) 50°C 50% hPEa20, d) 50°C 50% hPE20, and the symbols represent ◊ *Q*=0.44, × *Q*=0.92, □ *Q*=1.34 and Δ *Q*=1.85

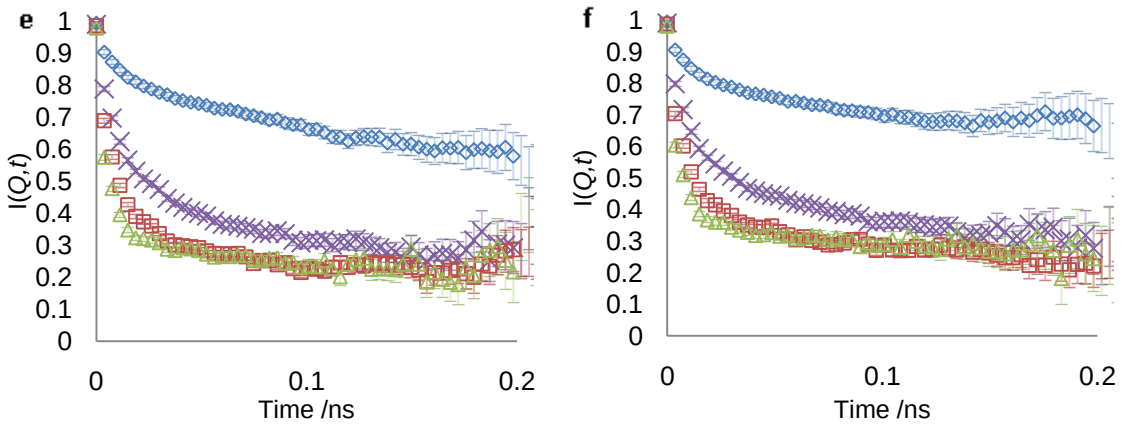

Figure 6:7 *I(Q,t)* versus time at constant *Q* (Å^{-1}) for three different temperatures where e) 100°C 50% hPEa20, f) 100°C 50% hPE20, and the symbols represent ◊ *Q*=0.44, × *Q*=0.92, □ *Q*=1.34 and Δ *Q*=1.85

A steep gradient in a *I(Q,t)* versus time graph often indicates a rapid motion. Therefore, by comparing *I(Q,t)* versus time graphs for the additive and the control at constant *Q* values a shift is revealed from a fast process at high *Q* and time less than approximately 22 ps to a slower one at low *Q* and at times longer than 22 ps. The fast process could be due to a vibrational relaxation and the slower process to conformational relaxation, diffusion-like behaviour[1, 8].

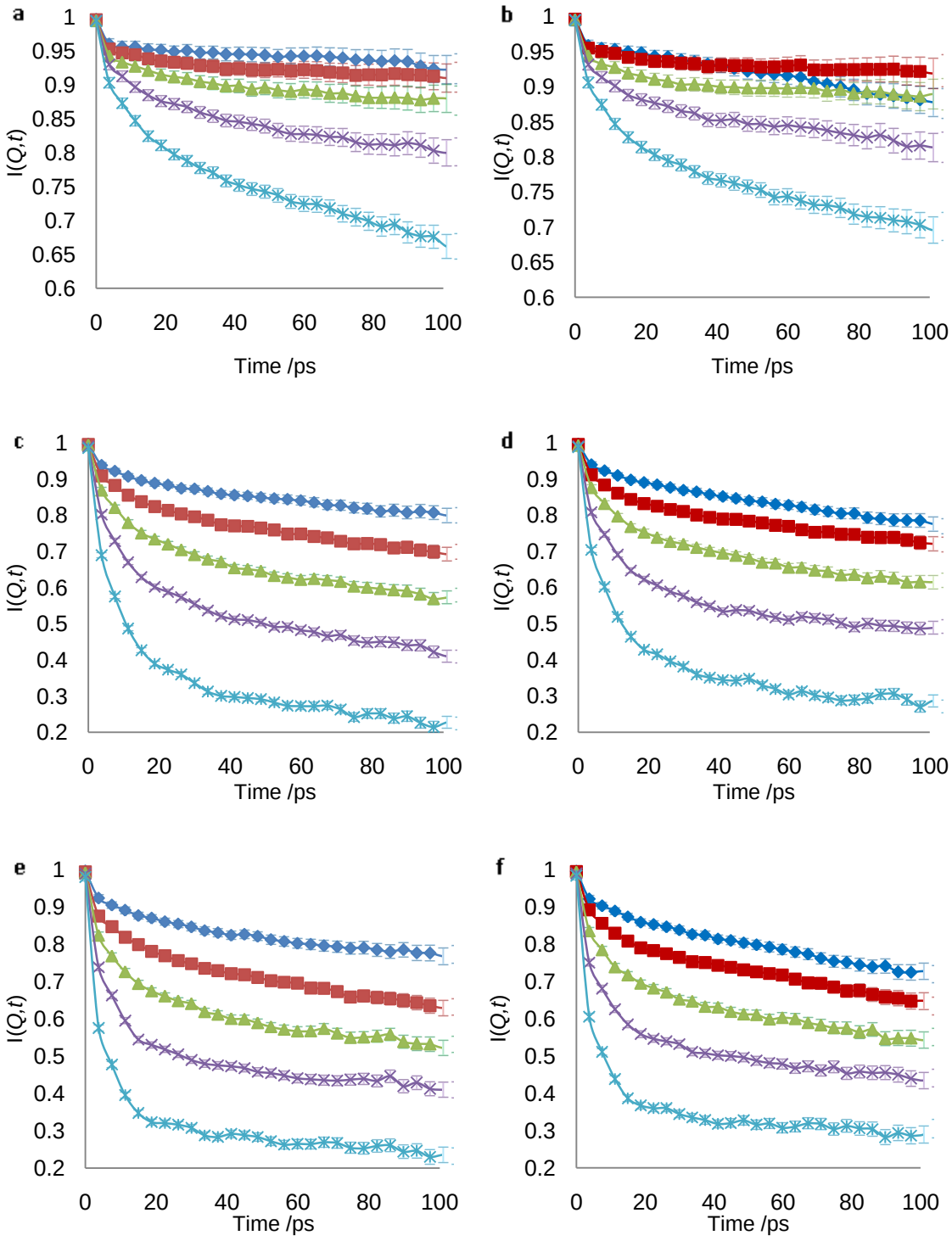

Figure 6:8 *I(Q,t)* versus time at constant *Q* (Å^{-1}) for all temperatures a) *Q*=0.44 50% hPEa20, b) *Q*=0.44 50% hPE20, c) *Q*=1.34 50% hPEa20, d) *Q*=1.34 50% hPE20, e) *Q*=1.85 50% hPEa20 and f) *Q*=1.85 50% hPE20, where the symbols represent ♦ 0°C, ■ 25°C, ▲ 50°C, × 75°C and ∗ 100°C

From figure 6:8 it is obvious that at higher temperatures the movement is faster, whereas, at lower temperature movement is slower but more constant.

The elastic intensity alone concluded that the number of elastic events was similar for the additive and the control, thus the two additives behave similarly in this matrix and therefore CF groups have no discernible influence in the dynamics. However, *I(Q,t)* gives a more sensitive measure between the differences in dynamics than the elastic intensity, where everything that is stationery is measured, whereas *I(Q,t)* is sensitive to movement (inelastic), figure 6:9. Thus the *I(Q,t)* plots for the highest and intermediate *Q* show some difference in motion between the additive and the control where the additive appears to be moving slightly faster. This could be a result of a more mobile chain end.

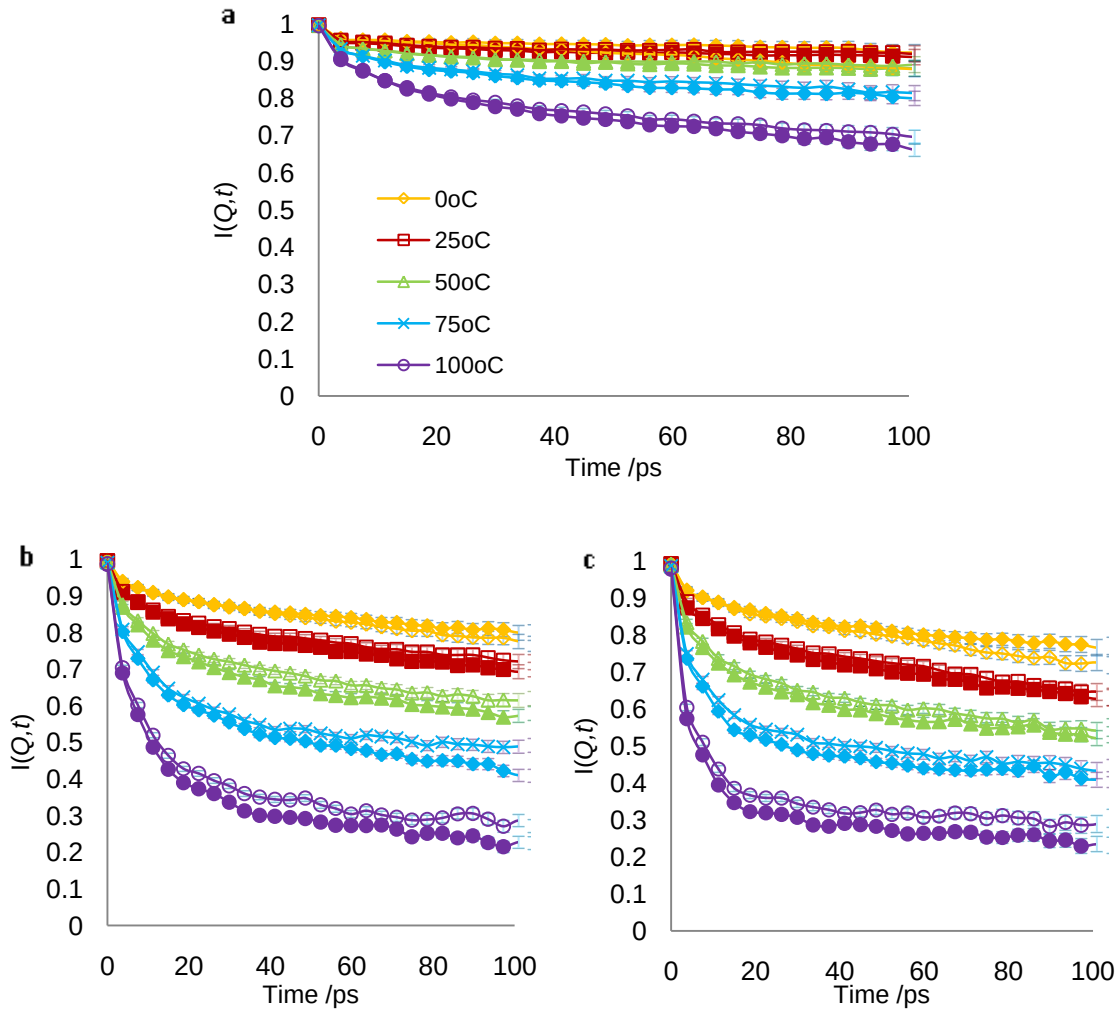

Figure 6:9 Comparison of *I(Q,t)* versus time at constant *Q* ($Å^{-1}$) at different temperatures between the additive and the control a) *Q*=0.44, b) *Q*=1.34 and c) *Q*=1.85, where the symbols represent ◊ 0°C, □ 25°C, Δ 50°C, × 75°C and O 100°C (solid for additive and open for control)

It should be noted that the process does not decay to zero for the blends, leaving open the possibility of another relaxation at longer times e.g. reptation.

6.1.1.3 Kohlrausch-Williams Watts (KWW) Equation

The time dependence of the different correlation functions can be approximated by the stretched exponential or Kohlrausch-Williams Watts (KWW) function[9, 10]:

Equation 6:9

Where ψ is a phenomenological shape parameter, $0< \psi \leq 1$ and for polymers ψ is typically close to 0.5[9]. τ_{KWW} is the KWW relaxation time and represents the extent to which different atoms in the viewing window have different motilities, i.e. different τ_{KWW} [6, 2].

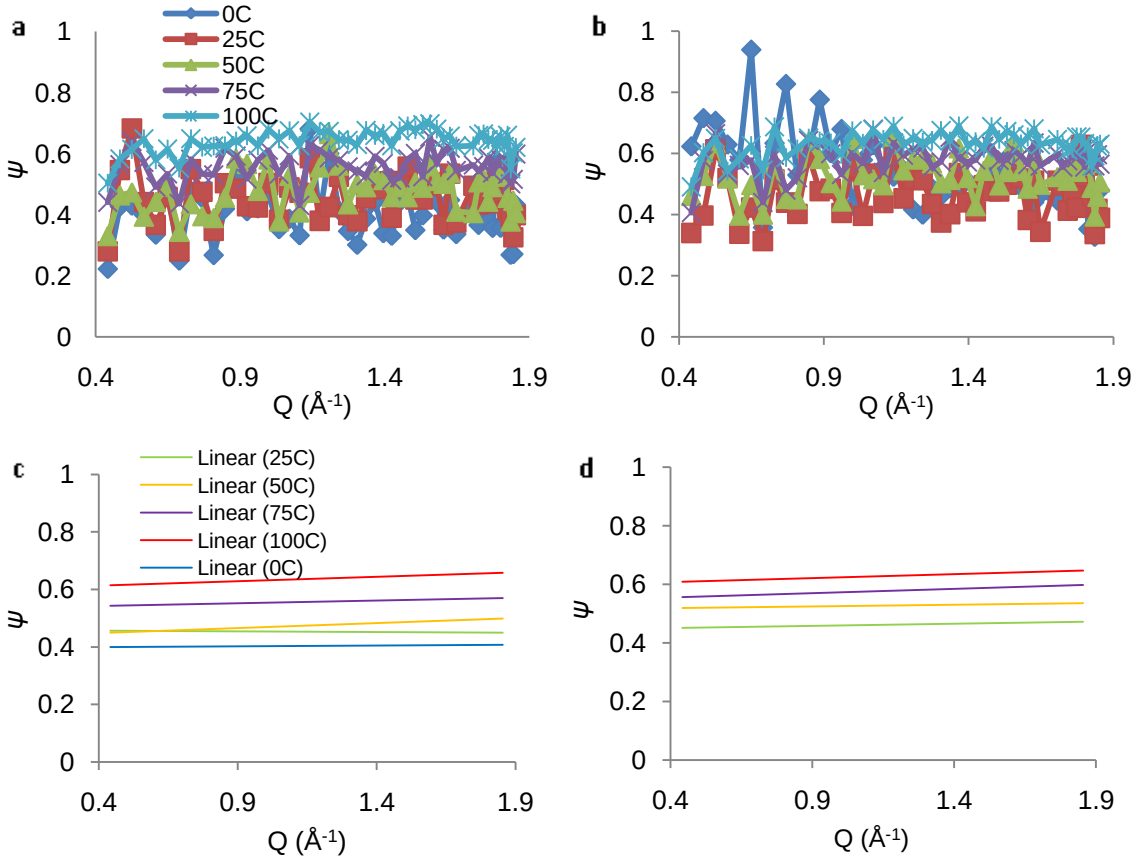

Figure 6:10 Stretching exponent (ψ) versus Q at various temperatures for a) 50% hPEa20, b) 50% hPE20, and the bottom two graphs are the linear "best fit" corresponding to c) 50% hPEa20 and d) 50% hPE20

For both polymers the stretching exponent is fairly constant through the entire Q range, as shown in figure 6:10. By examining specific Q ranges there appears to be no difference between the functionality of ψ with temperature for the control and the additive, as can be seen in figure 6:11.

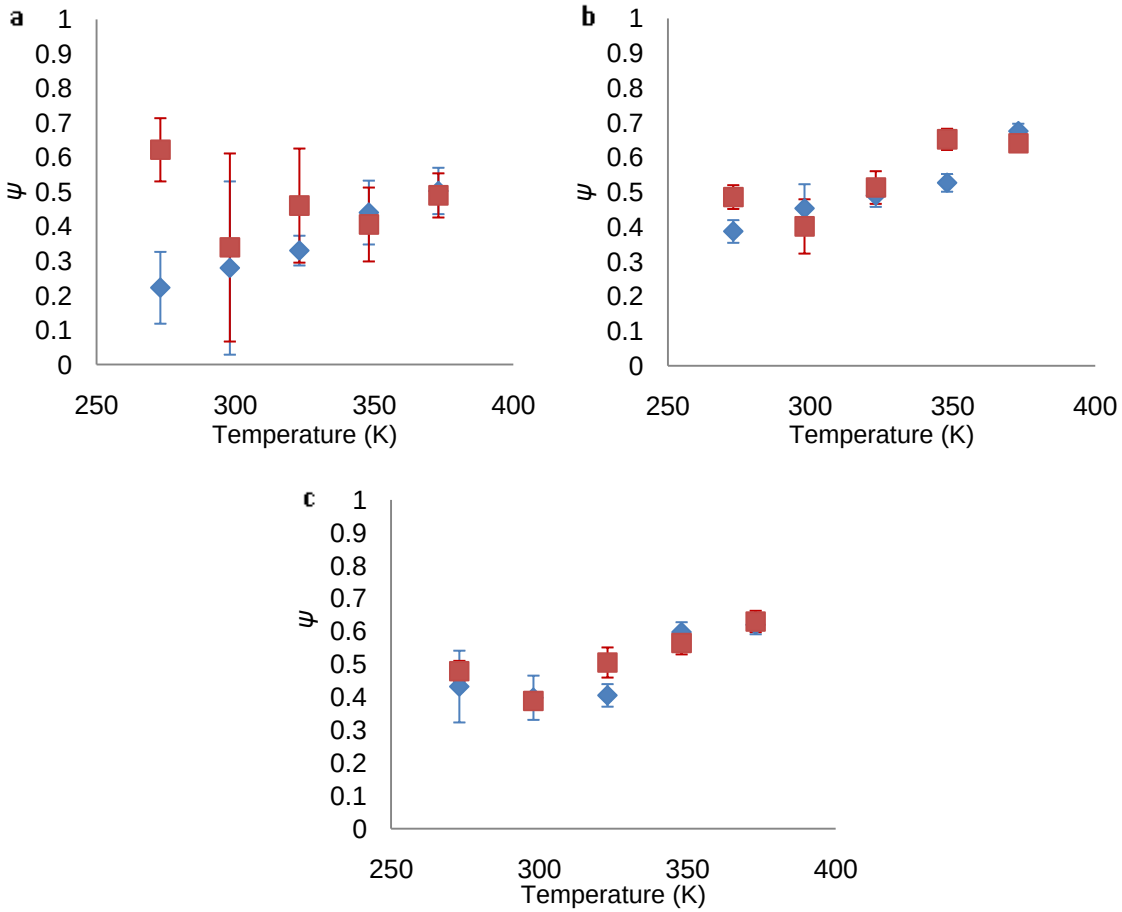

Figure 6:11 Stretching exponent versus Temperature where ■ is for hPE20 and♦ for hPEa20 at three different Q (Å^{-1}) values of a) Q=0.44, b) Q=1.34 and c) Q=1.85

As ψ is almost constant over the probed Q range an average ψ can be taken and plotted against temperature, figure 6:12. The temperature dependence of ψ implies that the distribution of relaxation times broadens as temperature decreases.

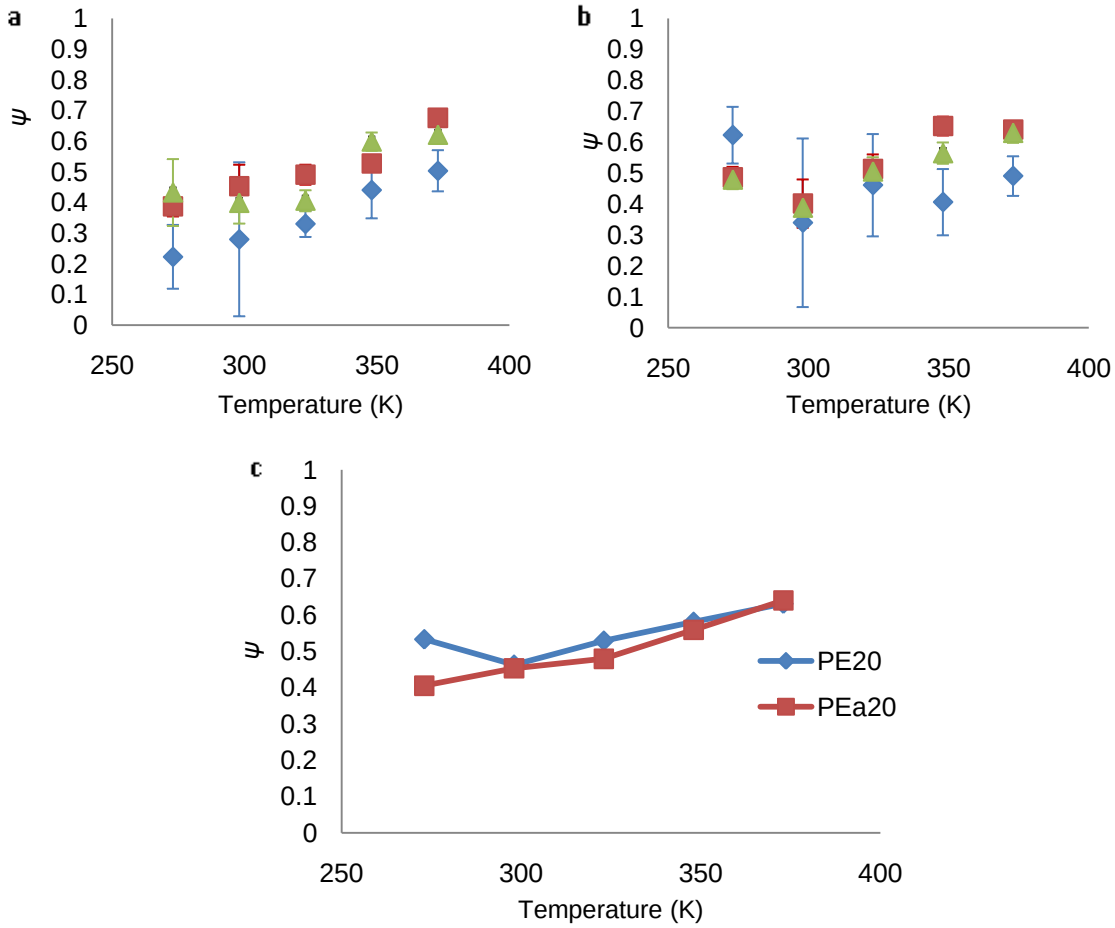

Figure 6:12 Stretching Exponent versus temperature for a) 50% hPEa20 and b) 50% hPE20 where ♦ Q=0.44Å^{-1}, ■ Q=1.34Å^{-1} and ▲ Q=1.85Å^{-1} and c) average ψ versus temperature

Following from equation 6:9 *I(Q,t)* van be solved by fitting tau_{KWW}, psi and background using a Fortran programme where:

Equation 6:10

Table 6:1 shows parameters obtained for a mid Q range, where Q=1.34 Å^{-1}, at 3 different temperatures chosen to be when the sample is crystalline, 0°C, midway, 50 °C, and around the melting temperature, 100 °C.

	Temp / °C	τ_{KWW}	ψ	Background
	0	1.578	0.4924	0.01
	50	0.6683	0.3603	0.01
Control	100	0.012	0.3489	0.01
	0	1.152	0.4261	0.3249
	50	0.08448	0.3696	0.27
Additive	100	0.01034	0.5969	0.22

Table 6:1 The parameters obtained from fitting *I(Q,t)* versus time for hPE20 and hPEa20 where Q=1.34 Å^{-1}

The relaxation time, τ_{KWW}, agrees with previous observations that hPEa20 moves slightly faster than the control, where τ_{KWW}(hPE20) > τ_{KWW}(hPEa20), figure 6:13, and ψ is within the range already calculated. The background term represents the material that does not relax within the experimental window, where the higher the background term the greater the proportion of material that does not relax within the experimental window. Interestingly, this suggests that the additive and the control have different numbers of mobile components which have slightly different dynamics. The additive is characterised by a smaller number of mobile units which have faster dynamics. Hypothetically, as the only difference between hPE20 and hPEa20 are 2x C_8F_{17} units, at the end of hPEa20, the higher background and faster dynamics obtained by QENS for hPEa20 could suggest that the groups are very slow moving, therefore not observed in the experimental window. The C_8F_{17} groups could cause aggregation, shown in experiments on similar materials[11]. The higher background and faster relaxations of the end-capped material is consistent with faster local dynamics (indicating the possibility of exclusion from the crystalline regions), and show long range dynamics possibly due to aggregation.

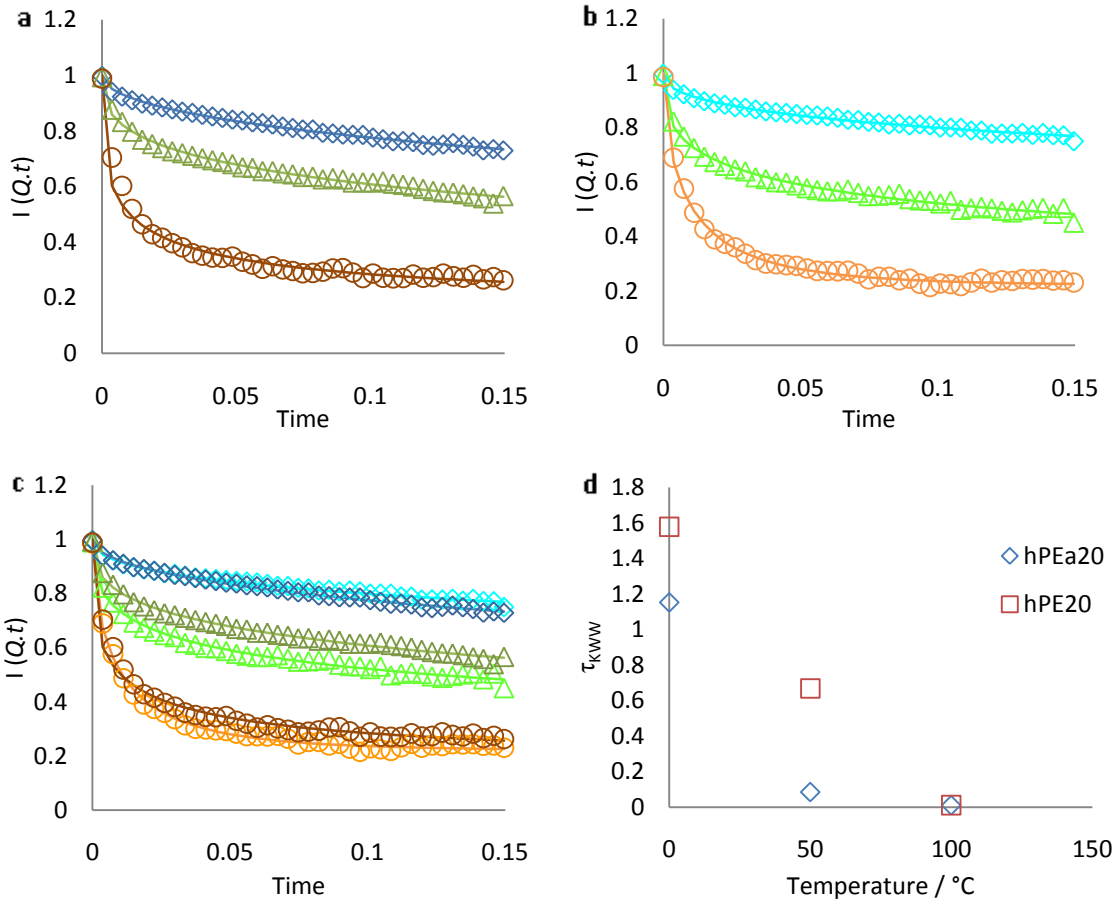

Figure 6:13 *I(Q,t)* versus time for a) hPE20, b) hPEa20 and c) combined sets where darker ◊ represents 0 °C, Δ represents 50 °C and O represents 100°C hPE20 and lighter hPEa20, d) τ_{KWW} versus time

If a sample has a thermally activated process it will follow Arrhenius behaviour. Normally Arrhenius temperature dependence is assumed for the relaxation time, where the activation energy, E_a, is the height of the potential barrier hindering the motion (energy barrier, for the conformational transition) and τ_0 is the relaxation time when temperature is infinite.

— Equation 6:11

Many polymers exhibit a well defined relationship between relaxation time and temperature, known as *time-temperature superposition* which is a consequence of thermally activated relaxation (Debye-type) processes.

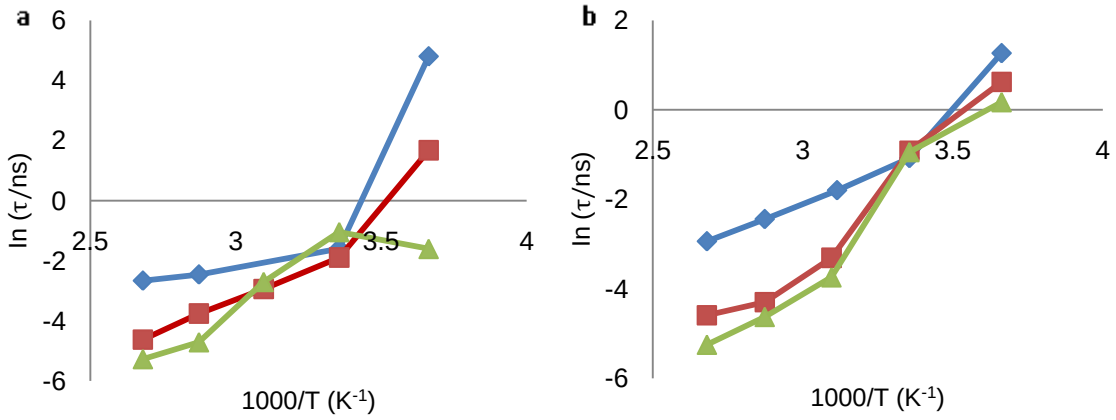

Figure 6:14 Arrhenius behaviour of the additive and the control Polymer a) 50% hPEa20 and b) 50% hPE20 where ♦ Q=0.44 Å^{-1}, ■ Q=1.34 Å^{-1} and ▲ Q=1.85 Å^{-1} where tau is represented in equation 6:10

The Arrhenius behaviour is followed at high temperature, figure 6:14, but as the temperature decreases the behaviour tends towards non-Arrhenius, i.e. the log plot does not have a simple linear dependence. This is not uncommon[12-14] and thus deviation from Arrhenius behaviour at low temperature indicates a marked increase in the activation energy[15, 16].

6.2 Small Angle Neutron Scattering (SANS)

SANS measures the time-averaged intensity of scattered neutrons versus Q, yields information about the static structure within the scattering medium. The advantages of SANS are that it can introduce or measure contrast e.g. density fluctuations and composition/concentration changes. However SANS measures in reciprocal space (Fourier) which is not real space therefore data has to be either inverted back or fitted to models describing structures in reciprocal space.

The measured SANS scattered intensity can be expressed as:

—— Equation 6:12

Equation 6:13

where the first three terms in equation 6:12 are instrument specific, incident flux $I_0(\lambda)$, detector solid angle, $\Delta\Omega$, and detector efficiency $\eta(\lambda)$ and λ is the wavelength of the neutron. The final three are sample specific. They include the sample transmission, T, sample volume, V, and the differential cross section (units of barn). When a sample is probed with neutrons some of the

incident radiation is transmitted through the sample, some is absorbed and some is scattered. All SANS data are rescaled to form a macroscopic cross section (units of cm^{-1}). This rescaling involves a measurement from the scattering sample $I_s(Q)$ and a measurement from the empty beam transmission $I_0(\lambda)$ which is the incident neutron beam intensity. The rescaled SANS scattered intensity can be expressed as:

— Equation 6:14

where $I_s(Q)$ is the intensity of neutrons detected in a unit detector cell. The scattering cross section can be measured as the ratio:

— ——— Equation 6:15

The absolute cross section (units cm^{-1}) is related to the microscopic cross section, dσ/ by the number density of scattering objects. Using a pulsed source $I(\lambda,Q)$ is measured and used to determine the detector efficiency, $\eta(\lambda)$[17]. Once the cross-section has been rescaled information about the different form factors can be obtained. SANS data are normally presented as the absolute differential scattering cross-section, dσ/dΩ, versus Q.

— Equation 6:16

where,

N_p*V_p = ϕ of scattering bodies
N_p = number concentration of scattering bodies
V_p = volume of one scattering body
$(\Delta\delta)^2 = (\delta_p-\delta_m)^2$ = contrast term if $(\Delta\delta)^2=0$ then there is no scattered flux

$P(Q)$ = form factor
$S(Q)$ = structure factor which includes the molecular weight and connectivity of each component
B_{inc} = incoherent background

The form factor, $P(Q)$, describes how $I(Q)$ is modulated by interference effects between radiation scattered by different parts of the same scattering body. Therefore it is very dependent on the shape of the scattering and van de Hulst's equation, which describes the form factor, has a shape parameter term, which in the case of polymers could be the radius of gyration.

The structure factor, *S(Q)*, describes how *I(Q)* is modulated by interference effects between radiation scattered by different scattering bodies. It depends on the degree of local order in the sample and has a peak corresponding to the average inter-particle distance (coordinate shell),

—

Equation 6:17

where, $d\sigma/d\Omega$ is *I(Q)*, b_H and b_D are the scattering lengths of the H and D atoms, -3.75×10^{-13}cm and 6.67×10^{-13}cm, respectively, v is the volume per one monomer . *P(Q)* provides intra-particle information (e.g. size and shape), whereas *S(Q)* provides inter-particle information (particle interactions).

For a mixture *S(Q)* can also be used to determine the Flory-Huggins interaction parameter, χ, which describes interactions between monomers of different species[18, 19]. According to the Random Phase Approximation[20] (RPA) the structure factor of a mixture of two components, A and B in the single-phase state is represented by:

— — — Equation 6:18

where ϕ and *N* are the volume fraction and degree of polymerisation respectively and χ is the Flory interaction parameter, *P(Q)* is the normalized form factor. For the *Q* range $Q<<1/R_g$ this is reduced to the Ornstein-Zernike equation:

— — Equation 6:19

— — — Equation 6:20

where ξ denotes the correlation length and is the weight average degree of polymerisation. For polydisperse polymers the degree of polymerisation is replaced by the weight average degree of polymerisation. The main limitation of the RPA is that it cannot be used to describe systems where strong interactions between polymer chains cause demixing, as in the case of microphase separation or phase separation in which the polymer chains are not randomly mixed. Blends of partially deuterated PE additive in perdeuterated matrix were examined using the SANS2d instrument at ISIS - typical data are shown in figure 6:15. The large scattering cross-section of the experimental data, figure 6:19, at low Q values, 0.005 $Å^{-1}$, shows that there is significant deviation

from the RPA suggesting relatively large structures in the blend, compared to the polymer dimensions indicated by the RPA simulation. A typical RPA is drawn in blue on figure 6:15a where the parameters are blends of different concentration PEb5 in dPE.

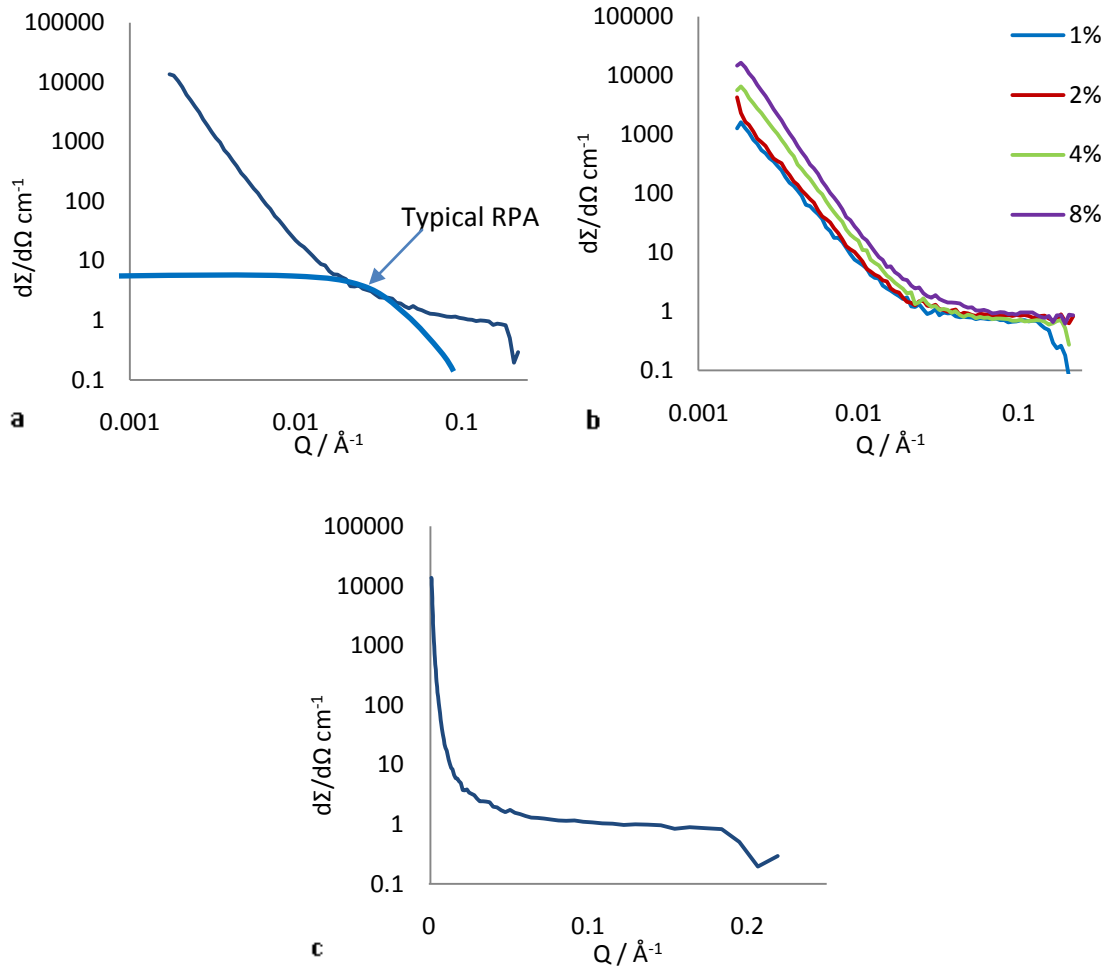

Figure 6:15 Absolute differential scattering cross section, dσ/dΩ, versus scattering vector, *Q*, for blends of a) 16% PEb5, b) 1-8% PEc5 and c) 16% PEb5 linear-log plot highlighting the regime at the higher regime

6.2.1 Analysis and Results

The very large $d\sigma/d\Omega$ values as Q tends to 0, figure 6:15c, together with the Q^{-4} dependence of $d\sigma/d\Omega$, figure 6:16, both indicate that the blend has sharp interfaces, almost certainly due to phase separation. (Unfortunately that matrix polymer used, supplied from Polymer Source, was contaminated, thus only the uncontaminated data will be presented below).

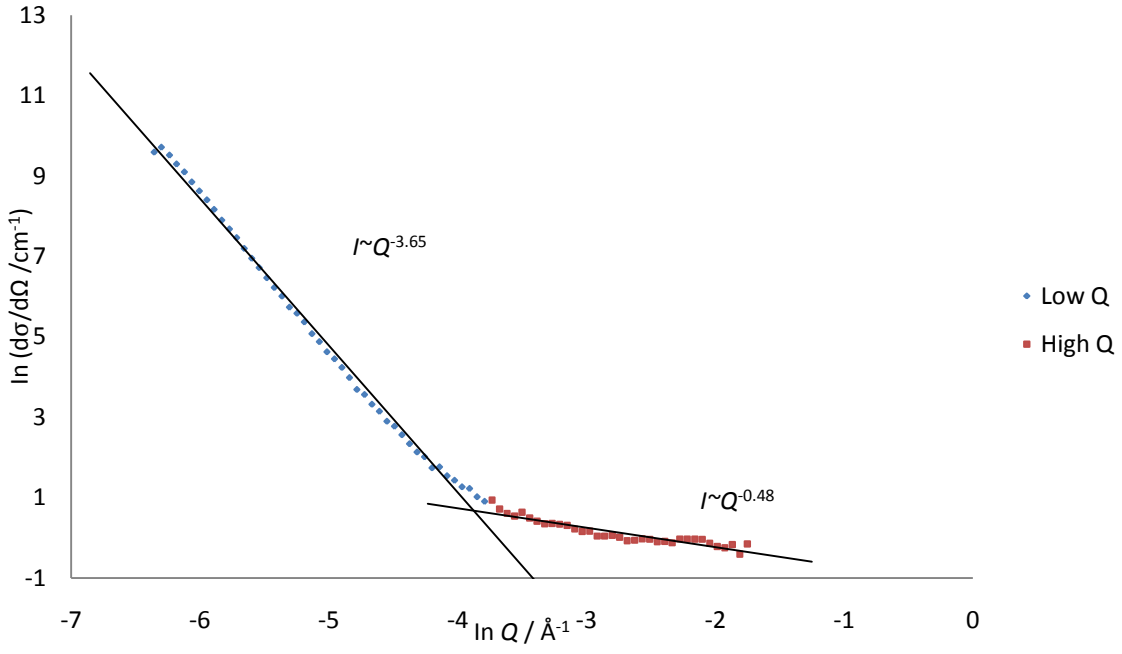

Figure 6:16 Example of Porod Law Plot for 8% PEc5 showing the two *Q* regions where "a" represents the Porod exponent, $I \sim Q^{-a}$

The power Law (I(Q) α Q^{-a}) exponent described the "dimensionality" of different shapes, figure 6:17 and 6:18. Because there are two power regions it suggests that there are two different "dimensions". This more sophisticated analysis cannot be performed as we cannot account for how much of each polymer (the additive or matrix) is in each region. However, it should be noted that longer annealing times might be appropriate to ensure that equilibrium has been reached, when mixing higher molecular weight polymers, thus allowing sufficient time for the preferred structure to develop.

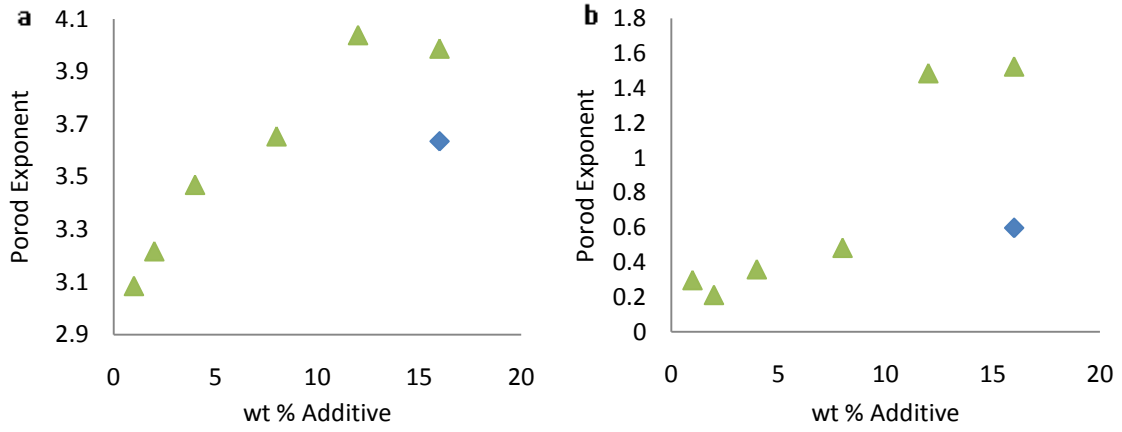

Figure 6:17 Power exponent for additive PEb5 and PEc5 at a) low *Q*(<0.23) and b) high *Q* (>0.23) where ♦PEb5 and ▲PEc5

The two exponents, -4 and -2, describe the following areas:

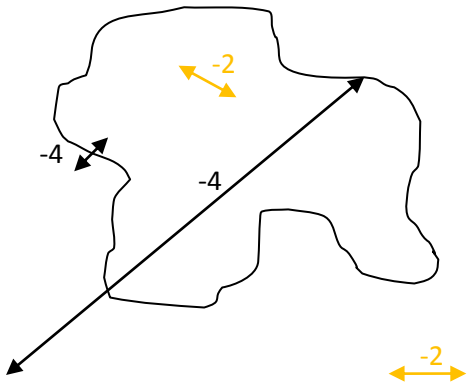

Figure 6:18 Porod exponent dimensionalities showing a region of amorphous polymer dispersed in another phase of amorphous polymer

At high *Q* the contrast can only be differentiated over small areas, implying that measurements are being taken of the polymer bulk ordering either inside or outside the large aggregates. At higher *Q* values when $I(Q) \alpha Q^{-2}$, as the Porod law indicates, the Ornstein-Zernike equation is valid and χ can be calculated. However, as already explained it is not possible to account for how much of each polymer (the additive or matrix) is in each region and this affects the intensity of the $I(Q) \alpha Q^{-2}$ area, figure 6:19.

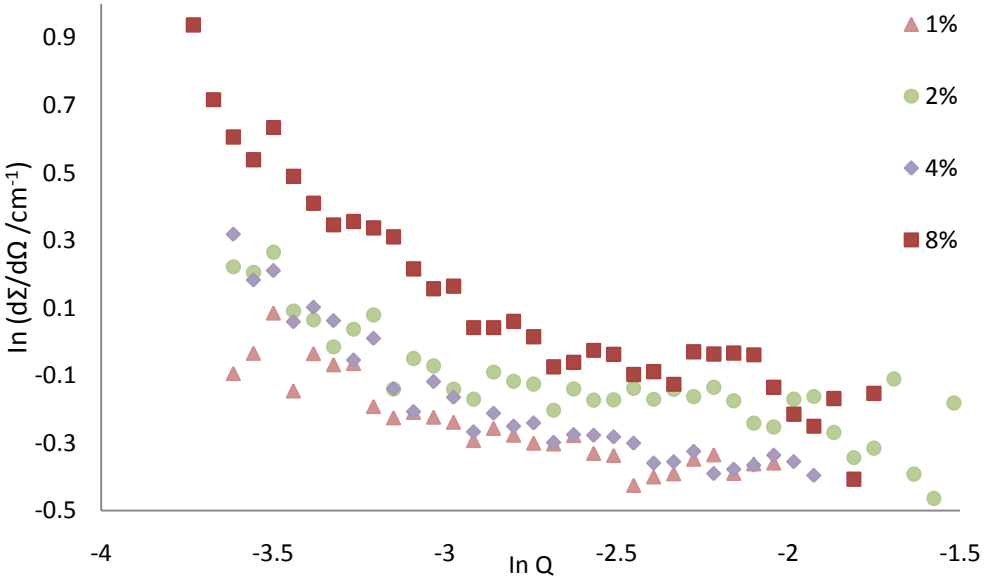

Figure 6:19 Graph showing the change in intensity for a Porod Plot of $I(Q) \alpha Q^{-2}$ region for PEc5

whereas, at lower *Q* SANS is sensitive to scattering from interfaces of larger objects where the surface area to volume ratio ($S_T = S/V$) can be calculated (b_v is the scattering cross-section) using the following equation[21] and figure 6:20 illustrates the results calculated.

—

Equation 6:21

—

($C_4H_6D_2$, $b_A = 1.74x10^{-6}$ Å^{-2} , C_4D_{28}, $b_B = 7.71x10^{-6}$ Å^{-2})

Equation 6:22

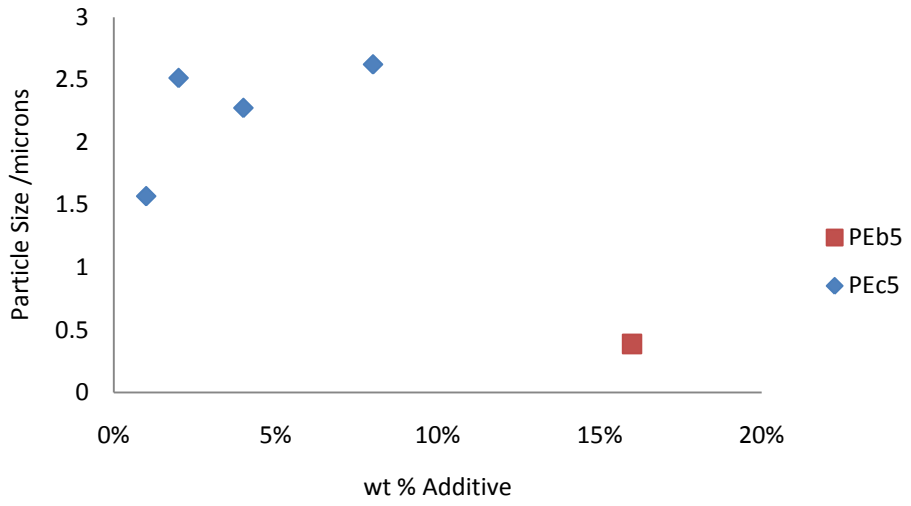

Figure 6:20 Particle sizes calculated for additives ■PEb5 and ♦PEc5 at different concentrations

The PEc5 additive particle size appears to increase as the percentage additive increases and is of the order of about 2 µm. The smaller PEb5 additive aggregates are approximately 4 times smaller, 0.5 µm. This is almost certainly due to the size of the head groups. Owing to these findings the structure was further investigated using transmission electron microscopy (TEM, carried out by Dr. Mendis, Dept of Physics, Durham University) using a similar system where additives, same as those used in the SANS experiments, were blended in various concentrations into a hydrogenated matrix, rather than deuterated. At the lower concentration additive mixtures there appear to be larger rod-like fibrils, figure 6:21.

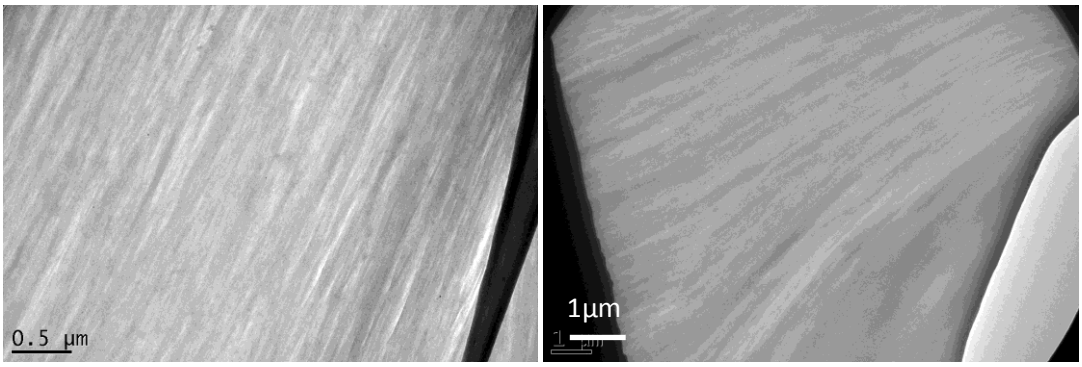

Figure 6:21 TEM images of 2% PEc5 in hPE200 matrix

Whereas at the higher concentration additive mixtures there appear to be a number of discrete objects of the order of 1.6µm, figure 6:22.

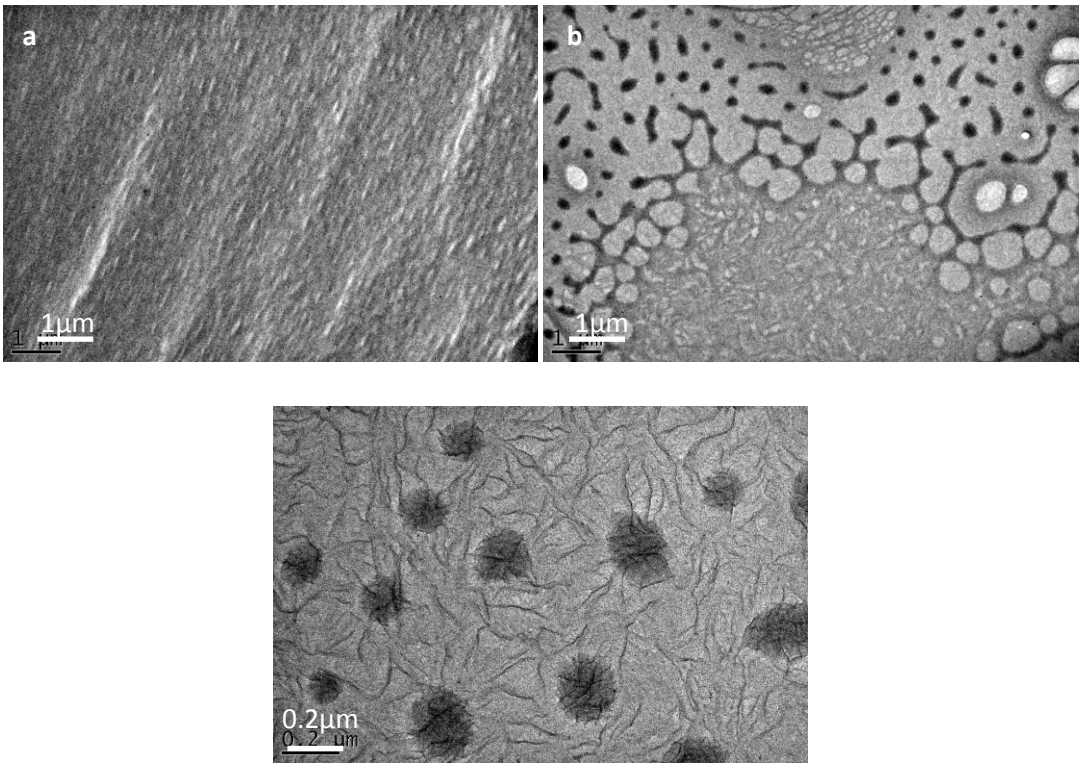

Figure 6:22 TEM images of 12% PEc5 in hPE200 matrix at different magnifications and areas, as indicated by the scales bars

The particle sizes measured using TEM were of a similar order of magnitude to those measured by SANS. However, as the films produced for TEM imaging (approximately 100 nm) were not mechanically stable the images look very different in different areas thus reducing the validity of the measured particle sizes.

6.3 Crystallinity

No fundamental property affects the physical properties of a polymer in such a vast way as the degree of crystallinity[22]. It can affect a polymer's storage modulus, permeability, density, brittleness, toughness and melting temperature, to name but a few. In this section the melting and crystallising temperature along with the decomposition temperature for a range of blended and unblended samples are described. A second polymer added to a semi crystalline polymer can act as a diluent, which could either decrease crystallinity by decreasing the concentration and nuclei numbers, or increase crystallinity by enhancing nucleation or increasing chain mobility[23]. Differential scanning calorimetry (DSC) was used to determine the melting temperature and the crystallisation temperature. Thermogravimetric Analysis (TGA) was used to determine the decomposition temperature for the unblended polymers and the same samples used for SANS. It should be noted that only one measurement was taken for each sample.

6.3.1 Thermogravimetric (TGA) Results and Discussion

A typical TGA trace is shown in figure 6:23 where the temperature of decomposition was defined as the temperature at which 98% of the mass of the original polymer remained. From the data illustrated in figure 6:23 it is clear that all of the materials made were highly stable over the annealing temperature range used in this study (120 °C). The TGA analysis results for the unblended polymers indicated that, figure 6:23, increasing the molecular weight for the fluorocarbon polymers resulted in an increased stability, whereas, increasing the number of fluorocarbon groups had no overall effect in the stability, within error. The hydrogenated polymers with no end- functionalisation decomposed at about the same decomposition temperature.

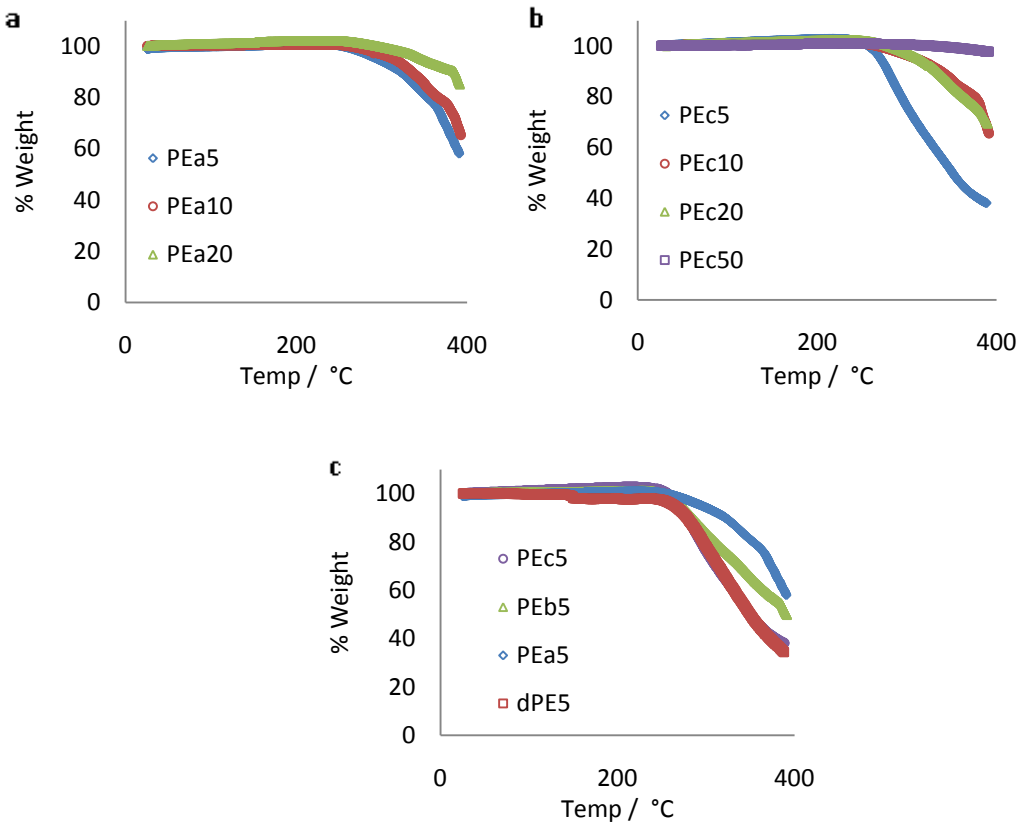

Figure 6:23 Thermogravimetric analysis results for the unblended polymers a) for type "a" additives, b) for type "c" additives and c) for 5 $kgmol^{-1}$ additives

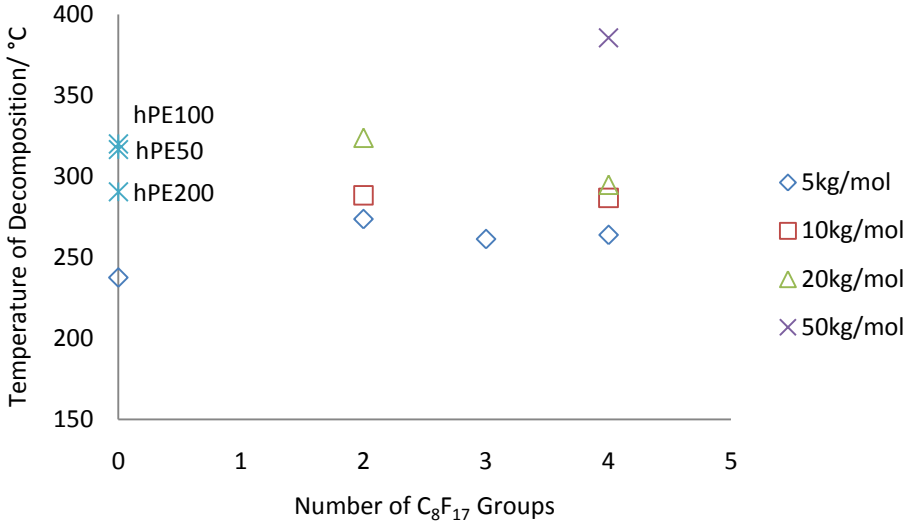

Figure 6:24 Decomposition temperatures measured by Thermogravimetric for the unblended polymers with different numbers of C_8F_{17} end-groups

The lower decomposition temperature of dPE5 was taken to be an anomalous result. In figure 6:23c at just after 100°C there is a drop in weight for dPE5, likely to be owing to solvent evaporation.

The greater the overall number of CF end-groups the lower the decomposition temperature (i.e. irrespective of the type of additive a 5 $kgmol^{-1}$ polymer will have proportionally more CF end-groups than a 10 $kgmol^{-1}$ polymer). These results are consistent with end-groups having lower stability than the polymer chains. Within the same molecular weight when the number of C_8F_{17} groups increases from 2 to 4 the decomposition temperature remains almost constant, decreasing slightly, again agreeing that the greater the numbers of CF groups the least stable the polymer. When these polymers are blended, table 6:1, with the matrix polymers used in the SANS study their stability is very similar across the range of additive and concentrations, however the temperate at which they decompose when blended is much higher, ~150°C, than their unblended constituent.

% Additive	% Matrix	PEa5		PEb5		PEc5	
		Matrix M_w $kgmol^{-1}$	Temp. of Decomp. /°C	Matrix M_w $kgmol^{-1}$	Temp. of Decomp. /°C	Matrix M_w $kgmol^{-1}$	Temp. of Decomp. /°C
1	99	79000	-	79000	428.87	82000	427.95
2	98	79000	419.98	79000	417.61	82000	413.51
4	96	79000	400.43	79000	409.91	82000	414.19
8	92	79000	398.06	79000	405.17	82000	406.98
12	88	79000	351.26	79000	395.1	79000	411.35
16	84	79000	216.8	82000	380.88	79000	400.13
100	0	-	273.66	-	261.32	-	261.84

Table 6:2 Blended polymer mixtures, used in SANS study, and their temperature of decomposition (temp. of decomp.)

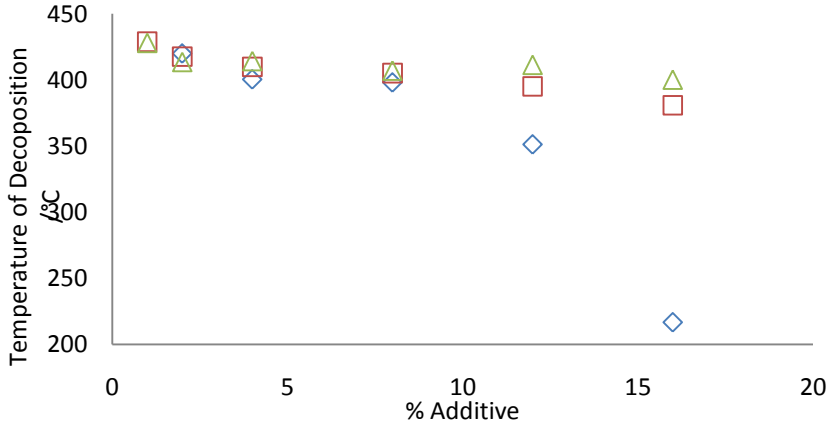

Figure 6:25 Thermogravimetric analysis results for the blended polymers at 2% decomposed for ◊PEa5, □PEb5 and ΔPEc5

6.3.2 DSC Results and Discussion

DSC was carried out on the unblended polymers and the samples used for SANS. These experiments were carried out to determine the influence of the additives on the crystallisation and melting behaviour of PE matrices.

6.3.2.1 Unblended Polymers

A typical DSC trace is shown in figure 6:26 where percentage crystallinity = (ΔH_m / 289)*100% - 80% for the sample shown below.

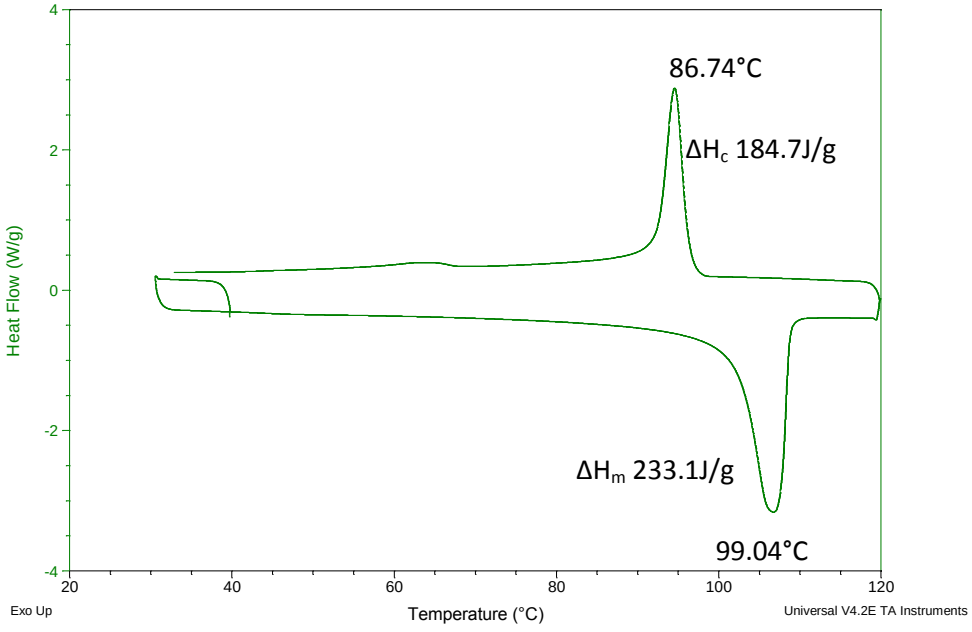

Figure 6:26 A typical DSC Plot and thermal energy change measured on hPE50

Figure 6:27 illustrates the melting and crystallising temperatures for the matrix polymers and a deuterated low molecular weight polymer, none of these polymers have been end-capped. For the hydrogenated matrix polymer, the change in molecular weight has no overall effect on the melting point, however, at lower molecular weight the T_m is lowest and the T_c highest indicating less hysteresis as smaller, imperfect, crystals are formed quickly and easier to melt. This is not uncommon as for higher molecular weight polymers as the reduced free volume from chain ends, has no effect on the melting point, however, it does have an effect on the crystallising temperature. As the molecular weight increases the number chain entanglements increases increasing the difficultly for the chains to align and form regular structures, in addition the melt becomes more viscous. These two influences compete with the increased thermodynamic driving force for crystallisation as the temperature decreases. Deuteration slightly reduces the melting point which is consistent with earlier work of Bates *et al*[25].

Chain ends are relatively free to move and the lower the molar mass the more chain ends which results in a reduced T_m because less energy is required to stimulate chain motion and melting. The deuterated polymer also has a slightly higher crystallising temperature suggesting that it enhances crystallisation. However, chain ends can be thought of as impurities and the more impurities the more possible nucleating sites which enhance crystallisation so T_c would be increased.

There is a dramatic increase in the percentage crystallinity, from 5 $kgmol^{-1}$ to 50 $kgmol^{-1}$ which was not considered as dPE5 was most likely "wet", figure 6:27. The percentage crystallinity decreases from 50-200 $kgmol^{-1}$ possibly because there are an enormous amount of chain entanglements in the melt and it is impossible for the amount of organisation required to produce a crystalline polymer to take place during crystallisation for larger polymers.

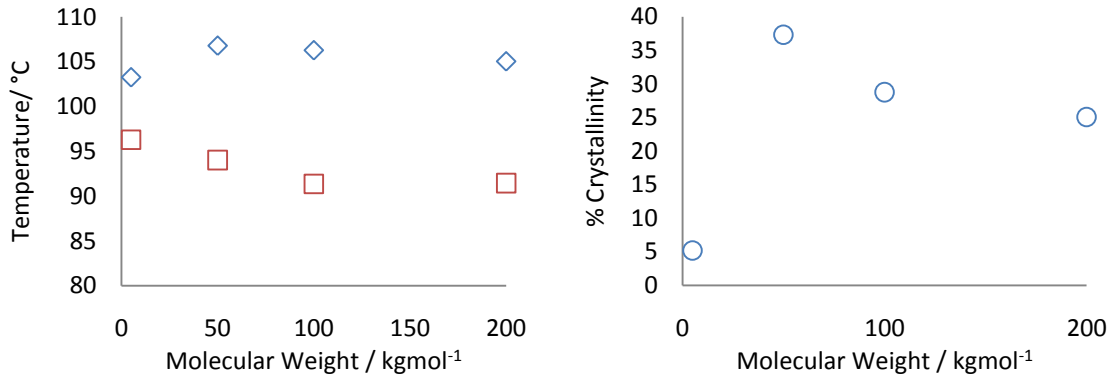

Figure 6:27 Melting (◊) & crystallising (□) temperature for various molecular weight unfunctionalised matrix polymers and the corresponding degree of crystallinity (O)

Figure 6:28 illustrates the thermal behaviour of the unblended functionalised additives. It is clear that the melting and crystallising temperature decreases as the number of fluorocarbon groups increases. As the molecular weight of the polymer is the same it must be the fluorocarbon chain ends that are suppressing crystallisation. T_c decreases by about the same amount as T_m which is consistent with the CF groups being excluded from the crystalline regions. Secondly, the percentage crystallinity reduces as the number of fluorocarbon groups increases which as with T_c implying there are fewer crystals, or less perfect crystals (or both).

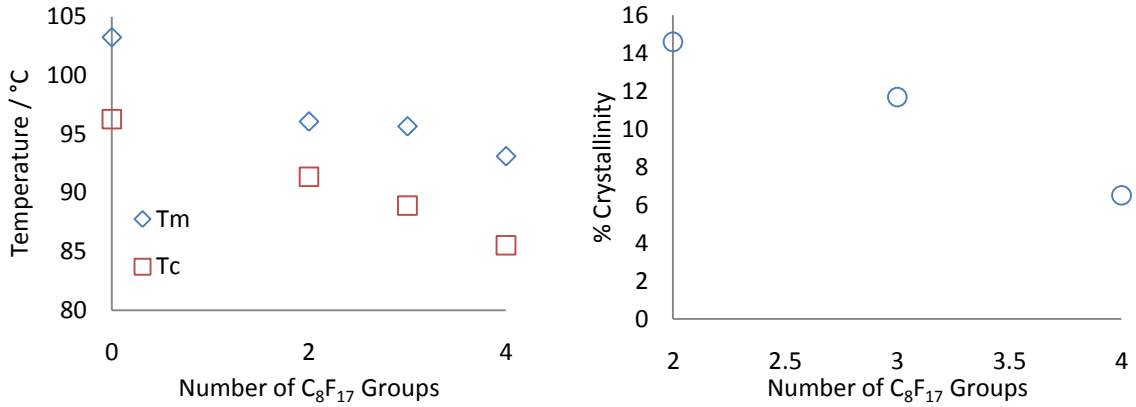

Figure 6:28 Effect of increasing the number of fluorocarbon groups on the 5 $kgmol^{-1}$ melting (◊) & crystallising (□) temperature and the corresponding degree of crystallinity (O)

The crystal size has an effect on T_m where the smaller the crystal the lower the melting temperature due to the greater contribution from the interfacial free energy[26], associated with the disordered chain ends emerging from the ends of the ordered crystallites. Lower molecular weight or more branching from the fluorocarbon chain ends has the effect of introducing defects into the crystals and so lowering their T_m. The results illustrated in figure 6:29 and 6:30 suggest that increasing the molecular weight of the additive, figure 6:29, and the number of fluorocarbon groups, figure 6:30, suppresses crystallisation. Paul and Barlow[24] identified five patterns of crystallinity development upon addition of a crystallisable diluent to a semi crystalline one:

- The diluent does not affect crystallisation
- The diluent retards the crystallisation rate
- The diluent prevents crystallisation (particularly at high concentrations)
- The diluent accelerates crystallisation
- The diluent provides enough thermal mobility to cause crystallisation of a normally non-crystalline polymer

All the data in figure 6:29 appear to show an initial increase in T_m, T_c and crystallinity then a gradual decrease with increasing molecular weight. This suggest competing effects of chain ends suppressing crystallinity at low molecular weight, where they dominate and viscosity inhibits melt crystallisation at high molecular weight.

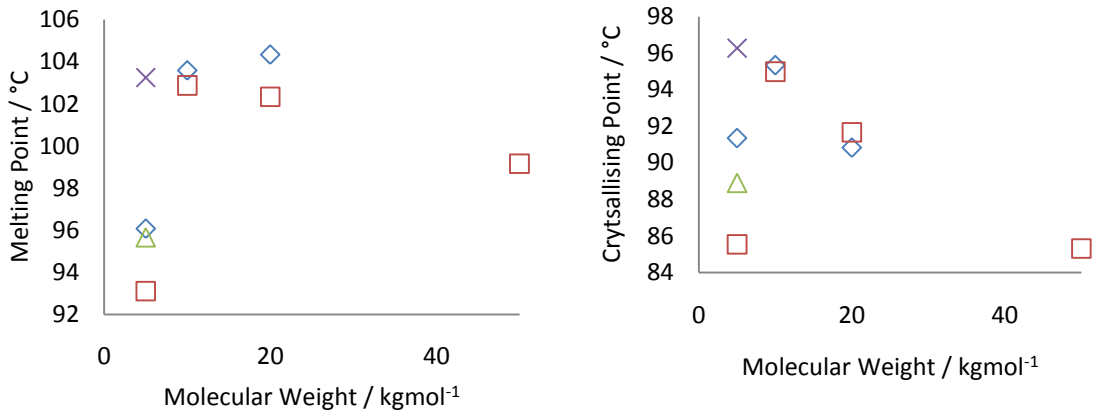

Figure 6:29 Effect of increasing the molecular weight of the additive on the melting and crystallising temperature, where represent ◊ additive "a", Δ additive "b", □ additive "c" and x dPE5

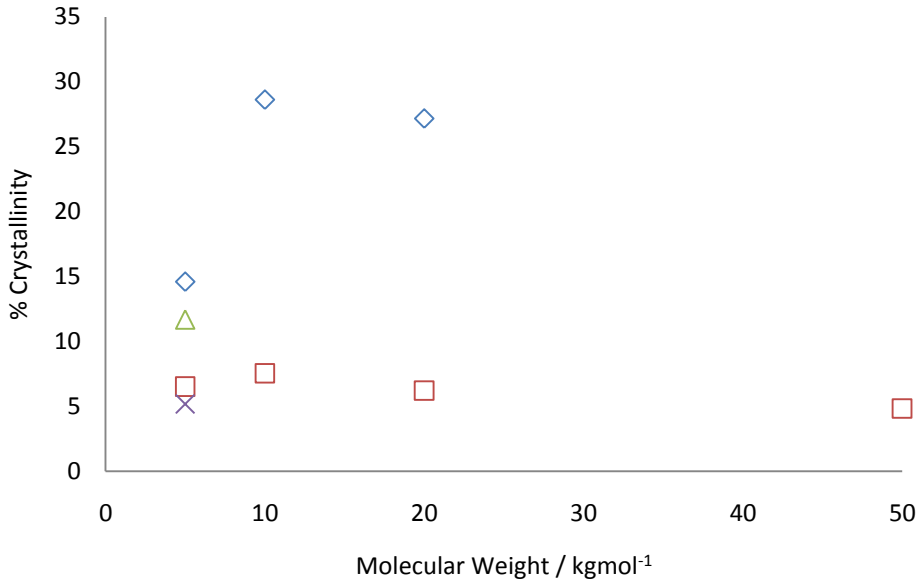

Figure 6:30 Effect of increasing the molecular weight of the additive on the degree of crystallinity where ◊ represents additive "a", Δ additive "b", □ additive "c" x dPE5

The molecular weight of the additive has little overall effect on the percentage crystallinity for additive "c", figure 6:30 and are inherently less crystalline due to their larger functional group. However for additive "a" the higher the molecular weight the higher the degree of crystallinity. This could be a result of the fluoro end-groups being excluded from the crystalline regions. Although the errors associated with the degree of crystallinity is associated with integrating the area under the melting peak.

There is a clear trend in decreasing crystallinity, for the data at 5 $kgmol^{-1}$, with increasing functionality a>b>c. This observation is consistent with previous conclusions that CF groups act as nucleating agents, thus the amount of crystallinity increases when present.

6.3.2.2 Blended Polymers from SANS Study

Three nominally similar batches of dPE from Polymer Source were used in SANS where a high temperature GPC, carried out by RAPRA, confirmed the molecular weight prior to the experiment. However, two (PE79.1 and PE79.2) samples gave anomalously high scattering. TA was carried out to explore the origins of the unexpected behaviour. The melting temperature for blends of additive "a" and "b" are very similar and almost constant, figure 6:31. However the much lower T_m of samples PE79.1 and PE79.2 indicates the possible presence of impurities or a poor level of saturated of PB. Only sample PE82 obtained satisfactory results so only these results shall be compared. These are PEc5 1-8% blends and PEb5 16% blend.

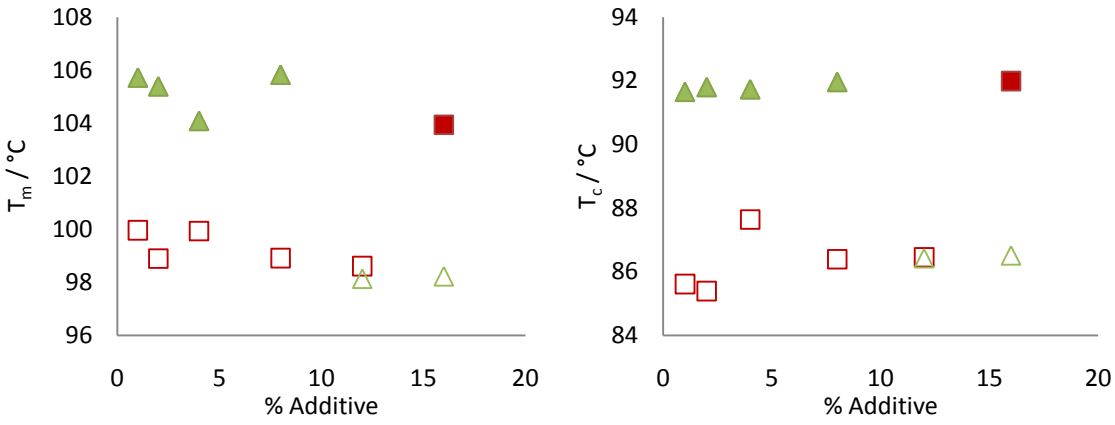

Figure 6:31 Melting and crystallising temperature for blended polymers where □ represents PEb5 and ΔPEc5 (open for blends using impure matrix and closed for those using the pure matrix)

For these blends the crystallisation temperature remains constant irrespective of the type of concentration of the additive. This is not expected for a truly homogeneous blend since the additives have melting temperatures in the range of 93-96 °C (c.f. figure 6:29), whereas the matrices melting temperature is approximately 106 °C (c.f. figure 6:27) and their presence if intimately mixed with the matrix should reduce the T_m of the blend. This could be due to the additive being excluded from the matrix or the crystalline regions. Although there is a slight decrease in the melting point as the concentration to additive is increased; this decrease is within error, so not regarded as significant.

6.3.2.3 Blended Polymers from QENS Study

DSC results have shown that the melting point of the QENS blend samples containing fluorinated additive, hPEa20, are slightly lower than those with the hydrogenated homopolymer, hPE20. T_m for the pure additive hPEa20 is between 104-107°C whereas for the pure homopolymer it is 5 °C higher (109-112°C). The T_c of the additive is between 83-97 °C whereas for the homopolymer it is 85 °C, table 6:3. This is consistent with previous results suggesting that the fluorocarbon groups suppress crystallisation. The samples used here are described in section 2.5.1.

Deuterated matrix dPE /g	Additive hPEa20 /g	Control hPE20 /g	% Added	T_m / ^{0}C	T_c / ^{0}C
0.205	0	0	0	95.38	80.18
0.02	0.051	0	20	95.75	87.18
0.172	0.074	0	30	95.73	88.50
0.261	0.26	0	50	95.88	90.34
0.201	0	0.051	20	94.40	89.86
0.175	0	0.075	30	103.93	92.57
0.206	0	0.202	50	105.72	94.85

Table 6:3 T_m and T_c for homopolymer and additive used in QENS study

In both cases increasing the additive concentration increases T_m and T_c. In this case the matrix is of high molecular weight and the additive possibly reduces the melt viscosity enabling better crystallisation.

6.4 Conclusion

The QENS, SANS and DSC results all suggest that the polymer blends have phase separated both above and below the melting point. Below the melt temperature a possible reason for this is that the additive is excluded from the crystalline regions. The dynamics explored by QENS for the additive and unfunctionalised control appear similar in the elastic window scan. However, there are small quantitative differences that indicate that the functional additive moves more easily, from the *I(Q,t)* plots. These results complement each other suggesting that the additive is excluded from the matrix and located in the amorphous regions.

Even in the case of some molten mixtures, where there are no crystalline regions, SANS indicates phase separation between PEc5 and its unfunctionalised matrix. The SANS surface area to volume ratio calculations show micron sized particles which were verified by TEM images. The final piece

of evidence suggesting phase separation is the thermal analysis results. These results suggest that CF groups are excluded from crystalline regions owing to the melting point and crystallisation point decreasing as number of CF groups increase. The thermal analysis also confirms that the pure additives are thermally stable and semicrystalline. The percentage crystallisation of the blends falls with increasing amount of fluorocarbon, which indicates that whilst fluorocarbons may assist nucleation, their presence leads to smaller, less perfect crystallites.

6.5 References

1. Arialdi, G.; Ryckaert, J. P.; Theodorou, D. N., *Chemical Physics* **2003,** *292* (2-3), 371-382.

2. Arialdi, G.; Karatasos, K.; Rychaert, J. P.; Arrighi, V.; Saggio, F.; Triolo, A.; Desmedt, A.; Pieper, J.; Lechner, R. E., *Macromolecules* **2003,** *36* (23), 8864-8875.

3. Lutz, T. R.; He, Y. Y.; Ediger, M. D.; Cao, H. H.; Lin, G. X.; Jones, A. A., *Macromolecules* **2003,** *36* (5), 1724-1730.

4. Sakai, V. G.; Maranas, J. K.; Peral, I.; Copley, J. R. D., *Macromolecules* **2008,** *41* (10), 3701-3710.

5. Sakai, V. G.; Arbe, A., *Current Opinion in Colloid & Interface Science* **2009,** *14* (6), 381-390.

6. Neelakantan, A.; Maranas, J. K., *Journal of Chemical Physics* **2004,** *120* (3), 1617-1626.

7. Qiu, X. H.; Ediger, M. D., *Macromolecules* **2000,** *33* (2), 490-498.

8. Neelakantan, A.; May, A.; Maranas, J. K., *Macromolecules* **2005,** *38*, 6598-6609.

9. Arbe, A.; Colmenero, J.; Monkenbusch, M.; Richter, D., *Physical Review Letters* **1998,** *81* (3), 590-593.

10. Bendler, J. T.; Shlesinger, M. F., *Macromolecules* **1985,** *18* (3), 591-592.

11. Ansari, I. A.; Clarke, N.; Hutchings, L. R.; Pillay-Narrainen, A.; Terry, A. E.; Thompson, R. L.; Webster, J. R. P., *Langmuir* **2007,** *23* (8), 4405-4413.

12. Gabrys, B.; Higgins, J. S.; Ma, K. T.; Roots, J. E., *Macromolecules* **1984,** *17* (4), 560-566.

13. Chahid, A.; Colmenero, J.; Alegria, A., *Physica A* **1993,** *201* (1-3), 101-105.

14. Chahid, A.; Alegria, A.; Colmenero, J., *Macromolecules* **1994,** *27* (12), 3282-3288.

15. Branca. C., f. A., Magazu. S., Maisano. G., Mangione. A., *Physica B* **2004,** (350), e355-e357.

16. Sakai, V. G.; Chen, C. X.; Maranas, J. K.; Chowdhuri, Z., *Macromolecules* **2004,** *37* (26), 9975-9983.

17. Heenan, R. K.; Penfold, J.; King, S. M., *Journal of Applied Crystallography* **1997,** *30*, 1140-1147.

18. Sasaki, S.; Tashiro, K.; Gose, N.; Imanishi, K., *Polymer Journal* **1999,** *31* (8), 677-686.

19. Tashiro, K.; Imanishi, K.; Izuchi, M.; Kobayashi, M.; Itoh, Y.; Imai, M.; Yamaguchi, Y.; Ohashi, M.; Stein, R. S., *Macromolecules* **1995,** *28* (25), 8484-8490.

20. de Gennes, P., *Scaling Concepts in Polymer Physics*. Cornell University, NY: 1979.

21. Higgins, J.; Benoit, H., *Polymers and Neutron Scattering*. Clarendon Press - Oxford Science Publications, London: 1996.

22. Fred W. Billmeyer, J., *Textbook of Polymer Science*. 2nd ed.; Wiley-Interscience, John Wiley & Sons, Inc, NY: 1971.

23. Long, Y.; Shanks, R. A.; Stachurski, Z. H., *Progress in Polymer Science* **1995,** *20* (4), 651-701.

24. Paul, D. R.; Barlow, J. W., *ACS* **1979**, *40*, 746.

25. Bates, F. S.; Keith, H. D.; McWhan, D. B.; *Macromolecules* **1987**, *20*, 3065

26. Harel, H.; *Composites Part A-Applied Science and Manufacturing* **2010**, *41* (9), 1066 - 1071.

7 Conclusion and Future Work

7.1 Conclusion

From this work six conclusions can be successfully drawn. Firstly, a wide range of novel multi-end functionalised polyethylene, of low polydispersity, were successfully synthesised. The synthesis required was involved and time consuming, requiring several different approaches until the desired product was obtained. Following the successful synthesis of seven different additives then deuteration to yield end-capped LLPDE which was, blended in different weight fractions, into hydrogenated LLDPE. The surface properties of these blends were then fully characterised.

The second conclusion that can be drawn is that as the additive concentration increases the surface excess of the additive increases, whether in the melt or in the crystalline state. This is similar to behaviour previously seen for amorphous analogues.

The third and fourth conclusions are that the lower the additive's molecular weight the greater its ability to segregate to the surface, and the matrix molecular weight has little importance. However, the greater the difference in molecular weight between the additive and the matrix the greater the resulting surface excess of additive. The CA and NRA measurements indicated that the lowest molecular weight additives, with the most fluorine groups, in the highest matrix (but matrix molecular weight is less crucial), are the most effective at decreasing the wettability of the film surface and have the highest surface excess. The surface energy results were discussed for the 5 $kgmol^{-1}$ additives in hPE200 matrices. For these blends the surface energies were lowest for PEc5 blends and highest for PEa5. These results suggested that the number of fluorocarbon groups was critical in order to obtain lower surface energies.

The fifth conclusion was made as a result of the XPS findings where it was concluded that surface roughness plays an important factor in determining surface wettability. The XPS results showed that PEb5 had the highest fluorocarbon concentration at the surface and produced overall the most efficient system. These results contradicted the CA predictions of surface fluorocarbon content, where the higher the fluorocarbon content the higher the CA. This is because surface roughness significantly contributes to the overall wettability of a surface, where the rougher the surface the higher the CA and the more hydrophobic the surface. The roughness may therefore be the most significant contributing factor to apparently anomalous results. For example at the lowest concentration of additives roughness dominates and the CA is unexpectedly high whereas at higher additive concentrations the roughness is less critical and the amount of fluorine at the surface dominates. This could give the "false" impression that a smaller amount of additive always

gives similar results as larger amounts, where in reality it does not. The effect of the surface roughness can be quantified simply as follows. The roughness, measured by AFM was between 5-10 nm, whereas the NRA surface excess layer was between 0-10 nm and NR 0-4 nm therefore roughness is a considerable parameter that needs further study.

The final conclusion is that many blends showed a strong tendency to phase separate. The results of the QENS, DSC, NRA, NR, CA and SANS results all indicated phase separation. SANS surface area to volume ratio calculations showing particles and images taken by TEM verified this. Below T_m a possible reason for phase separation was that the additive is excluded from the crystalline regions. The QENS results show that the additive moves more easily than the unfunctionalised additive. This suggests that the additive is excluded from the crystalline regions and located in the amorphous regions. Complementing the QENS results are the T_m and T_c values, measured by DSC. The melting and crystallisation point decrease as number of CF groups increases suggesting that CF groups are excluded from crystalline regions owing to the decrease in energy required to melt the crystalline regions. Following from this the NRA, NR and CA results intimate a possible "critical concentration" required to reach the highest surface excesses. Although the NR z* values are somewhat smaller than the NRA ones, the "critical concentration" is still observed implying that the additive and matrix become incompatible above a certain concentration resulting in phase separation. A possible explanation for this could be that the CF groups are excluded from the crystalline regions above a certain concentration.

7.2 Future Work

Three issues have to be resolved to draw any definitive conclusion with regards to the effect crystalline regions have on surface segregation. Firstly, the reason for phase separation has to be established. During the bulk studies (QENS, SANS) a perdeuterated matrix was used to maximise contrast and minimise incoherent scattering from the matrix. The incompatibility between the matrix and additive may be due to the large fluorocarbon groups and low molecular weight compatible (ethylene) groups, but could be further exacerbated by isotopic incompatibility. By reducing the isotopic contribution to incompatibility, using a hydrogenated matrix instead of a perdueterated one, not only can segregation due to isotopic incompatibility be eliminated but also a consistency between SANS, NR and NRA results achieved. To extract a reason for phase separation neutron beam time on SANS2d was applied for and the following proposal accepted: "*Understanding Melt Phase Aggregation in Semicrystalline Polymer Blends*". Although this experiment could not be scheduled during this study it will be extremely useful for future work.

Secondly, whether or not the matrix and additives mix within the amorphous regions, has to be understood. To resolve the molecular weight and functionality issue a second neutron proposal

was submitted, again for neutron beam time. The accepted proposal was entitled "*Miscibility of High Molecular Weight End-Functionalized Polymers in Semi-Crystalline Blends*". Again although this experiment could not be scheduled during this study it will be extremely useful for future work.

Thirdly, the rate of diffusion of the fluorinated additives, compared to unfunctionlised, in a matrix has to be understood to determine whether or not CF groups are excluded from crystalline regions. Another area to explore further would be whether or not the CA hysteresis, observed in this study, is a result of surface roughness due to CF groups or crystalline surface domains. By deliberately roughening the surface it can be made superhydrophobic and these results can be compared to those already obtained, which may indicate some conclusions.

Finally, atomistic molecular dynamic (MD) simulations fully overlap with the temporal and spatial ranges accessible by QENS. By performing these simulations the theoretical dynamics of the system could be compared to experimental results. However MD simulations are extremely difficult to perform and they can only simulate one molecule, whereas a polymer is huge, thus the model would need to be coarse grained. A more accessible experiment would be neutron spin echo which overlaps and extends the temporal and spatial ranges covered by QENS toward longer time and length scales. However, H/D labelling in NSE is not possible at local length scales and NSE is optimised to measure coherent signals[1, 2].

It would be interesting to extend this study to synthesis a high energy surface using NH_2 and OH end-groups. This work is of crucial importance for certain applications, e.g. bone mineralisation[3], adhesion and printing (with aqueous ink), because it is beneficial to have higher energy additives at the surface. It is not surprising that a blended additive that has high surface energy is depleted from the surface because of enthalpic factors. Although this is beyond the scope of this thesis examples of surface depleting additives include polymers end-capped with carboxylic acid groups[4-6], amine groups[3, 7, 8] and hydroxyl groups[3, 9]. By attaching lower energy groups next to higher energy ones at the end of a polymer chain the driving forces of lower energy groups segregating to the surface are capable of pulling high energy groups to the polymer surface. Surface reconstruction by changing the external conditions can then yield a high energy surface. There are other examples of similar polymers where an allyl amide functional perfluorinated ether is reacted to a silicon network through a hydrosilation reaction resulting in the surface properties to the PDMS elastomer being switchable[7]. Similarly if only a polar end architecture is available adsorption can be induced by annealing in a polar environment, e.g., dPS-COOH in a hPS matrix annealed in glycerol, prior to quenching in a glassy state[6, 10].

Further studies could also include studying the effect different annealing times, for different molecular weight polymers, have on the diffusion, crystallinity and structures obtained. The higher molecular weight the longer the diffusion time, so longer annealing would be required to obtain comparable amounts of diffusion and long range order. Also the crystallinity could be further studied using small and wide angle X-ray scattering and compared with the results obtained by DSC.

7.3 References

1. Arialdi, G.; Ryckaert, J. P.; Theodorou, D. N., *Chemical Physics* **2003,** *292* (2-3), 371-382.
2. Sakai, V. G.; Arbe, A., *Current Opinion in Colloid & Interface Science* **2009,** *14* (6), 381-390.
3. Toworfe, G. K.; Composto, R. J.; Shapiro, I. M.; Ducheyne, P., *Biomaterials* **2006,** *27* (4), 631-642.
4. Elman, J. F.; Johs, B. D.; Long, T. E.; Koberstein, J. T., *Macromolecules* **1994,** *27* (19), 5341-5349.
5. Frantz, P.; Leonhardt, D. C.; Granick, S., *Macromolecules* **1991,** *24* (8), 1868-1875.
6. Narrainen, A. P.; Clarke, N.; Eggleston, S. M.; Hutchings, L. R.; Thompson, R. L., *Soft Matter* **2006,** *2* (11), 981-985.
7. Thanawala, S. K.; Chaudhury, M. K., *Langmuir* **2000,** *16* (3), 1256-1260.
8. Jalbert, C. J.; Koberstein, J. T.; Balaji, R.; Bhatia, Q.; Salvati, L.; Yilgor, I., *Macromolecules* **1994,** *27* (9), 2409-2413.
9. Istratov, V.; Kautz, H.; Kim, Y. K.; Schubert, R.; Frey, H., *Tetrahedron* **2003,** *59* (22), 4017-4024.
10. Thompson, R. L.; Hardman, S. J.; Hutchings, L. R.; Narrainen, A. P.; Dalgliesh, R. M., *Langmuir* **2009,** *25* (5), 3184-3188.

Ion Beam Analysis

Ion beam analysis[1-7] is based on the interactions between accelerated charged particles and the electrons and nuclei of the bombarded material, causing them to slow down and possibly deviate from their original trajectory. As result of these interactions, particles or radiation whose energy carries information about the sample material is emitted. The three main interactions that can occur:

- An incident ion strikes a target ion which has greater ionic number. In this case the incident ion undergoes an elastic collision and is backscattered. This is the basis of Rutherford Backscattering.
- When the incident ion posses greater mass than the target ion it results in an elastic collision but the incident ion cannot be backscattered and instead continues in a forward direction and the lighter ion is recoiled from the sample. This is the basis of Elastic Recoil Detection.
- Nuclear reactions occur between the incident ion and target nucleus.

The detection of particles, or emissions from a sample after ion bombardment can reveal lots of information about a sample. Using MeV ion beam rapid quantitative analysis of elemental composition versus depth is obtained. The elemental sensitivity can be of the order of parts per million and the depth resolution of a few nanometres at its best. Some of the different techniques are illustrated in the figure A1:1; however only the techniques used in this these will be discussed in detail. Those are Rutherford Backscattering[4, 8], Elastic Recoil Detection[2, 9] and Nuclear Reaction Analysis.

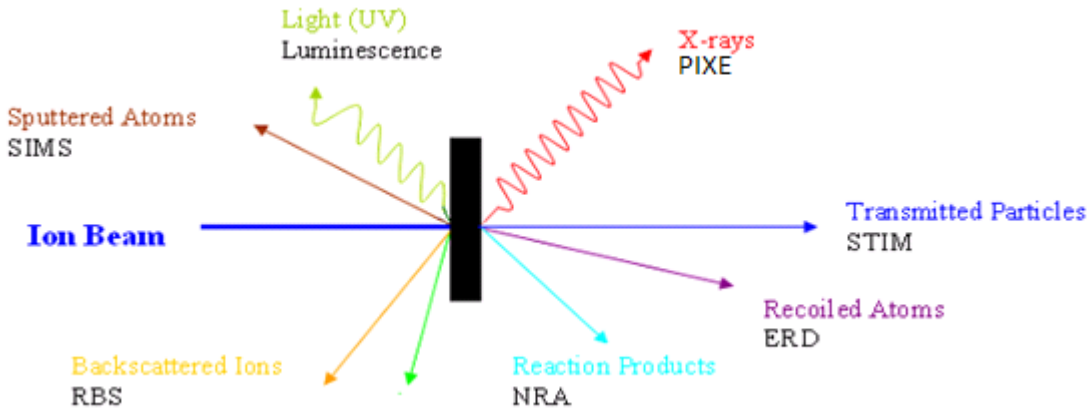

Figure A1:1 Illustration representing the types of Ion Beam Analysis Techniques[2]

A1.1 Rutherford Backscattering (RBS)

In RBS the most energetic recoil comes from the high mass elements at the sample surface, with lower mass elements at lower recoil energy. The probability of backscattering, which is governed by the Rutherford cross-section, increases with the square of the atomic number. The energy of a back scattered particles depend on the mass of the target atom, relative to the incident ion and the initial energy of the incident ion, and the depth at which the scattering took place. A typical use of RBS in polymer science is the study of surface modification.

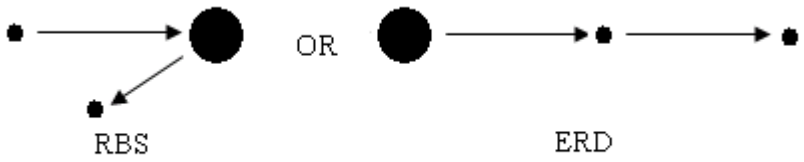

Figure A1:2 Image to illustrate the difference between RBS, where a sample projectile collides with a larger atom and ERD, where a large projectile collides with a smaller atom

As well as backscattering inelastic small angle scattering can also occur off the sample's electrons, resulting in a decrease in the energy of ions, which penetrate deep into the sample. Over short distances, the reduction in the projectile's energy is approximately proportional to the distance travelled through the sample. The amount of inelastic scattering in a material is dependent on the electronic distribution, in the sample and is known as the "stopping power"[10]. This is the reason why backscattering from nuclei deep within a sample give rise to backscattered ions detected at lower energy than from the same nuclei at surfaces.

When analysing RBS data the energy of the scattered projectile is measured and related to the mass of the scattered nucleus and its position in the matrix, creating a compositional depth profile. Thus, different nuclei will scatter incident ions with different energy, producing separate peaks in a plot of recoil count versus energy. Elements are determined by the position of the peak, depth by the width of the peak and concentration by the height.

The scattering cross section can be derived using simple Coulomb scattering and related to fundamental parameters such as the energy of the incident particle, its atomic number and mass. Knowledge of the scattering cross-section underlies converting the measured number of scattering events from a given target to the actual elemental concentration in the target. The probability of observing a scattered projectile is described by the differential (scattering) cross section is inversely proportional to E.

Equation A1:1

The typical set-up for either an RBS or ERD experiment is illustrated in figure A1:3.

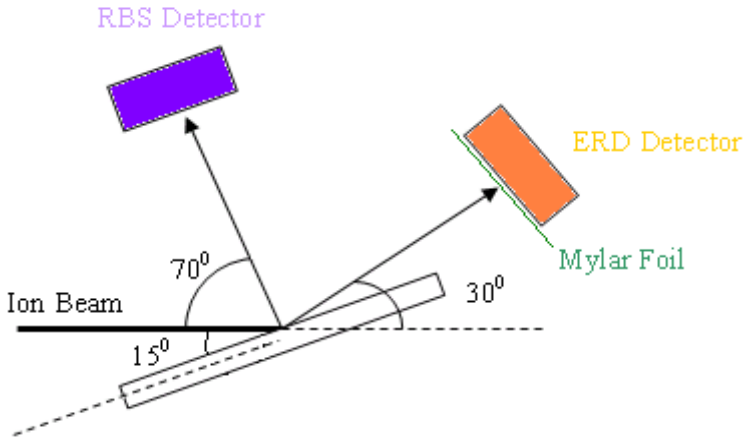

Figure A1:3 Typical ERD and RBS experimental set-up and detector angles used

A1.2 Elastic Recoil Detection (ERD)

When the interaction between a nucleus and a high energy ion beam is elastic and the recoil occurs at forward angles, typically between 20-60°, it is called ERD[4, 9, 11], often reported as forward recoil spectroscopy (FReS) in the literature. ERD is one of the few techniques that can quantify hydrogen depth distributions in virtually any material. When used in conjunction with deuterium labelling it can resolve the depth distribution of nearly identical polymers in blended films[12-14]. Using the same kinematic equations used for RBS it is clear that heavy ion projectiles

can easily recoil lighter ones which in some cases (if the geometry is correct) can then be ejected from the target and detected.

Any nucleus can be recoiled, if a heavy incident beam is used, and if the detector is placed at large recoil angles, this minimises signals from the forward scattered beam. ^{4}He is the most commonly used incident ion for detecting hydrogen or deuterium, since heavier elements (e.g. ^{12}C in the polymer) are not scattered forwards with sufficient energy to be detected, and beam damage is lower for low mass incident beams. A limitation of ERD is that the incident ion is also scattered towards the detector, and can saturate it, with comparable energy to the forward scattered nuclei of interest, so must be eliminated from the spectrum. A Mylar Foil placed between the sample and the detector reduces the kinetic energy of the forward scattered incident ions so that the user can discriminate between forward scattered projectiles and the signals of the recoiling nuclei. The energy loss when travelling through the foil is greater for heavier nuclei (He) than the lighter recoiled target nuclei so only the energy of the recoiled particle (^{1}H or ^{2}H) is measured at the detector.

Using ERD an elemental concentration depth profile is obtained and can reveal the hydrogen and deuterium content of polymer samples, where RBS cannot. The significant difference between RBS and ERD is that RBS registers the scattered projectiles where as ERD makes use of the ions recoiling from the bombarded sample. Further to this, during ERD depth profiles of all elements lighter than the incident beam can be obtained simultaneously.

Using appropriate calibration standards, films of known composition and thickness, it is possible to convert the spectrum channel number into a depth scale and the count number into a volume fraction a depth profile can be obtained.

A1.3 Nuclear Reaction Analysis (NRA)

When the incident beam energy is sufficient to overcome the Coulomb barrier a nuclear reaction between the incident beam and the certain isotopes in the sample can occur[4, 9, 11].

NRA, which can be performed resonantly - nuclear resonance profiling (NRP), or by article-induced gamma emission (PIGE) spectroscopy, is widely used to depth profile deuterium in a sample. Deuterium can be profiled using ^{3}He where the energy of the detected fast proton depends on the depth of the deuterium in the sample[15]. These are particle-particle nuclear reactions[1].

$$^{3}He + D \rightarrow \alpha + p + 18.353MeV$$

$$^{19}F + \alpha \rightarrow {}^{22}Ne + p + 1.67MeV$$

The limitation of this method is that only light elements can be profiled (atomic number<11) and that each element requires a specific incident ion beam, so multiple measurements may be necessary depending on the elements involved. Another disadvantage is that the reaction cross-section is much lower than the scattering cross-sections, so greater exposure to the ion beam is required, leading to beam damage. However, using the $^{2}H(^{3}He,p)\alpha$ nuclear reaction enables deuterium labelled polymers[16] to be studied and can be complementary to neutron scattering. It is also possible to detect the high energy protons in backscattering geometry, thus eliminating the need for Mylar foil, allowing excellent depth resolution (~6nm) to be obtained, with relative ease[16-18]. Another significant advantage that greater depths can be profiled as protons suffer very little energy loss on exiting the sample, thus the depth scale is controlled by the energy loss of the incident beam. Figure A1:4 illustrates a typical NRA spectrum where the emitted proton's energy is used to deuterium the depth profile of ^{2}H using a 0.7 MeV ^{3}He beam on deuterium containing polymer film. Particles were detected at 170° to incident beam using a Am/Cu/Pu Alpha particle source to confirm energy calibration of detector.

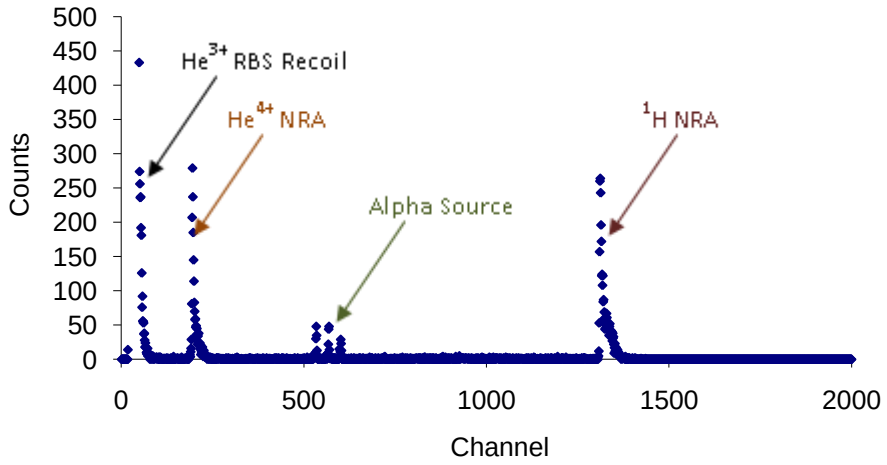

Figure A1:4 Typical NRA spectrum showing counts (of recoil particles detected) *vs* channel (energy of recoil particles) which can later be converted into a depth scale using

A1.4 Stopping Power

As an ion beam travels through a sample, the flux remains nearly constant but their energy decreases[4]. This reduction in the incident ion beams energy, is due to interactions with electrons[19] and is the basis of the depth measurement. The amount a given sample reduces the incident ion beams energy is referred to as its "stopping power". The stopping power is individual to each sample and is caused by Coulomb interactions with target nuclei and interactions with bound and free electrons. The stopping power is approximately linear with increasing atomic number of the

target nucleus. Electronic interactions are the main mechanism for energy loss in ion scattering techniques because for MeV scattering nuclear energy loss is approximately three orders of magnitude smaller than electronic energy loss. There are numerous electrons in the target thus the incident ion slows down in an almost continuous fashion. The energy loss with depth, *-(dE/dx)*, due to momentum transfer between incident ions and electrons can be calculated for any sample and decreases with increasing incident energy and varies approximately systematically at high energy with 1/*E* (this is true for some but not all energy ranges). Because of this systematic variation it can be readily converted into a depth-profile. The electronic stopping power, *S*, is:

Equation A1:2

where *1* denotes the incident ion, *2* denotes the nucleus, *m* the mass, *Z* the atomic number, *v* the velocity and *I* the excitation energy of the electrons[20].

For a sample that is not a pure element, such as a polymer, Bragg's rule is usually used to calculate the stopping power. This assumes that the target atoms contribute independently to the total energy loss, regardless of bonding. This allows the stopping power to be calculated from the elemental stoichiometry and the density. Alternatively the stopping power can be calculated experimentally by measuring the energy loss, *dE*, of a film of known thickness, *dx*. Stopping powers for polymers should be directly measured where possible because elemental densities do not always match the polymer density. There is freely available software program SRIM®[19, 21] that can calculate the stopping powers in virtually any material, including polymers.

As a general rule of thumb, the energy loss of MeV ^{4}He ions in most hard materials is 30-60 eV/Å, but for polymers this value is generally smaller[19], 20 eV/Å. Stopping powers are relatively constant in thin films, although the energy loss by the incident beam occurs by discrete interactions both on entry and exit. The thin film approximation uses one value to represent energy loss but can only be used for very thin films and only really used when computationally it is difficult to do otherwise. For thicker targets the energy loss for the incoming ^{4}He and outgoing H/D (in ERD) are significant and therefore the energy dependence on the stopping power of the sample must be considered. The thick film approximation is usually used for ERD and the Mylar Foil (δE_s) and the thin film approximation for RBS.

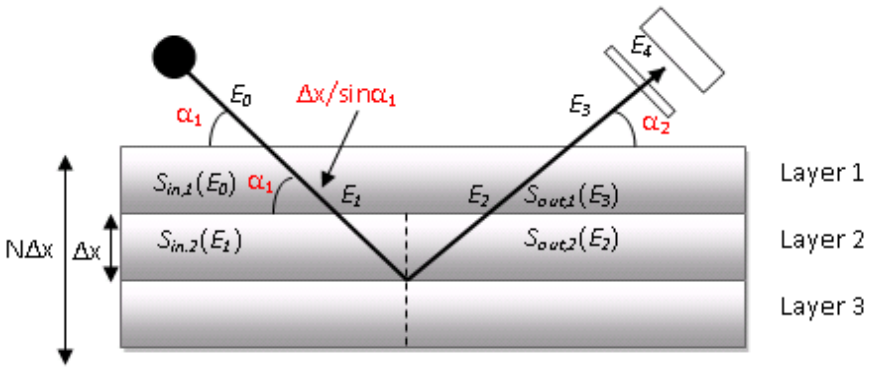

Figure A1:5 Illustration schematically defining the parameters involved in the Thick Target Approximation Definition used in ion beam analysis

Figure A1:5 describes the Thick Film Approximation where the sample is divided into N layers each of thick thickness Δx. For small changes in depth (Δx) the stopping power (S) in that layer can be considered to be constant, as in the thin film approximation

At each layer E_1 and E_2 are related by $E_{1,j} = kE_{2,j}$. Here, the energy of the ion in layer j-1 can be derived from the recurrent relations, where $S_{in,j-1}$ is evaluated at $E_{in,j-1}$ where,

Equation A1:3

Equation A1:4

The values of S_{in} and S_{out} are derived from the stopping powers of the constituent elements using Braggs rule where,

Equation A1:5

A1.5 Limitations of Ion Beam Analysis

Ion beam analysis has very few limitations compared to other surface science techniques. Single measurements are required to determine the depth distribution and gradual compositional changes which take ~30 minutes. Sample preparation is fairly straightforward and the data fitting is relatively simple. However, spatial resolution is limited and a lack of chemical bonding information is provided.

A1.5.1 Depth Resolution

Depth profiling techniques, such as ion beam analysis, measure concentration in a direct space perpendicular to the sample surface. By measuring perpendicular (RBS and ERD) to the sample surface a maximum depth of 10 microns could be easily reached however the resolution is not

likely to be better than 300 nm. Using a grazing incidence beam (NRA) can achieve much better depth resolutions at the surface, ~5 nm, to a maximum depth of ~150 nm. The main determining factors for depth resolution are the energy resolution capabilities of the detector and the energy loss of the ion beam as it penetrates the sample.

To reach the best resolution different factors need to be optimised and often the optimisation of one comes at the expense of another e.g. depth range versus resolution. Each technique in IBA has different depth resolution capabilities; therefore, it is a key factor to consider when choosing an appropriate method for interfacial studies. For example, ERD has relatively poor depth resolution owing to the high straggling of the beam in the Mylar foil. Straggling is the fluctuation in statistical energy loss[4]. As a beam travels through a sample multiple small-angle collisions with the nuclei in the sample occur causing the beam to spread. Because of the statistical nature of these interactions, the energy loss of the ions has a Gaussian distribution with a width corresponding to the energy straggling. The energy spread due to straggling is approximated from the Bohr Theory and predicts that straggling is independent of energy and increases with the square root of the film thickness.

Depth resolution is defined as:

Equation A1:6

The best depth resolution is achieved when ΔE_{tot} is at a minimum and the effective stopping power is at a maximum. Assuming the individual factors are uncorrelated and can be characterised by a Gaussian distribution then[6]:

Equation A1:7

ΔE_D is the detector energy resolution and is constant, but may decay over time. ΔE_s and ΔE_f are energy loss due to straggling in both the sample and the filter respectively. The straggling in the filter is the largest contribution to the total energy resolution loss. ΔE_m is the energy broadening due to multiple scattering. This is particularly important for glancing angle geometries (ERD) and recoil collisions below the surface. It is very similar to straggling where the individual particles lose energy via many individual encounters with electrons. ΔE_s and ΔE_m can be calculated for individual experimental set-ups. Finally ΔE_G is the geometrical broadening error due to beam divergence and the finite acceptance angle of the detector. This is because the ion beam has finite width, because

of the strong dependence on the kinematic factor and on θ, and the detector has finite area, which reflects a distribution of path lengths and energy loss in the sample. The surface roughness effect on ΔE_{tot} can normally be ignored apart from in ERD where glancing angle geometry is used.

Depth resolution can be improved by increasing the effective energy loss, $(dE/dx)_{eff}$. The detectors are in a fixed position but by rotating the sample α can be optimized and improve the overall depth resolution. There are several ways which the depth resolution can be optimized. If,

Equation A1:8
Equation A1:9
Equation A1:10

- $S_{in,He} >> S_{out,H}$ therefore by increasing the path length of ^{4}He (i.e. decreasing α, which changes x/sinα, see the *thick film approximation*) will increase [S]. But by increasing the path length of the ions inside the sample it increases the multiple scattering (ΔE_m) which increases ΔE_{tot} and deteriorates the depth resolution. A balance needs to be achieved.
- Decreasing E_0 results in an increase in $S_{in,He}$ and $S_{out,H}$ but by using a lower beam energy the range is lower.
- Increasing the atomic mass of the projectile the kinematic factor is increased and *[S]* increased. This may however lead to unwanted beam damage of the sample.
- Finally, by reducing ΔE_F, the largest contributor to ΔE_{tot}, it can be reduced. This is achieved by reducing E_0 (increases *[S]*) which enables the use of a thinner filter.

A1.5.2 Beam Damage

Organic materials, especially polymers, are very susceptible to beam damage because of their covalent bonds. The ionising radiation used in IBA tends to break these bonds leading to chain scission or cross linking; as such IBA is a destructive technique. The C-H bonds in the amorphous regions of polyethylene may cross link because the damaged fragments may diffuse and react. This is not possible in crystalline regions hence tendency only to get scission, leaving reactive sites, in the crystalline regions[22].

To check for beam damage the same spot on a sample can be analysed several times. To avoid beam damage the acquisition time should be limited to the minimum required to obtain statically good data. Figure A1:6 illustrates the beam damage obtained for a typical set of samples where the measurement has been repeated on the same spot using a beam charge of 5 μC. It is obvious from the counting times used, 5.0 μC, that beam damage in negligible as the integral under the peaks are similar.

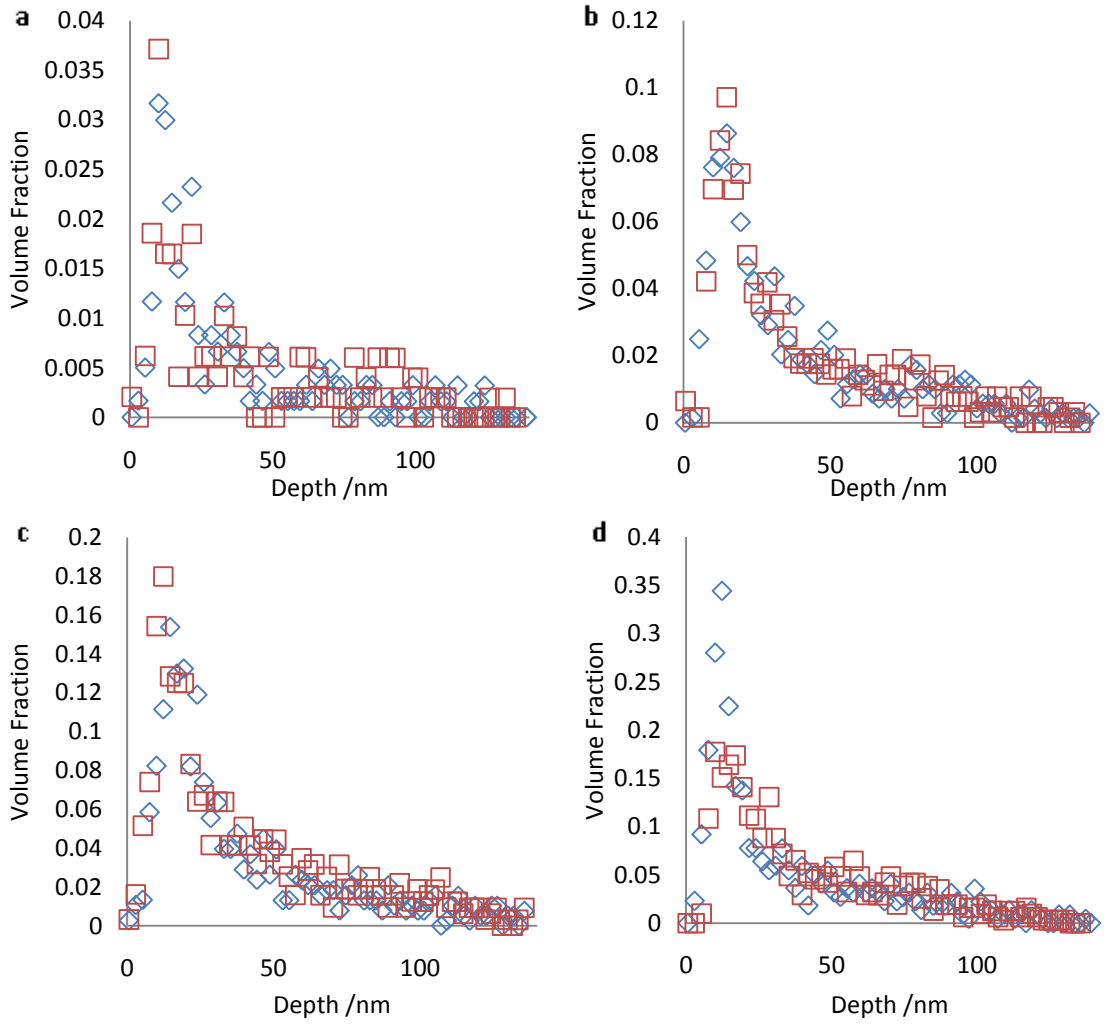

Figure A1:6 Typical NRA data (blue) illustrating the beam damage (red) after 5μC counting caused to a two blend compositions, perpendicular to the surface of a) 2% additive, b) 8% additive, c) 16% additive and d) 20% additive

A1.6 References

1. Feldman, L. C. a. M., J.W, Fundamentals of Surface and Thin Film Analysis, Prentice Hall; Facsimile edition. 1986.
2. Tesmer, J. R.; Nastasi, M.; Barbour, J. C.; Maggiore, C. J.; Mayer, J. W., *Handbook of Modern Ion Beam Materials Analysis*. Materials Research Society: Pittsburgh, 1995; p 704.
3. Malmqvist, K. G., *Radiation Physics and Chemistry* **2004,** *71* (3-4), 817-827.
4. Breese, M. B. H., Jamieson, D.N., King, P.J.C., *Materials Analysis using a Nuclear Microprobe*. John Wiley & Sons, NY: 1996.
5. Chakraborty, P., *Ion Beam Analysis of Surfaces and Interfaces of Condensed Matter Systems*. Nova Science Publishers Inc.: New York, 2002.
6. Composto, R. J.; Walters, R. M.; Genzer, J., *Materials Science & Engineering R-Reports* **2002,** *38* (3-4), 107-180.
7. Geoghegan, M. In *MeV ion beam profiling of polymer surfaces and interfaces*, Conference on Polymer Surfaces and Interfaces III, Durham, England, Jul; Richards, R. W.; Peace, S. K., Eds. John Wiley & Sons Inc: Durham, England, 1997; pp 43-73.
8. Chu, W. K., *Backscattering Spectroscopy*. Academic Press: New York, 1978; p 399.
9. Jones, R. A. L.; Richards, R. W., *Polymers at Surfaces and Interfaces*. Cambridge University Press.
10. Genzer, J.; Rothman, J. B.; Composto, R. J., *Nuclear Instruments & Methods in Physics Research Section B- Beam Interactions with Materials and Atoms* **1994,** *86* (3-4), 345-354.
11. Richards, R. W., *Scattering Methods in Polymer Science*. Ellis Horwood Limited: 1995.
12. Crist, B.; Green, P. F.; Jones, R. A. L.; Kramer, E. J., *Macromolecules* **1989,** *22* (6), 2857-2858.
13. Dai, K. H.; Kramer, E. J.; Shull, K. R., *Macromolecules* **1992,** *25* (1), 220-225.
14. Jones, R. A. L.; Kramer, E. J.; Rafailovich, M. H.; Sokolov, J.; Schwarz, S. A., *Physical Review Letters* **1989,** *62* (3), 280-283.
15. Gall, T. P.; Kramer, E. J., *Polymer* **1991,** *32* (2), 265-271.
16. Payne, R. S.; Clough, A. S.; Murphy, P.; Mills, P. J., *Nuclear Instruments & Methods in Physics Research Section B- Beam Interactions with Materials and Atoms* **1989,** *42* (1), 130-134.
17. Ansari, I. A.; Clarke, N.; Hutchings, L. R.; Pillay-Narrainen, A.; Terry, A. E.; Thompson, R. L.; Webster, J. R. P., *Langmuir* **2007,** *23* (8), 4405-4413.
18. Chaturvedi, U. K.; Steiner, U.; Zak, O.; Krausch, G.; Schatz, G.; Klein, J., *Applied Physics Letters* **1990,** *56* (13), 1228-1230.
19. Ziegler, J. F.; Biersack, J. P.; Littmark, U., *The Stopping Range of Ions in Solids*. Pergammon Press: New York, 1985.
20. Bardos, G.; Gavrilenko, G. M., *Acta Physica Hungarica* **1986,** *59* (3-4), 393-399.
21. Ziegler, J. F.; Ziegler, M. D.; Biersack, J. P., *Nuclear Instruments & Methods in Physics Research Section B-Beam Interactions with Materials and Atoms* **2010,** *268*, 1818-1823.
22. Martinez-Pardo, M. E.; Cardoso, J.; Vazquez, H.; Aguilar, M., *Nuclear Instruments & Methods in Physics Research Section B-Beam Interactions with Materials and Atoms* **1998,** *140* (3-4), 325-340.

Neutron Scattering

Neutrons are subatomic particles found in an atom's nucleus which are slightly heavier than protons. They have no electrical charge and can be characterised by a wave. The wave form, of neutron scattering, can be described in terms of de Broglie relations. Due to particle-wave duality, thermal neutrons can be described as a wave with a wavelength of a few Angstroms where the wavelength of thermal neutrons is 10^4-10^6 times larger than the size of an atomic nucleus and comparable to intermolecular spacing. Nuclei therefore act as point scatters (neutron are scattered isotropically) and scattering remains constant as the scattering angle increases. de Broglie describes waves as having momentum, *k*, and by using the de Broglie relationship the momentum transfer, *Q*, is defined as having a definite value for any wavelength, figure A2:1.

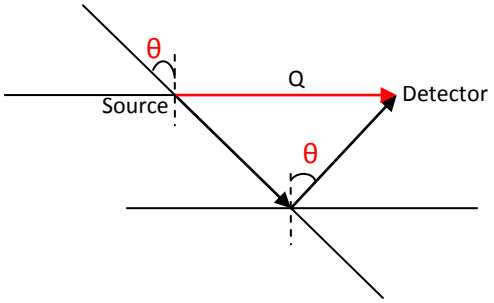

$$Q = k_f + k_i$$

$$E = E_f + E_i$$

Figure A2:1 Illustration schematically defining the parameters involved in the neutron scattering

Unlike electrons neutrons have no electrical interaction with matter, are sensitive to the position of atomic nuclei and their absorption is small. Due to their weakly interacting nature with most materials neutrons are very penetrating and useful probes for examining the structure[1, 2], both bulk (e.g. SANS[3-6]) and surface composition of materials (e.g. reflection[5, 7-12]), and the dynamics[13, 14] of a system[15-17].

Only a single neutron scattered at a point is scattered isotropically but when a large number of coherent scattering events are involved the incident neutrons may be diffracted or reflected. Under the Bragg condition, *Q* is perpendicular to the scattering planes and:

Equation A2:1

must be satisfied where the distance between two adjacent scattering planes is *d*:

$$r_j - r_i = d$$ Equation A2:2

Equation A2:3

— by substituting into Bragg's equation when n=1 — Equation A2:4

Lower *Q* values correspond to longer d-spacing (intermolecular distances) in the probed structure so can be used to study the large intermolecular spacing between polymers/colloids.

Neutrons are produced from either continuous reactors or spallation sources. Utilising nuclear fission reactions, operate in a continuous neutron generation mode where the neutron flux available is ultimately limited by the ability to remove heat from the reactor. Spallation sources function in a pulsed (time-of-flight) mode and can potentially go to higher fluxes as a non-continuous process allows for better heat removal. Beams of high kinetic energy hydrogen ions are produced and injected into a synchrotron ring, where they are accelerated to reach much higher energy, 800 MeV (in the case of ISIS), then steered to hit a neutron rich, e.g. tantalum, or mercury source. In summary continuous reactors generate some neutrons all of the time, whereas, spallation sources generate many neutrons some of the time. The incident flux can be calculated by:

Equation A2:5

I(Q) is the intensity of neutrons scattered at different angles and is manipulated from the van Hove formulation.

Equation A2:6

It contains information on the size, shape and interactions between scattering bodies.

where *N* is the number of scattering bodies, *V* is the volume of the scattering body, $\Delta\rho$ the contrast factor, *P(Q)* the form factor and gives intra-particle information (size and shape) and *S(Q)* is the structure factor. The structure factor gives inter-particle information (particle interactions) and *B* is the background signal. *I(Q)* is also known as the *differential cross-section* ($d\sigma/d\Omega$) and is

more precisely the number of neutrons scattered into a certain area in a certain time[17], figure A2:2.

Equation A2:7

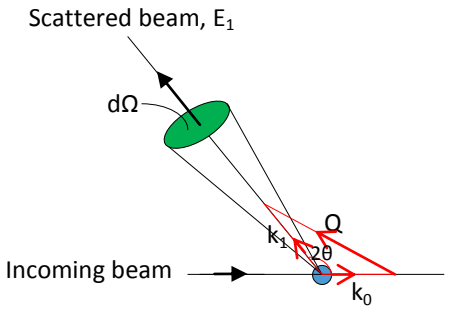

Figure A2:2 Illustration schematically defining the parameters involved in calculating the differential cross-section used in neutron scattering

There are two types of scattering that a neutron can undergo; *elastic* and *quasielastic/inelastic* scattering. During elastic scattering a materials structure is investigated and the dynamics are probed by quasi/inelastic scattering.

Elastic scattering (ΔE=0) can be used to probe structure, e.g. coherent SANS where S(Q) is measured. Quasielastic scattering (QENS), due to the reorientation or translational diffuse motions of particles in the samples materials, is incoherent and probes self-diffusion[18] on the pico-second (vibrations) and the nano-second (relaxation) scale. Analysis is made of Doppler line broadening of otherwise elastically scattered neutrons. Inelastic scattering ($\Delta E \neq 0$, $\Delta Q \neq 0$) probes a materials dynamics. Examples include coherent inelastic scattering such as NSE, NMR, Raman spectroscopy, all of which measure collective motion.

Most neutron scattering instruments operate in the diffraction mode, of which there are four types.

- To measure the structure of crystalline bulk samples single diffractometers would be used which probe high Q>0.1 $Å^{-1}$
- To measure the structure of an amorphous samples a diffuse and liquid scattering instrument is used. These diffractometers can probe high Q ranges.
- A SANS instrument can be used to probe the bulk of both amorphous and crystalline samples and it investigate at lower Q ranges (0.4 $Å^{-1}$ to 0.001 $Å^{-1}$)

- Finally to investigate a sample's surface a reflectometer must be used. Reflectometers can only measure amorphous sample surface structure and do not operate in the diffraction mode the *Q* range is generally low and similar to SANS.

The single scattering theory, used in diffraction mode, is based on the first *Born Approximation*, which applies to thermal/cold neutrons. The *scattering cross-section* (σ) of an element is the apparent "area" it *offers during scattering*,

Equation A2:8

where *b* is the *scattering length*.

Because neutrons are scattered isotropically the scattering event can be characterised by a single parameter, the neutron scattering length, *b*. The neutron scattering length represents the apparent "size" of the element during scattering. If b is negative it means the scattered neutron wave function is out of phase with respect to the incident neutron wave function. The scattering length varies greatly among elements/isotopes and is determined experimentally by transmission measurements. The *Fermi pseudopotentical* models the interaction between a neutron, located at , and a neutron with scattering length b_j at position . By using the Born Approximation of Fermi's Golden Rule the *double differential cross-section* can be calculated at it is this quantity that is measured in a neutron scattering experiments. The double differential cross-section calculates the *dynamic structure factor*, *S(Q,E)*, used to quantify neutron scattering where a change of neutron energy on scattering is measured. The double differential cross section is represented by:

Equation A2:9

These factors together gives *S(Q,ω)* which contains all the physics of the system, e.g. the scattering function and response function:

Equation A2:10

The dynamic structure factor, *S(Q,ω)*, is measured by most quasieleastic/inelastic neutron scattering spectrometer. If a Fourier time transform is performed on this the *time dependent*

structure factor is obtained *S(Q,t).* This is measured by neutron-spin-echo spectrometers. The initial value of this, S(*Q*,*t*=0) is the so called *static scattering factor*, *S(Q).* SANS instruments measure *S(Q). S(Q,t)* and *S(Q)* are sometimes called the time dependent density-density correlation function and the density-density correlation function respectively.

Equation A2:11

A2.1 Definition of Coherent and Incoherent Scattering

Coherent scattering concerns the correlations between the positions different atoms at different times and the collective excitations in the sample, *collective motion*[19] and is where reemission occurs at the same frequency as the incident radiation leading to interference. During coherent scattering neutrons interact with the whole sample; therefore the scattered waves from different nuclei interact with each other. This is owing to the scattered waves having relative phases. Depending on the relative distance between the two atoms information can be obtained about the structure of the material. This is due to the interaction of a neutron wave with different atoms at different positions and times. If the coherent scattering is elastic then information about the equilibrium structure can be obtained. Coherent scattering experiments are not only structural, they tell us about collective dynamics – how atoms move with respect to each other. The technique most commonly used for this is Neutron Spin-Echo[17].

Incoherent scattering provides information on the time-dependent correlations between different positions of the same atom and single particle excitations in the sample, *self diffusion*[18]. In general QENS is used to probe self diffusion via the Doppler broadening of the scattered energy spectrum, Figure A2:3. When neutrons interact independently with each nucleus incoherent scattering occurs. The scattered waves from each different nucleus do not interfere instead the intensities accumulate. This could be due to the interaction of a neutron wave with the same atom at different positions and different times, thus providing information about atomic diffusion.

Coherent scattering depends on *Q* and is therefore the part that contains information about the scattering structures, whereas, incoherent scattering is featureless (*Q* independent) and contains information on the material scattering density only.

A2.2 Scattering Cross Section

The scattering cross section can be written simply as the sum of the two coherent and incoherent contributions:

Equation A2:12

Therefore the double differential cross section can be written as:

Equation A2:13

Following from the Fermi average for cases where i=j (incoherent) and i≠j (coherent) are and then the Fermi pseudo potential can be written as the sum of two components and the double differential cross-section becomes:

Equation A2:14

The equation defines the initial, k_0, and final, k_1, momentum at a position, *R(0)*, at time zero and a given time, *R(t)* with an certain energy, ω. The first term gives coherent scattering and the second the incoherent. The coherent and incoherent scattering cross sections in all directions are defined as for the coherent scattering and for the incoherent scattering.

N.B. the scattering length has the dimensions length 1fm = 10^{-13} cm, where 1 barn = 10^{-24} cm^2

In order to separate out the coherent and incoherent scattering during a neutron experiment one can use either (1) polarized neutron along with a polarized analyser, (2) align the nuclear spins or as in my experiments (3) use D_2 labelling.

For any molecule (e.g., "A_mB_n") the coherent scattering cross section then the incoherent scattering cross section is determined by summing the spin and composition incoherent scattering cross sections. The total scattering cross section is the sum of the incoherent and coherent scattering cross sections. After this you can calculate the scattering length density (SLD) which is defined as the ratio of the scattering length per molecule and the molecular volume. Finally, the macroscopic scattering cross section needs to be calculated. This is the product of the microscopic cross sections times the number of molecules per unit volume. Table A2:1 list the relevant SL and SCS for C, H and D.

Atom	Scattering Length / fm		Scattering Cross Section / barn		
	Coherent	Incoherent	Coherent	Incoherent	Total
C	b_c = 6.65	0	5.551	0.001	5.551
H	b_H = -3.739	25.274	1.76	80.26	82.02
D	b_D = 6.671	4.04	5.59	2.05	7.64
F	b_F = 5.654	-0.082	4.012	0.0008	4.0178

Table A2:1 Scattering Lengths and Cross Sections for C, H, D and F

Remember is coherent scattering lengths and are incoherent scattering lengths.

A2.2.1 Scattering Cross Section

For molecule A_mB_n

Number fraction of A, —— Number fraction of B, —— where

Therefore, Equation A2:15

e.g. one polyethylene repeat unit – CH_2

Number fraction of C, ——

Number fraction of H, ——

The coherent cross-section per atom = 0.00956barn and per CH_2 molecule = 3×0.00956 =0.029barn

A2.2.2 Incoherent Scattering Cross Section

Incoherent scattering has two contributions from:

(1) Spin incoherence from different atoms which every element has, unless its spin is zero. Spin incoherence occurs because of the different atoms in the molecule. So for a molecule A_mB_n

Spin incoherent cross-section =

(2) Composition Incoherence is a combination of the isotopic incoherence, from different isotopes in the molecule and disorder scattering. So again for a molecule A_mB_n

Composition Incoherent cross-section =

The total incoherent scattering cross-section =

Equation A2:16

N.B to convert from fm^2 to barn divide by 100

e.g. one polyethylene repeat unit – CH_2

Total incoherent scattering cross-section =

The incoherent cross-section per atom = 53.75 barn and per CH_2 molecule = 3×56.53 =169.58 barn

A2.2.3 Total Scattering Cross Section

Equation A2:17

For molecule A_mB_n

Equation A2:18

For one polyethylene repeat unit – CH_2

The total cross-section per atom = 56.63barn and per CH_2 molecule = 3×56.63 =169.89 barn

A2.2.4 Macroscopic Scattering Cross-Section

The macroscopic scattering cross-section is the product of the microscopic cross-sections times the number of molecules per unit volume.

Equation A2:19

Equation A2:20

For a system containing pure CH_2 then:

A2.2.5 Scattering Length Density

The scattering length density is required to calculate neutron contrast factors. For a molecule A_mB_n

Equation A2:21

For one polyethylene repeat unit – CH_2

Volume = $14/(N_A \times 1.21) = 1.92\times10^{-23}\ cm^3$ **(N.B. 1×10^{-13} cm=1 fm)**

A2.2.6 Scattering Length Density for Mixtures

For a mixture of $C_4H_6D_2$ blended in C_4H_8 then the volume fractions are and .

Volume ($C_4H_6D_2$) = $58\ gmol^{-1}/(N_A \times 1.21\ gcm^{-3}) = 7.96\times10^{-23}\ cm^3$

Volume (C_4H_8) = $56\ gmol^{-1}/(N_A \times 1.21\ gcm^{-3}) = 7.68\times10^{-23}\ cm^3$

Total SLD =

From this depending on what % $C_4H_6D_2$ is in the mixture you can calculate the SLD, or from the SLD measure you can determine the volume fraction of $C_4H_6D_2$ at the surface, for the case of NR.

A2.2.7 Contrast Factors

The contrast term is the difference in SLD values between components within a sample. The scattering intensity is proportional to the contrast factors; therefore, by changing the relative amounts of deuterium the SLD can be adjusted. In a blend of *A* molecules in a *B* molecule matrix:

— — Equation A2:22

— — Equation A2:23

If i.e. would result is the differential cross-section, so *Q*=0 and there would be no coherent neutron scattering.

Contrast matching is an isotopic labelling technique based on the dramatic difference between the b of H and D. By contrast matching you can simplify the scattering pattern.

In the work presented in this thesis, the materials studied were EF-$C_6H_4D_2$ (end-functionalised partially deuterated polybutadiene) blended in C_6D_8 (fully deuterated polyethylene) for SANS and QENS and had EF-$C_6H_4D_2$ blended in C_6H_6 (fully hydrogenated polybutadiene) for NR.

A2.3 Scattering Functions

During a neutron scattering experiment only *I(Q,t)* and , S(Q,ω) are experimentally observed. *I(Q,t)* is the intermediate scattering function providing information on the sample's state as a function of time and momentum. A space Fourier transform of the pair correlation function, G(,t) (describing the position of the nuclei in space and time) yields *I(Q,t)*. By performing a time Fourier transform of *I(Q,t)* the structure factor, S(Q,ω), is obtained providing information on a samples state as a function of energy and momentum.

A2.4 Neutron Measurements

Neutrons incident on a sample can do one of three things:

- be transmitted through the sample without interaction (no change in energy or momentum)
- be scattered (change in momentum and/or energy)
- be absorbed.

Option 1:Transmission

Travelling through a sample without interaction is the simplest neutron measurement to acquire. To measure this, called the samples transmission, a monochromatic beam, collimation and simple detectors are all that is required. The measurements yield information on the sample content, figure A2:3.

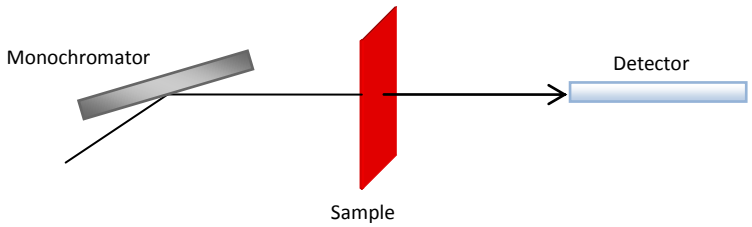

Figure A2:3 Transmission beam path during neutron scattering

Transmission, T_s, is measured as a ratio of the direct beam intensity with the sample and the direct beam intensity without the sample. SANS experiments carry out transmission measurements where a flat slab sample (appropriate for SANS) of thickness "*d*" (typically ~1mm) and total macroscopic cross section, Σ_t are measured, where the total cross section per unit sample volume, Σ_t, is the sum of the coherent, incoherent and absorption cross sections per unit volume where,

Equation A2:24

Equation A2:25

Equation A2:26

The absorption, or neutron capture, cross section, Σ_a, can be calculated accurately from the tabulated absorption cross sections of the elements. The incoherent cross section, Σ_i, the coherent cross section, Σ_c, can only be estimated.

Option 2: Scattering

Two scattering techniques are relevant to the work presented in this thesis. The first type is elastic neutron scattering, figure A2:4, where the scattered intensity is measured at various *Q*. This is a way of resolving $Q=(4\pi/\lambda)\sin(\theta/2)$. It is performed by either step-scanning or using a position sensitive detector.

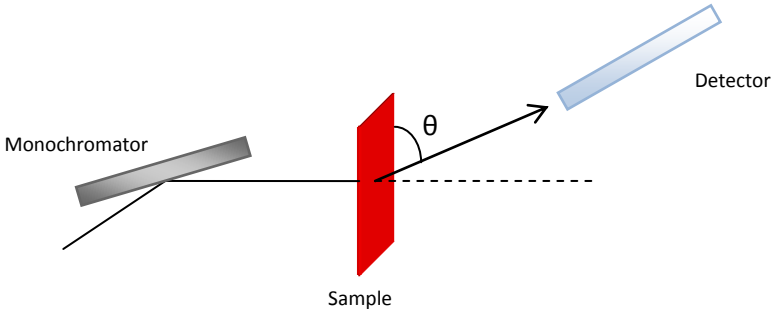

Figure A2:4 Elastic scattering beam path during neutron scattering

The above set-up is used to investigate the structure of either crystalline or amorphous samples.

The second type is quasielastic/inelastic neutron scattering. Quasielastic is a form of inelastic where the energy transfer peak is located around E=O (zero peak position but with a finite peak width). It requires monochromation and collimation but before detection can take place the energy of the scattered neutron is analysed. The analysis requires a crystal analyser (or a time-of-flight method) in order to resolve the energy transfer during scattering. Both *Q* and *E* are resolved. QENS corresponds to the energy transfer around zero and investigates diffusion modes. Inelastic scattering corresponds to the finite energy transfer and investigates several modes including phonon and optic. Triple axis, time-of-flight and backscattering spectrometers can all be used.

A2.5 References

1. Pozzo, D. C., *Langmuir* **2009,** *25* (3), 1558-1565.
2. Whitten, A. E.; Jacques, D. A.; Hammouda, B.; Hanley, T.; King, G. F.; Guss, J. M.; Trewhella, J.; Langley, D. B., *Journal of Molecular Biology* **2007,** *368* (2), 407-420.
3. Voets, I. K.; de Keizer, A.; de Waard, P.; Frederik, P. M.; Bomans, P. H. H.; Schmalz, H.; Walther, A.; King, S. M.; Leermakers, F. A. M.; Stuart, M. A. C., *Angewandte Chemie-International Edition* **2006,** *45* (40), 6673-6676.
4. Heenan, R. K.; Penfold, J.; King, S. M., *Journal of Applied Crystallography* **1997,** *30*, 1140-1147.
5. Rogers, S. E.; Terry, A. E.; Lawrence, M. J.; Eastoe, J.; Cabral, J. T.; Chan, A., *Materials Today* **2009,** *12* (7-8), 92-99.
6. Hammouda, B., *Polymer Reviews* **2010,** *50* (1), 14-39.
7. Thomas, R. K., *Annual Review of Physical Chemistry* **2004,** *55*, 391-426.
8. Penfold, J.; Richardson, R. M.; Zarbakhsh, A.; Webster, J. R. P.; Bucknall, D. G.; Rennie, A. R.; Jones, R. A. L.; Cosgrove, T.; Thomas, R. K.; Higgins, J. S.; Fletcher, P. D. I.; Dickinson, E.; Roser, S. J.; McLure, I. A.; Hillman, A. R.; Richards, R. W.; Staples, E. J.; Burgess, A. N.; Simister, E. A.; White, J. W., *Journal of the Chemical Society-Faraday Transactions* **1997,** *93* (22), 3899-3917.
9. Richards, R. W., *Scattering Methods in Polymer Science*. Ellis Horwood Limited: 1995.
10. Pynn, R., *Neutron Scattering: A Primer*. 1990.
11. Clifton, L. A.; Neylon, C.; Terry, A. E.; Dicko, I. C.; Diddens, I. A., *Materials Today* **2009,** *12* (7-8), 86-91.
12. Jones, R. A. L.; Richards, R. W., *Polymers at Surfaces and Interfaces*. Cambridge University Press.
13. Tehei, M.; Franzetti, B.; Wood, K.; Gabel, F.; Fabiani, E.; Jasnin, M.; Zamponi, M.; Oesterhelt, D.; Zaccai, G.; Ginzburg, M.; Ginzburg, B. Z., *Proceedings of the National Academy of Sciences of the United States of America* **2007,** *104* (3), 766-771.
14. Sakai, V. G.; Arbe, A., *Current Opinion in Colloid & Interface Science* **2009,** *14* (6), 381-390.
15. Penfold, J., *Current Science* **2000,** *78* (12), 1458-1466.
16. Russell, T. P., *Annual Review of Materials Science* **1991,** *21*, 249-268.
17. Higgins, J.; Benoit, H., *Polymers and Neutron Scattering*. Clarendon Press - Oxford Science Publications: 1996.
18. Neelakantan, A.; Maranas, J. K., *Journal of Chemical Physics* **2004,** *120* (1), 465-474.
19. Neelakantan, A.; Maranas, J. K., *Journal of Chemical Physics* **2004,** *120* (3), 1617-1626.
20. Crowley, T. L.; Lee, E. M.; Simister, E. A.; Thomas, R. K., *Physica B* **1991,** *173* (1-2), 143-156.
21. Crowley, T. L.; Lee, E. M.; Simister, E. A.; Thomas, R. K.; Penfold, J.; Rennie, A. R., *Colloids and Surfaces* **1991,** *52* (1-2), 85-106.

Conferences, Seminars, Publications and Awards

A3.1 Conferences

A3.1.1 Oral Contributions

- Novel Applications of Surfaces and Materials (11th to 15th April 2010, Manchester) – Tailoring the Surface of Polyethylene
- Molecular Spectroscopy User Group (5th March 2010, Oxford) – Using Molecular Probes to study Dynamics.
- Durham University Interdisciplinary Science colloquia – opening speaker (October 2009) Adsorption on Semi-crystalline polymers.

A3.1.2 Poster Presentations

- Zing Conference - "Polymer Chemistry Conference - Frontiers in Polymers and Biomaterials" (19 - 22 November 19 2010, Mexico)
- Royal Society of Chemistry – "Macro2010" (11-16 July 2010, Glasgow)
- IRC Spring Meeting (23rd March 2010, Durham)
- Institute of Physics - "Physical Aspects of Polymer Science" (14 - 16 Sep 2009, Bristol)
- Institute of Physics - "19th International Conference on Ion Beam Analysis" (7– 11 Sep 2009, University of Cambridge, UK)

A3.1.3 Attended

- High Polymer Research Group - "50th Anniversary Meeting" (25 – 19 April 2010, Pott Shrigley, Cheshire)

A3.2 Seminars

- Organiser of the Durham University science Soft Matter colloquia - Involving over 60 speakers from all 4 sciences (2009-2010)
- IRC Polymer Course Interdisciplinary Research Centre (IRC) Polymer Science and Technology Course (2007):
    - Polymer Physics

A3.3 Publications

- "pH-Controlled Polymer Surface Segregation" Thompson, Richard L., Hardman, Sarah J, Hutchings, Lian R., Narrainen, Amilcar Pillay, Dalgliesh, Robert M., Langmuir, **25**, 5, 2009, 3184-3188

A3.4 Awards

- Young Persons Lecture Competition (North East Division) 1nd place (2010)
- RSC Travel bursary of £100 for MACRO2010 attendance
- D H Richards Bursary of £100 for Zing Polymer Chemistry attendance
- Young Persons Lecture Competition (North East Division) 2nd place (2008)
- Durham University Teaching Induction for Postgraduates: Preparing to Teach – Demonstrating (2007)
- Durham University Teaching Induction for Postgraduates: Preparing to Teach – Assessment in the Sciences (2007)